Physics of wastewater flow and pathogen transport processes from a soil-based at-grade effluent treatment system and associated groundwater contamination risks in Alberta, Canada

by

Amanuel Oqbit Weldeyohannes

A thesis submitted in partial fulfillment of the requirement for the degree of

Doctor of Philosophy

in

Soil Science

Department of Renewable Resources

University of Alberta

Abstract

Understanding of wastewater flow and transport processes and treatment effectiveness through the soil-absorption field of soil-based wastewater treatment systems remains a challenge. In addition, Alberta regulators and the on-site wastewater industry wanted to quantify the effectiveness of the new LFH At-grade soil-based wastewater absorption and treatment system design. An extensive field research program was executed at Wetaskiwin Rest Stop, Central region of Alberta, a site that has been receiving secondarly treated and ultraviolet disinfected effluent via pressurized effluent distribution at-grade laterals since 2007. The specific objectives were to investigate: i) hydrologic response to effluent infiltration from at-grade line sources under shallow groundwater conditions, ii) fate and transport of pathogens under boundary conditions typical of on-site water treatment systems (OWTS), and iii) groundwater contamination risks associated with OWTS. Following site characterization, field-scale tracer experiment was conducted using *E.coli* and Bromide as step and pulse inputs respectively. Groundwater response to effluent infiltration, wastewater plume movement, *E.coli* and virus concentrations were monitored in nests of monitoring wells over time. Finally, using the field measurements, HYDRUS 2D was used to investigate groundwater contamination risks associated with OWTS.

Considering the existing regulatory requirement of 7-day effluent travel depth through the vadose zone that has been established in Alberta, a residence time assumed to be enough for pathogens attenuation in the vadose zone, weekly cycle hydrologic responses were interpreted. Findings indicated: i) significant

hydrologic response to effluent infiltration from at-grade line sources at a weekly scale, ii) effluent reaching the groundwater for approximately 15% of the time in the spring and summer periods when effluent loading rate of ≥5 cm^3 cm^{-2} d^{-1} encountered a groundwater at ≤0.5 m below the ground surface. These conditions also coincided with the significant 7-day cycle of the effluent input function due to traffic on the highway and use of the facilities. The results suggest consideration of both surface effluent loading and regional hydrologic conditions when designing at-grade wastewater treatment systems to minimize potential groundwater contamination risks; iii) the vadose zone of ≥0.88 m thick, the vertical separation between the at-grade lines and the top of the groundwater level, filtered *E.coli* bacteria that were present in the infiltrating effluent to acceptable levels achieving the 7-day effluent travel depth design criteria, however it didn't perform well for some viruses, and iv) initial groundwater depth from the surface is critical for designing at-grade effluent treatment systems. Under the prevailing site boundary conditions and assuming a homogenous medium, a loading rate up to 15 cm^3 cm^{-2} d^{-1} poses less threat when the initial depth to groundwater is at ≥2 m.

In practical terms therefore, matching effluent loading rate vis-a-vis the effluent receiving site characteristics is critical particularly during the spring snow melt and summer period. In addition to the design criteria of OWTS, inclusion of performance criteria as standard of practices for these systems is suggested. The findings presented in this thesis contribute significantly to the understanding of

wastewater flow and transport under boundary conditions typical of OWTS and shallow groundwater conditions.

Dedication

I dedicate this work to my family, my wife (Rahwa) and our children (Jolien, Mathias and Aryam) for their love, encouragement and patience as well as to the memory of my *late* parents and parents-in-law for the (then) unwavering support, prayers and encouragement. Specially, my mother and my father-in-law who took the lead to heaven recently at the completion stage of this work.

Acknowledgements

"Commit to the Lord whatever you do and your plans will succeed." (Prob. 16:3). All credit goes to the almighty God for his loving care, for bestowing me with all the talents and patience needed for the entire work.

First of all, I have to thank my family, my wife Rahwa Ghirmay and our Children Jolien, Mathias and Aryam for their support and words of encouragement over the years. My greatest thanks go to my wife Rahwa who has always been there for me, for her love and for taking care of our children in my absence. She has unselfishly sacrificed her wants and needs over the years to help me achieve my dreams. Now it's my turn to help you make your dreams come true. I would also like to thank my children Jolien, Mathias and Aryam. You have taught me the meaning of true sacrifice and have inspired me to be the best person I can be. I love you all!

My special thanks go to my supervisor Dr. Miles Dyck and co-supervisor Dr. Gary Kachanoski. Thank you for everything you have taught me, your ongoing unreserved support and encouragement. Thank you for the opportunities you have given and continue to give. Your mentorship, guidance and critiques throughout the thesis writing were incredible that I can't imagine this could have been completed without your support. Words are not enough to express my gratitude to you both, thank you!

I also thank to Dr. Carl Mendoza, for agreeing to be part of my supervisory committee. Your encouraging comments and suggestions throughout the research work were greatly helpful and appreciated. A special thanks go to Dr. Gary Parkin for taking the time to review my thesis as my external examiner and to Dr. Scott Chang for agreeing with a short notice to review my thesis as an internal examiner. My sincere thanks also go to Dr. Gro Lilbaek, the (then) postdoctoral fellow, your support during the inception of my program were very helpful, thank you so much. Thank you to Dick Puurveen for your unreserved help and ongoing support. You are a friend and a mentor indeed. Thank you all!

My sincere thanks go to Alf Durnie from Alberta Municipal Affairs for your continued support to the project, Danny Shold from Cherdan Construction Co. and Edon Management Wetaskiwin for providing access to the research site

and for sharing the documents about the site infrastructure and continued support while I was at the site.

I extend my sincere thanks to Andre Christensen for your unreserved support during the field work including night shifts, encouragement and continued friendship. No words to express but you are a real man, thank you. Special thanks go to my field assistants at different stages of my field program: Philip Chanasyk, Katelyn Zinz, Heather Shurgot, Sawyer John Desaulniers, Russell Green Osberne, Leah Predy, Leanne Chai, Lauren, Nate, Jennifer Martin, and Nicholas Beranek. I am also greatly indebted to my lab group: Hailong He, Mekonnen Giweta, Cory Kartz, Sunny Song, Giovanna Dragonetti, Pamela Sabbagh, Syed Mostafa, Ju Zhang, Amy Gainer, Kelly Kneteman, Manjila Shahidi, Tina Harms, Kyle Kipps, Ali Zolfaghari, Sheryl Ramnarine and Christina Hebb for their support and friendship.

My thanks also go to the staff of the Provincial Laboratory of the University of Alberta Hospital: Dr. Norman Neumann and his staff - Candis Scott, Dr. Xiao-Li Pang, Min Cao, and to the staff of the Natural Resource Analytical Laboratory of my department: Alan Harms, Xin (Jean) Zhang and Donna Friesen, thank you for your help during the analysis of my samples. To Amanda Brown, Tammy Frunchak, Christie Nahos, Mike Abley, Nash Goonewardena, Ian Paine Annette Bussey, Darlene Saunders and all support and academic staff of my department for everything you have done to keep the wheels turning.

I am indebted to the University of Alberta, Alberta Water Research Institute (Alberta Ingenuity) and Memorial University of Newfoundland for funding my research program, Syngenta Graduate Scholarship in Sustainable Agriculture for scholarship award, the Faculty of Graduate Studies and Research and Graduate Students Association of the University of Alberta for bursaries and funding for professional development.

At last but not the least, I extend my sincere thanks to all my family, friends whose names have not been mentioned here (simply because the list is too long) for their prayers, friendship, encouragement, continued moral support and comforting my family throughout my study.

God bless you all!!

Table of Contents

LIST OF TABLES

LIST OF FIGURE

List of Acronyms and Symbols

β	Fitting parameter for straining function [-]
α	van Genuchten model fitting parameter related to inverse air-entry suction
θ	Soil water content [L^3 L^{-3}]
η	Dimesntionless time parameter
η_0	Overall single-collector contact efficiency [-]
$\phi_n(s)$	Phase signal
ω_o	Non-dimensional wavelet frequency
$\psi_o(\eta)$	Wavelet base function
θ_r	Residual soil water content [L^3 L^{-3}]
θ_s	Saturated soil water content [L^3 L^{-3}]
ψ_{str}	Dimensionless depth-dependent straining function [-]
Δt	Time interval [T]
$\hat{R}^2_{XY}(f_K)$	Coherency spectra
$\hat{S}^{(P)}_{XX}(f_K)$	Periodogram
$\hat{S}_{XX}(f_K)$	Estimated power spectrum of series X
W_n^{XY}	Cross wavelet transform of time series X and Y
$\overline{v_t}$	Average vertical Darcy flow velocity [L T^{-1}]
$\overline{\theta_v}$	Average soil water content [L^3 L^{-3}]
$S_{XX}(f_K)$	Power spectrum of series X
g_o	Specified bottom boundary gradient [L L^{-1}]
a	Microbe attachment (collision) efficiency [-]
A	Surface area[L^2]
AWI	Air-water interface
Br	Bromide
C_0	Bulk (influent) microbe concentration [M L^{-3}]
CBF	Clean Bed Filtration
CDE	Convective-Dispersion-Equation
$COV[X,Y]$	Covariance of X and Y
CV	Coefficient of variation
C_w	Concentration in aqueous phase [M L^{-3}]
CWT	Continuous wavelet transform
D	Hydrodynamic dispersion [L^2 T^{-1}]
$d(t)$	Depth to groundwater from the ground surface ([L]
$D1$ to $D3$	Down-gradient sites 1 to 3 with respect to source zone
d_{10}	Particle size diameter for which 10% of all particles in the volume distribution are smaller [M L^{-3}]
$d_{7,w}$	7-day travel depth [L]

d_a	Arithmetic mean diameter of collector (sand grain) [L]
d_c	Average diameter of spherical collector [L]
DFT	Discrete Fourier Transform
d_g	Geometric mean diameter of collector (sand grain) [L]
DI	De-ionized water
DLVO	Derjaguin-Landau-Verwey-Overbeek
d_p	Diameter of particle (e.g. virus, bacteria) [L]
DWT	Discrete wavelet transform
E.coli	Escherichia coli
E[∗]	Expectation operator
EC	Electrical conductivity
EM	Electromagnetic
E_s	Surface evaporation [L T^{-1}]
ET_{os}	Potential evapotranspiration estimated by Penman Montieth method [L T^{-1}]
ET_{tr}	Potential evapotranspiration estimated by an empirical expression developed by Maule *et al*.(2006) for the prairie region of Canada1 [L T^{-1}]
ET_{tru}	Potential evapotranspiration estimated by an empirical expression developed by Maule *et al*.(2006) for the prairie region of Canada2 [L T^{-1}]
F	Fourier frequency [T^{-1}]
FAST	Fixed Activated Sludge Treatment
f_K	Spectral frequency [T^{-1}]
FT	Fourier Transform
GW	Groundwater
H	Pressure head [L]
ID	Internal diameter [L]
K	Radiation extinction by canopy [-]
k_{att}	Microbial attachment rate coefficient [T^{-1}]
k_{det}	Microbial detachment rate coefficient [T^{-1}]
K_{eq}	Equilibrium distribution coefficient [L^3 M^{-1}]
K_s	Saturated hydraulic conductivity [L T^{-1}]
k_{str}	Microbial straining coefficient [T^{-1}]
L	Length [L]
LAI	Leaf area index [L^2 L^{-2}]
LFH	Layers of leafy, fermented, humic organic matter found at the surface of the soil profile in a forested area
MAC	Maximum Acceptable Concentration
MW	Monitoring well
N	van Genuchten model fitting parameter related to pore size distribution

N	Total number of sampling points or total number of sample size
OWTS	On-site wastewater treatment system
P	Porosity of a porous medium [L^3 L^{-3}]
P	Precipitation [L T^{-1}]
Pdf	Probability Density Function
PSD	Particle size distribution
PVC	Polyvinylchloride
PW	Piezometer well
P_z	Empirical root distribution parameter
$q(t)$	Effective surface flux density [L^3 L^{-2} T^{-1}]
$q_{efflu}(t)$	Area-averaged surface effluent flux density [L^3 L^{-2} T^{-1}]
R	Retardation factor, $R = 1 + \rho_b K_{eq} / f$ [-]
R^2	Coefficient of determination
RMSE	Root mean squared error
S	Wavelet scaling parameter [T]
$S(z,h)$	Sink term related to root water extraction [L^3 L^{-3} T^{-1}]
S1 to S4	Source zone sites 1 to 4
SCF	Dimensionless soil cover fraction defined
SD	Standard deviation
SI	Sensitivity index [L L^{-1}]
S_m	Attached microbe concentration [M M^{-1}]
S_p	Potential root water uptake rate [L^3 L^{-3} T^{-1}]
SWA	solid-water-air-interface
SWE	Snow water equivalent [L T^{-1}]
SWI	Solid-water-interface
t	Time [T]
t_0	Duration of microbe injection [T]
TFM	Transfer Function Model
T_p	Potential transpiration [L T^{-1}]
TRF	Total rainfall [L T^{-1}]
U1 to U2	Up-gradient site1 and 2 with respect to the source zone
UV	Ultraviolet
v	Interstitial pore velocity; $v = V/p$ [L T^{-1}]
$V(t)$	Effluent volume [L^3]
Var[X]	Variance of X
$W_{j,m}$	Bartlett Window
WT	Water table well
WTC	Wavelet coherency
x	Spatial distance (horizontal) [L]
Xn	Discrete time series X
XWT	Cross-wavelet transform

Yn	Discrete time series Y
z	Spatial distance (depth) [L]
z^*	Empirical parameter related to depth of maximum root intensity
Z_R	Maximum rooting depth [L]
ρ_b	Dry bulk density of porous medium [M L^{-3}]
λ	Fourier perio [T]
SZ	Effluent source zone
$2D$	Two dimensional domain
$3D$	Three dimensional domain

1. GENERAL INTRODUCTION

1.1. Background

The earth's fresh water resources account for only 2.5% of the planet's total water resources and the remaining 97.5% is salt water (UNESCO, 2012). Only 30% of the fresh water is accessible to sustain life on earth and it exists as surface (0.3%) and in groundwater (29.7%) bodies. Contamination due to lack of sanitation and use of agrochemicals (UNESCO, 2012) further reduces availability of fresh water resources. Thus, research to quantify the problems and to develop mitigation strategies for water quality problems is required to help policy-makers develop water management policies and regulations.

Canada is endowed with approximately 7% of the world's renewable freshwater resources (Environment Canada, 2004). However, the Canadian people and Canadian industries are among the world's highest per capita water users, ranked second only to the United States. As the population increases, the demand for clean water will continue to grow, but risks to water quality will likely also grow. About 30% of Canadians rely on groundwater supplies and yet groundwater users frequently report municipal water shortages (Environment Canada, 2004). Therefore, in areas with water shortages, wastewater management and reuse may be an option, but potential environmental and health risks need to be considered (Ganoulis, 2012; Hanjra *et al.,* 2012).

In Canada the use of treated wastewater is at an experimental stage. At small scales, wastewater treated in decentralized systems is used mostly for landscape irrigation and toilet flushing; and water treated in centralized systems is used for agricultural, golf course and urban landscape irrigation (Exall *et al.*, 2006; Exall, 2004). Many other countries with water shortages also use treated wastewater for agricultural purposes (e.g., Pedrero *et al.,* 2010). Adoption of treated wastewater use depends on water availability, economic incentives, regulatory feasibility and public acceptance (Menegaki *et al.,* 2007). If there is scarcity of water, the public will likely use treated wastewater (Hanjra *et al.,* 2012;

Mutengu *et al.,* 2007; Pedrero *et al.,* 2010; Qadir *et al.,* 2010; Weber *et al*., 2006).

Management and mitigation measures should be in place to avoid potential health and environmental risks associated with wastewater disposal (Scandura and Sobsey, 1997; WHO, 2003). Potential sources of wastewater include agricultural, industrial, and municipal activities (e.g. fertilizer and pesticide use, sewage disposal systems). Septic tanks, marginally treated wastewater from on-site wastewater treatment systems, sewage sludge (biosolids), and animal feeding operations are among potential sources of human and animal pathogenic microbes (Gerba and Smith, 2005; US-EPA, 1977). Pathogens are infectious microbes such as viruses, bacteria and protozoa that can cause diseases (Barnett and Ormiston, 2007). Among the pathogenic microorganisms of concern that can possibly be transported through soil along with wastewater flow include: bacteria - *Escherichia coli* (*E. coli*) O157:H7, *Salmonella spp*., *Shigella spp*., *Vibrio cholera*, *Yersinia enterocolitica*, *Y.pseudo-tuberculosis*, *Leptospira spp., Frsncisella tularensis, Dyspepsia coli*, enterotoxine forming *E.coli, Pseudomonades, Listeria*, and *Helicobacter*; viruses - *hepatitis, polio viruses, coxsackie viruses, ECHO viruses*, *rotavirus*, and *Norwalk* agents; and parasites - *Cryptosporidium*, *Cyclospora*, *Toxoplasma*, *Microsporidia*, and *Giardia* (e.g. Katz *et al.,* 2009; Gerba and Keswick, 1981; Matthess and Pekdeger, 1981). Other organic contaminants such as pharmaceutical and personal care products may also co-exist in these wastewaters (Crockett, 2007; Carrara *et al*., 2008; Lapworth *et al*., 2012; Lishman *et al.,* 2006).

The vadose zone, the unsaturated zone between the ground surface and water table, plays an important role in controlling water flow processes, attenuating pathogens and other contaminants or their transport to groundwater resources (Last *et al.,* 2004; McCarthy and McKay, 2004). As an intrinsic part of the hydrologic cycle, the vadose zone controls the interrelationships between precipitation, infiltration, surface runoff, evapotranspiration and groundwater recharge (Harter and Hopmans, 2004). Lin (2010) described the vadose zone-

groundwater interface as one of the critical zone interfaces that affects landscape-soil-water-ecosystem-climate relationships.

Near-surface water balance and geochemical conditions (e.g. weathering of rocks, precipitation and dissolution of chemical compounds) are affected by vadose zone processes (e.g. infiltration, redistribution, deep percolation, attachment and detachment processes). These processes in turn significantly influence the fate and transport of dissolved compounds and colloids. The persistence of contaminants in the subsurface is largely determined by the extent of degradation, sorption and volatilization processes (Chiou, 1989) that occur in the vadose zone and therefore it is often considered to be a natural filter for contaminants, protecting groundwater from pollution. For example, the transport of bacteria through soils is governed by a complex set of interrelated physical, chemical, and biological processes, which in turn control cell growth, survival, and attenuation (Steenhuis *et al.,* 2011). However, a shallow vadose zone or the presence of preferential flow paths, i.e., warm holes, cracks, and tree roots, may expedite the movement of water and contaminants deeper into the ground by limiting the aforementioned filtering processes (e.g. Beven and Germann, 1982). Thus, intentional or accidental spills of wastes/chemicals on the ground at various scales necessitate research for better environmental management and risk assessment.

1.2. Evolution of Wastewater Treatment Systems

1.2.1. Wastewater Treatment Options and Trends

The first known wastewater disposal system, a water closet at Knossos Palace in Crete, was used by king Minos in the 17th century BC; (US-EPA, 2002). Later, up to 1850 AD, similar systems were in use by other societies in Europe (e.g. Greek, British and Romans). Nonetheless, the systems were not environmentally sustainable because the wastewater was discharged to surface waters leading to the contamination of lakes, rivers, streams, and coastal areas and became the cause of disease outbreaks like cholera and typhoid fever. These health and environmental concerns motivated the innovation of centralized

wastewater treatment systems in the 20th century. In centralized systems, the wastewater is treated away from the source (off-site) and these systems are commonly used in urban settings. However, due to aging of these off-site systems and high costs for building new centralized systems, on-site wastewater treatment systems (OWTS) are becoming alternative options (McCray and Christopherson, 2008). The OWTS are decentralized systems that treat wastewater at or near the source of generation and they are increasingly used in individual homes, hotels, motels and resorts in rural areas or in remote public park places in Canada, the United States and many other countries (e.g. US-EPA, 1997). The OWTS are also gaining popularity in urban settings because of the above-mentioned limitations with centralized systems. In Alberta an estimated 300,000 private sewage systems (including septic tanks) are in use and are increasing at an approximate rate of 7000 per year (Durnie, 2008).

1.2.2. Wastewater and Emerging Contaminants

Emerging contaminants in both surface and groundwater bodies have been a growing concern in recent years (Lapworth *et al.*, 2012; Katz *et al.*, 2009; Katz and Griffin, 2008). These emerging contaminants are those contaminants such as pathogens and organic compounds that have appeared in human populations for the first time, or have occurred previously but are increasing in incidence or expanding into areas where they have not previously been reported, especially over the last 20 years (WHO, 2003). Waterborne emerging pathogens include protozoa, bacteria and viruses such as *Cryptosporidium parvum, Eschericha coli* 0157:H7, poliovirus, Norwalk virus and others (Crockett, 2007). Emerging organic contaminants are pharmaceutical and personal care products such as gemfibrozil and diclofenac (e.g. Lishman *et al.,* 2006; Krkosek, 2006). Over the years, technological advances have led to the invention of various wastewater treatment techniques including physical, chemical and biological treatment systems that are operated at off-site (centralized) and on-site (decentralized) facilities. However, most conventional wastewater treatment systems have been designed to remove well-known contaminants such as suspended solids, organic

matter, and some nutrients (e.g. Pescod, 1992). Therefore, the control of bacteria, viruses, protozoa; and organic compounds such as pharmaceutical and personal care products, industrial and life-style compounds, and caffeine remains a challenge (Crockett, 2007; Carrara *et al*., 2008; Lap worth *et al*., 2012).

Crockett (2007) highlighted the potential survival of emerging pathogens at significant concentrations for longer periods (>7 days) in the environment and the difficulty to remove or inactivate them by the existing water and wastewater treatment mechanisms. Lapworth *et al* (2012) also reported widespread groundwater contamination by organic compounds. Katz *et al* (2009) observed elevated levels of carbamazepine (a pharmaceutical compound) and enteroviruses in groundwater down gradient of a septic tank drainfield. Similarly, Katz and Griffin (2008) also detected organic wastewater, pharmaceutical compounds and microorganisms in groundwater in a large spring basin in north-central Florida, possibly originating from septic tank effluent. These findings suggest revisions are needed of the existing regulatory standards and industrial practices. Therefore, assessment of the eco-toxicological risks associated with these contaminants is required to backup regulatory standards.

It is likely that there is no "silver bullet" method or system that can remove or inactivate all known contaminants. Hence, a combination of two or more treatment systems could be an option such as UV disinfection and sand filtration (Crockett, 2007). In summary, together with the improvement of analytical methods for measuring/detecting emerging pathogenic microorganism and organic compounds, studies on the fate, transport and survival of these pathogens and organic contaminants in the environment should continue to ensure good quality water resources and the environment.

1.2.3. Microbial Source Tracking

Routine analyses of all pathogenic microorganisms that may exist in drinking water and wastewater is not practical or economical with the available detection methods. Instead, indicator microbes (e.g. bacteria) are selected as fecal tracers (Health Canada, 2006; Bartram and Pedley, 1996). The following four

bacterial genera are commonly used as target organisms in microbial source tracking studies: *Escherichia*, *Enterococcus*, *Bacteroides*, and *Bifidobacterium* (Simpson *et al.,* 2002). Microbial source tracking is a method that allows researchers to identify the source(s) of fecal contamination using indicator microorganisms - natural or surrogates - and chemicals (Mesquita and Emelko, 2012; Scott *et al.,* 2002). *Escherichia coli* (*E. coli*) and fecal *enterococci* are tracked by bacterial strain isolation methods while non-culturing approaches are used for *Bacteroides* and *Bifidobacterium* species. However, the use of *E. coli* and fecal enterococci is easier than the other two because they are relatively easy to detect.

E. coli is a rod-shaped, gram-negative, gammaproteobacterium in the family *Enterobactericeae,* and belongs to the fecal coliform group of bacteria (Ishii and Sadowsky, 2008). It inhabits the intestines of humans and other warm-blooded animals (Health Canada, 2006; Savageau, 1983). As *E. coli* is sensitive to environmental stresses like temperature, sunlight, type of microflora and water chemistry, it has a very short life about 4–12 weeks in water and its re-growth in water is also limited. Therefore, the presence of *E. coli* in water would indicate recent fecal contamination of the water (Health Canada, 2006, 2013; WHO, 2004; Edberg *et al*., 2000). In Canada, the maximum acceptable concentration (MAC) of *E. coli* in drinking water is none detectable per 100 mL (Health Canada, 2006).

There are three classes of *E. coli* based on antibody reaction with three types of antigens: the somatic (O), capsular (K) and flagellar (H) antigens (Nataro and Kapel, 1998). *E. coli* O157:H7 is one of the shiga toxin-producing serotypes with combination of O and H antigen, which cause well-known diseases such as hemorrhagic colitis and hemolytic uremic syndrome in humans (Paton and Paton, 1998; Karmali, 1989). They are among the endemic types of pathogens that have been of concern to public health and the environmental. This bacterium can contaminate soil, vegetables and water bodies when untreated or marginally treated sludge and effluents are applied as manure, irrigation water and/or leached to the groundwater. Waterborne disease outbreaks (e.g. due to *E. coli* O157:H7, noroviruses) were reported in the United States, Canada and other parts of the

world including recent years (Corapcioglu and Haridas, 1984; Craun, 1985; Yates *et al.,* 1988; Bruce-Grey-Owen Sound Health Unit, 2000; Craun *et al*., 2006; Clark *et al.,* 2010; Borchardt *et al.*, 2011; Moffatt and Struck, 2011) and from indirect sources linked to eating contaminated food stuffs such as fresh spinach, cheese, raw, refrigerated, prepackaged cookie dough and ground beef (CDC, 2009, Scallan *et al.,* 2011).

1.3. Biocolloids Fate and Transport through Saturated and Unsaturated Media

Biocolloids are nano- to micron-sized organic particles including, but not limited to, bacteria, viruses, and spores that exist in the environment (Steenhuis *et al.*, 2011). The fate and transport of biocolloids through saturated and unsaturated porous media has been and continues to be an area of research interest for protecting groundwater resources, evaluating pathogen risks to groundwater supplies, designing better wastewater and water treatment systems, and assessing natural and enhanced bioremediation processes (Bales *et al.,* 1995; Brennan *et al*., 2010*;* Gerba and Smith, 2005; Ginn *et al.*, 2002; Keller and Auset, 2007; Johnson *et al.,* 2007; Steenuis *et al.*, 2011; Scandura and Sobsey, 1997; Stevik *et al.*, 2004; Tufenkji, 2007). Therefore, it is important to understand and develop theory about the mechanisms of biocolloid transport processes.

The main transport mechanisms of biocolloids are advection, diffusion, dispersion and adsorption; and they are also subjected to biochemical and physical removal/retention mechanisms (e.g. Keller and Auset, 2007; Sen, 2011; Stevik *et al.*, 2004). The physical retention processes include straining, interception, diffusion to the walls of the transport media and gravitational deposition. These processes result in the attachment of the cell to the matrix of the porous media (e.g. soil). Microbial growth, die-off, predation, and parasitism are among the biological processes. There is also a chemical-driven transport process called chemotaxis, a phenomenon of directional movement of single-celled organisms toward to (positive chemotaxis) or away from (negative chemotaxis) a higher chemical concentration (Stevik *et al.,* 2004). Some of the aforementioned

processes, such as die-off, increase removal of the biocolloids while others increase attenuation through attachment/detachment mechanisms (Dowd and Pillai, 1997; Gordon and Toze, 2003; Nasser *et al*., 1993). Biocolloidal transport and retention mechanisms are the subjects of much recent research.

Biocolloid retention and transport processes have been modeled using the Derjaguin–Landau–Verwey–Overbeek (DLVO), theory of colloidal stability or the Clean Bed Filtration (CBF), theory of deposition (Steenhuis *et al.*, 2011; Tufenkji, 2007). The application of DLVO theory for modeling the behavior of biocolloids is limited because it assumes spherical colloids, uniform charge density and impermeable colloid surfaces, however biocolloids are inherently nonspherical, soft, have deformable and nonhomogeneous surfaces and they respond to chemical changes in the environment (Ginn *et al.,* 2002; Tufenkji *et al.*, 2006). The CBF theory explains the collision of a biocolloid to a collector surface such as soil grain as induced by interception, gravitational deposition and Brownian motion. However, CBF theory also assumes packed beds of spherical collectors, which again limits its use to approximate spherical matrix grains while most natural subsurface porous media have a wide range of pore and particle sizes, complex pore geometry, rough pore walls, tortuous flow paths, and considerable surface heterogeneity (Bradford and Torkzaban, 2008; Johnson *et al.*, 2007; Kretzschmar *et al.,* 1994).

Johnson *et al* (2007) introduced additional retention mechanisms such as colloid wedging between grain-to-grain contacts in multiple collectors and their associated flow dynamics; Torkzaban *et al* (2008) used a combination of DLVO and other porous media properties such as ionic strength and suggested that the straining rate in a given porous medium is a complicated mechanism, coupled with such parameters as pore size distribution, hydrodynamics, solution chemistry and water content. Torkzaban *et al* (2008) observed an increase in straining rate with increase in ionic strength but with decrease in water content and flow rate of the system.

Among the possible interfaces by which microorganisms are attached to porous media are shown in Figure 1-1 and these are: i) the solid-water interface

(SWI) also known as enhanced attachment, ii) air-water interfaces (AWI) - common with hydrophobic biocolloids and iii) air-water-solid interfaces (AWS) also referred as contact line (Schijven and Hassanizadeh, 2000). Such attachment mechanisms delay microbial transport and provide extra time for their inactivation and die-off. The attachment and inactivation processes are also influenced by the soil solution chemistry such as ionic strength and pH (Torkzaban *et al.*, 2006; Michen and Graule, 2010; Zevi *et al.,* 2009). Zevi *et al* (2009) observed reduced preferential retention of biocolloids at the AWS interfaces as ionic strength increases.

Researchers have shown that pathogens can be transported long distances in groundwater and surface waters (Keswick and Gerba, 1980) and may persist for significant periods in the environment (Dowd and Pillai, 1997). The fate and transport of pathogens are affected by physical, chemical and biological properties of a porous media through which transport takes place (Yates *et al.,* 1988). The soil water content, ionic strength, presence of metal oxides and pH of the soil dictate virus transport (Bales *et al.,* 1995; Chu *et al*., 2003; Torkzaban *et al.*, 2006). Similarly, the survival of bacteria is also affected by particle size distribution, soil moisture and organic matter contents (Brennan *et al.,* 2010). Chu *et al* (2003) found greater removal or inactivation of viruses under unsaturated flow through high metal oxide soils. Bales *et al* (1995) observed net attachment at pH = 5.7 and net detachment at pH = 6-8 of viruses from a sandy soil.

Microbe retention in the soil increases as the water saturation decreases. In unsaturated soil where pores are partially filled with air, the transport volume is reduced and processes of attachment (adsorption) take place that retard microorganisms transport. Brennan *et al* (2010) observed greater survival of facultative bacteria (e.g. *E.coli*) in soils with high clay content and saturated soils and they suggested it could be due to a potential decrease of larger microbes (e.g. protozoa) in the anaerobic conditions that could have grazed on bacteria. They also noted that soil structure variability induced microbe transport variation; and

that formation of biofilms could also shield the bacteria from predators (Brennan *et al.,* 2010).

1.4. Modeling Biocolloid Fate and Transport Through Soils

1.4.1. Governing Transport Equations

A general form of the one-dimensional convective-dispersion equation (CDE) for homogeneous media under steady state flow is (e.g. Schijven and Hassanizadeh, 2000; Yates *et al.,* 1988)

$$\frac{\partial C}{\partial t} = D\frac{\partial^2 C}{\partial z^2} - v\frac{\partial C}{\partial z} \qquad [1.1]$$

Where: C is microbe concentration in aqueous phase [M L^{-3}], D is hydrodynamic dispersion coefficient [L^2 T^{-1}), t is time [T], z is spatial distance [L], and v is pore water velocity [L T^{-1}].

Eq. [1.1] describes only the main physical transport processes similar to conservative tracers for steady state flow conditions. Including the fate of microbes due to physicochemical processes of filtration, as the case is for microbes, Eq. [1.1] becomes:

$$\frac{\partial C}{\partial t} + \frac{\rho_b}{\theta}\frac{\partial S_m}{\partial t} = D\frac{\partial^2 C}{\partial z^2} - v\frac{\partial C}{\partial z} \qquad [1.2]$$

Where: S_m is attached microbe concentration to the solid phase [M M^{-1}], ρ_b is porous media bulk density [M L^{-3}] and θ is the steady state volumetric water content of porous media [L^3 L^{-3}].

Equilibrium adsorption of microbes can be described by instantaneous (time independent) models: linear, Langmuir and Freundlich isotherms (Yates *et al.,* 1988). For the special case of linear isotherms, $S_m = K_{eq}C$, and Eq. [1.2] is reduced to:

$$R\frac{\partial C}{\partial t} = D\frac{\partial^2 C}{\partial z^2} - v\frac{\partial C}{\partial z} \quad [1.3]$$

Where: $R=1+\rho_b K_{eq}/\theta$ is the retardation factor and K_{eq} is equilibrium distribution coefficient [L^3 M^{-1}].

However, for suspended microbes, a time-dependent (kinetic) adsorption model may be more appropriate than instantaneous equilibrium. Schijven and Hassanizadeh (2000) described a two-stage kinetic model. In the first stage, microbes are transferred from the bulk fluid to the matrix surface via mass transport. In the second stage, the microbes are attached to the surfaces following physicochemical interactions. The rate at which a retained microbe concentration changes with time is given by:

$$\frac{\rho_b}{p}\frac{\partial S_m}{\partial t} = k_{att}C - \frac{\rho_b}{p}k_{det}S_m \quad [1.4]$$

Where: k_{att} is microbial attachment rate coefficient [T^{-1}] and k_{det} is microbial detachment rate coefficient [T^{-1}] and p is porosity of the media at saturation [L^3 L^{-3}]. The attachment rate coefficient, k_{att}, is related to single-collector contact efficiency (η_0) [-] and microbe attachment (collision) efficiency (a) [-] by:

$$k_{att} = \frac{3(1-n)}{2d_c}\eta_0 a \quad [1.5]$$

Bradford *et al* (2003) extended the classical CBF by including physical straining (with no detachment) as:

$$\frac{\rho_b}{p}\frac{\partial S_m}{\partial t} = k_{att}C - k_{str}\psi_{str}C \quad [1.6]$$

$$\psi_{str} = \left(\frac{d_c+z}{d_c}\right)^{\beta} \quad [1.7]$$

Where: k_{str} is microbial straining coefficient [T^{-1}], ψ_{str} is depth-dependent straining function [-], d_c is average diameter of spherical collector [L] and β is a fitting parameter for straining function [-] and it controls the shape of the spatial distribution of retained colloids.

1.4.2. Transfer Functions: Stochastic Approaches

A transfer function is a stochastic model, which uses a solute travel probability density function (pdf) measured at a given depth to predict transport to greater depths. A widely used transfer function model (TFM) was proposed by Jury (1982) to predict transport of a surface applied solute to any given depth in the soil system. Since then the TFM has been used by many researchers (e.g.; Jury *et al.*, 1982; Utermann *et al.*; 1990; Mattern and Vanclooster, 2010) to estimate solute travel time through the unsaturated zone.

The TFM assumes the vadose zone is a black box that the internal transport mechanisms are unknown but can be inferred from the field measured travel pdf (Jury, 1982). The hypothesis behind the TFM is that infiltrating water at the surface transmits through the vadose zone and reaches at a given depth, z, passing through all possible pathways and conduits in the transport volume (which may be less than the volumetric water content). Another assumption is that conservative solutes move in solution along with the water flow at similar velocities. In the TFM, dispersion is explained by the pdf because the main cause for dispersion is assumed to be the variability in flow velocities (Jury, 1982).

1.4.3. Physical Based models: Numerical Analysis

Conditions in "real world" field settings are often transient and much more complex than the simple systems described by the steady state CDE (Eq. [1.1]) and some transfer function models. With the continuing progress in high-speed computing, numerical solutions to the governing flow and transport equations are allowing much more complex field conditions to be simulated.

Process-based modeling refers to a procedure by which the behavior of a system is simulated through the numerical solution of coupled, governing partial

differential equations. In the context of flow and transport through porous media, the transient flow field is simulated through numerical solution of the Richards equation, which informs numerical algorithms such as particle tracking or numerical solutions of the CDE (Gogu and Dassargues, 2000; Godfrey, 1983; Bossel, 1994). HYDRUS is an example of a process-based model applicable for flow and transport in variably saturated condition (Šimůnek and Šejna, 2007).

1.5. Discussion and Synthesis

To date, considerable improvements have been made toward the developments of theories regarding biocolloid fate and transport in laboratory bench-scale column experiments; and results from these experiments have helped to identify factors important for field-scale investigations. However, macro-scale parameters, aquifer characteristics (e.g. preferential pathways), and natural field conditions (e.g. transient conditions) are often difficult to mimic at a laboratory scale suggesting the need for field-scale investigations. Field conditions may enhance biocolloid attachment/detachment mechanisms relative to the laboratory scale. Up-scaling of laboratory results to field situations may also underestimate attachment mechanisms due to field heterogeneity, environmental factors (e.g. climate) and native microbial activity (Charles *et al.,* 2008). Hence, regulatory guidelines and best management practices are better assessed and developed based on field-scale observations.

Pathogen removal and retention mechanisms are greatly influenced by saturated and unsaturated flow conditions and other soil physicochemical and biological properties (Yates *et al.,* 1988). The retention of pathogens on soil surfaces is expected to increase with an increase in thickness of the unsaturated zone (Urbano and Thibault, 2005; Schwientek *et al.,* 2009). The thickness of the unsaturated zone (vadose zone) also by definition controls the travel distance and therefore directly influences travel time of contaminants from the source point to groundwater. Schwientek *et al* (2009) suggested the need for high vertical resolution of sampling to accurately detect transit time of contaminants through

the vadose zone. In addition to vadose zone thickness, the degree of saturation influences the efficiency of retention processes (Figure 1.1).

At-grade wastewater line sources are commonly used in areas where the water table is close to the ground surface (e.g. ≤0.9 m, Converse *et al.,* 1990; Safety Code Council, 2012; 0.3 to 1.2 m US-EPA, 1999). Development of local groundwater mounding below on-site wastewater discharge fields reduces the thickness of the unsaturated zone (Finnemore, 1993) causing a shorter travel time and/or travel distance of contaminants and biolcolloids before reaching the groundwater and may reduce the attenuation of pathogens. This local rise in water table also changes biogeochemical processes in the soil. An increase in soil water content decreases biodegradation processes substantially because of the decrease in oxygen and may thereby increase the risk of groundwater contamination. This is because the kinetics of aerobic biodegradation is much faster compared to anaerobic conditions.

Oxidation-reduction conditions of a wastewater plume zone affect fate and transport of contaminants. Carrara *et al* (2008) observed a correlation between the transport of pharmaceutical compounds such as salicylic acid and diclofenac and an oxidation-reduction zone of a wastewater plume. Almost no pharmaceutical compound was detected in the aerobic zone, but its detection increased in the NO_3^--, Mn(IV)- and Fe(III)-reducing zones. Other researchers (Robertson *et al.,* 1998; Harman *et al*., 1996) also observed attenuation of nutrients such as phosphorus in a relatively thick unsaturated zone conducive for the oxidation of a wastewater plume. Dominant chemical precipitation reactions were observed largely being completed within the vadose zone resulting in accumulation of phosphorus-rich solids near infiltration area (Robertson *et al.,* 1998). Harman *et al* (1996) observed higher attenuation of phosphorus either by sorption or precipitation in the unsaturated zone. However, aerobic conditions do not guarantee the attenuation of all contaminants. For example, Robertson (2003) found well-oxidized wastewater plumes at sites with 2 to 5 m thick unsaturated zones had high NO_3-N concentrations and Harman *et al* (1996) also found increased levels of NO_3-N at the water table compared to the effluent's

concentration, suggesting oxidation of NH_4-N favored by aerobic conditions in the unsaturated zone. Robertson (2008) observed decreased concentrations of NH_4-N at the water table and in the plume zone compared to that in the effluent as a result of its oxidation to nitrate. Other strategies such as phytoremediation may be used to decrease nitrate loading.

For on-site wastewater treatment systems that discharge the effluent on the ground surface via at-grade lines, a biomat may develop. A biomat is a layer of biological growth and inorganic residue that develops at the wastewater-soil interface and extends up to about 2.5 cm into the soil matrix (Barnett and Ormiston, 2007). It controls the infiltration of pre-treated wastewater through the infiltrative surface/zone in medium to coarse textured soils. In engineered wastewater filtration media, reverse flushing of a filter with clean water is one of the common practices to suppress biomat formation and thereby increases efficiency of the filtration system. However, in the field, reverse flushing is not possible. So biomat formation may pose problems for at-grade systems especially after long term use and it may be important to consider biomat formation in dealing with flow and transport from at-grade line sources under shallow groundwater boundary conditions.

Intermittent changes of soil water content in response to event-based infiltration of effluent are commonly observed in on-site wastewater treatment systems. Depending on the magnitude of the dosing cycles, infiltration of the effluent influences the underlying groundwater table. In the saturated and unsaturated zones, the air-water and solid-water interfaces may also change with the changes in soil water content and potentially affect biocolloid retention and transport processes. Thus, understanding and predicting these physical flow and transport processes in the saturated and unsaturated soils remains a challenge (Sen, 2011). Also the US-EPA (2013) recently issued concerns with OWTS. About 10 to 20% of the OWTS in the US fail each year causing environmental pollution and putting public health at risk. Moreover, the potential of bacteria transport in the subsoil below 1-m depth is poorly understood, which suggests consideration when assessing risk to groundwater (Brennan *et al.,* 2010).

Therefore, characterization of wastewater flow and transport processes in fields receiving effluent via at-grade line sources helps in the development of regulatory guidelines and design protocols for on-site wastewater treatment systems. Thus, the general objective of this study is to better understand wastewater flow and transport processes of effluent released from at-grade line sources under shallow water table conditions.

1.6. Objectives, Thesis Structure and Relevance of the Research

1.6.1. General Objective

In Alberta approximately more than a quarter-million private sewage systems (septic tanks) are in use and are increasing at an approximate rate of 7000 per year (Durnie, 2008), but the environmental risks, especially with respect to groundwater contamination associated with these systems, have not been well quantified. Further, regulatory guidelines for LFH at-grade systems are currently being developed for Alberta and research is required to reinforce these regulations. Therefore, the general objective of the research in this thesis is: to increase the understanding of multi-dimensional unsaturated and saturated flow and transport under boundary conditions typical of on-site wastewater treatment systems (OWTS) under shallow groundwater conditions in order to quantify groundwater contamination risks associated with these systems.

To address this objective, a field research program was executed at the Wetaskiwin rest stop, 80 km south of Edmonton, which is under the supervision of Alberta Infrastructure (Figure 2-1). Our assumption was that the site-specific measurements of the flow and transport processes are representative of the physics of flow and transport processes typical of other at-grade wastewater sites and could be further generalized through the development of a numerical flow and transport model.

1.6.2. Thesis Structure and Specific Objectives

The thesis objectives were addressed in the respective chapters as follows: in this chapter, the general background on the historical evolution of on-site

wastewater treatment systems, wastewater flow and transport (biocolloid), emerging contaminants and associated risks to public health and the environment were briefly described. Synthesis of our present understanding of OWTS with respect to at-grade effluent dispersal and associated problems with these systems was presented and potential research questions were outlined for this PhD thesis. Finally, the research objectives, approaches, importance and relevance of this PhD thesis work were presented.

In chapter two, the study site description, historical review and physiographic characterization are presented. The site has been receiving an ultraviolet disinfected effluent via at-grade line sources for over four years. However, the extent of wastewater plume (if it exists), groundwater flow pattern and potential risks to groundwater pollution have not been studied. Therefore, the specific objectives for this chapter were: (i) to describe the study site, (ii) to characterize in-situ spatial and temporal groundwater flow and wastewater plume extent, and (iii) to identify groundwater flow direction and estimate wastewater plume center of mass.

A time series covariance of effluent infiltration and groundwater response was the main topic of Chapter 3 to investigate hydrologic response to surface applied effluent. In this chapter, a time series analysis was conducted to unveil the groundwater response to effluent infiltration from the at-grade line sources and to understand groundwater mounding beneath an at-grade infiltration field. The specific objectives were: (i) to quantify the groundwater fluctuation over time (ii) to identify groundwater response to effluent infiltration and detect any groundwater mounding under the at-grade line sources and (iii) to estimate vadose zone thicknesses with respect to these groundwater fluctuations and whether these variations pose environmental risks.

In Chapter four, field scale flow and transport study and observed breakthrough of *E.coli* and bromide tracers are described and synthesized. The specific objectives were (i) to identify wastewater flow pathways and transport through the saturated and unsaturated zones; (ii) to quantify flow and transport

parameters and (iii) to examine and evaluate effective vadose zone thickness that potentially filter/treat wastewater before pathogens reach the groundwater.

Combining the information from the previous chapters, a process model for on-site at-grade wastewater treatment systems (OWTS) is presented in Chapter 5 to investigate groundwater pollution risks associated with these systems. The specific objective was to investigate groundwater contamination risks associated with OWTS via simulation of an actual site and then introducing scenarios including high water table (high means close to the ground surface) to up-scale (generalize) for similar at-grade systems.

Chapter six concludes with general discussion highlighting the main contributions of this PhD thesis and future works in this line.

1.6.3. Outcome and Relevance of the Research

This research will contribute to a better understanding of a multidimensional unsaturated and saturated water flow and transport under boundary conditions of typical of on-site wastewater treatment systems and shallow groundwater conditions.

The outcome of the research will help to develop guidelines and procedures for designing environmentally friendly septic systems and wastewater treatment plants, decision making tools for the design of cost-effective wastewater treatment systems as well as groundwater risk assessment programs.

Immediate beneficiaries of the research will be:

- Researchers in academic and research institutions: research results will benefit researchers in various soil, groundwater and contaminant transport studies, nutrient balance, biodegradation studies on the site and elsewhere.
- Infrastructure Engineers: optimization studies for effluent disposal/dispersal, designing efficient and effective septic systems and OWTS.

- Decision makers including but not limited to Government, Public, Municipal and Environmental Health Officers: in developing wastewater treatment design guidelines, groundwater risk assessment procedures, drinking water standards and environmental impact assessment (EIA) procedures.

1.7. References

Bales, R. C., S. Li, K. M. Maguire, m. T. Yahya, C. P. Gerba, and R. W. Harvey, 1995. Virus and bacteria transport in a sandy aquifer, Cape Cod, MA. *Groundwater, 33:653-661.*

Barnett, H. and Ormiston, A. W., 2007. Manual for on-site wastewater design and management : Technical report to support Policy development. Horizons Regional Council, New Zealand. ISBN: 1-877413-69-0 Report No: 2007/EXT/778. Available on line: http://www.horizons.govt.nz/assets/horizons/Images/one_plan/On-Site%20Wastewater%20Design%20Manual_April%2007.pdf

Bartram, J. and S. Pedley, 1996. Microbiological analyses. Chapter 10, In J. Bartram and R. Ballance (eds.), Water quality monitoring - A practical guide to the design and implementation of freshwater quality studies and monitoring programmes. UNEP/WHO, Chapman & Hall, London ISBN 0 419 22320 7 (Hbk).

Beven K. and P. Germann, 1982. Macropores and water flow in soils. *Water Resour. Res. 18: 1311-1325.*

Borchardt, M. A., K. R. Bradbury, E. C. Alexander Jr., R. J. Kolberg, S. C. Alexander, J. R. Archer, L. A. Braatz, B. M. Forest, J. A. Green, and S. K. Spencer, 2011. Norovirus Outbreak Caused by a New Septic System in a Dolomite Aquifer. *Groundwater, 49:85-97.*

Bossel, H. 1994. Modeling and simulation. A. K. Peters Ltd., Wellesley, MA, 484 p.

Bradford, S. A. and S. Torkzaban, 2008. Colloid transport and retention on in unsaturated porous media: A review of interface-, collector-, and pore-scale processes and models. *Vadose Zone J. 7:667–681.*

Bradford, S. A., J. Simunek, M. Bettahar, M. Th. van Genuchten, S. R. Yates, 2003. Modeling colloid attachment, straining, and exclusion in saturated porous media. *Environ Sci Technol. 37:2242–50*.

Brennan, F. P., V. O'Flaherty, G. Kramers, J. Grant and K. G. Richards, 2010. Long-term persistence and leaching of *E.coli* in temperate maritime soils. *Appl. Environ. Microbio. Dio:10.1128/AEM.02335.09.*

Bruce-Grey-Owen Sound Health Unit, 2000. The investigative report on the Walkerton outbreak of waterborne gastroenteritis. May–June, Owen Sound, Ontario. Available on line: http://www.publichealthgreybruce.on.ca/Water/Public_Drinking/Walkerton/Report/REPORT_Oct00.PDF

Carrara, C., C. J. Ptacek, W. D. Robertson, D. W. Blowes, M. C. Moncur, ED Sverko, and S. Backus, 2008. Fate of pharmaceutical and trace organic compounds in three septic stsyem plumes, Ontario, Canada. *Environ. Sci. Technol. 42:2805-2811.*

CDC, 2009. *E. coli* outbreak investigations. Available on line: http://www.cdc.gov/ecoli/outbreaks.html

Charles, K. J., F. C. Souter, D. L. Baker, C. M. Davies, J. F. Schijven, D. J. Roser, D. A. Deere, P. K. Priscott, and N. J. Ashbolt, 2008. Fate and transport of viruses during sewage treatment in a mound system. *Water Res. 42, 3047–3056*.

Chiou, C. T. 1989. Theoretical considerations of the partition uptake of nonionic organic compounds by soil organic matter.. In, Sawhney, B.L., and K Brown (eds), Reactions and movement of organic chemicals in soils. SSSA Special Publication Number 22. Soil Science Society of America, Inc. Madison, WI. pp. 1-29.

Chu, Y., Y. Jin, T. Baumann, and M. V. Yates, 2003. Effect of soil properties on saturated and unsaturated virus transport through columns. *J. Environ. Qual. 32:2017–2025.*

Clark, W.F., J. M. Sontrop, J. J. Macnab, M. Salvadori, L. Moist, R. Suri and A. X. Garg, 2010. Long term risk for hypertension, renal impairment, and cardiovascular disease after gastroenteritis from drinking water contaminated with Escherichia coli O157:H7: a prospective cohort study. *BMJ 2010;341:c6020*. doi:10.1136/bmj.c6020

Converse, J. C., E. J. Tyler, and J. O. Peterson, 1990. Small scale wastewater management project. Wisconsin at-grade soil absorption system: Siting, design and construction manual. University of Wisconsin-Madison. Available online: http://www.mde.state.md.us/programs/Water/BayRestorationFund/OnsiteDisposalSystems/Documents/Onsite%20Systems/Wisconsin%20At%20Grade%20Manual.pdf

Corapcioglu, M. Y., and A. Haridas, 1984. Transport and fate of microorganisms in porous media: a theoretical investigation. *J. Hydrol. 72:149–69.*

Craun, G. F., 1985. A summary of waterborne illness transmitted through contaminated groundwater. *J Environ. Health. 48:122–127.*

Craun, M. F., G. F. Craun, R. L. Calderon and M. J. Beach, 2006. Waterborne outbreaks reported in the United States. *J. Water Health, 4(Suppl. 2): 19-30.*

Crockett, C. S., 2007. The role of wastewater treatment in protecting water supplies against emerging pathogens. *Water Environ. Res. 79:221-232.*

Dowd, S. E, S. D. Pillai, 1997. Survival and transport of selected bacterial pathogens and indicator viruses under sandy aquifer conditions. *Environ Sci Health, Part A: Environ Sci Eng. Toxic Hazard Subst. Control. 32A:2245–58*.

Durnie, A, 2008. An on-site sewage and septage management framework in Alberta framework Alberta. Available on line:

http://www.environmentconference.alberta.ca/docs/Session-33_presentation.pdf

Edberg, S. C., E. W. Rice, R. J. Karlin, M. J. Allen, 2000. Escherichia coli: the best biological drinking water indicator for public health protection. *J. Appl. Microbiol., 88: 106S-116S.*

Environment Canada, 2004. Threats to Water Availability in Canada. National Water Research Institute, Burlington, Ontario. NWRI Scientific Assessment Report Series No. 3 and ACSD Science Assessment Series No. 1. 128 p. Available on line: https://www.ec.gc.ca/inre-nwri/default.asp?lang=En&n=0CD66675-0&offset=4&toc=show

Exall, K. 2004. A review of water reuse and cycling, with reference to Canadian practice and potential: 2. Applications. *Water Qual. Res. J. Canada. 39:13-28.*

Exall, K., J. Marsalek, and K. Schaefer, 2006. Water reuse in canada: Opportunities and challenges. In P. Hlavinek, T. Kukharchyk, J. Marsalek and I. Mahrikova (eds.), Integrated urban water resources management. *Proceedings of NATO Advanced Research Workshop. p 253–262*.

Finnemore, E. J., 1993. Estimation of groundwater mounding beneath septic drain fields. *Ground water 31:884-889*.

Ganoulis, J., 2012. Risk analysis of wastewater reuse in agriculture. *Inter. J. of Recycling of Org. Waste in Agri. 1:1-9*.

Gerba, C. P and J. E. Jr. Smith, 2005. Sources of pathogenic microorganisms and their fate during land application of wastes. *J. Environ. Qual. 34:42–48.*

Gerba, C.P. and B. H. Keswick, 1981. Survival and transport of enteric viruses in groundwater. In: W. Van Duyvenbooden, P. Glasbergern and H. Van Lelyveld (Eds.), Quality of Groundwater. *Studies in Environ. Sci., Elsevier, 17:511-515.*

Ginn, T. R., B. D. Wood, K. E. Nelson, T. D. Scheibe, E. M. Murphy, T. P. Clement, 2002. Processes in microbial transport in the natural subsurface. *Adv. Water Resour. 25:1017-1042.*

Godfrey, K. 1983. Compartmental models and their applications. Academic Press, New York, NY, pp.291.

Gogu, R. C. and A. Dassargues, 2000. Current trends and future challenges in groundwater vulnerability assessment using overlay index methods. *Environ. Geol. 39:549-559.*

Gordon C, S. Toze, 2003. Influence of groundwater characteristics on the survival of enteric viruses. *J Appl. Microbiol. 95:536–44*.

Hanjra, M. A., J. Blackwell, G. Carr, F. Zhang, T. M. Jackson, 2012. Wastewater irrigation and environmental health: Implications for water governance and public policy. *Int. J. Hyg. Envir. Heal. 215:255–269.*

Harman, J., W. D., Robertson, J. A. Cherry and L. Zanini, 1996. Impacts of a sand aquifer from an old septic system: Nitrate and phosphate. *Ground Water, 34:1105-1114.*

Harter, T. and J. W. Hopmans, 2004. Role of vadose-zone flow processes in regional-scale hydrology: review, opportunities and challenges. In R. A. Feddes, G. H. de Rooij, J.C. van Dam (eds.) Unsaturated zone modeling: Progress, challenges and applications. 179-208. Kluwer Acad. Publ. The Netherlands. Available on line: http://hopmans.lawr.ucdavis.edu/papers+ppt+zip/harter&hopmans.pdf

Health Canada, 2006. Guidelines for Canadian Drinking Water Quality: Guideline Technical Document — *Escherichia coli*. Water Quality and Health Bureau, Healthy Environments and Consumer Safety Branch, Health Canada, Ottawa, Ontario. Available on line: http://www.hc-sc.gc.ca/ewh-semt/alt_formats/hecs-sesc/pdf/pubs/water-eau/escherichia_coli/escherichia_coli-eng.pdf

Health Canada, 2013. Guidance on waterborne bacterial pathogens. Water, Air and Climate Change Bureau, Healthy Environments and Consumer Safety Branch, Health Canada, Ottawa, Ontario (Catalogue No. H129-25/1-2014E-PDF).

Ishii, S. and M. J. Sadowsky, 2008. *Escherichia coli* in the environment: Implications for water quality and human health. *Minireview, Microbes Environ. 23:101-108.*

Johnson, W. P., M. Tong, and X. Li, 2007. On colloid retention in saturated porous media in the presence of energy barriers: The failure of α, and opportunities to predict η. *Water Resour. Res. 43:W12S13, doi:10.1029/2006WR005770.*

Jury, W. A., 1982. Simulation of Solute Transport Using a Transfer Function Model. *Water Resour. Res. 18:363-368*.

Jury, W. A., L. H. Stolzy and P. S**house**, 1982. A field test of the transfer function model for predicting solute transport. *Water Resour. Res. 18:369-378*.

Karmali, M. A. 1989. Infection by verocytotoxin-producing Escherichia coli. *Clin. Microbiol. Rev. 2:15-38*.

Katz, B. G., and D. W. Griffin, 2008. Using chemical and microbiological indicators to track the impacts from the land application of treated municipal wastewater and other sources on groundwater quality in a karstic springs basin. *Environmental Geology 55: 801-821*.

Katz, B.G., Griffin, D.W., Davis, J.H., 2009. Groundwater quality impacts from land application of treated municipal wastewater in a large karstic spring basin: chemical and micbiological indicators. *Sci. Total Environ. 407:2872-2886*.

Keller A. A. and M. Auset, 2007. A review of visualization techniques of biocolloid transport processes at the pore scale under saturated and unsaturated conditions. *Adv. Water Resour. 30:1392-1407 doi:10.1016/j.advwatres.2006.05.013*.

Keswick, B. H. C. P. Gerba, 1980. Viruses in groundwater. *Environ. Sci. Technol. 14:1290-1297.*

Kretzschmar, R., W. P. Robarge, and A. Amooregar, 1994. Filter efficiency of three saprolites for natural clay and iron oxide colloids. *Environ. Sci. Technol. 1994, 28, 1907-1915.*

Krkosek, W. 2006. Creating the winning conditions for technological innovation in municipal water and wastewater infrastructure: A policy discussion. *Freshwater for the future: policies for sustainable water management in Canada. Conference proceedings*. pp.135-146. Ottawa: Policy Research Initiative. Available on line: http://www.infc.gc.ca/research-recherche/results-resultats/wr-at/pri-prp/pri-prp-eng.html

Lapworth, D. J., N. Baran, M. E. Stuart, and R. S. Ward, 2012. Emerging organic contaminants in groundwater: A review of sources, fate and occurrence. *Environ. Poll. 63:287-303*.

Last, G. V., E. J. Freeman, K. J. Cantrell, M. J. Fayer, G. W. Gee, W. E. Nichols, B. N. Bjornstad and D. G. Horton, 2004. Vadose zone hydrogeology data package for Hanford assessments. Prepared for the U.S. department of energy under contract DE-AC05-76RL01830.

Lin, H. 2010. Earth's critical zone and hydropedology: Concepts, characteristics, and advances. *Hydrol. Earth Syst. Sci. 14:25–45. doi:10.5194/hess-14-25.*

Lishman, L., S. A. Smyth, K. Sarafin, S. Kleywegt, J. Toito, T. Peart, B. Lee, M. Servos, M. Beland, P. Seto, 2006. Occurrence and reductions of pharmaceuticals and personal care products and estrogens by municipal wastewater treatment plants in Ontario, Canada. *Sci. Total Environ. 367:544-558*.

Massoudieh, A. and T. R. Ginn, 2010. Colloid-facilitated contaminant transport in unsaturated porous media. In G. Hanrahan (ed.). Modelling of Pollutants in Complex Environmental Systems, Volume II. ILM Publications, a trading division of International Labmate Limited. 259-287.

Mattern, S. and M. Vanclooster, 2010. Estimating travel time of recharge water through a deep vadose zone using a transfer function model. *Environ. Fluid Mech. 10:121–135.*

Matthess, G., and A. Pekdeger, 1981. Concepts of a survival and transport of model of pathogenic bacteria and viruses in groundwater. *Sci. Total Environ. 21:149-159.*

McCarthy, J. F., and L. D. McKay, 2004. Colloid transport in the subsurface: past, present, and future challenges. *Vadose Zone J. 3:326–337.*

McCray, J. E. and S. H. Christopherson, 2008. On-site wastewater systems and interactions with the environment. ASCE , *J. Hydrol. Engin. 653-654.*

Menegaki, A. N., N. Hanley, K. P. Tsagarakis, 2007. The social acceptability and valuation of recycled water in Crete: A study of consumers' and farmers' attitudes. *Ecol. Econ. 62:7–18.*

Mesquita, M. M. F. and M. B. Emelko, 2012. Bacteriophages as surrogates for the fate and transport of pathogens in source water and in drinking water treatment processes. In I. Kurtboke (ed.) Bacteriophages. *Publisher InTech, ISBN 978-953-51-0272-4, pp.57-80.*

Michen, B. and T. Graule, 2010. Isoelectric points of viruses. J. Appl. Microbiol. 109:388–397.

Moffatt, H., and S. Struck, 2011. Water-borne disease outbreaks in Canadian small drinking water systems. *National Collaborating Centres for Public Health*, *.pp16.*

Mutengu, S., Z. Hoko, F. S. Makoni, 2007. An assessment of the public health hazard potential of wastewater reuse for crop production. A case of Bulawayo city, Zimbabwe. *Phys. Chem. Earth 32:1195–1203.*

Nasser, A. M., Y. Tchorch and B. Fattal, 1993. Comparative survival of *E. coli*, F^+bacteriophages, HAV and Poliovirus-1 in wastewater and groundwater. *Wat. Sci. Tech. 27:401-407.*

Nataro, J. P. and J. B. Kaper, 1998. Diarrheagenic *Escherichia coli*. *Clin. Microbiol. Rev. 11:142–201.*

Paton, J. C. and A.W. Paton, 1998. Pathogenesis and diagnosis of shiga toxin-producing *Escherichia coli* infections. *Clin. Microbiol. Rev. 11:450-479.*

Pedrero, F., I. Kalavrouziotis, J. J. Alarcón, P. Koukoulakis, T. Asano, 2010. Use of treated municipal wastewater in irrigated agriculture—Review of some practices in Spain and Greece. *Agr. Water Manage. 97:1233–1241.*

Pescod, M. B., 1992. Wastewater treatment and use in agriculture - *FAO irrigation and drainage paper 47.*

Qadir, M., D. Wichelns, L. Raschid-Sally, P. G. McCornick, P. Drechsel, A. Bahri, and P. S. Minhas, 2010. The challenges of wastewater irrigation in developing countries. *Agr. Water Manage. 97:561–568.*

Robertson, W. D., 2003. Enhanced attenuation of septic system phosphate in noncalcareous sediments. *Ground Water, 41:48-56.*

Robertson, W. D., 2008. Irreversible phosphorus sorption in septic systems plumes? *Groundwater 46:51-60.*

Robertson, W. D., S. L. Schiff and C. J. Ptacek, 1998. Review of phosphate mobility and persistence in 10 septic system plumes. *Ground Water, 36:1000-1010.*

Safety Code Council, 2012. Alberta private sewerage systems 2009 standard of practice handbook. Available on line: http://www.safetycodes.ab.ca/Public/Documents/PSSSOP_Handbook_Version_12_Online_Feb_21_2012b.pdf

Savageau, M.A., 1983. Escherichia-coli habitats, cell-types, and molecular mechanisms of gene-control. *Am. Nat. 122:732-744.*

Scallan, E., R. M. Hoekstra, F. J. Angulo, R. V. Tauxe, M. Widdowson, S. L. Roy, J. L. Jones, and P. M. Griffin, 2011. Foodborne Illness Acquired in the United States—Major Pathogens. *Emerg. Infect. Dis. 17:7-15*. DOI: 10.3201/eid1701.P11101.

Scandura, J. E. and M. D. Sobsey, 1997. Viral and bacterial contamination of groundwater from on-site sewage treatment systems. *Water Sci. Technol. 35:141-146.*

Schijven, J. F. and S. M. Hassanizadeh, 2000. Removal of viruses by soil passage: Overview of modeling, processes, and parameters. *Crit Rev Environ. Sci. Technol. 30:49–127.*

Schwientek, M., P. Maloszewski, F. Einsiedl, 2009. Effect of the unsaturated zone thickness on the distribution of water mean transit times in a porous aquifer. *Journal of Hydrology 373:516–526.*

Scott, T. M., J. B. Rose, T. M. Jenkins, S. R. Farrah, and J. Lukasik, 2002. Microbial source tracking: current methodology and future directions. *Appl. Environ. Microbiol. 68:5796–5803*.

Sen, T. K., 2011. Processes in pathogenic biocolloidal contaminants transport in saturated and unsaturated porous media: A Review. *Water Air Soil Pollut*. Springer, DOI: 10.1007/s11270-010-0531-9

Simpson, J. M., J. W. Santodomingo and D. J. Reasoner, 2002. Microbial Source Tracking: State of the Science. *Environ. Sci. Techol. 36:5279-5288.*

Šimůnek, J. and M. Šejna, 2007. HYDRUS 2D/3D Software Package for Simulating the Two- and Three-Dimensional Movement of Water, Heat and Multiple Solutes in Variably-Saturated Media. *User Manual, Version 1.02. PC-Progress, Prague, Czech Republic*.

Steenhuis, T. S., V. L. Morales, M. E. Cakmak, A. E. Salvucci, W. Zhang, 2011. Biocolloids: transport and retention in soils. In J. Gliński, J. Horabik, and J. Lipiec (eds.), Encyclopedia of Agrophysics. DOI 10.1007/978-90-481-3585-1, © Springer Science+Business Media B.V. 66-71.

Stevik, T. K., K. Aa, G. Ausland, J. F. Hanssen, 2004. Retention and removal of pathogenic bacteria in wastewater percolating through porous media: a review. *Water Res. 38:1355-1367.*

Torkzaban, S., S. A. Bradford, M. Th. van Genuchten, S. L. Walker, 2008. Colloid transport in unsaturated porous media: The role of water content and ionic strength on particle straining. *J. Contamin. Hydrol. 96:113–127.*

Torkzaban, S., S. M. Hassanizadeh, J. F. Schijven, H. A. M. de Bruin, and A. M. de Roda Husman, 2006. Virus Transport in Saturated and Unsaturated Sand Columns. *Vadose Zone J. 5:877–885*.

Tufenkji, N., 2007. Modeling microbial transport in porous media: Traditional approaches and recent developments. *Adv.Water Resour. 30:1455–1469.*

Tufenkji, N., D. R. Dixon, R. Considine, and C. J. Drummond, 2006. Multi-scale Cryptosporidium/sand interactions in water treatment. *Water Res. 40:3315–3331*.

UNESCO, 2012. Managing water under uncertainity and risks. *The United Nations World Water Development Report 4 Vol. 1.*

Urbano, L. D. and C. Thibault, 2005. Pattern of saltwater contamination resulting from tsunami inundation of small islands. *Transactions 17th Caribbean Geological Conference, San Juan, Puerto Rico July 17-22, 2005.*

US-EPA, 1977. The Report to Congress: Waste disposal practices and their effects on groundwater. Washington, DC.

US-EPA, 1997. Response to the Congress on the use of decentralized wastewater treatment systems. Available on line: http://water.epa.gov/infrastructure/septic/upload/septic_rtc_all.pdf

US-EPA, 1999. Decentralized systems technology fact sheet mound systems. EPA 832-F 99-074.

US-EPA, 2002. On-site wastewater treatment systems manual. EPA/625/R-00/008, February 2002. Office of Water, Office of Research and Development U.S. Environmental Protection Agency (EPA). Available on line: http://www.norweco.com/pdf/EPA/625R00008.pdf

US-EPA, 2013. Septic (Onsite/Decentralized) Systems. Available on line: http://water.epa.gov/infrastructure/septic/

Utermann, J., E. J. Kladivko, and W. A. Jury, 1990. Evaluating pesticide migration in tile-drained soils with a transfer function model. *J. Environ. Qual. 19:707-714*.

Weber, S., S. Khan, J. Hollender, 2006. Human risk assessment of organic contaminants in reclaimed wastewater used for irrigation. *Desalination 187:53–64.*

WHO, 2003. Emerging issues in water and infectious diseases. ISSN 1728-2160.

WHO, 2004. Guidelines for drinking water quality. 3rd ed. Volume 1 Recommendations, Geneva. Available on line: http://www.who.int/water_sanitation_health/dwq/GDWQ2004web.pdf

Yates, M. V., S. R. Yates, and C. P. Gerba, 1988. Modeling microbial fate in the subsurface environment. *Crit. Rev. Env Contr. 17:307-344*. DOI: 10.1080/10643388809388339.

Zevi, Y. A. Dathe, B. Gao, W. Zhang, B. K. Richards, and T. S. Steenhuis, 2009. Transport and retention of colloidal particles in partially saturated porous media: Effect of ionic strength. *Water Resour. Res. 45:W12403, doi:10.1029/2008WR007322.*

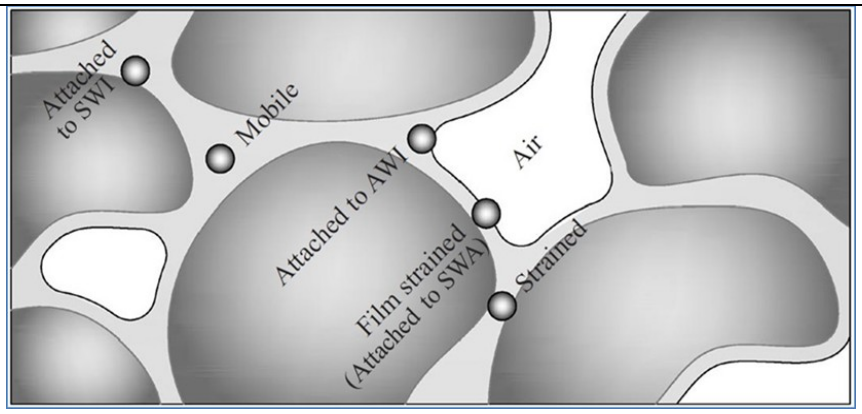

Figure 1-1: Colloid retardation mechanisms in unsaturated porous media (Modified after Massoudieh and Ginn, 2010).

2. STUDY SITE DESCRIPTION, HYDROLOGY AND WASTEWATER PLUME DELINEATION

2.1. Introduction

The main purpose of this chapter is to describe the study site and the general methodology used for conducting the initial environmental site assessment (Alberta Environment, 2001). More emphasis is given to the approaches employed to characterize the groundwater flow patterns and wastewater plume identification. The specific and detailed methods pertaining to each experiment and data analysis that were used throughout the thesis work are given in chapters 3, 4 and 5. Therefore, the specific objectives for this chapter were (i) to describe the study site, (ii) to characterize in-situ spatial and temporal groundwater flow and wastewater plume extent, and (iii) to identify groundwater flow direction and estimate wastewater plume center of mass.

2.2. Study Site Description

The research in this thesis was conducted between 2010 and 2012 at the Wetaskiwin Rest Stop, Alberta, Canada. The Wetaskiwin Rest Stop is located on the Queen Elizabeth II Highway, northbound, 80 km south of Edmonton and 25 km southwest of Wetaskiwin (N52°53.709 W113°38.548). Based on the Alberta legal land classification system, the site is located at 10-24-045-26 W4M (Figure 2-1). The Rest Stop is equipped with seven toilets, two urinals, seven hand-washing sinks and septic tanks. At the Rest Stop, an on-site wastewater treatment system equipped with Ultraviolet (UV) disinfection and LFH at-grade line sources was established by the Alberta Municipal Affairs as a pilot project in 2007. The system serves a travelers rest stop located in Central Alberta on Queen Elizabeth II highway.

A site history review and physiographic characterization of the study site was conducted during the inception of the research project in summer 2010. A desktop review of documents and site visits were carried out to examine historical and current uses of the study site, potential risks associated with the Rest Stop facility and the on-site wastewater treatment system. The design and installation

of the on-site wastewater treatment system consisting of the ultraviolet-disinfection and at-grade effluent dispersal lines (Cherdan Construction Ltd), regional (HCL, 2008) and local (APTRYX, 2007) groundwater hydrology and lithology were reviewed. An on-site meeting and field tour was conducted between the research team (Dr. Kachanoski, Dr. Dyck, Dr. Lilbaek and Mr. Weldeyohannes) and representatives from relevant stakeholders including Alberta Municipal Affairs, Alberta Environment, Alberta Infrastructure and Edom Management and a memorandum of understanding was reached. The research perspective, access to the study site and logistics were discussed and agreed by all the participants on May 06, 2010.

2.2.1. Physiographic and Hydrogeologic Setting

A review of the regional physiographic and hydrogeologic setting of the study site was conducted. The hydrogeologic map of Wetaskiwin County is given in Figures 2-2 to 2.5 (HCL, 2008). The specific location of the study site is indicated in Figures 2-2 and 2-3. The surficial deposits of the region were divided into upper and lower deposits (HCL, 2008). The upper surficial deposit was composed of till, clay, silt, sand and gravel deposited by glacial melt water. The upper deposit is approximately 30 m thick and within this 30 m thickness, there is a 2 m thick layer of sand and gravel that is believed to be an aquifer, but its exact location has not been verified. The lower surficial deposit is generally less than 2 m thick but can reach up to 5 m along the linear bedrock lows. Fluvial and lacustrine deposits of shale, sandstone and coal compose the lower surficial deposit. The main hydrogeologic (water conducting) unit of the lower deposit is sandstone.

Regional bedrock and surface elevation data was obtained from the Alberta groundwater assessment database (HCL, 2008) and it was analyzed using interpolation by Kriging in Surfer (Golden Software, Inc., 2009) and is presented in Figure 2-4. The surficial deposit and bed rock cross-section (C-C′) of the study site as interpreted from Figure 2-4 is given in Figure 2-5. The three-dimensional color representation of Figure 2-4 indicates the regional surface topography

overlaid by contours of the bedrock elevation. The elevation of the top bedrock surface ranges between 720 to 1100 masl (Figures 2-2 to 2-3).

The surface topography of the study area was characterized as having a level to gentle slope (2 to 2.5%) to the northeast with few undulations. Regionally, the study site is located at a low elevation (Figure 2-4). At the site, seasonal groundwater fluctuation is common and groundwater flows to northeast towards the Bearhills Lake, which is located at approximately 3.5 km northeast of the study site. There is an ephemeral creek within the fenced area north of the at-grade laterals, which is active after snowmelt and flows from west to east as shown in Figure 2-1. Past the creek to the north, the site outside of the forested area is nearly flat and stays wet for about two to three months after snow melt. There are also unnamed creeks at about 200 m to the northeast and at about 800 m to the east and Maskwa Creek located at 1.4 km east of the site and it flows to the Bearhills Lake (APTRYX, 2007).

Average groundwater table elevation at the site was 1.1 m below the ground surface during 2011 and 2012, with a seasonal averages of 0.685 m and 0.871 m below ground in the spring and summer of 2011 and 2012 respectively (see Table 2-1 for each season). Earlier measurements of the site's water table level also showed that the groundwater was at 0.85 to 1.20 m and 0.58 to 0.93 m below the ground surface in 2003 and 2005 respectively (APTRYX, 2007). These observations indicated the annual variability of groundwater level and it was likely attributed to annual precipitation variability.

2.2.2. Soil, Vegetation Cover and Land Uses

The soils at the study site belong to the Chernozemic order (Soil Classification Working Group, 1998). Two pits and nine hand auger soil sampling sites were used to characterize the soils of the study site. The two pits were located at approximately 52 m apart (see Figure 2-6a). In both pits a diagnostic Ah horizon and the soil color Value and Chroma indicated that the soils of the study site were classified as Black to Dark Gray Chernozemic great group. Chernozemic soils are common to the Prairie region of Canada with natural grassland vegetation (Pennock *et al.,* 2011). The B-horizon was

characterized as Btgj (Figure 2-9) showing a juvenile development stage of gleyed horizon indicating regular, periodic saturated and anoxic conditions. Apart from the similarities in the surface horizon and texture, variations in soil hydrology were evident between the two soil pits. In pit #1, an elluviated and gleyed layer was observed at 20-33 cm depth below the ground surface and the gleying feature persisted throughout the pit depth (78+ cm). However, in pit #2, there was no evidence of elluviation layer and gleyed features were only observed beyond 68 cm depth below the ground surface.

A total of 63 disturbed soil samples were collected from the nine sampling locations at 20-cm depth intervals from 0 to 1.40 m depth using a hand auger. The nine sampling locations were distributed in three zones with respect to Zone B (Figure 2-1): 1) three at 5 m up-gradient; 2) three in the mid-source zone; and 3) three at 5 m down-gradient (Figure 2-6a). The soil samples were air dried and passed through 2 mm sieve and particle size distribution (PSD) of each sample was determined using a standard hydrometer method (Kaddah, 1974). Table 2-2 shows average PSD profile for each sampling location. On average the soil texture ranged from clay loam to sandy loam.

Undisturbed soil cores were also collected using a Geoprobe hydraulic coring rig for soil hydraulic property determination. The cores were extracted from three sampling locations (A, B, C; Figure 2-6a) from the ground surface to depths of 1.68, 2.20 and 2.0 m respectively. The soil cores were sliced in to 3-5 cm thick segments with 4-5 cm internal diameter (ID) making a total of 110 cores from the three sites. Hanging water column and pressure extraction techniques (Reynold and Topp, 2006) were used to determine the moisture retention curve of the samples. The soil water content in the soil cores was measured at seven predetermined matric potential values (0, 0.05, 0.1, 0.3, 1, 5 and 15 bar). Soil hydraulic parameters (θ_r, α, n) were obtained by fitting a van Genuchten-Mualem model (Equation 2-1 and 2-2) to the measured data using a RETC program ver. 6.02 (van Genuchten, 1980; van Genuchten *et al.,* 2009) (Table 2-3).

$$\theta(h) = \theta_r + \frac{\theta_s - \theta_r}{[1+(\alpha h)^n]^{1-\frac{1}{n}}} \qquad \text{for } h < 0 \qquad [2\text{-}1]$$

$$\theta(h) = \theta_s \qquad \text{for } h \geq 0 \qquad [2\text{-}2]$$

Where: θ is the volumetric water content [L^3 L^{-3}], h soil water pressure [L], subscripts r and s refer to residual and saturated volumetric water content respectively, α [L^{-1}], and n [-] are van Genuchten model fitting parameters related to inverse air-entry suction and to the measure of pore size distribution respectively.

Vegetation Cover

The study site was covered by a mix of lawn grass (park) and forest species. The grassed (park) area was covered with turf grasses, which was frequently mowed and it was interspersed with some trees including willow (*Salix alba*[1]) crabapple (*Malus komarovii*), ash (*Fraxinus nigra*), and maple (*Acer griseum*). The forested area was dominated by trembling aspen (*Populus tremuloides*) and poplar reaching approximately 8-10 m in height. The forest floor and open patches were also rich with understory herbal plants including green alder (*Alnus acuminata*), raspberry (*Rubus idaeus*), bunchberry (*Cornus canadensis*) and sarsaparilla (*Smilax regelii*).

Settlements

There were about three permanent settlement areas located within 2 to 4 km of the study site. There was also a potential for residential development in the Louis Bull reservation area that would likely increase groundwater users and wastewater generation on the east side of the study site.

Climate

Wetaskiwin County is categorized under the humid, warm to cool summers and severe winter climatic region of Alberta (HCL, 2008). A two-year

[1] Sources for the Scientific names: (Alberta Agriculture and Rural Development, 2003)

(2011-2012) weather data that was recorded at the study site's weather station, which was established in July 2010 (Figure 2-1), is summarized in Table 2-4a. The mean monthly temperatures ranged between a high of 16.9° C in July to a low of -10.0° C in December and the mean annual temperature of 2.92° C. Also the mean total rainfall and snow water equivalent for the two years (2011 and 2012) were 351 mm and 94 mm respectively. For those years, the average potential evapotranspiration (ETos) was 471 mm, indicating a mean deficit of 26 mm assuming only the contribution of total rainfall and snow water equivalent to the annual precipitation (Table 2-4b).

2.2.3. Wastewater source, volume and conveyance system

A schematic representation of the wastewater management and conveyance system is presented in Figure 2-6b. On average the Rest Stop generates a total of 8 to 9 m^3 of wastewater daily. The Rest Stop facilities were used more on Fridays and Saturdays compared to other days of a week, and more in the summer compared to the other seasons. Observed water consumption at the Rest Stop has been consistent since the establishment of the facility in the Fall of 2007. Earlier records of water use at the facility ranged between 8.90 $m^3\ d^{-1}$ to 20.8 $m^3\ d^{-1}$with an average peak of 11.0 $m^3\ d^{-1}$ during the peak days (Friday to Sunday), while during the non-peak days (Sunday through Thursday) the average water use reached only 5.68 $m^3\ d^{-1}$ (APTRYX, 2007). Our findings, observed in the two years 2011-2012, were also consistent with those earlier results showing a mean daily effluent discharge of 8.94 $m^3\ d^{-1}$.

The wastewater from the Rest Stop was first conveyed into three consecutive settling septic tanks labeled as 1-2-3 in Figure 2-6b. The solid part was allowed to settle down in those tanks and it was hauled to a different place on a monthly basis. The liquid part, however, was pumped to the next tanks via subsurface pipes for further treatment before it was disposed of to the soil absorption field. The wastewater treatment processes in the latter tanks included anaerobic, aerobic biological treatment, Fixed Activated Sludge Treatment (FAST) and UV-disinfection. The UV-disinfected effluent was pumped off to soil absorption field via pressurized at-grade line sources.

2.2.3.1. Design of the At-Grade Line Sources and Effluent Application

There were three at-grade zones (A, B and C) that received approximately equal amounts of UV-disinfected effluent. The layout of the at-grade line sources for the three zones is shown in Figures 2-1 and 2-7. The at-grade lines were polyvinylchloride (PVC) pipes with 3.175 cm ID and they are referred to hereafter as laterals. In one zone there were five laterals each 40 m long. The laterals were laid above the ground surface supported by 10 cm pegs (Figure 2-7d) and they were aligned at approximately parallel to surface topography within 3.5 to 5.5 m interval between consecutive laterals.

The laterals had nozzles/emitters at every 0.5 m, which were facing up ward but every fifth one facing down to drain/clear effluent at the end of each dosing event. A black arc-shaped Quick4® standard chamber (Infiltrator Systems Inc., 2006) was used to cover the laterals (Figure 2-7a-c). The function of the chamber (width = 0.85 m and height= 0.31m) was to redirect the upward infiltrating back from the chambers' roof to the ground as rain form (Figure 2-7c). This design also ensured uniform wetting of the infiltration bed effectively for a 0.61 m width (excluding ~0.12 m buffer zone on both sides). The chamber was covered by a 0.30 m thick woodchip cover to protect the laterals from freezing during winter, from rodents, and because it was also esthetically pleasing (Figure 2-7a). The research presented in this thesis was conducted on "at-grade North (zone B)" in four laterals as shown in Figures 2-1 and 2-6a.

The system of effluent application was event-based as a function of the influent volume that was generated at the source (Rest Stop facility). In turn, the influent volume was dependent on the number of users at the facility. In the pump dose tanks (e.g. Tank#7 for zone B, Figure 2-6b); the water level was controlled by a pressure transducer in the tank such that the pump was triggered when a pre-determined water level in the tank was reached. During the experiment period, there were two main water level settings that control the time of effluent application: a regular event (for water level between 12.5 and 27.9 cm) and a veto event (for water level above 27.9 cm). In the regular event, a 0.330 m^3 effluent volume was applied to one lateral (A= 24.4 m^2) for a pulse duration of

195 sec. In the veto dosing event, however, the pulse input was 0.61 m^3 in one lateral (A=24.4 m^2) for a duration of 360 sec. In the event of enough effluent volume in the tank to trigger the pump, an alternate effluent dosing to a next lateral occurs after one hour interval; that is, in those scenarios the pump was off for only one hour in between laterals. Therefore on an average summer day, the four laterals in Zone B, where this research was focused, would receive 11 pulse events, which sum to a total volume of 3.87 m^3 applied to 97.6 m^2 of infiltration area per day corresponding to a flux density of 1.38 $cm^3cm^{-2}d^{-1}$.

2.2.3.2. Surface Effluent Flux Distribution

The woodchips and infiltration chambers were removed to verify effluent surface flux uniformity on the infiltration beds on April 18 and19, 2012 (Figure 2-8). The effluent surface flux was uniform in all the nozzles (emitters) throughout the length of the laterals. In addition, the infiltration surface was examined for biomat formation, a layer of biological growth and inorganic residue that develops at the wastewater-soil interface and extends up to about 2.5 cm into the soil matrix (Barnett and Ormiston, 2007). There was no biomat or indication of biomat formation, which justified that there was no hydraulic overloading and the effluent was infiltrating easily into the soil. If formed, biomat can hinder water infiltration through infiltrative surfaces in medium to coarse textured soils. The chambers and woodchips were replaced back after the investigation was completed.

2.3. Characterization of Groundwater

2.3.1. Electromagnetic Induction (EM) Survey

A non-destructive geophysical method was used for an initial wastewater plume assessment. The geophysical instruments, including Electromagnetic Induction (EM) are noninvasive geophysical instruments that are designed to penetrate earthen materials and provide images of shallow subsurface (0-6 m) (e.g. Roy *et al.*, 2009; Kachanoski *et al.*, 1988). Electromagnetic induction operates by transmitting pulses of radio-frequency electromagnetic energy into the subsurface

and it measures travel time of the electromagnetic energy from the antenna to the interface of interest (e.g. water table). It's widely in use for mapping subsurface electrical conductivity (EC), spatial and temporal variations of water table depth and flow pattern (Sheets and Hendrickx, 1995; Roy *et al.*, 2009; Harman *et al.,* 1996). In this study EM38-MK2 and EM31 (Geonics, 2009) were used for a preliminary reconnaissance of the subsurface bulk EC spanning from the ground surface to depths of 3 m and 6 m respectively (Figure 2-10c and 2.10b). The subsurface bulk EC was considered as a tracer for the wastewater plume.

Approximately 150 m by 120 m area within and outside the at-grade line sources was surveyed by traversing swath lines at every 5 m intervals. The bulk EC data was processed using Kriging linear interpolation method in Surfer program (Golden Software, Inc., 2009) (Figure 2-11a). Based on the bulk EC spatial distribution map and field conditions, ten transects (each 20 to 40 m long) were selected for groundwater well sites (Figure 2-11b).

2.3.2. Groundwater Measurement

2.3.2.1. Groundwater Well Construction

Inexpensive aluminum (Al) pipes with 1.27 cm internal diameter (ID), which are referred to hereafter as water table and piezometer standpipes, were used to characterize the site in terms of i) spatial and temporal distribution of hydraulic head, ii) groundwater flow patterns, and iii) preliminary investigation of the spatial extent of wastewater plume. The standpipes were perforated/screened by a 1.6 mm drill bit and a drill press making 4 holes per 2 cm interval around the standpipe with 1 cm offset (Figure 2-12). The screen length for the water table standpipes was between 2.1 to 2.5 m and 0.1 m for the piezometers (Figure 2-13).

A solid metal rod was used to drive the Al standpipes into the ground during installation. The metal rod was selected such that it fit inside the standpipe and slid in and out easily after installing the standpipes to the ground. The metal rod was designed with one end sharp point and bolted-head on the other end and it was at least 2 cm longer than the standpipes (Figure 2-13). The standpipes and metal rods were washed with plenty of tap water and rinsed three times with

deionized (DI) water. They were air dried and blotted with paper towel. During transportation from the laboratory to the field the standpipes and metal rods were wrapped with plastic to prevent from contamination (Figure 2-12c).

2.3.2.2. Groundwater Well Installation

Prior to well installation and soil sampling, underground utilities were identified and located by Alberta One-Call and the resulting map for the identified existing underground lines is given in Appendix 2-A.

Firstly, the metal rod was fitted into a standpipe and driven into the ground with the sharp tip pointing into the ground while pounding on the bolted head side using a sledge hammer. Secondly, after the standpipe had reached the desired depth, the metal rod was pulled out by gripping at the bolted head with wrench. The metal rod was washed and rinsed with DI water before each well installation. During the field rinsing, a plastic sheet (tarp) was laid on ground below a washing pan to avoid cross-contamination (Figure 2-12b). The dirty water was transferred to a plastic container and it was dumped into the toilet.

A total of 84 standpipes (i.e., 70 water table standpipes and 14 piezometer standpipes) were installed in eight transects (Figure 2-6a). At first 6 water table standpipes; that is, three on transect 5 (approximately parallel to the laterals; Figure 2-6a) and the other three on transect 8 (approximately perpendicular to the center of the laterals; Figure 2-6a) were installed at 5 m intervals. Based on the observed water level in the six wells, additional water table standpipes were installed in those transects at 1 m intervals for the first 10 m distance from the source zone and then at 4, 8 and 16 m intervals thereafter for longer distances (>10 m) away from the source zone. Additional wells were installed in the other transects in a similar way.

2.3.2.3. Gradients and Groundwater Flow Directions

Groundwater levels in the standpipes were measured manually using a Solinst water level meter at weekly to biweekly intervals in the summer of 2010. The local groundwater hydrology in terms of spatial distribution and flow direction was characterized using the 84 standpipes distributed over a 1.5 ha area

within and outside Zone B. The 14 piezometer standpipes were installed in 7 nests comprising of two piezometers standpipes (deep and shallow). Additionally, one water table standpipe was also included at five of the piezometer nest sites and in the remaining two nests, only one deep and one shallow piezometer standpipe were installed. The water table standpipes were screened from 0.40 m to 2.60 m depth below ground surface (Figure 2-13). The screen interval of the shallow piezometer standpipes was between 0.80 to 0.90 m below the ground surface in the clay loam geologic material while for those of the deep piezometers it was between 2.40 to 2.50 m below the ground surface on a sandy clay loam material.

The site is hydrologically very complex because the vertical and horizontal gradients showed temporal and spatial variability. Pressure head data was obtained from a nest of monitoring wells to calculate the hydraulic gradients (details are presented in Chapter 4). Average vertical gradients along a transect are given in Figure 2-14 only for the spring and summer seasons because most of the wells were dry and measureable gradients were hardly obtained for the fall and winter seasons. The source zone is shown by a rectangular box and the arrows indicate direction of vertical gradients (positive downward and negative upward gradients). With the increase of surface fluxes (snow melting, summer precipitation and effluent fluxes) downward gradient dominates (see arrows in Figure 2-14). On average the vertical gradient ranged between -0.131 to 0.234 with an average of 0.043 and horizontal was 0.02.

The spatial distribution of hydraulic heads (water table elevation) in all the wells were analyzed and mapped using a linear Kriging algorithm in Surfer (Golden Software, Inc., 2009). A snapshot plot of the water table elevation map for November 09, 2010 is presented Figure 2-15a. The groundwater flow direction was drawn perpendicular to the equipotential lines (water table contours) (Figure 2-15a). A three-point problem approach (Fetter, 2001) was also used to calculate equipotential lines and the direction of flow (Figure 2-15b). In this procedure, the distance between the piezometer standpipes and hydraulic heads at a given interval along the line were calculated. Equipotential lines connecting

equal hydraulic heads were drawn. Finally, groundwater flow lines perpendicular to the equipotential lines were drawn along the hydraulic gradient (Figure 2-15b).

2.3.3. Hydrochemistry

A total of 228 groundwater samples were obtained from 74 water table and two piezometer standpipes (three samples from each well) for hydrochemical assessment and results are summarized in Table 2-5. One sample from each well was used for EC and pH determination and the remaining two samples were used for the other chemical constituents that are described below. The groundwater samples were collected using a waterra tubing and waterra foot valves and then transferred to clean sample bottles.

pH and EC of the 76 groundwater samples were analyzed on-site immediately after sampling by a portable Thermo Orion 5-plus multimeter, while the samples for chloride and the other ion analyses were packed in cooler boxes appropriately at ≤ 4 ^{o}C. The samples were brought to the lab and stored in a freezer until further analyses. These samples were then filtered through 0.45μm filters and they were analyzed within a week of the sampling date. 40 out of the 76 samples were analyzed for Nitrate (NO_3^--N), Nitrite (NO_2^--N), Phosphate (PO_4^- P), Sulphate ($SO_4^{=}$), Bromide (Br^-), Chloride (Cl^-) concentrations by Ion Chromatograph (Dionex 600) standard method in the Natural Resources Analytical Laboratory of our department. In addition, Cl^- ion concentration was analyzed in the 76 samples by Cl-probe connected to a portable Thermo Orion 5-plus multimeter. .

2.4. Wastewater Plume Delineation

The spatial distribution of the groundwater EC and Cl were processed and mapped using Kriging linear interpolation in Surfer (Golden Software, Inc., 2009). The concentrations of both EC and Cl in the groundwater showed a strong linear relationship ($R^2 = 0.89$) and thus only the EC distribution map is presented in Figure 2-16. For comparison, a hand drawn contour map (not shown here) was also produced using linear interpolation and it was similar to the map generated in the surfer program.

The estimated wastewater plume flow direction and width are given by the yellow, dotted lines in Figure 2-16 and the plume flow direction coincided with the groundwater flow direction (Figure 2.15). The plume width was within the width of the laterals (40 m) and it moved approximately 10 m down gradient along the estimated flow direction over the three years since the wastewater system has been operating corresponding to a velocity of 1 cm d^{-1}. From the estimated velocity and average porosity of 0.56 cm^3 cm^{-3}, a 0.56 cm d^{-1} groundwater flux was estimated. The estimated groundwater flux was close to the horizontal Darcy groundwater flux of 0.765 cm d^{-1} that was calculated using a horizontal hydraulic gradient of 0.02 and a field observed *Ks* of 38.27 cm d^{-1}. The finding infers that convective transport and longitudinal dispersion along the groundwater flow direction dominates the lateral transverse dispersion because the plume was within the width of the at-grade lines.

2.5. Summary of Findings

In this chapter, the study site and summary methodology employed in the initial environmental site assessment process were described and summary of the findings are as follows.

- The study site physiographic and hydrogeologic setting were described.
- Preliminary wastewater plume extent was identified from the spatial distribution of subsurface bulk EC obtained with the help of electromagnetic induction (EM) and by installing inexpensive groundwater wells.
- Spatial and temporal groundwater hydrology and flow direction were characterized and a water table map was produced.
- Hydrochemistry of the groundwater results revealed (Figure 2-16) the impact of the wastewater on groundwater.
- Assuming EC as the wastewater tracer, groundwater EC distribution map was produced, the wastewater plume extent was delineated and its flow direction was identified.
- Wastewater plume center of mass was estimated.

The specific methods pertaining to each of the experiments and data analysis throughout the PhD thesis work are presented in the next chapters (Chapter 3, 4 and 5).

2.6. References

Alberta Agriculture and Rural Development, 2003. Alberta Range Plants and Their Classification. Available on line: http://www1.agric.gov.ab.ca/$department/deptdocs.nsf/all/agdex146/$file/3400600.pdf?OpenElement.

Alberta Environment, 2001. Phase 1 Environmental site assessment guideline for upstream oil and gas sites. *Environmental Service Environmental Sciences Division*. Pub. No: T/573 ISBN: 0-7785-1422-6 On-line Edition.

APTRYX, 2007. Innovative solutions for your onsite wastewater needs: Report. APTRYX Onsite Wastewater Inc. Duffield, Alberta.

Barnett, H. and Ormiston, A. W., 2007. Manual for on-site wastewater design and management : Technical report to support Policy development. Horizons Regional Council, New Zealand. ISBN: 1-877413-69-0 Report No: 2007/EXT/778. Available on line: http://www.horizons.govt.nz/assets/horizons/Images/one_plan/On-Site%20Wastewater%20Design%20Manual_April%2007.pdf

Geonics Ltd, 2009. EM38-MK2 ground conductivity meter operating manual. Geonics, Ltd. Ontario, Canada.

Golden Software, Inc. 2009. Surface mapping system. Surfer Version 9.11.947.

Harman, J., W. D., Robertson, J. A. Cherry and L. Zanini, 1996. Impacts of a sand aquifer from an old septic system: Nitrate and phosphate. *Ground Water, 34:1105-1114.*

HCL, 2008. Regional groundwater assessment. For County of Wetaskiwin. Part of North Saskatchewan River basin. Parts of Tp 044 to 048, R 22 to 28, W4M & Tp 045 to 047, R 01 to 07, W5M. Prepared for the country of

Wetaskiwin. Hydrogeological Consultants Ltd. (hcl) 1.800.661.7972 . File No.: 07-771.03.

Infiltrator Systems Inc., 2006. The Quick4® Standard Chamber. Available on line: www.infiltratorsystems.com.

Kachanoski, R. G., E. G. Gregorich and I. J. Van Wesenbeeck, 1988. Estimating spatial variations of soil water content using noncontacting electromagnetic inductive methods. *Can. J. Soil Sci. 68:715-722.*

Kaddah, M. T. 1974. The Hydrometer method for detailed particle size analysis - 1. Graphical interpretation of hydrometer readings and test methods. *J. Soil Sci. 118:102-108.*

Pennock, D., A. Bedard-Haughn1, and V. Viaud, 2011. Chernozemic soils of Canada - Genesis, distribution, and classification. *Can. J. Soil Sci. 91:719-747.*

Reynold, W. D. and G. C. Topp, 2006. Soil water desorption and imbibition: tension and pressure techniques. In M. R. Carter and E. G. Gregorich (eds.) Soil sampling and methods of analysis. 2nd Ed. Chapter 72. *Can. Soc. Soil Sci. Taylor & Francis Group, LLC.*

Roy, J. W., J. M. Robillard, S. B. Watson, and M. Hayashi, 2009. Non-intrusive characterization of methods for wastewater affected groundwater plumes discharging to an alpine lake. *Environ. Monit. Assess. 149:201-211*.

Sheets, K. R. and Jan M. H. Hendrickx, 1995. Noninvasive soil water content measurement using electromagnetic induction. *Water Resour. Res.* 31:2401-2409.

Soi1 Classification Working Group, 1998. The Canadian system of soil classification. *Agric. and Agri-Food Can. Publ. 1646 (Revised). 187 pp.*

van Genuchten, M. Th., 1980. A closed-form equation for predicting the hydraulic conductivity of unsaturated soils. *Soil Sci. Soc. Am. J., 44: 892-898.*

van Genuchten, M. Th., J. Simunek, F. J. Leij, and M Segina, 2009. Code for quantifying hydraulic functions of unsaturated soils. Available on line: www.hydrus3d.com.

Table 2-1: Average seasonal groundwater level below ground surface observed at the study site over two years (see details in Chapter 3)

Season	2011	2012	Mean
	d(t)[†] (m)		
Spring	-0.641	-0.686	-0.664
Summer	-0.728	-1.056	-0.892
Fall	-1.346	-1.536	-1.441
Winter	-1.242	-1.460	-1.351
Mean	-0.989	-1.185	-1.087

[†] *d(t)* is depth to groundwater from the ground surface

Table 2-2: Average particle size distribution with depth along a transect perpendicular to the at-grade line sources

Location	Depth (cm)	%Sand	%Silt	%Clay	Textural class[††]
Up-gradient	0-20	47.2	37.2	15.6	Loam
	20-40	54.8	25.9	19.4	Sandy Loam
	40-60	47.2	25.7	27.1	Sandy Clay Loam
	60-80	38.9	33.4	27.7	Loam
	80-100	31.2	46.7	22.1	Loam
	100-120	42.3	39.3	18.4	Loam
	120-140	62.2	23.6	14.3	Sandy Loam
Source zone	0-20	54.1	30.4	15.5	Sandy Loam
	20-40	54.6	26.5	18.9	Sandy Loam
	40-60	54.5	26.5	19.1	Sandy Loam
	60-80	57.9	21.3	20.8	Sandy Clay Loam
	80-100	49.7	28.6	21.7	Loam
	100-120	50.2	31.0	18.7	Loam
	120-140	45.9	34.4	19.7	Loam
Down-gradient	0-20	41.5	35.7	22.8	Loam
	20-40	37.8	38.9	23.3	Loam
	40-60	36.7	34.3	29.1	Clay Loam
	60-80	23.7	40.0	36.3	Clay Loam
	80-100	25.3	41.0	33.7	Clay Loam
	100-120	24.0	50.8	25.2	Silty Loam
	120-140	29.0	46.0	25.0	Loam

[††] Canadian soil texture classification system (Soil Classification Working Group, 1998).

Table 2-3: Soil hydraulic properties

depth (cm)	$\theta(\psi=-15bar)$ ($cm^3\ cm^{-3}$)	$\theta s(\psi=0bar)$ ($cm^3\ cm^{-3}$)	θs ($cm^3\ cm^{-3}$)	θr ($cm^3\ cm^{-3}$)	α (cm^{-1})	n (-)
0-20	0.306	0.610	0.607	0.018	0.0194	1.124
20-40	0.290	0.579	0.571	0.038	0.0118	1.140
40-60	0.280	0.551	0.542	0.0211	0.0080	1.140
60-80	0.343	0.512	0.505	0.022	0.0138	1.067
80-100	0.331	0.590	0.580	0.029	0.0175	1.093
100-120	0.287	0.624	0.606	0.006	0.0143	1.128
120-140	0.199	0.539	0.510	0.014	0.0045	1.231
140-160	0.186	0.501	0.478	0.014	0.0033	1.250
160-180	0.189	0.521	0.489	0.027	0.0014	1.338
Mean	0.268	0.559	0.543	0.021	0.0104	1.168
Stand. Dev.	0.061	0.044	0.050	0.010	0.006	0.087

θ is the volumetric water content [$L^3\ L^{-3}$], ψ suction pressure [L], subscripts *r* and *s* refer to residual and saturated volumetric water content respectively, α [L^{-1}], and *n* [-] are van Genuchten model fitting parameters related to inverse air-entry suction and to the measure of pore size distribution respectively.

Table 2-4: Summary weather data from a locally established weather station

Year	Descriptive statistics	Mean annual air temp.	Annual ETos (Penman)	Annual ETos when T>=5°C	Annual ETtr (Maule *et al., 2006*)	Annual ETtr when Temp>=5°C	Annual ETtru (Maule *et al*., 2006)	Annual ETtru when Temp>=5°C
		°C	mm	mm	mm	mm	mm	mm
2011	Mean	2.74	535.82	465.49	651.02	562.46	476.56	473.89
2012	Mean	3.10	555.04	475.50	670.91	596.49	487.09	510.10
2011-2012	Mean	2.92	545.43	470.49	660.96	579.47	481.82	492.00

Table 2-4: Summary weather data (cont…)

Year	Annual total event rain fall (TRF)	Annual total event rain fall when Temp>5	Annual total snow water equivalent (SWE)	Annual total precipitation (TRF+SWE)	Annual water balance (TRF+SWE-ETos)	Remark
	mm	mm	mm	mm	mm	
2011	502.18	409.98	109	518.98	53.49	surplus
2012	400.29	291.58	78	369.58	-105.92	deficit
2011-2012	451.24	350.78	93.5	444.28	-26.21	deficit

Table 2-5: Descriptive statistics for some hydrochemical parameters tested in groundwater sample

	pH	EC	Cl^-	NO_2^- - N	Br^-	NO_3^- - N	PO_4^{2-}	SO_4^{2-}
		$mS\ cm^{-1}$	$mg\ L^{-1}$					
Mean	7.44	3.25	706.89	2.37	n.d	37.92	n.d	67.96
SD	0.16	1.17	339.25	1.89	n.d	33.06	n.d	39.44
CV	0.02	0.36	0.48	0.80	n.d	0.87	n.d	0.58

SD = standard deviation, CV = coefficient of variation, n.d. = non-detectable, instrument detection limit = 0.5 $mg\ L^{-1}$

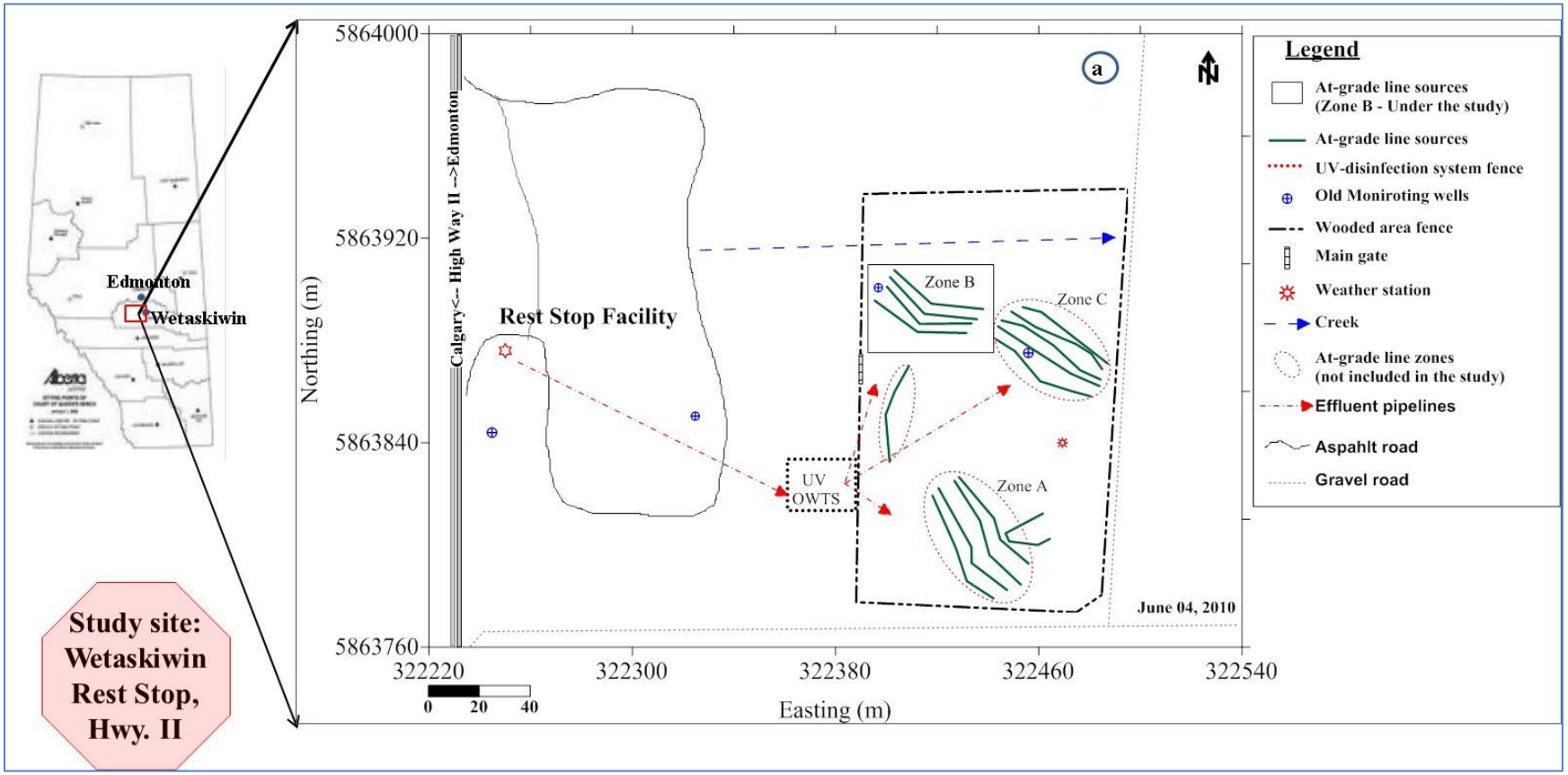

Figure 2-1: Study site overview map (a) existing features. The coordinates were projected according to the North American Datum 83 (NAD 83) and are in zone 12.

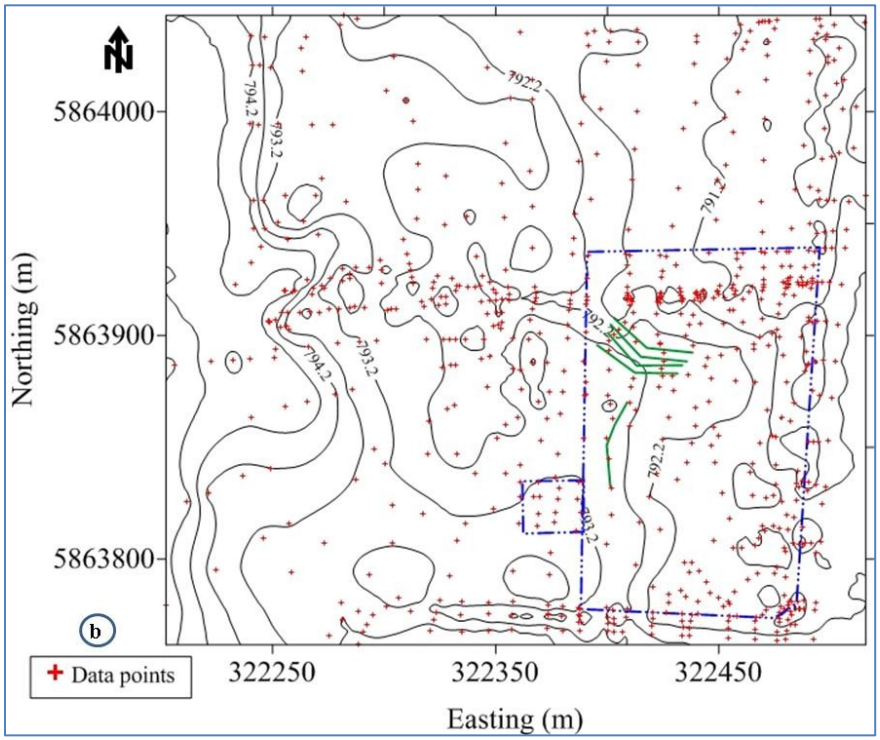

Figure 2-2: Study site overview map (b) contour map showing majority of the study site. The coordinates were projected according to the North American Datum 83 (NAD 83) and are in zone 12.

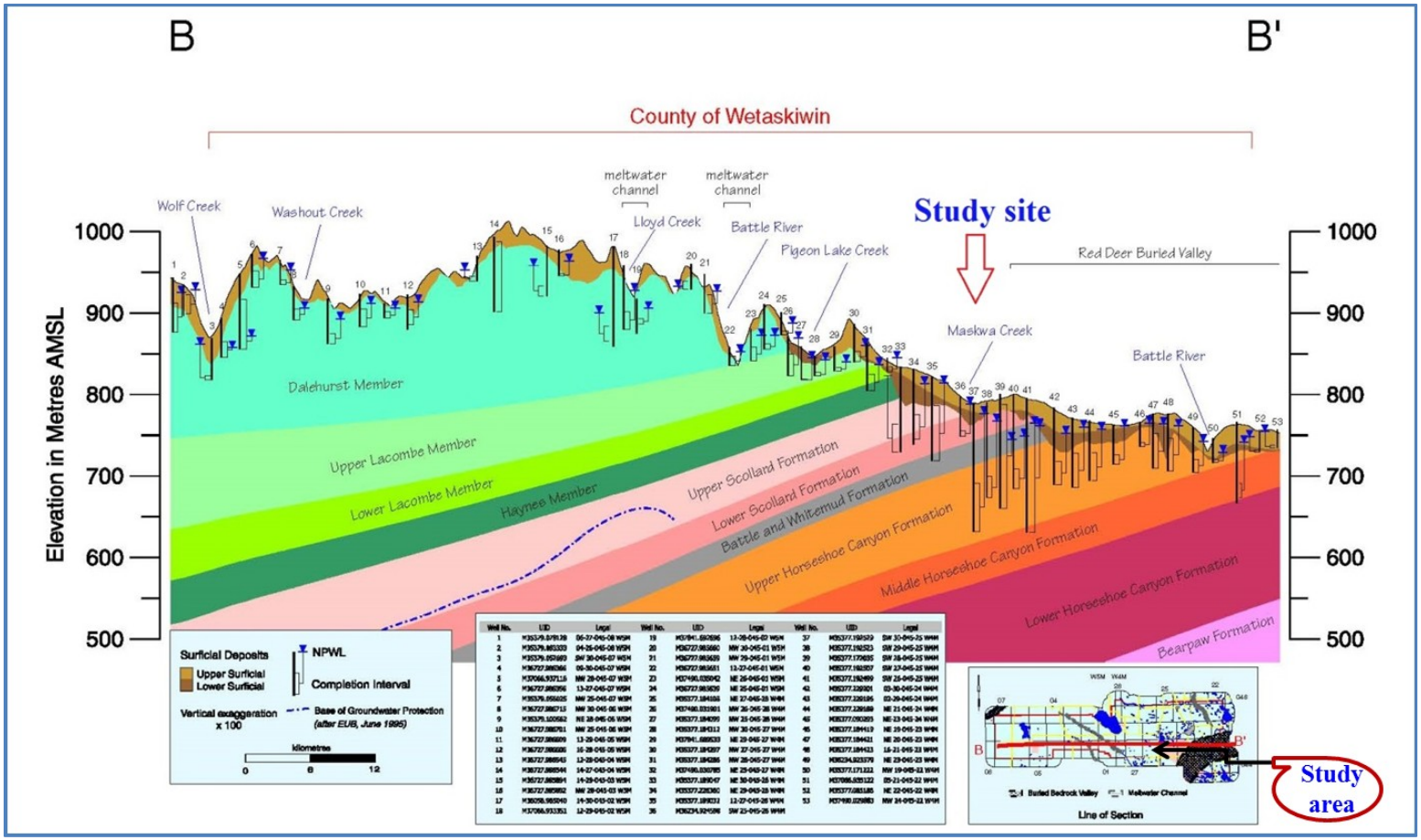

Figure 2-3: Bedrock and aquifer stratigraphy: West-East cross-section of Wetaskiwin County (After HCL, 2008).. The Figures shows the bedrock lows from the East to West direction. In addition the surficial deposits are deeper in the east part of the County.

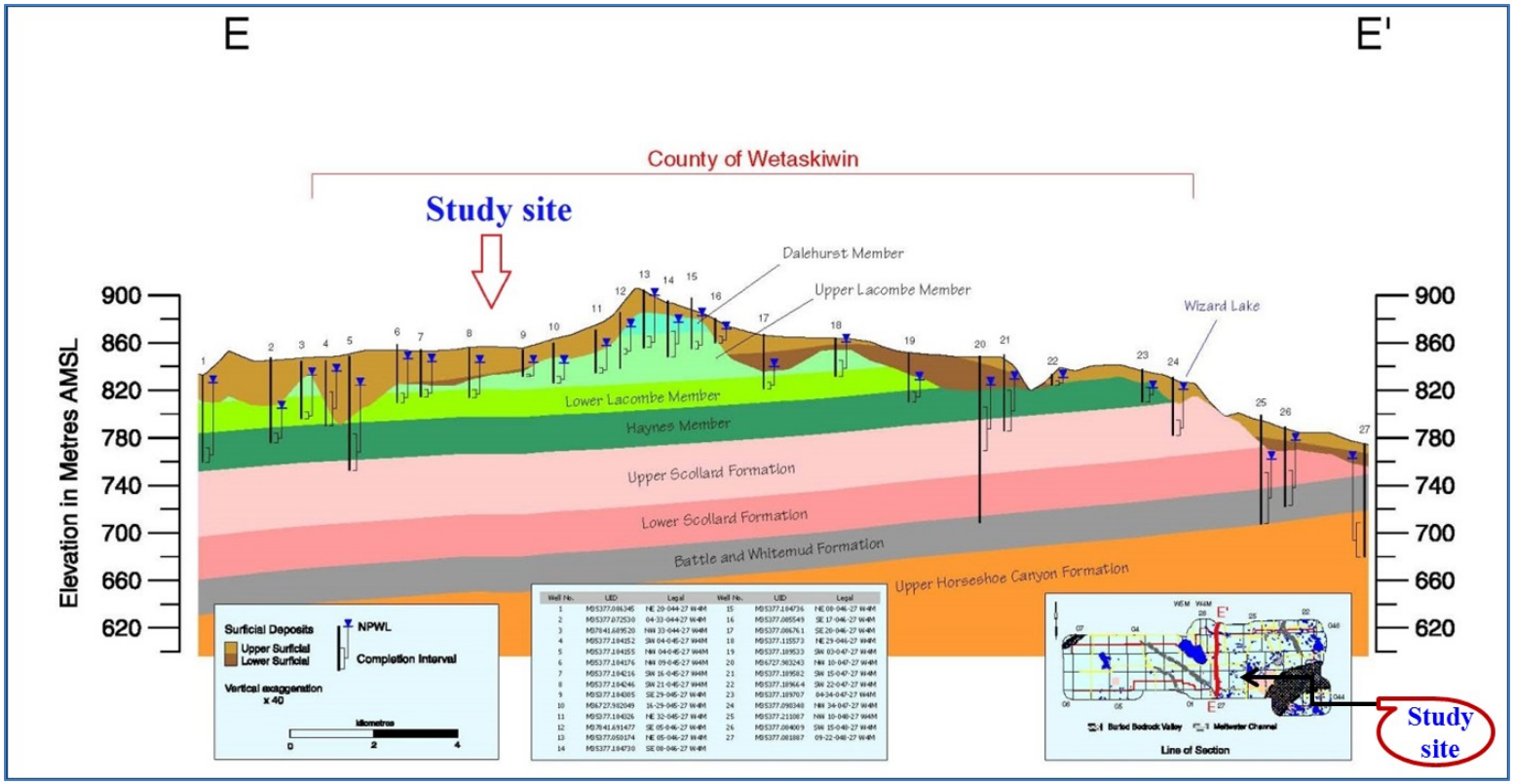

Figure 2-4: Bedrock and aquifer stratigraphy: South-North cross-section of Wetaskiwin County (After HCL, 2008). The bed rock stratification is nearly parallel to the ground surface with a slight slope to the south and the surficial deposits are deeper in the south side.

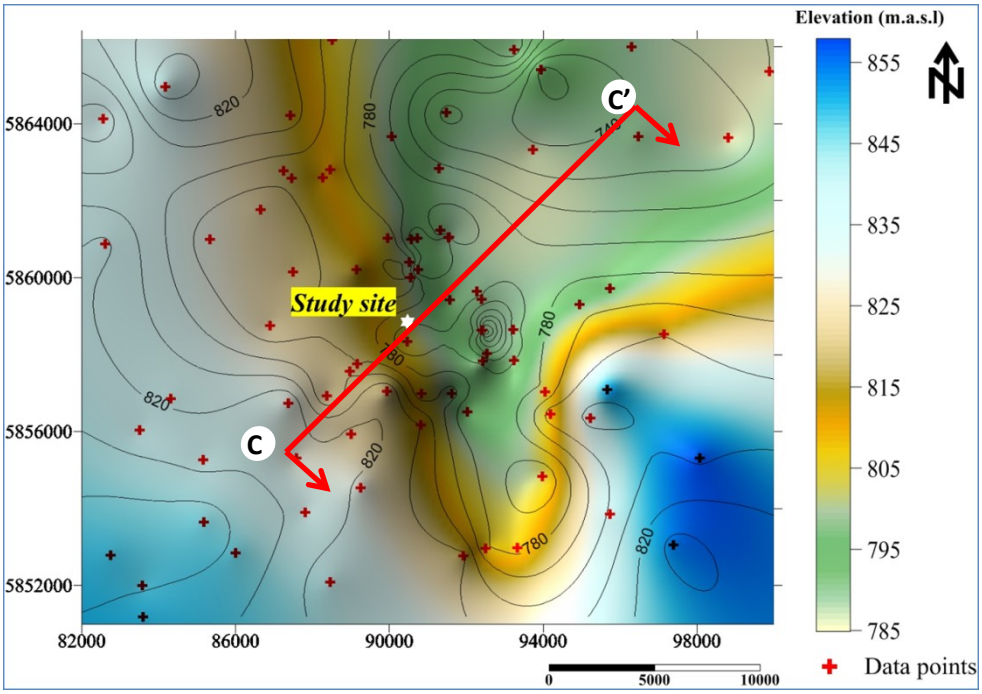

Figure 2-5: Regional topographic map of Ground surface contours (3D map) and top bed rock elevation (Contour lines).

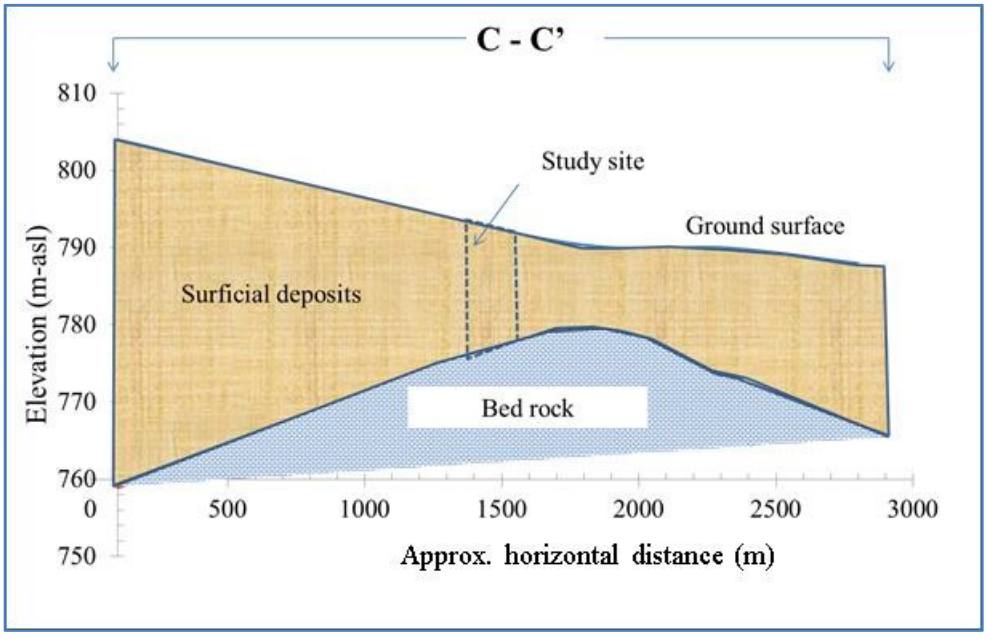

Figure 2-6: Aquifer and bed rock across the C-C' cross-section of the study area given in Figure 2-4 (the map was produced using information extracted from Alberta Groundwater Center, HCL, 2008). The coordinates were projected according to the North American Datum 83 (NAD 83) and are in zone 12.

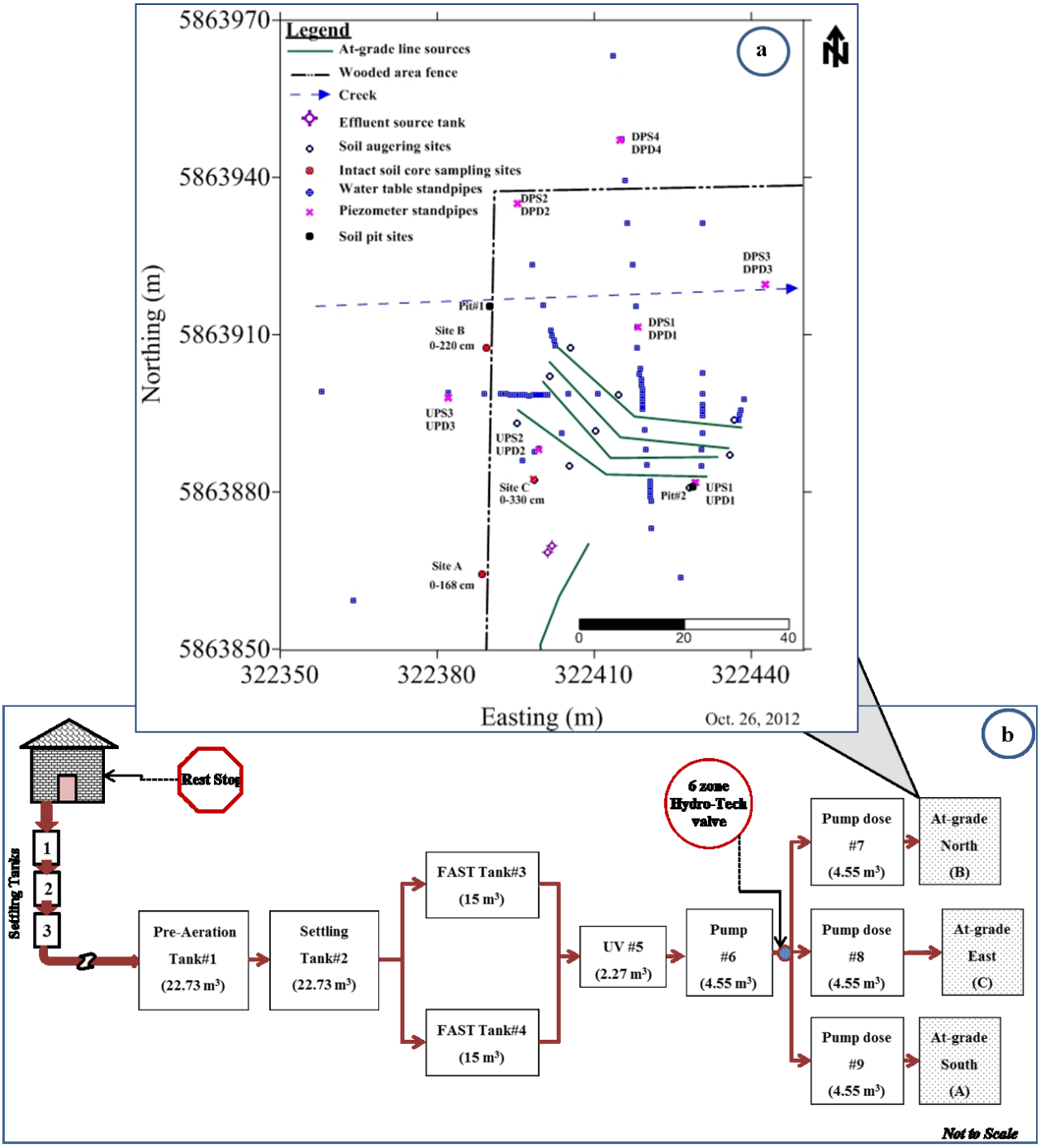

Figure 2-7: Study site with sampling points (a) and schematic representation of the wastewater source, conveyance and distribution system (b). The coordinates were projected according to the North American Datum 83 (NAD 83) and are in zone 12.

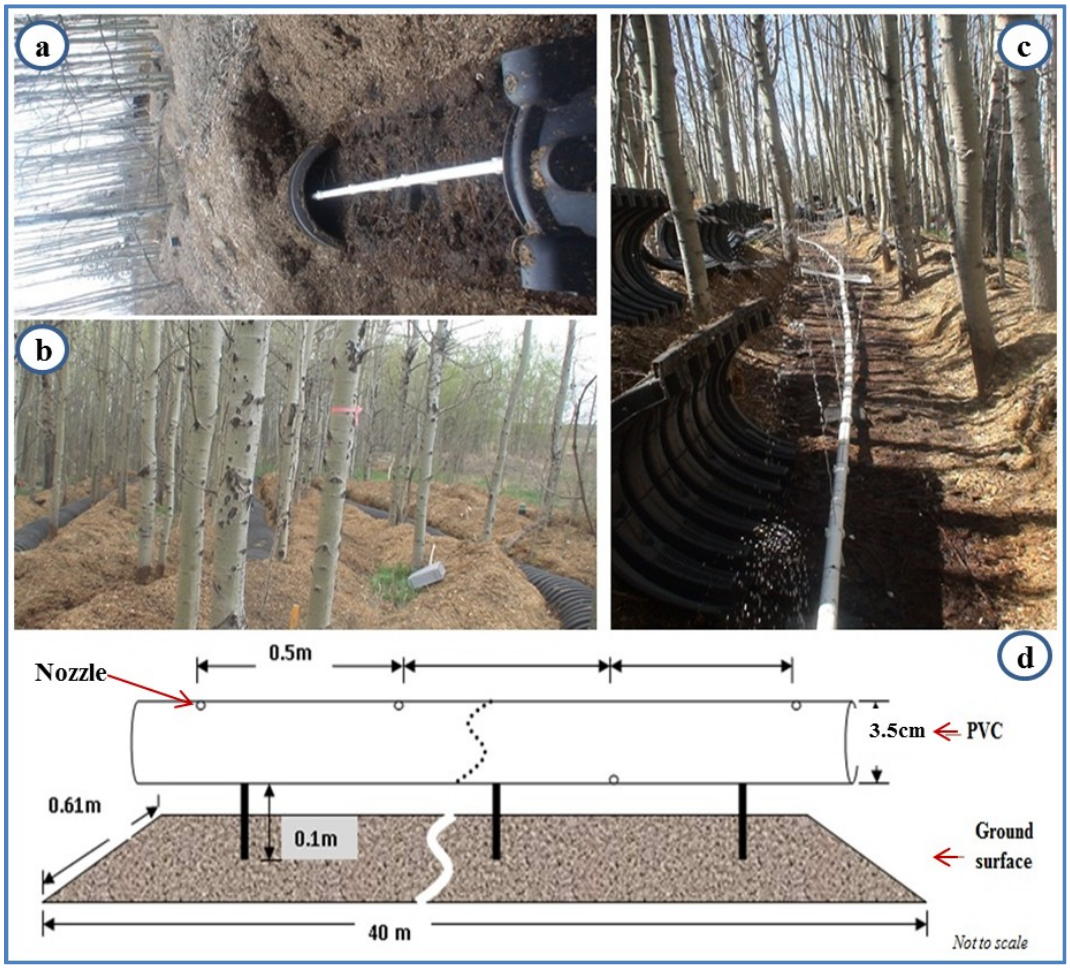

Figure 2-8**:** At-grade line sources lay out with wood chip cover (a), infiltration chamber (b), effluent application (c) and dimensions of the laterals and infiltration bed (d).

Figure 2-9: Dosing rate determination on April 19, 2012. The flow rates visually inspected along each lateral and the flow was uniform in all nozzles in a lateral.

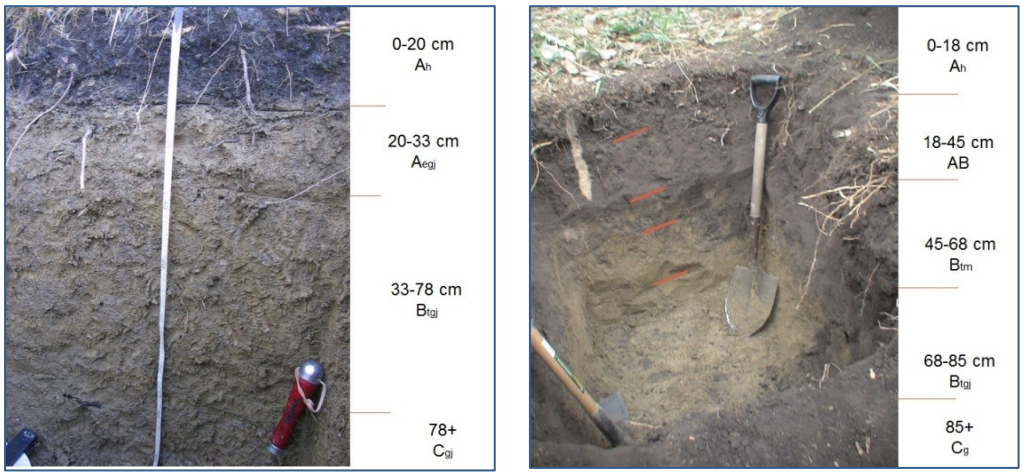

a) Pit#1 adjacent to a creek bank.

b) Pit#2 5 m up-gradient of the at-grade lines

Figure 2-10: Soil profile description: Dark Gray Chernozem (a) and Black Chernozem (b).

Figure 2-11: Topographic survey (a) and subsurface bulk electrical condcutivity (EC) survey (b) EM31 and c) EM38.

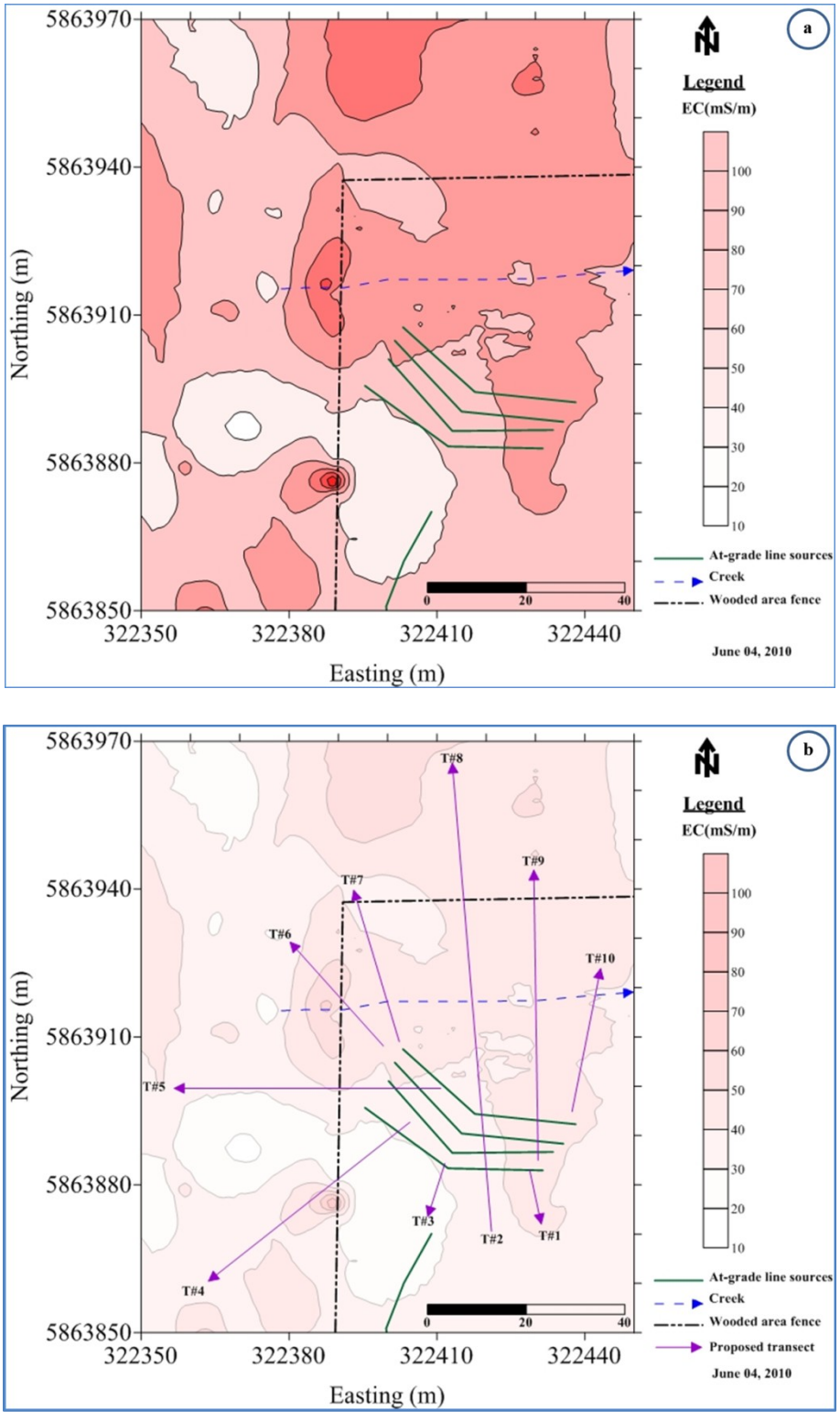

Figure 2-12: Subsurface bulk EC map (a) and proposed transects for groundwater well sites (b). The coordinates were projected according to the North American Datum 83 (NAD 83) and are in zone 12.

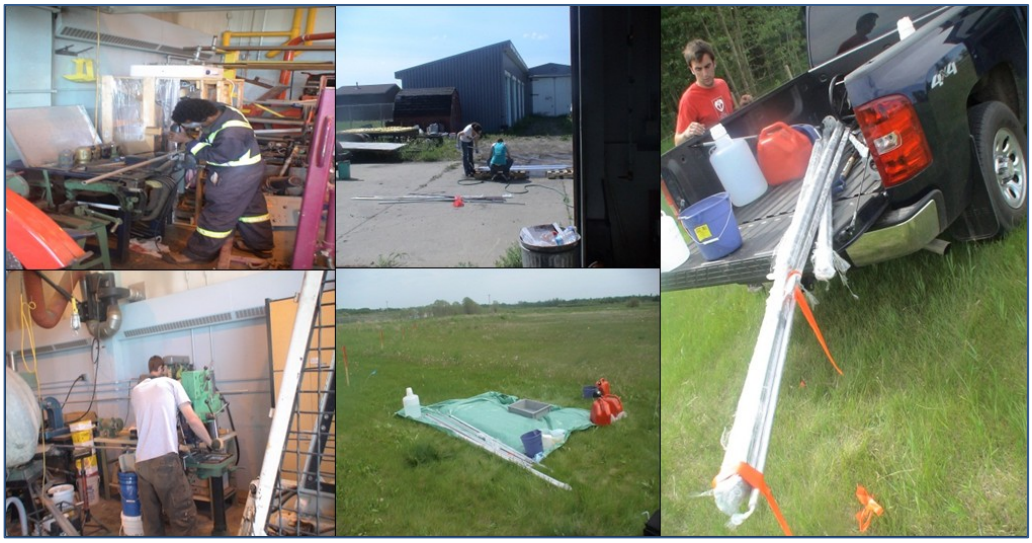

a) Drilling standpipes b) Washing standpipes c) Handling standpipes

Figure 2-13: Pictorial representation of drilling and handling of the standpipes.

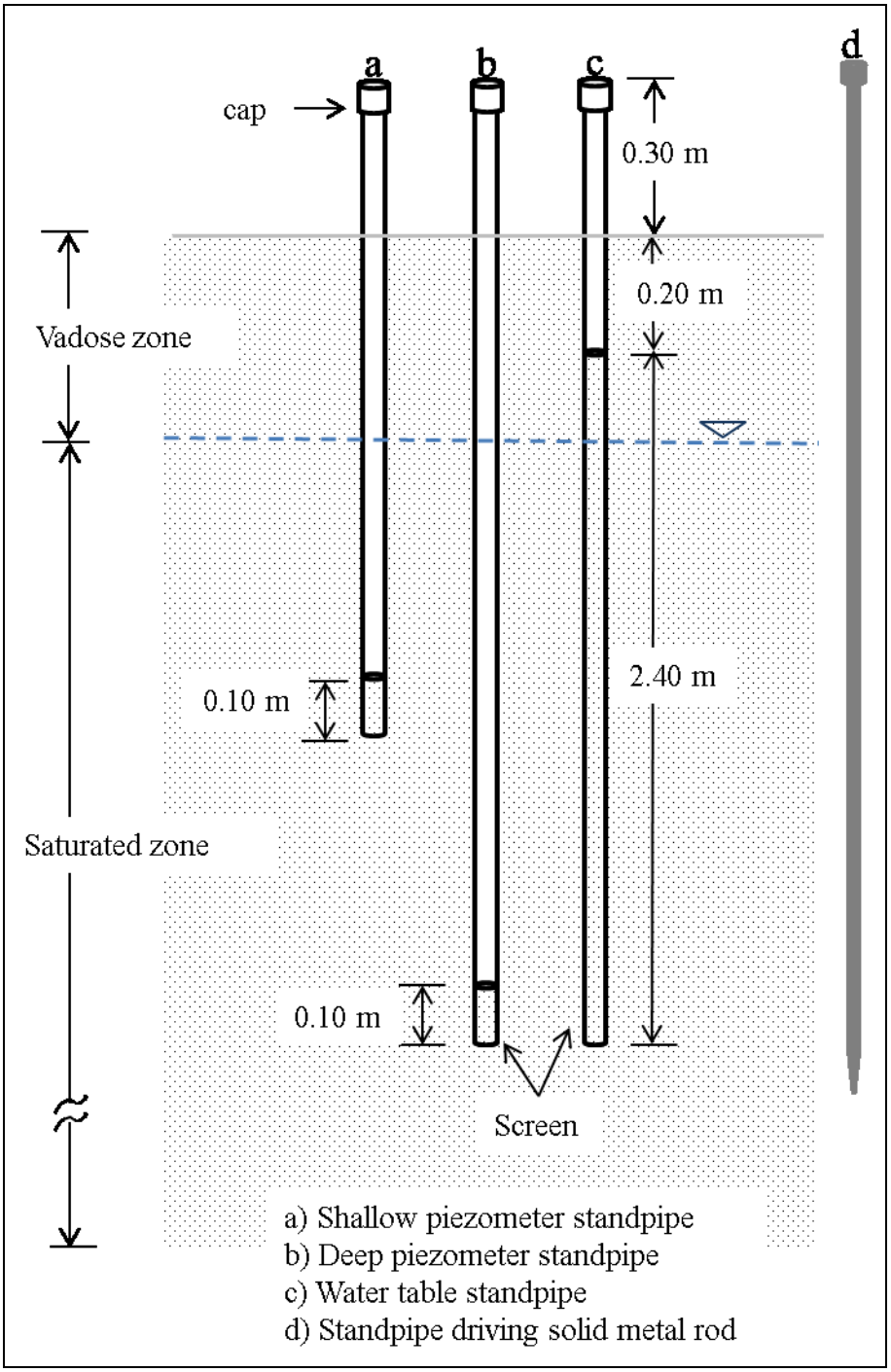

Figure 2-14: Water table and piezometer standpipes.

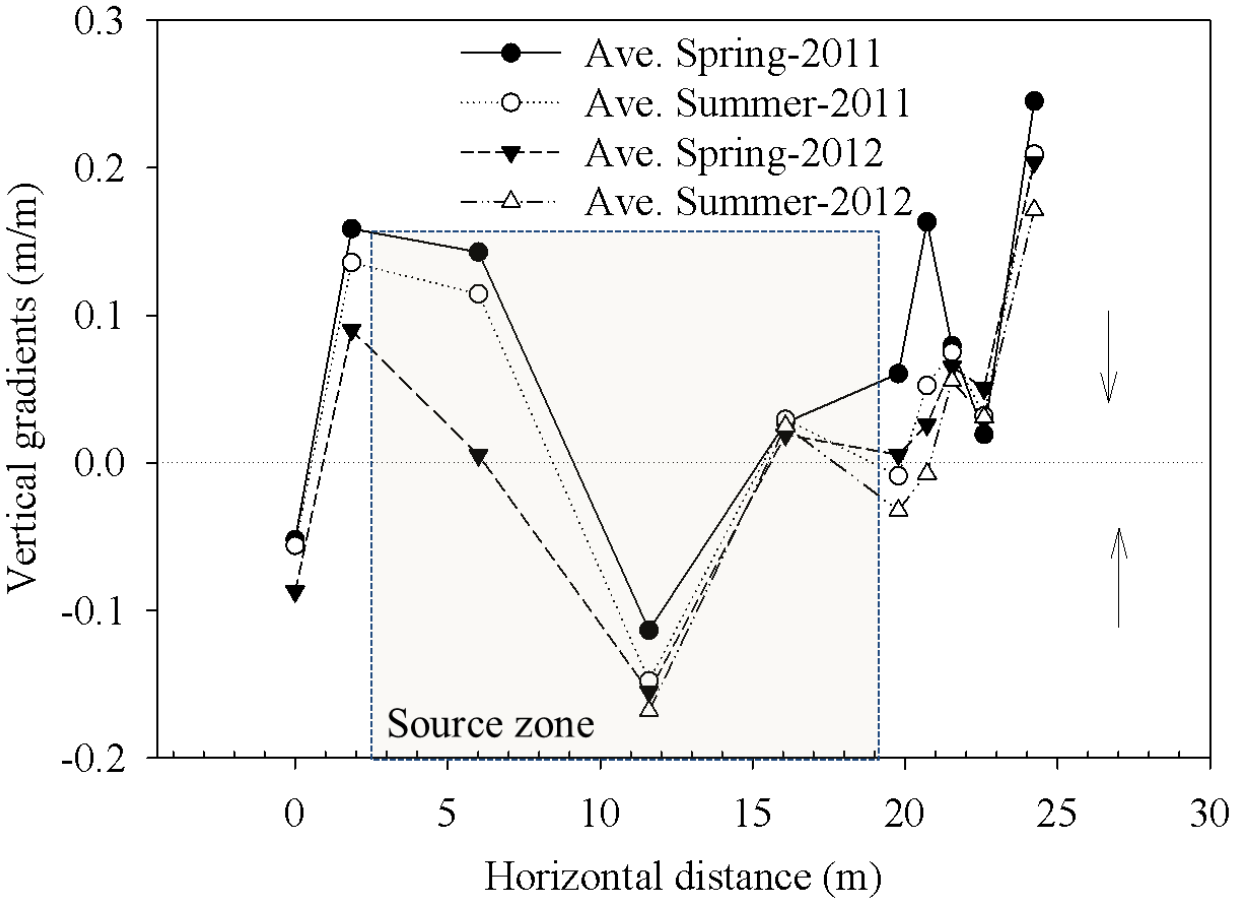

Figure 2-15: Vertical hydraulic gradients observed in the Spring and Summer seasons of 2011 and 2012. The rectangular box indicates the effluent source zone and the arrows show direction of the vertical gradients.

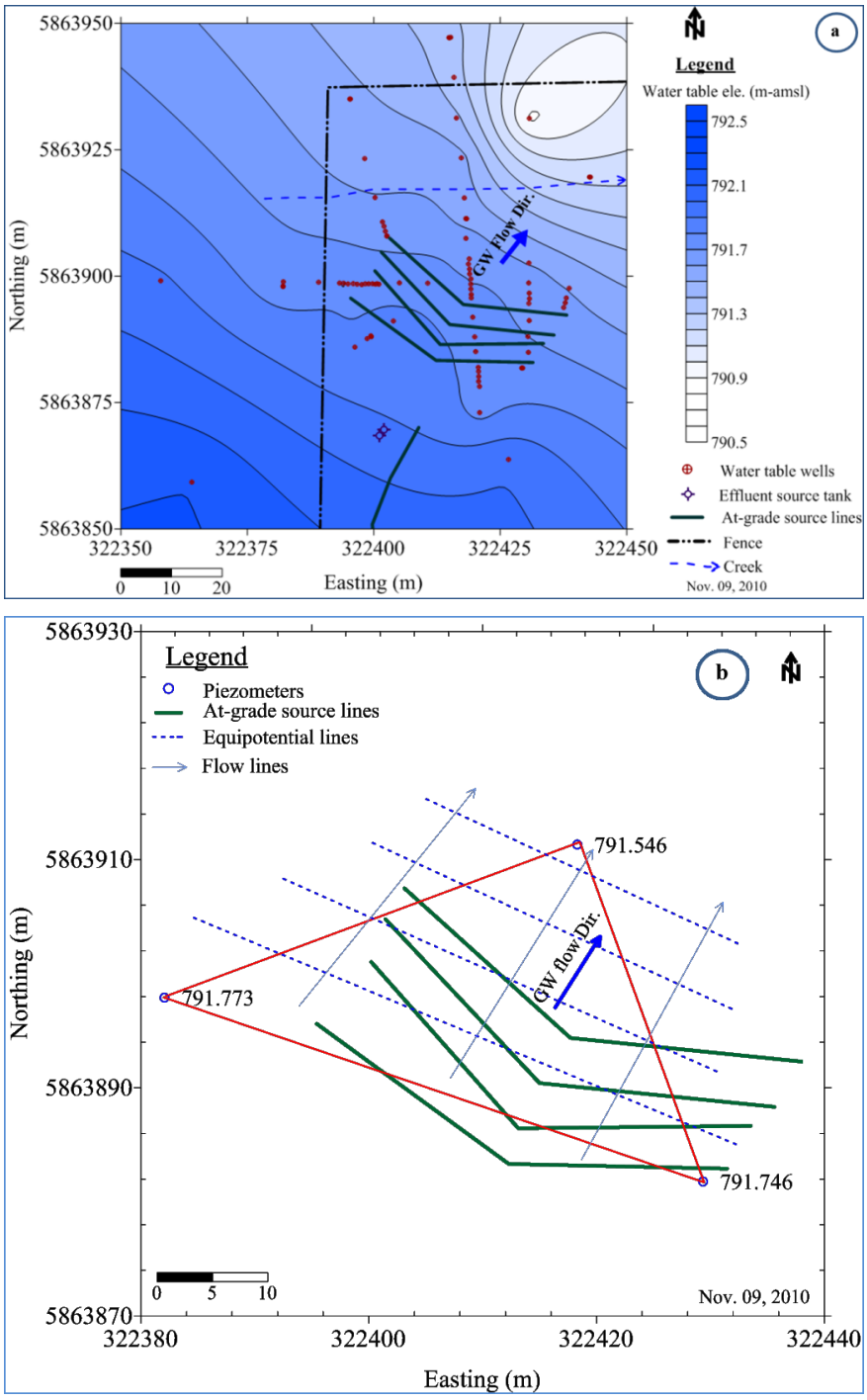

Figure 2-16: Water table contour map and groundwater flow direction (a) water table contour map and (b) three-point problem approach. The coordinates were projected according to the North American Datum 83 (NAD 83) and are in zone 12.

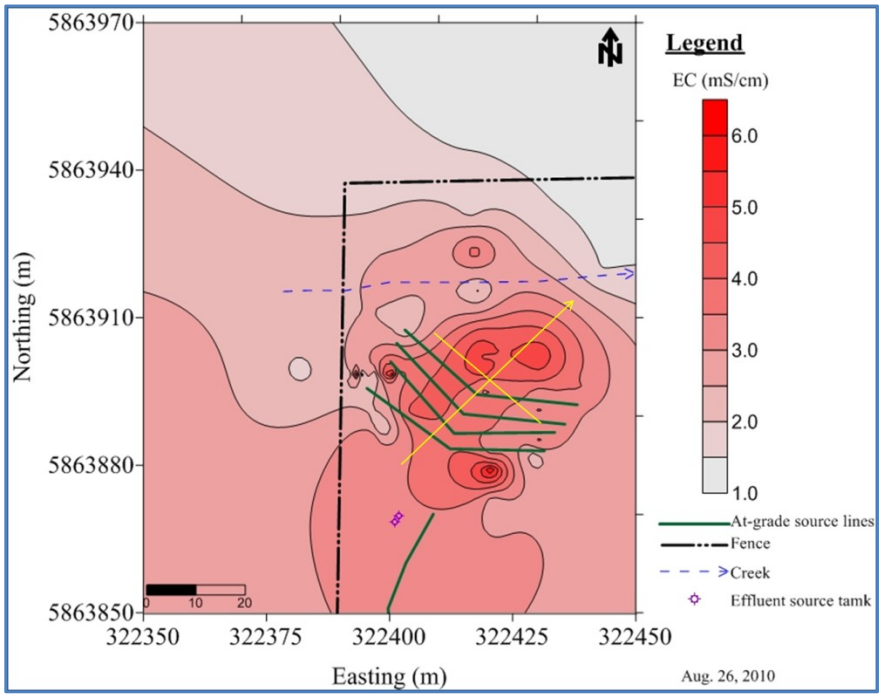

Figure 2-17: Groundwater EC contour map. The coordinates were projected according to the North American Datum 83 (NAD 83) and are in zone 12.

3. HYDROLOGIC RESPONSE TO EFFLUENT INFILTRATING FROM AT-GRADE LINE SOURCES TO SHALLOW GROUNDWATER

3.1. Introduction

As population increases, domestic water use and wastewater generation continue to grow, requiring construction of new wastewater treatment facilities and strategies. In areas with water shortages, recycling and reuse of wastewater for irrigation of parks, highway medians, golf courses; toilet and urinal flushing; and industrial purposes such as for cooling water, boiler feed, fire protection and dust control (Stanley, 2010) may be practical options, but potential public and environmental health risks need to be considered (Ganoulis, 2012). Wastewater treatment systems/facilities are classified as centralized systems, or decentralized systems. In urban settings, wastewater is transported from household sources to large centralized facilities. Alternatively, on-site wastewater treatment systems (OWTS) treat the wastewater at the source of its generation. On-site wastewater treatment systems are commonly used in individual homes, in rural areas or in remote public park places where the centralized systems are not practical and available. They are also becoming popular in urban settings because of aging infrastructure and high cost for building new centralized systems (McCray and Christopherson, 2008; McCray *et al*., 2005; Lowe *et al*., 2008; Durnie, 2008; Sen, 2011). In Alberta an estimated 300,000 private sewage systems are in use with an increase by approximately 7000 per year (Durnie, 2008).

In the last two decades, many studies on wastewater flow in the subsurface have been carried out, but the physical flow and transport processes from the infiltration surface through the soil treatment zone are still poorly understood (Sen, 2011; McCray and Christopherson, 2008). Lowe *et al* (2008) evaluated purification performance of OWTS using three engineered treatment units: a septic tank; a septic tank with a textile filter unit; and a septic tank with membrane bioreactor. The performance of the systems was assessed based on the percent removal efficiency of each treatment unit for total suspended solids, five-day carbonaceous biochemical oxygen demand, dissolved organic carbon and nitrogen. Purification efficiency increased from a septic tank alone to a septic tank with bioreactor, however, the operational complexity, maintenance requirement, energy use and costs also increased in that order (Lowe *et al*., 2008).

Understanding of the flow and transport processes in soil under boundary conditions typical of OWTS is needed to develop guidelines for the construction of safe, efficient and effective OWTS, particularly in areas with shallow groundwater conditions. Localized

groundwater mounding below an on-site wastewater discharge fields can reduce the thickness of the unsaturated zone (e.g. Finnemore, 1993), providing a shorter travel distance for contaminants to reach the groundwater and effectively limiting effluent treatment time (i.e., residence time in the vadose zone). Local and temporal water table fluctuations may also change the aeration status of the soil, which subsequently affects biogeochemical processes. For example, an increase in soil water content can decrease the kinetics of biodegradation processes because of a decrease in oxygen (Carrara *et al*., 2008; Robertson, 2008; Robertson, 2003; Robertson *et al.,* 1998; Harman *et al.,* 1996). Hence, the potential contamination risks to groundwater, public and environmental health associated with OWTS need to be quantified.

Environmental and human health risks associated with OWTS are the contamination of ground- and surface-waters with pathogenic microorganisms. Risks to surface water can be managed by designing OWTS such that all wastewater infiltrates into the soil. The probability of pathogenic microorganisms contaminating groundwater depends on the travel time of the pathogen through the unsaturated zone (treatment zone) and the longevity of the pathogen in the soil environment. In general, a residence time of 7 days in the unsaturated zone (treatment zone) is thought to be effective for reducing the pathogenic load of wastewater to safe levels (Safety Code Council, 2012).

Therefore, quantifying groundwater contamination risks at OWTS involves quantifying the natural variations in the unsaturated zone thickness (i.e., depth to groundwater) and the short-term influence of infiltrating wastewater on the unsaturated zone thickness. Because groundwater levels at OWTS are likely influenced by regional hydrology and wastewater infiltration, and because the pathogens are carried in the wastewater, accurate risk assessment requires isolating the influence of the infiltrating wastewater on unsaturated zone thickness, and this may be achieved with signal processing tools.

Signal analysis methods are robust time series analysis tools used in the natural sciences (Boggess and Narcowich, 2009). Among the signal processing tools, spectral and wavelet analyses are commonly used. Spectral analysis assumes that the underlying processes are stationary in time with continuous, constant and periodic waves up to infinity (Boggess and Narcowich, 2009; Si, 2008; Wendroth *et al.,* 2012). Wavelets as signal analysis tools have been recognized since the 1980s and provide both time and frequency domain representations of a continuous, non-stationary signal (Boggess and Narcowich, 2009; Holman *et al.,* 2011).

Torrence and Compo (1998) and Grinsted *et al* (2004) have given wavelet analysis toolkits that include statistical significance testing. To date, the application of wavelet analysis to groundwater response has been limited to groundwater response to large scale climate changes (Torrence and Compo, 1998; Grinsted *et al.,* 2004; Holman *et al.,* 2011; Perez-Valdvia *et al.,* 2012). However, localized non-stationary processes may exist, for example, due to population growth and its impact on land development and increased wastewater discharges that are part of on-site wastewater treatment systems. Thus, understanding local groundwater response to a local surface boundary condition and separating that response from regional groundwater fluctuations is also important for effective groundwater resources management.

This study is part of an in-situ field-scale project examining wastewater flow and pathogen transport under an at-grade OWTS with a shallow groundwater table. Groundwater response to effluent infiltrating from at-grade line sources was measured to understand groundwater mounding beneath an at-grade infiltration field. Specific objectives were (i) to quantify the groundwater fluctuation over time (ii) to identify groundwater response to effluent infiltration and detect any groundwater mounding under the at-grade line sources and (iii) to estimate vadose zone thicknesses with respect to these groundwater fluctuations and whether these variations pose environmental risks.

3.2. Materials and Methods

3.2.1. Site Description

The study was conducted at the Wetaskiwin Rest Stop (N52°53’43’’and W113°38’33’’), located 80 km south of Edmonton, Alberta, Canada (Figure 3-1). The Rest Stop is equipped with seven toilets, two urinals, seven hand washing sinks and septic tanks. An on-site wastewater treatment system equipped with Ultraviolet (UV) disinfection and at-grade line sources was established by the Alberta Municipal Affairs as a pilot project in 2007.

The study site has been receiving ultraviolet- (UV) disinfected effluent for more than four years via pressurized at-grade line sources (polyvinyl chloride, PVC), which are referred to hereafter as laterals. In total, there were three zones, each with five laterals, which distribute the UV-disinfected effluent to the ground surface. The laterals were covered by dome-shaped Quick4® standard chambers (width = 0.85 m and height= 0.31m; Infiltrator Systems Inc., 2006) to guide effluent infiltration and to ensure uniform wetting of the infiltration bed. The current

study was conducted in the northern most zone with four laterals (Figure 2-1, Chapter 2). The northern zone was selected because it was away from the influence of the other two zones as observed by the groundwater flow direction. Each lateral (L=40 m and ID = 3.175 cm) was laid above the surface raised by 0.1 m pegs and distributed the effluent over a 40 m long by 0.61 m wide infiltration bed. The laterals have nozzles every 0.5 m, which were facing upward except for every fifth one which faced down. The effluent sprinkles through the nozzles and showers back to the ground after hitting the infiltration chamber. The infiltration chamber was covered with a 0.3 m thick layer of woodchips to protect from freezing in the winter, from rodents, and for esthetics.

3.3. Groundwater Monitoring Wells Installation and Data Collection

An initial survey to determine wastewater plume extent and direction was conducted by measuring bulk electric conductivity (EC) spatial distribution in the subsurface using non-contacting electromagnetic induction instruments (EM38 and EM31) (Geonics Ltd, 2009). From the EM data, a bulk EC spatial distribution map was produced and 8 transects were identified for groundwater (GW) well sites. A dense grid of 88 GW wells (74 water table wells, WT and 14 piezometer wells, PW with ID=1.25 cm, the WT screen depth ranges between 2.1 to 2.4 m and that of PW was 0.1 m) were installed in the 8 transects, at a lateral distance between wells from 1 m to 16 m in a transect, over a 1.5 ha area within and outside the effluent source zone. The groundwater level in the 88 wells was measured manually using a Solinst water level meter on a regular basis (weekly to biweekly) in the summer of 2010. In addition, groundwater samples from these wells were tested on-site for pH and EC using a portable Thermo Orion 5-plus meter. The spatial distribution of hydraulic head and EC maps were produced in Surfer (Golden Software, 2010) and were used to estimate the groundwater flow direction and extent of wastewater plume (see Figure 2-15 and 2-16 in Chapter 2).

Following the detailed site characterization of groundwater flow direction and the wastewater plume extent, an additional 11 GW wells (ID=2.54 cm, screen depth = 2.4 m) were installed within the source zone (Figure 3-1) and wastewater plume as delineated by the electrical conductivity values. In these 11 GW wells, pressure transducers (Solinst Gold Levelogger, Model 3001) were deployed and groundwater levels were recorded every hour for more than two-years (795 days) starting from the end of October 2010.

Event-based effluent applications were recorded with an Aquaworx event recorder (Pinnacle Environmental Technologies, Ltd.) that was connected to a pressure transducer located at the effluent source tank. An area-averaged effluent surface flux density, q_{efflu} ($L^3L^{-2}T^{-1}$) was calculated based on the number of effluent application events and known application volume per event, V (L^3) per unit infiltration area, A (L^2) over time, Δt (T) as follows

$$q_{efflu}(t) = \frac{V(t)}{A \times \Delta t} \quad [3.1]$$

A meteorological station was established at the site and it recorded daily solar radiation, rainfall (tipping bucket and rain gauge), wind speed and direction, relative humidity and air temperature. Potential evapotranspiration, ETos, was calculated from the weather data by the Penman Montieth method (Allen *et al.,* 1998) for the days when the air temperature was ≥5 ^{0}C. Summary weather data is presented in Table 2-3b (see Chapter 2).

Effective effluent surface flux density, *q(t)*, (t=1,2…N) was calculated by adding effluent flux and precipitation and subtracting evapotranspiration. Precipitation and evapotranspiration had generally small contributions compared to effluent surface flux because they were on the order of mm/day and the surface effluent fluxes were on the order of cm/day. In calculating *q(t)*, snow water equivalent (SWE) was not included because it was not practical to measure daily SWE and snowmelt infiltration wasn't measured directly.

An average $\bar{\theta}_v$ (0.56 cm^3 cm^{-3}) (Table 2-2), obtained from a laboratory measurement of the soil hydraulic properties, which was also similar with the maximum water content (0.554 cm^3 cm^{-3}) measured in the field using a Time Domain Reflectometry (Topp *et al.,* 1980), and the daily effective surface flux density, $q(t)(cm^3cm^{-2}d^{-1})$; were used to determine an average daily vertical Darcy flow velocity, $\bar{v}_t(cm\ d^{-1})$ as

$$\bar{v}_t = \frac{q(t)}{\bar{\theta}_v} \quad [3.2]$$

The 7-day travel depth, $d_{7,w,}$ for each 7 day period, it was calculated by a moving sum function:

$$d_{7,w} = \sum_{w=l}^{l+6} \bar{v}_w \, \delta t \, , \qquad l = 1, 2, \ldots N - 6 \qquad [3.3]$$

Where: l is a time index and N is the number of sampling points in the time series. This function calculates the travel time for each consecutive 7-day period in the time series. The 7-day travel depth is an important index for comparison of an effective treatment time required in soil-based wastewater treatment systems to the groundwater depth (Safety Code Council, 2012). In addition, the 7-day cycle also coincides with weekly peaks in facility use and effluent application on weekends.

Disturbed soil samples (total number=63) were collected at 20 cm intervals from the surface to 1.40 m for particle size analysis at nine random sampling locations within the source zone and at 5 m up-and down-gradient of the source zone (Figure 2-8a). The particle size distribution (PSD) was determined by a standard hydrometer method (Kaddah, 1974). On average, the soil at the site was characterized by sand (43.3%, CV = 27%), silt (34.2%, CV = 23.7%) and clay (22.6%, CV = 25.5%) soil separates.

3.4. Data Analysis

The focus of the data analysis was to quantify the risks of effluent impacting groundwater at the Wetaskiwin site and to provide a general framework for this type of risk assessment at other OWTS. At this site, wastewater is exposed to UV light, reducing pathogen loads, but the process is not 100% efficient and, because pathogens such as *E coli* reproduce rapidly, it is not reasonable to assume that wastewater infiltrating into the soil is pathogen free. Further, if the UV system were to malfunction, it is important to understand the probability that most of the effluent would be treated in the unsaturated treatment zone at the site. Because 7-days is generally considered to be an effective treatment time for soil-based wastewater treatment systems (Safety Code Council, 2012), the data analysis framework presented here seeks to quantify the risk of wastewater effluent impacting the groundwater at the site within 7 days of application. Therefore, we employed three statistical methods to quantify the covariance between the effective effluent surface flux density and elevation of the groundwater table: 1) standard covariance over moving temporal windows, 2) spectral analysis and 3) wavelet spectra.

At the Wetaskiwin site (and probably at most other OWTS), the depth to the groundwater table directly beneath the wastewater laterals (output signal) is influenced by two input signals: 1) the hydrological processes outside of the effluent infiltration zone; and 2) the effective effluent surface flux density within the effluent infiltration zone. Each input signal operates over unique temporal and spatial scales and the risk assessment tools must be able to separate the influence of these two signals. Time series analysis methods such as spectral analysis and wavelet analysis are able to partition the variance of and covariance between individual signals into discrete temporal scales or frequencies. Thus, to quantify the time-dependent local groundwater response from only the local effective surface flux, spectral and wavelet analysis tools were employed in addition to the standard covariance. Analyses of the power spectra, coherency and cross spectra of *q(t)* and *d(t)* signals were used to identify the localized groundwater response to the effluent infiltration. Detailed descriptions and applications of the spectral analysis are available (e.g. Si, 2008; Dyck and Kachanoski, 2011; Wendroth *et al*., 2012) and for the wavelet analysis in Farge, 1992; Graps, 1995; Holman *et al.,* 2011; Torrence and Compo, 1998; Carmona *et al.,* 1998; Grinsted *et al.,* 2004; Perez-Valdivia *et al.,* 2012; and thus only a summary description is presented here.

(i) Standard Variance and Covariance

For standard and time series analysis, input (effective surface effluent flux) and output (groundwater elevation) signals are represented as discrete series, X_n and Y_n. n=0, 1, 2…N-1. The total variance of a series is the expectation of squared deviations from the mean:

$$Var[X] = E[X^2] - (E[X])^2 \qquad [3.4]$$

Where: $E[\cdot]$ is the expectation operator. The total covariance between two series is expressed as:

$$COV[X,Y] = E[XY] - E[X]E[Y] \qquad [3.5]$$

The covariance between two series may be normalized by the product of their variances to estimate the coefficient of determination (R^2):

$$R^2 = \frac{COV[X,Y]^2}{Var[X]Var[Y]} \quad [3.6]$$

Because we were specifically interested in the 7-day time periods, we also calculated weekly (7-day) covariance between the effective effluent surface flux and the groundwater elevations using a 7-day moving window:

$$COV_i[X,Y] = COV\left[X_{i+j}Y_{i+j}\right] \quad i = 0 \ldots N-7 \quad j = 0 \cdots 6 \quad [3.7]$$

(ii) Spectral analysis

In spectral analysis, the Fourier transform (FT) is used to decompose the total variance of a time series into variance as a function of frequency or period (called the periodogram). Sine and cosine functions are the building blocks of the FT. The spectral Fourier domain representation of a time series, X_n, is given by (e.g. Dyck and Kachanoski, 2011):

$$X_n = \int_{-1/2}^{1/2} e^{i2\pi fn} dT(f) \quad [3.8]$$

Where: X_n is the n^{th} observation of the process, f is Fourier frequency ($|f| \leq 1/2$), $i = \sqrt{-1}$, dT(f) are random amplitudes and phases for sine (out of phase, imaginary) and cosine (in phase, real) components of the signal. From Euler's formula, $e^{i2\pi fn}$, is expressed by the sum of sine and cosine functions.

The power spectrum is used to estimate the variance of a process, X_n at each frequency, f of a time series,X_n, n=0, 1, 2…N-1. For this work, the power spectrum was estimated with the Discrete Fourier transform (DFT) by implementing a Bartlett window, $W_{j,M}$, (Percival and Walden, 1993) in Mathcad program version 15 software (Parametric Technology Corporation) (Dyck and Kachanoski, 2011) as:

$$W_{j,M} = \sum_{j=-M}^{M} \begin{vmatrix} 1 - \frac{|j|}{M}, |j| < M; \\ 0, |j| \geq M \end{vmatrix} \quad [3.9]$$

$$\hat{S}_{XX}(f_K) = \langle \hat{S}_{XX}^{(p)}(f_K) \rangle = \sum_{j=-M}^{M} W_{j,M} \left[\frac{1}{N} \left| \sum_{t=1}^{N} X_n e^{-2\pi f_{K+j} t} \right|^2 \right] \quad [3.10]$$

Where: $f_K = K/N$ (K = 1, 2…N/2), $\hat{S}_{XX}(f_K)$ is estimated power spectrum of series X, the time interval in this case is 1-day; j is the lag index and $M \leq N$ is the window parameter controlling the degree of smoothing by lag or smoothing window, $\hat{S}_{XX}^{(p)}(f_K)$ is periodogram, $\langle \cdot \rangle$ denotes expectation operator.

The covariance of two time series, X and Y, as a function of time scale can also be quantified using a cross-spectrum, which is given by:

$$\hat{S}_{XY}(f_K) = \langle \hat{S}_{XX}^{(p)}(f_K) \hat{S}_{YY}^{(p)*}(f_K) \rangle = \sum_{j=-M}^{M} W_{j,M} \left[\hat{S}_{XX}^{(p)}(f_{K+j}) \hat{S}_{XX}^{(p)*}(f_{K+j}) \right] \quad [3.11]$$

Where: $\hat{S}_{YY}^{(p)*}(f_K)$ is the complex conjugate of $\hat{S}_{YY}^{(p)}(f_K)$.

An analogue to the coefficient of determination (R^2) in regression analysis, spectral coherency was also used to quantify a time-dependent linear relationship between two time series, X and Y as a function of frequency (Kachanoski and de Jong, 1988). The coherency spectra, $\hat{R}^2{}_{XY}(f)$ was estimated by using:

$$\hat{R}^2{}_{XY}(f) = \frac{\left| \hat{S}_{XY}(f_K) \right|^2}{\hat{S}_{XX}(f_K) \hat{S}_{YY}(f_K)} \quad [3.12]$$

From Kachanoski *et al* (1985) and Si (2008), the critical value, ρ_{XY}, for $\hat{R}^2{}_{XY}(f)$ is given by:

$$\rho_{XY} = 1 - (1 - \alpha)^{\left[\frac{2}{\nu - 2}\right]} \quad [3.13]$$

Where ν is the degrees of freedom at $(\alpha/2)$ and $(1 - \alpha/2)$ probabilities. The degrees of freedom for Bartlett window is proportional to its width (16 degrees of freedom for M=5; Eq.

[3.9], making the critical value, ρ_{XY}, 0.355 and 0.491 at 95% and 99% confidence level respectively).

(iii) Wavelet analysis

The Fourier Transform (FT) uses a single window for all frequencies and thus the resolution of the analysis is equally spaced at all locations in the time-frequency domain. Spectral analysis is therefore, good for stationary processes (e.g. Torrence and combo, 1998). The Wavelet transform decomposes a time series into time and frequency domains simultaneously. Wavelets are wave-like oscillations that travel for one or more periods and are nonzero only over a finite interval instead of propagating infinitely the way sines and cosines do (Boggess and Narcowich, 2009). Wavelet power spectra provide information on both the amplitude of any "periodic" signal within the series, and how this amplitude varies with time. Thus, wavelet analysis is more appropriate for non-stationary processes (Torrence and combo, 1998). Stationarity is only assumed over the width of the wavelet finite interval.

A wavelet is defined by a basis function, $\psi_0(\eta)$, which is a function of a dimensionless time parameter, η. The function $\psi_0(\eta)$ must have zero mean and be localized in both the time and the frequency domains to be admissible function (Farge, 1992; Graps, 1995; Holman *et al.,* 2011; Torrence and Compo, 1998). A number of pre-defined sets of wavelet basis functions have been proposed (e.g. Morlet, Haar, Cauchy, Mexican hat) and detailed reviews of these are available (e.g. Torrence and Compo, 1998; Carmona *et al.,* 1998; Farge, 1992). In this study we have used the Morlet basis function because it gives a good balance between time and frequency localization (Torrence and Compo, 1998; Grinsted *et al.,* 2004; Perez-Valdivia *et al.,* 2012). The Morlet basis function is given by:

$$\psi_0(\eta) = \pi^{\frac{1}{4}} e^{-i\omega_0\eta} e^{-\frac{\eta^2}{2}} \qquad [3.14]$$

Where: ω_0 is non-dimensional frequency and it was given a value of 6 to satisfy admissibility (Farge, 1992; Grinsted *et al.,* 2004). Meaning, when $\omega_0 = 6$, the Morlet basis function was assumed a modulated Gaussian waveform and the errors due to non-zero mean were smaller than the typical computer round-off errors (Farge, 1992).

Similar to the Fourier transform, the wavelet transform can be done either by discrete- or continuous-wavelet transform (DWT and CWT, respectively). The CWT of a discrete sequence X_n is defined as a convolution of X_n with a scaled and translated version of $\psi_0(\eta)$ as given by (Torrence and Compo, 1998):

$$W_n(s) = \sum_{n'}^{N-1} X_{n'} \psi^* \left[\frac{|n'-n|\delta t}{s}\right] \qquad [3.15]$$

Where: $|a| = a \cdot a^*$, s (T) is the wavelet scaling parameter, also inversely related to the frequency, $\delta t(T)$ and n is the localized time index and N is the number of sampling points in the time series. The scaling parameter, s, is calculated as: $s_j = s_0 2^{j\delta j}$; $j = 0,1,\ldots,J;\ J = \delta j^{-1}\log_2\left(\frac{N\delta t}{s_0}\right);\ \delta j \leq 0.5;$ and $\lambda = 1.03s$ (λ is Fourier period) (Torrence and Compo, 1998). In the present study, for N=685, δt =1day, s_0=2δt, δj=1/12, and J=73, were used giving a total of 72 scales that range from 2 to 128 days. The value of δj gave a smooth picture of the wavelet power.

In contrast to the CWT, which assesses the periodicities and phases of cycles within a single dataset, the cross wavelet transform (XWT) estimates the cross wavelet power (covariance) of two time series. For two given time series, X_n, (n=0, 1, 2…N) and Y_n, (n=0, 1, 2…N), the XWT is given by (Holman *et al.,* 2011):

$$W_n^{XY} = W_n^X(s) W_n^{Y^*}(s) \qquad [3.16]$$

Where: $W_n^X(s)$, is the CWT of time series X_n, and $W_n^{Y^*}(s)$ is the complex conjugate of $W_n^Y(s)$, the CWT of the time series Y_n.

The cross wavelet spectrum can be decomposed into the amplitude or cross wavelet power $|W_n^{XY}(s)|$ and the phase $\phi_n(s)$, which indicates the delay between the two signals at time t and scale s as:

$$W_n^{XY} = |W_n^{XY}(s)| e^{n\phi_n(s)} \qquad [3.17]$$

A third component of wavelet analysis is the wavelet coherence (WTC). It is given by normalizing two time series data to the single wavelet power spectrum. The WTC is calculated as (Holman *et al.,* 2011):

$$WTC = \frac{|W_n^{XY}(s)|}{[W_n^X(s)W_n^{Y^*}(s)]^{0.5}} \quad [3.18]$$

The WTC ranges from 0 to 1 and measures the cross correlation of two time series as a function of frequency (Torrence and Compo, 1998), that is the local correlation between the time series in time-frequency space. Values close to 1 indicate more correlated time series.

The time series signals of depth to groundwater level from ground surface, (*d(t)*), and the corresponding effluent flux density, (*q(t)*), were processed using spectral and wavelet analysis methods discussed above. The time series data was processed and mapped in MATLAB® using the program written by Grinsted *et al* (2011) for the wavelet and in Mathcad for the spectral analysis (Dyck and Kachanoski, 2011).

The statistical significance tests (5%) were also conducted based on a null hypothesis of white noise data generated using Monte Carlo techniques, compared with the red noise of the input signal (Torrence and Compo, 1998; Gilmans *et al* (1963).

3.5. Results and Discussion

The groundwater hydrographs (depth to water table, *d(t)*), effective effluent surface flux density (*q(t)*), daily rainfall and evapotranspiration observed during the study period (2011 to 2012) are presented in Figure 3-2. The wells designated with a "U1 and U3 are at 3- and 10-m up-gradient of the source zone respectively; those designated with an "S1 to S4 are within the effluent source zone; and those designated with a "D1 to D3 are at 3-, 9- and 12-m down-gradient of the source zone respectively (Figure 3-1). Descriptive statistics and Pearson correlation matrix showing the covariance between *q(t)* and *d(t)* as well as between *d(t)* of the wells in- and out-side the source zone are also given in Tables- 3-1 and 3-2. In the two years (2011 and 2012), the average depth to groundwater measured from the wells with respect to the ground surface was between 0.88 to 1.22 m (Table 3-1). Zooming in to the spring and summer seasons, the groundwater level at the source zone reached as close as 0.221 m below the ground surface and an average of 0.76 m below the ground surface in those two years (Figure 3-3).

The total variance of *d(t)* in the site decreased from up-gradient to down-gradient direction. The percent coefficient of variation (CV%) was also higher in the down-gradient zone and relatively lower in the source and the up-gradient zones (Table 3-1). The relatively lower CV% in the source zone would mean lower extent of variability of *d(t)* in relation to the mean *d(t)*, attributed to the regular effluent surface flux which offsets groundwater level decreases during periods of low rainfall. The depth to water table decreases from up-gradient to down-gradient following the surface topography as the ground surface slope gets flatter in that direction. At the site, a linear trend of bedrock from southwest to northeast (i.e. in the down-gradient direction) approaching to the ground surface was shown in the regional Wetaskiwin County hydrogeologic study (HCL, 2008; see Figures 2-2 to 2-3 in Chapter 2). Therefore, the surface and subsurface conditions are likely controlling the shape of the groundwater level at the site.

From the Pearson correlation matrix (Table 3-2), all correlations were significant ($P<0.001$). However, a slightly higher correlation between *q(t)* and *d(t)* was observed in the 4 wells located within the source zone compared to either the up- or the down-gradient wells. The difference between the correlation coefficients, of *q(t)* and *d(t)* in the source zone ($0.484 \geq r \geq 0.463$) and outside the source zone (up-gradient: $0.450 \geq r \geq 0.441$, and down-gradient: $0.458 \geq r \geq 0.447$) suggested that the response of *d(t)* to *q(t)* was the highest in the source zone, but the correlation coefficients for all wells had the same level of significance ($P<0.001$).

The correlation among depths to groundwater, *d(t),* for the wells within and outside the source zone were likely high because the annual cycle of *q(t)* coincided with the annual hydrologic cycles. The annual precipitation (total rainfall and snow water equivalent, SWE) was 519 and 370 mm in 2011 and 2012 respectively (Table 2-3b, Chapter 2). On the Canadian Prairies, snowfall contribution is about 25% of the annual precipitation (Environment Canada, 2010), which is consistent to the SWE of 109 and 78 mm observed in the study site for 2011 and 2012 respectively. The groundwater response to the regional spring snowmelt and the summer precipitation is shown by the groundwater rising significantly closer to the ground surface in the spring (April and May; Figure 3-2c). However, at the same time, the road traffic and the rest stop visitors increased as indicated by the increase in the effluent surface flux density (Figure 3-2b). Therefore, the Pearson correlation does not clarify whether the relationships between effective surface flux and groundwater depth were the result of similar seasonal cycles between

the two series or because of the actual influence of surface-applied effluent on groundwater levels. Standard Pearson correlations are significantly influenced by trends or cycles at the scale of the entire series and, therefore, are likely not precise enough to estimate the relationship between wastewater effluent fluxes and groundwater table response. Further, the effect of the effective effluent flux on the depth to groundwater is likely much smaller than the large, regional snowmelt input. Snowmelt over the entire groundwater catchment likely influences the depth to groundwater directly below the effluent infiltration zone and this may obscures the effluent flux influence on the depth to groundwater.

To quantify the covariance in the two signals at frequencies or periods smaller than that of the entire dataset, 7-day moving window covariance, and spectral and wavelet cross spectra were estimated. Wavelet and spectral cross spectra and coherency spectra can identify significant covariance at many scales and frequencies.

The 7-day moving window covariance estimates in Figure. 3-2d show two discrete peaks in 2011 and 2012, but these peaks occurs at different times of the year. Figure 3-3 zooms in the periods of high 7-day covariance observed in the 2011 and 2012. In 2011, two periods of high covariance between effective effluent flux and groundwater depth in the source zone are apparent from June 16 to 27 and from July 21 to August 07 (Figure 3-3g). The 7-day travel depth (Eq. [3.3]) also exceeds the depth to groundwater during those periods. In 2012, two periods of increased covariance between effective effluent flux and groundwater depth in the source zone are apparent for March 11 - 25, and for April 11 – 24 (Figure 3-3h). During the April period of high covariance, the estimated 7-day travel depth exceeded the depth to groundwater, but not during the March period. In the April period, there was a very high magnitude surface flux event on April 18,2012 that occurred because the laterals were being flushed out for maintenance as well as testing the equalization of flow along each lateral. It is also likely that the estimated effective effluent flux during the March period was underestimated because snowmelt infiltration was not included as part of effective effluent flux estimation. Maximum daily air temperature (Figure 3-2b) during the March period of high covariance was consistently above zero (as high as 10 ^{o}C) suggesting that a snowmelt infiltration event at the regional scale created shallower groundwater conditions that coincided with high effluent surface fluxes. Therefore, standard covariance calculated over a 7-day window show that the effect

effluent surface fluxes influence the depth to groundwater at very discrete times of the year at the weekly scale. Spectra and wavelet analysis also quantify this covariance over multiple scales.

A periodogram (Eq. [3-10] was used to estimate the contribution of annual and weekly cycle variance to the total variance of the time series *d(t)*, *q(t)*, daily rainfall, *RF(t)* and potential evapotranspiration, $ET_{os}(t)$ (Figure 3-4). The annual cycle represented approximately 25%, 10%, and 83% of the total variance of *q(t)*, *RF(t)* and $ET_{os}(t)$ respectively. Similarly, the weekly cycle (7-day cycle) represented approximately 5.43%, 0.002%, and 0.047% of the total variance of *q(t)*, *RF(t)* and $ET_{os}(t)$ respectively. For the dependent variable, *d(t)*, the periodogram indicated that the annual cycle contributed approximately 78, 80 and 76% of the total variance of *d(t)* observed in the up-gradient, source zone and down-gradient zones respectively. The weekly cycle contribution to the total variance of *d(t)* was 0.0004%, 0.01% and 0.0013% in the up-gradient, source zone and down-gradient zones respectively (Figure 3-4). In the source zone, the weekly variance contribution of *d(t)* was 2 to 3 orders of magnitude higher than the down-gradient and up-gradient sites respectively clearly indicating a local influence of the effluent surface flux. In the three zones (up-gradient, source zone and down-gradient), the average periodogram (Figure 3-4a-c) showed a decreasing variance with decreasing temporal scale (increasing frequencies) from approximately a year to 3.3-days, indicating autocorrelated temporal patterns. The total variance was also in the following order: up-gradient > source zone > down-gradient (Table 3-1).

Cross-spectra of *q(t)* and *d(t)* for each well and by location (up-, down-gradient and source zone) are given in Figure 3-5. In all the sites, the cross-spectrum (covariance as a function of time-scale) of *q(t)* and *d(t)* showed relatively high covariance at longer time-scales (>20 days), and the covariance values at the longer time scale (>20 days) was about the same for the three zones (Figure 3-5 and Table 3-3). However, the covariance at 7-day period was apparent only in the source zone. The individual cross-spectra for each site were very similar (Figure 3-5) and hence comparing the averages of each site is justified.

Averages of *d(t)* and *q(t)* cross-spectra and coherency are presented in Figures 3-6a and 3-6b respectively. Similar to the individual cross spectra, the average cross spectra showed a high covariance at the 7-day scale only in the source zone, which is likely a reflection of the weekly cycle in the facility use (i.e., much more use and higher effluent fluxes on the weekends). The coherency of the time series, *q(t)* and *d(t),* indicated the weekly increase in application rate and resulted in a statistically detectable response in *d(t)* in the source zone only ($\hat{R}^2_{XY}(f)$=0.51),

with lower impact on the down-gradient ($\hat{R}^2_{XY}(f)$=0.14) and up-gradient zones ($\hat{R}^2_{XY}(f)$=0.12) (Table 3-3). The increased cross-spectrum at the 7-day scale was also consistent with the significant (P<0.05) coherency values observed at that scale (Figure 3-5b and Table 3-3); i.e., the high coherency was a result of higher covariance (cross spectrum) rather than low variance (power spectra) of the effluent and depth to groundwater level (see Eq. [3-12]). Other significant coherency values (P<0.05) in the source zone, were also observed at other time-scales (2.4-, 5.5- and 20-days), but the cross-spectrum during those periods was not as strong and thus gives less confidence to the significant coherency observed in those periods. Therefore, we could infer that the groundwater responds to the effluent infiltration on a weekly cycle because both of the cross-spectrum and coherency between *q(t)* and *d(t)* were statistically significant.

From these findings, the frequency-dependent covariance of *q(t)* and *d(t)* as well as groundwater response to effluent infiltration at weekly scales were evident. Therefore, wavelet analysis was used to investigate the amplitude of the periodic signals and how this amplitude varies with time in order to identify specific times of the year that are at high risk in terms of the effluent reaching the groundwater table.

The wavelet cross-spectrum between the two time series, *q(t)* and *d(t)*, was used to quantify the covariance of the two series in time-frequency space. The cross-spectrum in a two-dimensional (2-D) contour map and a weekly cross-spectrum of *q(t)* and *d(t)* are given in Figures 3-7 and 3-8 respectively. For comparison, the 2-D map are grouped with respect to the source zone (i.e., up gradient – the top two Figures, source zone – the middle four Figures; and down gradient – the bottom three Figures). A significant (P<0.05) cross-spectrum between *q(t)* and *d(t)* was observed at some frequencies (periods) and times over the two years of observation (Figure 3-7). The bold contours in the wavelet cross-spectrum indicated statistically significant (P<0.05) covariance of *q(t)* and *d(t)* (Figure 3-6). The arrows, especially in the significant contours, indicate a phase relationship between the time series: the right pointing arrows indicated that the *q(t)* and *d(t)* were in-phase, the left pointing arrows showed that the *q(t)* and *d(t)* were out of phase and the up and down pointing arrows showed that one time series was leading the other by 90^o (Grinsted *et al*., 2004; Holman *et al.,* 2011).

In the 2-D wavelet cross-spectrum contours, relatively more significant (P<0.05) regions were observed in the source zone (S1 to S4) compared to either the up- or the down-gradient sites (Figure 3-7). The arrows in the significant regions were pointing to the right indicating in-

phase covariance existed between *q(t)* and *d(t)*. Therefore, the next sections focus on the covariance of *q(t)* and *d(t)* observed in the source zone because this zone was also the immediate effluent recipient and became a source to the other zones. Further, as stated in the previous paragraph, the statistically significant ($P<0.05$) regions were time-frequency localized, i.e., spring and summer time of a year at shorter frequencies (less than a month cycle). Hence focusing to those time periods was justified.

Because of the observed weekly cycle effluent discharge (facility use) and the significant spectral cross-spectra and coherency at this scale, the coefficients of wavelet cross-spectra for the weekly period were extracted from the 2-D cross-spectrum plot. Recalling that the cross-spectrum has two components, the cospectrum (in-phase covariance, also called real component) and quadrature spectrum (out-of-phase covariance, also called imaginary component), only the real component was considered because it was in agreement with the standard weekly covariance of *q(t)* and *d(t)*. In addition, an in-phase covariance between *q(t)* and *d(t)* was observed by the arrows pointing to the right direction in the significant regions. By isolating the weekly period covariance as a function of time enables identification of the riskiest times of the year, when significant wavelet cross-spectrum matches with peak groundwater level. A time series focusing on the spring and summer periods for the two years (2011-2012) compares the weekly surface flux and groundwater depth covariance (e and f) and wavelet cross-spectrum (g and h) to the corresponding picks in the groundwater hydrograph (c and d) and effective surface flux density (a and b) is presented in Figure 3-8.

Both, standard 7-day moving window covariance and 7-day scale wavelet cross spectra indicate that the two signals, *q(t)* and *d(t)* significantly covary at only certain periods of the year (in the spring and summer times). In approximately 153 days, in the months between March to August, the weekly peaks of wavelet cross-spectrum and the standard covariance between *q(t)* and *d(t)* were compared graphically (Figure 3-8 e to h). In those times of the year, on average the groundwater level rose approximately 1.22 m following the snowmelt, summer precipitation and surface effluent flux (Figure 3-8a-d and Figure 3-2c). It is evident from the groundwater hydrograph (Figure 3-2c) that the regional groundwater hydrology has a significant influence over the groundwater fluctuation. Furthermore, there is a time coincidence in the spring and summer seasons that effluent surface fluxes also increase and the vadose zone becomes thin, favoring a short travel time or travel distance for the effluent to reach the top of the water table

(Figure 3-8c and d). Therefore, such a scenario needs careful investigation and analysis to identify risky periods as effluent travel depth exceeds *d(t)*.

For soil-based wastewater treatment systems, the Alberta Safety Code Council has regulated a minimum vertical separation required between a point of effluent infiltration and a water table or an impervious layer (Safety Code Council, 2012). The vertical separation considers the quality of the effluent and the depth of the suitable soil such that the effluent travels through the vadose zone for at least 7 days prior to reaching the groundwater table. For a primary treated effluent (septic tank effluent) and a secondary treated effluent (treatment plant effluent), the recommended vertical separation between the infiltration surface and the water table is 1.5 and 0.9 m, respectively. On the basis of these regulatory requirements and the weekly response coherency and cross-spectrum, we determined the 7-day effluent travel depth ($d_{7,w}$) for this site and compared it to the observed vadose zone thickness (*d(t)*).

The 7-days travel depth, $d_{7,w}$, was calculated using Eq. [3.3] and it was compared to the observed *d(t)* within the source zone (Figure 3-8c and d). An equal number of days were considered for 2011 and 2012 focusing on the spring and summer time to assess potential risks of groundwater pollution when water table was close to the ground surface. The months were selected that showed the smallest values of *d(t)* and the observed covariance from wavelet cross-spectrum (Figure 3-8g and h). The number of days when the 7-day travel depth exceeded the observed *d(t)*s were calculated and percentages were obtained (Table 3-4). On average, the estimated 7-day travel depth exceeded the observed *d(t)* for approximately 15% and 7% of the days sampled (153 days) in 2011 and 2012 respectively. The riskiest times of the years at which the effluent surface flux had reached the groundwater were observed when *q(t)* was greater or equal to 5 cm^3 cm^{-2} d^{-1} and *d(t)* less than the 7-day travel depth (Table 3-4). The conditional probability of $q(t) \geq 5$ cm^3 cm^{-2} d^{-1} when $d(t) \leq 0.5$ m also showed comparable probability to that of the 7-day travel depth exceeding *d(t)*. Thus, 5 cm^3 cm^{-2} d^{-1} and 0.5 m gives the threshold values of *q(t)* and *d(t)* respectively meaning when $q(t) \geq 5$ cm^3 cm^{-2} d^{-1} and $d(t) \leq 0.5$ m coincide, there is a high probability that the surface applied effluent reaches groundwater posing risks to groundwater quality. The probability of the 7-day travel depth was small for the year 2012 because generally 2011 was a wetter year than 2012 (Figure 3-2a) and hence the water table level remained close to the ground surface for extended period in 2011.

3.6. Conclusion

The present study investigated local groundwater response to effluent infiltrating from at-grade line sources. The average fluctuation of the groundwater level was between 0.30 m and 1.53 m below ground level, spanning a range of 1.22 m depth during the study period (2011-2012). This fluctuation was greatly controlled by the annual regional hydrologic cycles and also local surface effluent flux as observed from the periodograms of *q(t)* and *d(t)*. In-depth inspection of the local groundwater response to the effective surface flux density by using a 7-day moving window estimates of covariance, and spectral and wavelet cross spectra revealed a time-dependent covariance between *q(t)* and *d(t)*. It was shown that the local effective surface flux density had significant influence on the local depth to groundwater beneath the at-grade line sources at very discrete times of the year at the weekly scale. Fine tuning of the two signals (*q(t)* and *d(t)*) using spectral analysis (cross-spectrum and coherency) confirmed that the two signals showed significant coherency values ($P<0.05$) consistent to the cross-spectrum observed at a weekly scale. The weekly cycle is important because there is a significant 7-days cycle of the input function, *q(t)* due to traffic on the highway and use of the facilities. Therefore, we could infer that the groundwater responds to the effluent infiltration on a weekly cycle because both of the cross-spectrum and coherency between *q(t)* and *d(t)* were statistically significant. Furthermore, wavelet cross-spectrum between the two time series, *q(t)* and *d(t)*, was significant ($P<0.05$) at some frequencies (periods) and times over the two years of observation in the spring and summer seasons. In those two seasons of a year, the groundwater depth was close to the ground surface following the snowmelt and summer precipitation and interestingly, the effluent surface fluxes were also coincidentally higher.

Further, a 7-day travel depth was estimated to identify the potential risks where by the 7-day travel depth exceeds the minimum observed *d(t)*. It was found that the estimated 7-day travel depth exceeded up to 15% of the time between 2011 and 2012 when $q(t) \geq 5$ cm^3 cm^{-2} d^{-1} and $d(t) \leq 0.5$ m coincided . Therefore, $q(t) \geq 5$ cm^3 cm^{-2} d^{-1} and $d(t) \leq 0.5$ m can be considered as threshold values. The 7-day travel depth was very broad estimate because it was calculated assuming a uniform porosity ($\theta = 0.56$ cm^3 cm^{-3}) and vertical flow normal to the water table. Other observations such as preferential flow pathways, e.g. plant root channels, may also result in expedited water flow and transport in the vadose zone. Such conditions can potentially reduce the remediation effectiveness of the vadose zone. Therefore, it is important to consider time-

dependent groundwater responses and to determine the minimum travel depth (travel time) separation between effluent source (typical of an OWTS) and shallow groundwater boundary conditions to meet the 7-day travel time regulatory requirement.

In our study, the OWTS design at Wetaskiwin Rest Stop has failed to meet the requirements in that the 7-day travel depth had reached groundwater water for up to 15% of the spring and summer periods. A threshold of effective surface flux and depth to groundwater has been proposed to avoid risks of groundwater contamination for the OWTS under the prevailing boundary conditions. Possible recommendations could be: i) to add storage tank/s to reduce effluent loading rate in shallow groundwater systems, ii) to increase application area (if applicable) to distribute the effluent loading, iii) to design the at-grade line sources with mounding on the top of the ground surface.

3.7. References

Allen, R., L.S. Pereira, D. Raes, and M. Smith. 1998. Crop evapotranspiration – Guidelines for computing crop water requirements. *FAO Irrigation and Drainage Paper N° 56*. Rome, Italy.

Boggess, A. and F. J. Narcowich, 2009. A first course in wavelets with Fourier analysis. 2nd ed. John Wiley & Sons, Inc. pp. 315.

Carmona R, W. L. Hwang, B. Torresani, 1998. Practical time-frequency analysis: Gabor and wavelet transforms with an implementation in S (Wavelet analysis and its applications). Vol 9. Academic, San Diego.

Carrara, C., C. J. Ptacek, W. D. Robertson, D. W. Blowes, M. C. Moncur, ED Sverko, and S. Backus, 2008. Fate of pharmaceutical and trace organic compounds in three septic stsyem plumes, Ontario, Canada. *Environ. Sci. Technol. 42:2805-2811*.

Durnie, A., 2008. An on-site sewage and septage management framework in Alberta framework Alberta. Available on line: http://www.environmentconference.alberta.ca/docs/Session-33_presentation.pdf

Dyck, M. F. and R. G. Kachanoski, 2011. Scale-dependent covariance of soil physical properties above and below a soil horizon interface: Pedogenic versus anthropogenic influences on total porosity. *Can. J. Soil Sci. 91:149-159*.

Environment Canada, 2010. Water: Snow and Ice. Available on line: http://www.ec.gc.ca/eau-water/default.asp?lang=En&n=B98C0EB3-1.

Farge, M. 1992. Wavelet transform and their application to turbulence. *Ann. Rev. Fluid Mech. 24:395-457*.

Finnemore, E. J., 1993. Estimation of groundwater mounding beneath septic drain fields. *Ground water 31:884-889*.

Ganoulis, J., 2012. Risk analysis of wastewater reuse in agriculture. *Inter. J. of Recycling of Org. Waste in Agri. 1:1-9*.

Geonics Ltd, 2009. EM38-MK2 ground conductivity meter operating manual. Geonics, Ltd. Ontario, Canada.

Gilman, D. L., F. J. Fuglister and J. M. Mitchell, Jr., 1963. On the power spectrum of the red

Golden Software, Inc. 2009. Surface mapping system. Surfer Version 9.11.947.

Graps, A. 1995. An introduction to wavelets. *IEEE Computer Sci. and Eng., 2:50-61*.

Grinsted, A., J. C. Moore, and S. Jevrejeva, 2004. Application of the cross wavelet transform and wavelet coherence to geophysical time series. *Nonlinear Processes in Geophysics, 11:561-566*.

Grinsted, A., J. C. Moore, and S. Jevrejeva, 2011. Cross wavelet and wavelet. Available on line: http://www.pol.ac.uk/home/research/waveletcoherence/

Harman, J., W. D., Robertson, J. A. Cherry and L. Zanini, 1996. Impacts of a sand aquifer from an old septic system: Nitrate and phosphate. *Ground Water, 34:1105-1114.*

HCL, 2008. Regional groundwater assessment. For County of Wetaskiwin. Part of North Saskatchewan River basin. Parts of Tp 044 to 048, R 22 to 28, W4M & Tp 045 to 047, R 01 to 07, W5M. Prepared for the country of Wetaskiwin. Hydrogeological Consultants Ltd. (hcl) 1.800.661.7972 . File No.: 07-771.03.

Holman, I. P., M. Rivas-Casado, J. P. Bloomfield, and J. J. Gurdak, 2011. Identifying non-stationary groundwater level response to north Atlantic ocean-atmosphere teleconnection patterns using wavelet coherence. *Hydrogeol. J., doi:10.1007/s10040-011-0755-9*.

Infiltrator Systems Inc., 2006. The Quick4® Standard Chamber. Available on line: www.infiltratorsystems.com

Kachanoski, R. G. and E. de Jong, 1988. Scale dependence and temporal persistence of spatial patterns of soil water storage. *Water Resour. Res. 24:85-91*.

Kachanoski, R. G., D. E. Rolston, and E. de Jong, 1985. Spatial variability of a cultivated soil as affected by past and present microtopography. *Soil Sci. Soc. Am. J. 49:1082-1087*.

Kaddah, M. T. 1974. The Hydrometer method for detailed particle size analysis - 1. Graphical interpretation of hydrometer readings and test methods. *J. Soil Sci. 118:102-108.*

Lowe, K. S., S. M. Van Cuyk, .R. L. Siegrist and J. E. Drewes, 2008. Field evaluation of the performance of engineered on-site wastewater treatment units. ASCE , *J. Hydrol. Engin. 735-743.*

McCray, J. E. and S. H. Christopherson, 2008. On-site wastewater systems and interactions with the environment. ASCE , *J. Hydrol. Engin. 653-654.*

McCray, J. E., S. L. Kirkland, R. L. Siegrist, and G. D. Thyne, 2005. Model parameters for simulating fate and transport of on-site wastewater nutrients. *Ground Water, 43:628-639.*

Percival, D. B. and A. T. Walden, 1993. Spectral analysis for physical applications: Multitaper and conventional univariate techniques. Cambridge University Press, USA.

Perez-Valdivia, C., D. Sauchyn, and J. Vanstone, 2012. Groundwater level and teleconnection patterns in the Canadian Prairies. *Water Resour. Res., 40, W07516, doi:10.1029/2011WR010930*.

Robertson, W. D., S. L. Schiff and C. J. Ptacek, 1998. Review of phosphate mobility and persistence in 10 septic system plumes. *Ground Water, 36:1000-1010.*

Robertson, W. D., 2003. Enhanced attenuation of septic system phosphate in noncalcareous sediments. *Ground Water, 41:48-56.*

Robertson, W. D., 2008. Irreversible phosphorus sorption in septic systems plumes? *Groundwater 46:51-60.*

Safety Code Council, 2012. Alberta private sewerage systems 2009 standard of practice handbook. Available on line: http://www.safetycodes.ab.ca/Public/Documents/PSSSOP_Handbook_Version_12_Online_Feb_21_2012b.pdf

Sen, T. K., 2011. Processes in pathogenic biocolloidal contaminants transport in saturated and unsaturated porous media: A Review. *Water Air Soil Pollut. Springer*, DOI: 10.1007/s11270-010-0531-9

Si, B. C., 2008. Spatial scaling analyses of soil physical properties: A review of spectral and wavelet methods. *Vadose Zone J., 7:547-562*.

Stanley, S., 2010. Global lessons on water reuse for industrial applications in Alberta. WaterTech 2010. April 21-23, 2010, Fairmont Banff Springs. Available on line at: http://www.esaa-events.com/proceedings/watertech/2010/pdf/Presentation16.pdf

Topp, G. C., J. L., Davis and A. P. Annan, 1980. Electromagnetic determination of soil water content: Measurements in coaxial transmission lines. *Water Resour. Res. 16:574-582.*

Torrence, C. and G. P. Compo, 1998. A practical guide to wavelet analysis. *Bull. Amer. Meteor. Soc., 79:61-78*.

Wendroth, O., S. Koszinski, and V. Vasquez, 2012. Soil spatial variability. In P. M. Huang, Y. Li, and M. E. Sumner (eds.). Handbook of soil sciences: Properties and processes. 2nd ed. 10-1 - 10-25.

Table 3-1: Descriptive statistics of *q(t)* and *d(t)* observed in nine wells for 685-days

Statistic	*q(t)* ($cm^3cm^{-2}d^{-1}$)	Depth to water table, *d(t)* (-m)								
		Up-gradient		*Source zone*				*Down-gradient*		
		U3	U1	S1	S2	S3	S4	D1	D2	D3
Mean	2.402	1.166	1.168	1.220	1.149	1.054	1.067	1.056	0.916	0.877
Variance†	2.490	0.179	0.171	0.165	0.158	0.155	0.157	0.154	0.136	0.138
Maximum	16.501	1.725	1.721	1.768	1.686	1.603	1.605	1.578	1.418	1.360
Minimum	-0.288	0.173	0.254	0.353	0.288	0.221	0.245	0.214	0.132	0.083
Median	2.168	1.305	1.292	1.357	1.280	1.136	1.186	1.181	1.042	0.980
Mode	1.355	1.670	1.440	1.695	1.614	1.566	1.329	1.525	1.353	1.179
CV‡	65.697	36.286	35.456	33.248	34.572	37.387	37.075	37.215	40.200	42.330

†Units: $cm^6cm^{-4}d^{-2}$ for *q* and m^2 for depth to water table below ground surface
‡Units: Coefficient of variation (CV) in percent

Table 3-2: Pearson correlation coefficient matrix of *q(t)* and *d(t)* for the nine wells in the 685 days

Well ID		*Up-gradient*		*Source zone*				*Down-gradient*		
	q(t)	U3	U1	S1	S2	S3	S4	D1	D2	D3
q(t)	1									
U3	0.441*	1								
U1	0.450*	0.995*	1							
S1	**0.470***	0.992*	0.994*	1						
S2	**0.463***	0.987*	0.986*	0.996*	1					
S3	**0.484***	0.965*	0.962*	0.972*	0.972*	1				
S4	**0.467***	0.990*	0.992*	0.998*	0.995*	0.974*	1			
D1	0.447*	0.989*	0.987*	0.994*	0.996*	0.969*	0.995*	1		
D2	0.458*	0.991*	0.991*	0.995*	0.994*	0.966*	0.996*	0.997*	1	
D3	0.452*	0.980*	0.976*	0.987*	0.994*	0.977*	0.989*	0.991*	0.989*	1

* All are significant at $p<0.001$ between *q(t)* and *d(t)* as well as *d(t)* between the wells.

Table 3-3: Spectral covariance and coherency values for one year and 7-day cycle in the three sites

Site	Covariance		Coherency	
	~1 year	7 days	~1 year	7 days
Up-gradient	~ 1.28×10^{-2}	2.31×10^{-5}	~ 0.345	0.116
Source	~ 1.26×10^{-2}	3.15×10^{-4}	~ 0.390	0.512
Down-gradient	~ 1.24×10^{-2}	-2.18×10^{-5}	~ 0.394	0.138

Table 3-4: Probability of 7-day travel depth past the observed *d(t)*s in the source zone during spring and summer periods (N=153 days) in 2011-2012

Well ID	[£]Sample size (days)	Prob. of 7-day travel depth > *d(t)*	Prob. *d(t)* ≤0.5 m	Joint prob. of 7-day travel depth > *d(t)* and *d(t)* ≤ 0.5 m	Joint prob. of *q(t)*≥ 5 $cm^3\ cm^{-2}\ d^{-1}$ and *d(t)* ≤ 0.5 m	Conditional prob. of *q(t)*≥ 5 $cm^3\ cm^{-2}\ d^{-1}$ given *d(t)*≤0.5 m
	2011					
S1	153	0.111	0.118	0.065	0.033	0.278
S2	153	0.150	0.255	0.124	0.033	0.128
S3	153	0.176	0.359	0.163	0.039	0.109
S4	153	0.170	0.340	0.150	0.039	0.115
Mean	153	0.150	0.222	0.124	0.033	0.147
	2012					
S1	153	0.065	0.000	0.000	0.000	-
S2	153	0.065	0.039	0.026	0.007	0.167
S3	153	0.085	0.144	0.085	0.033	0.227
S4	153	0.092	0.144	0.092	0.033	0.227
Mean	153	0.072	0.065	0.052	0.013	0.200

[£] The number of days show from April 1 to August 31 for 2011 and from March 1 to July 31 for 2012. The months were selected based on the observed groundwater level below the ground level [*d(t)*], which was the shallowest possible in the year.

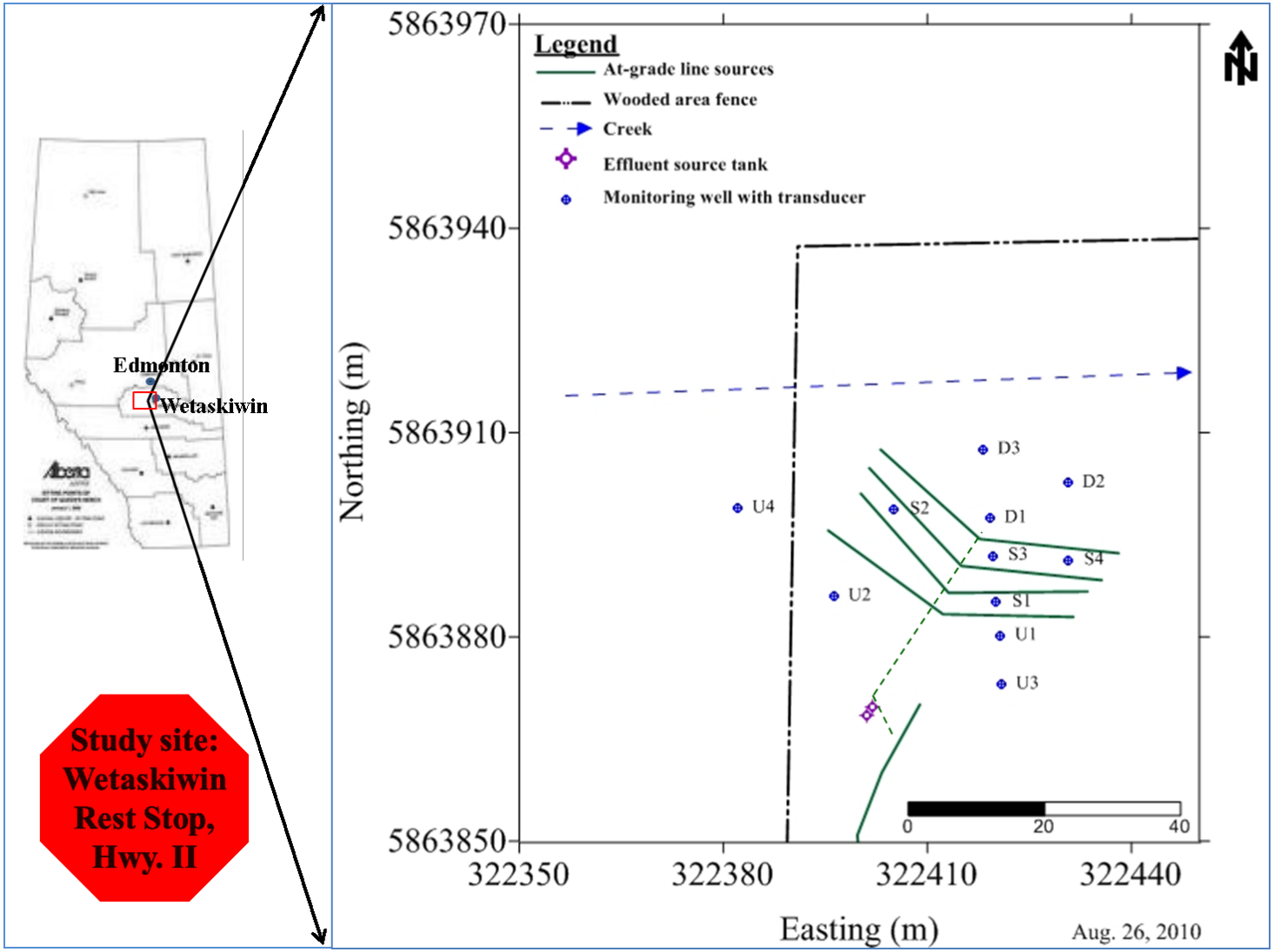

Figure 3-1: Study site and monitoring wells with transducer. The coordinates were projected according to the North American Datum 83 (NAD 83) Zone 12

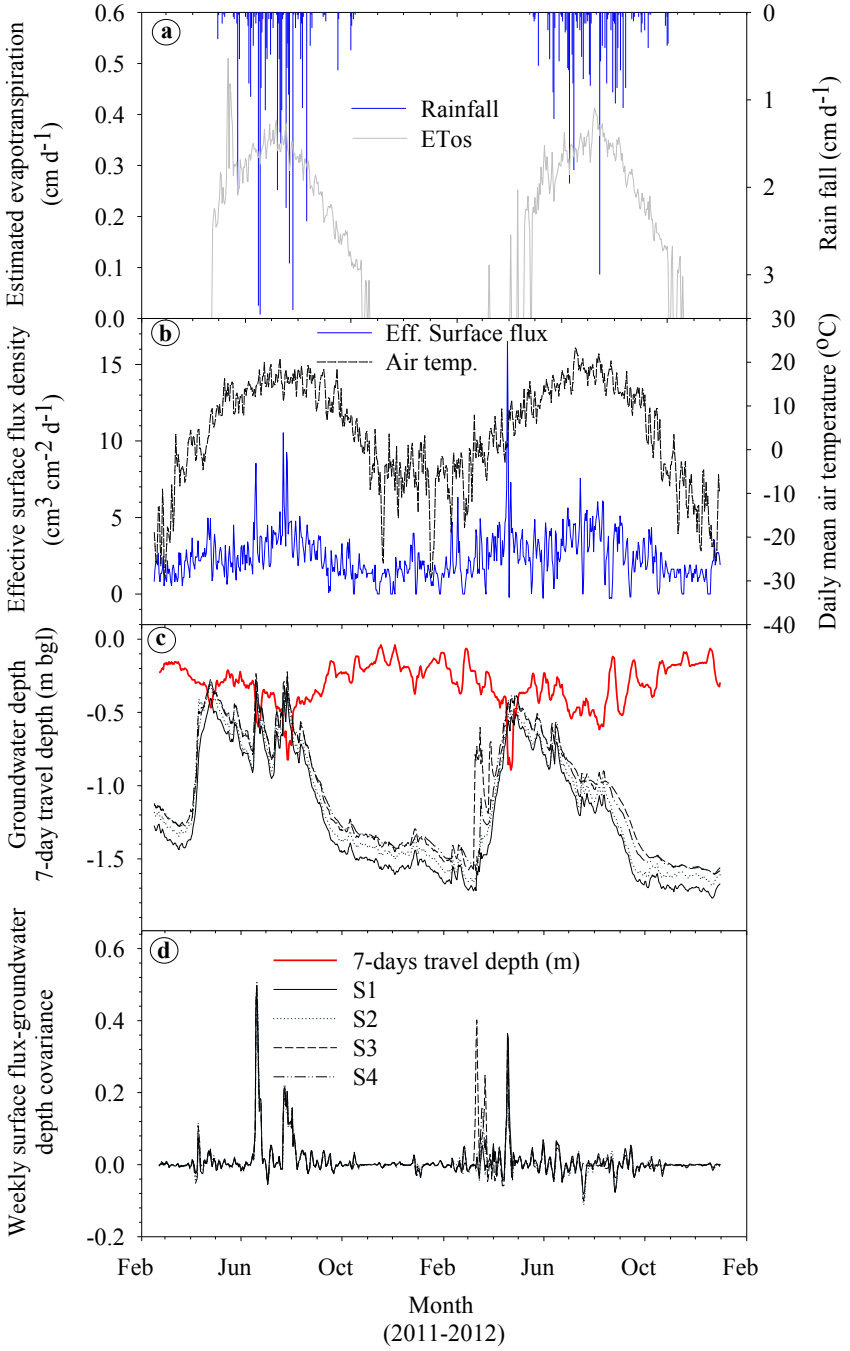

Figure 3-2: (a) Daily potential evapotranspiration, ETos and rainfall measured on-site (b) daily effluent surface flux density and daily mean air temperature, (c) groundwater hydrograph and 7-day travel depth, and (d) weekly effluent surface flux and groundwater depth covariance observed between Feb. 16, 2011 to Dec. 31, 2012 (685 days).

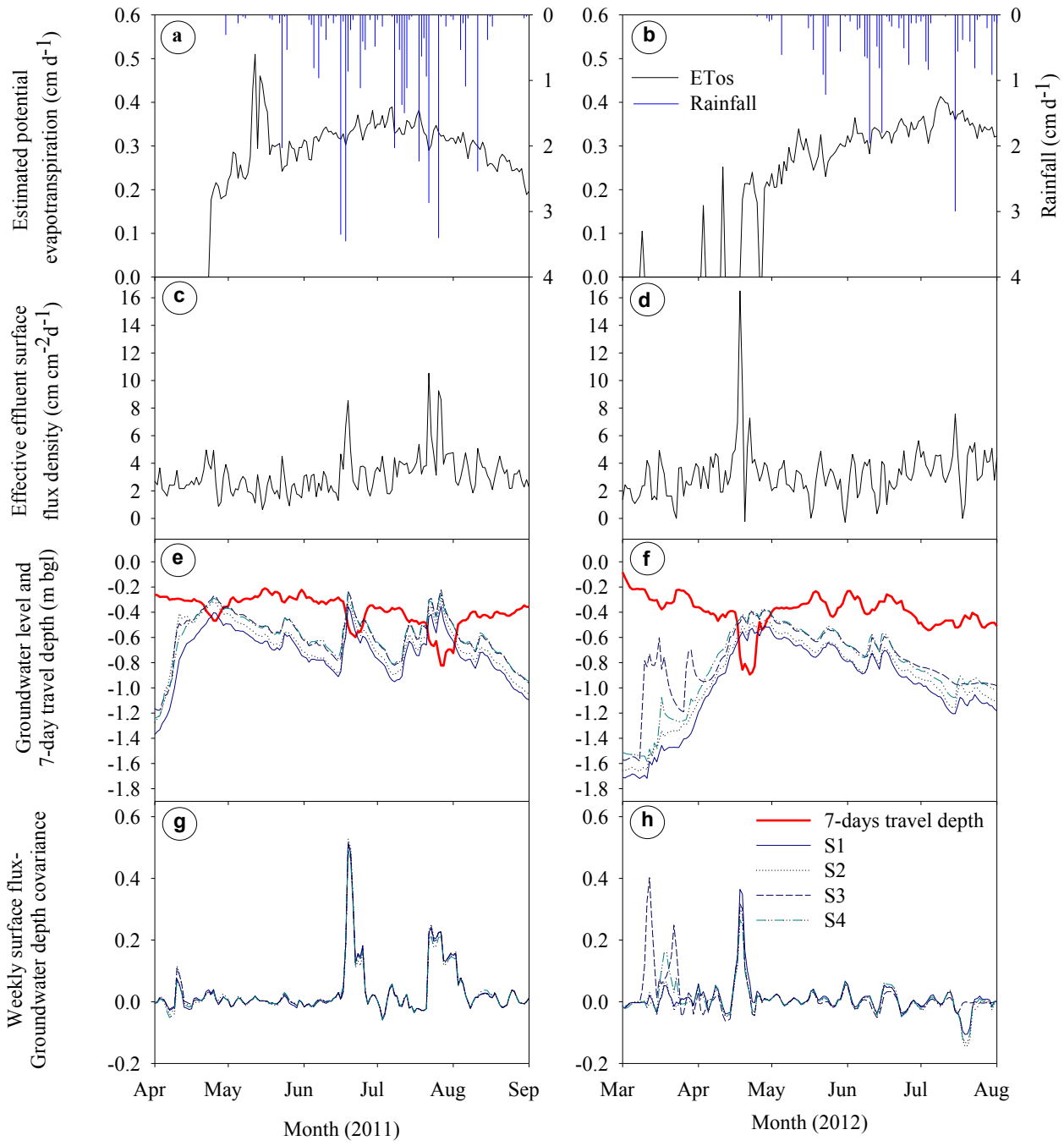

Figure 3-3: Time series focusing on the spring and summer periods for the two years (2011-2012). The graphs compare the weekly atmospheric boundary conditions for (a) and (b),. effective surface flux density (c) and (d), groundwater hydrographs (e) and (f), and surface flux and groundwater depth covariance (g) and (h).

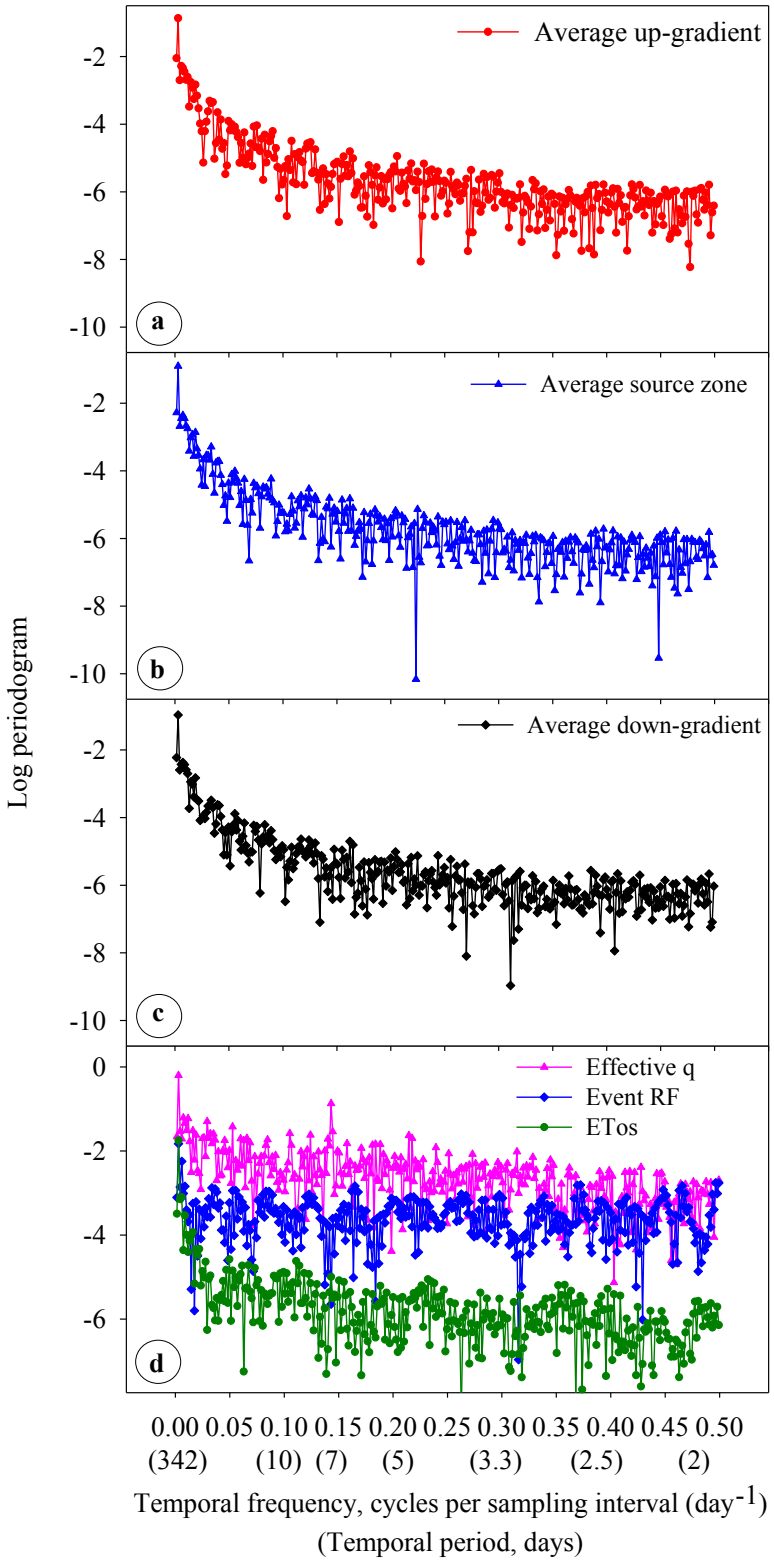

Figure 3-4: Periodogram of (a-c) dependent variable, *d(t)* and (d) independent variables, *q(t)*, daily RF and ETo measured on-site.

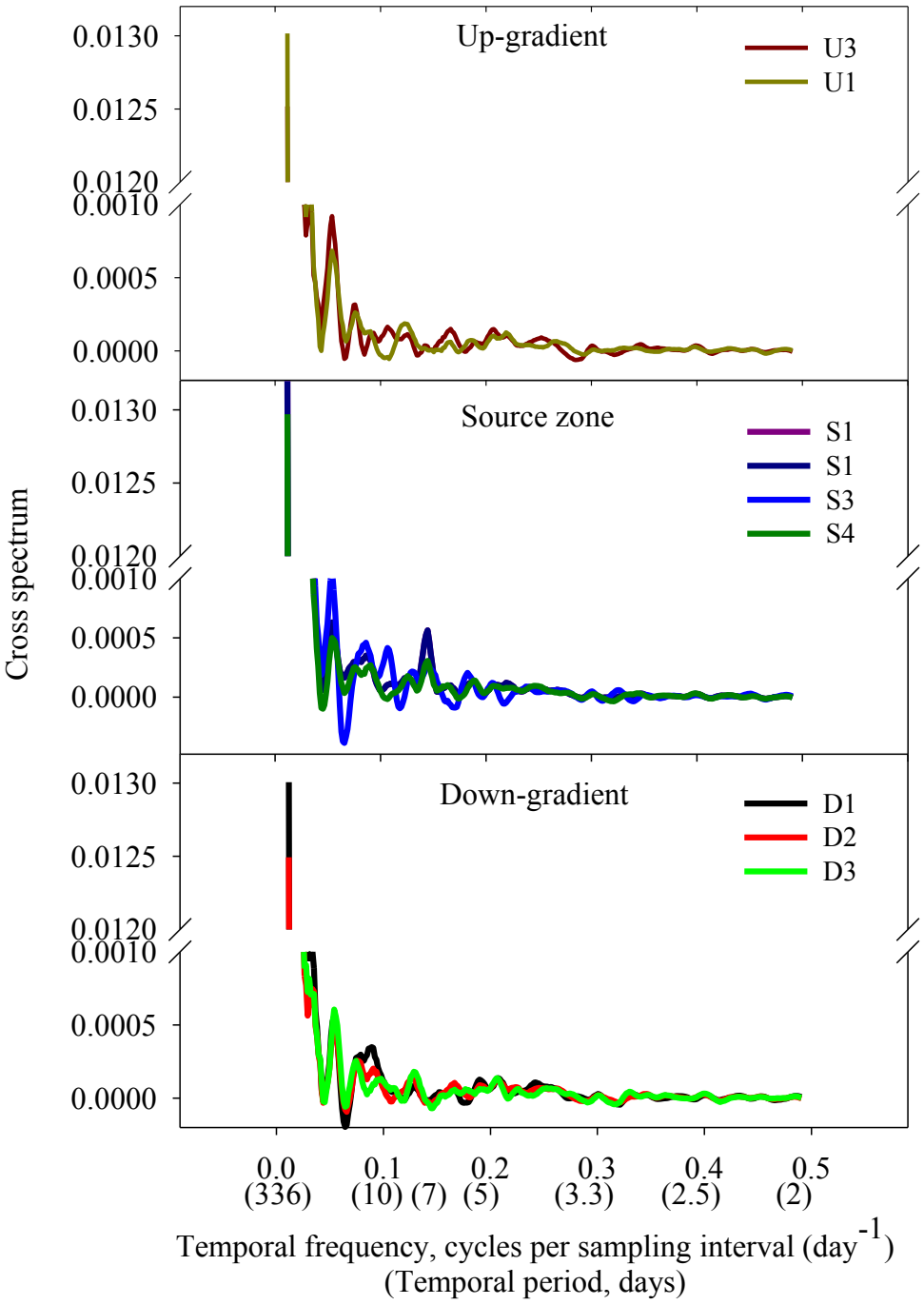

Figure 3-5: Cross-spectra between *q(t)* and *d(t)* for nine wells sorted by site. in the source zone, the spectral power picks at the weekly cycle.

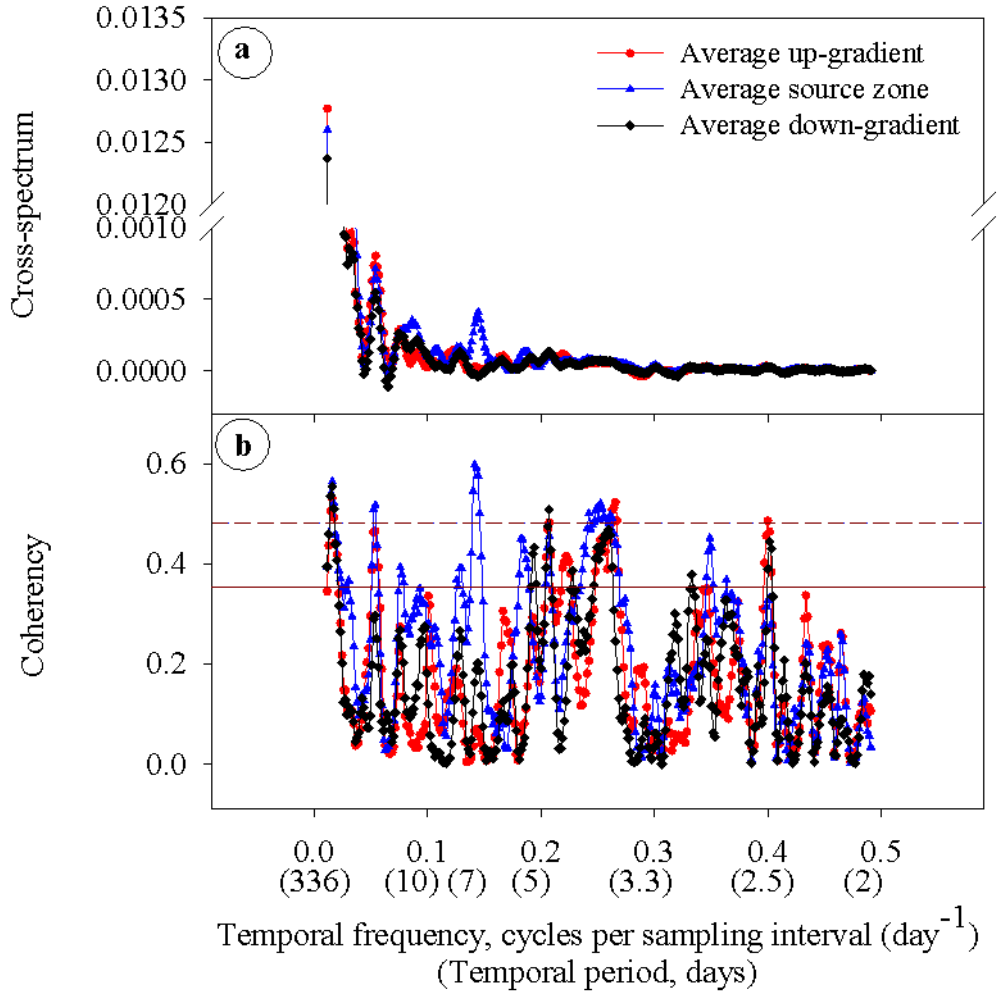

Figure 3-6: Average of *q(t)* and *d(t)* a) spectral cross-spectrum and b) spectral coherency for up-, down-gradient and source zones. The solid and dashed lines in (b) represent the significant coherency values at the 95% and 99% confidence levels respectively.

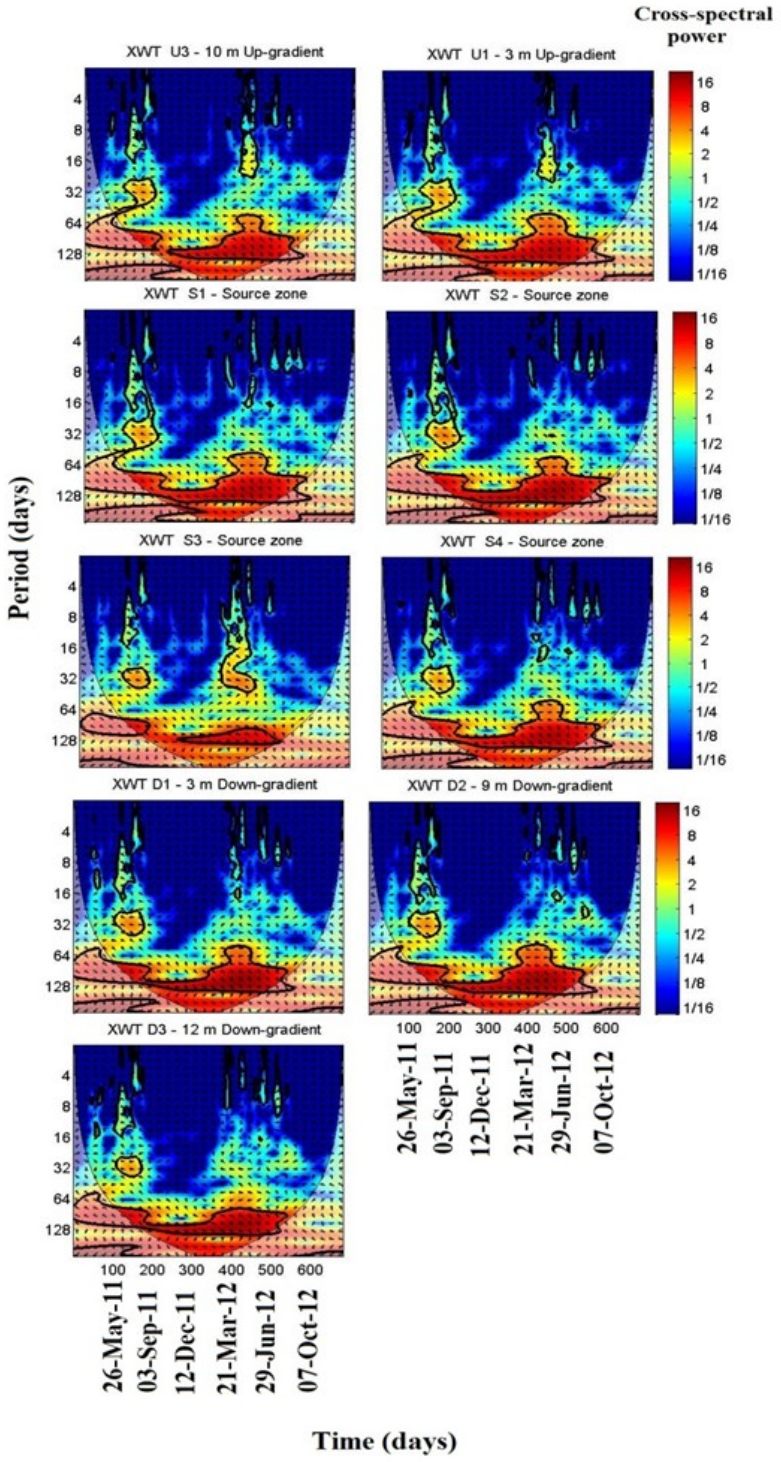

Figure 3-7: Comparison of wavelet cross-spectrum between effective surface flux density, *q(t)* and depth to water table, *d(t)* in the three zones (i.e., up-gradient: the top two Figures, source zone: the middle four Figures; and down-gradient: the bottom three Figures).

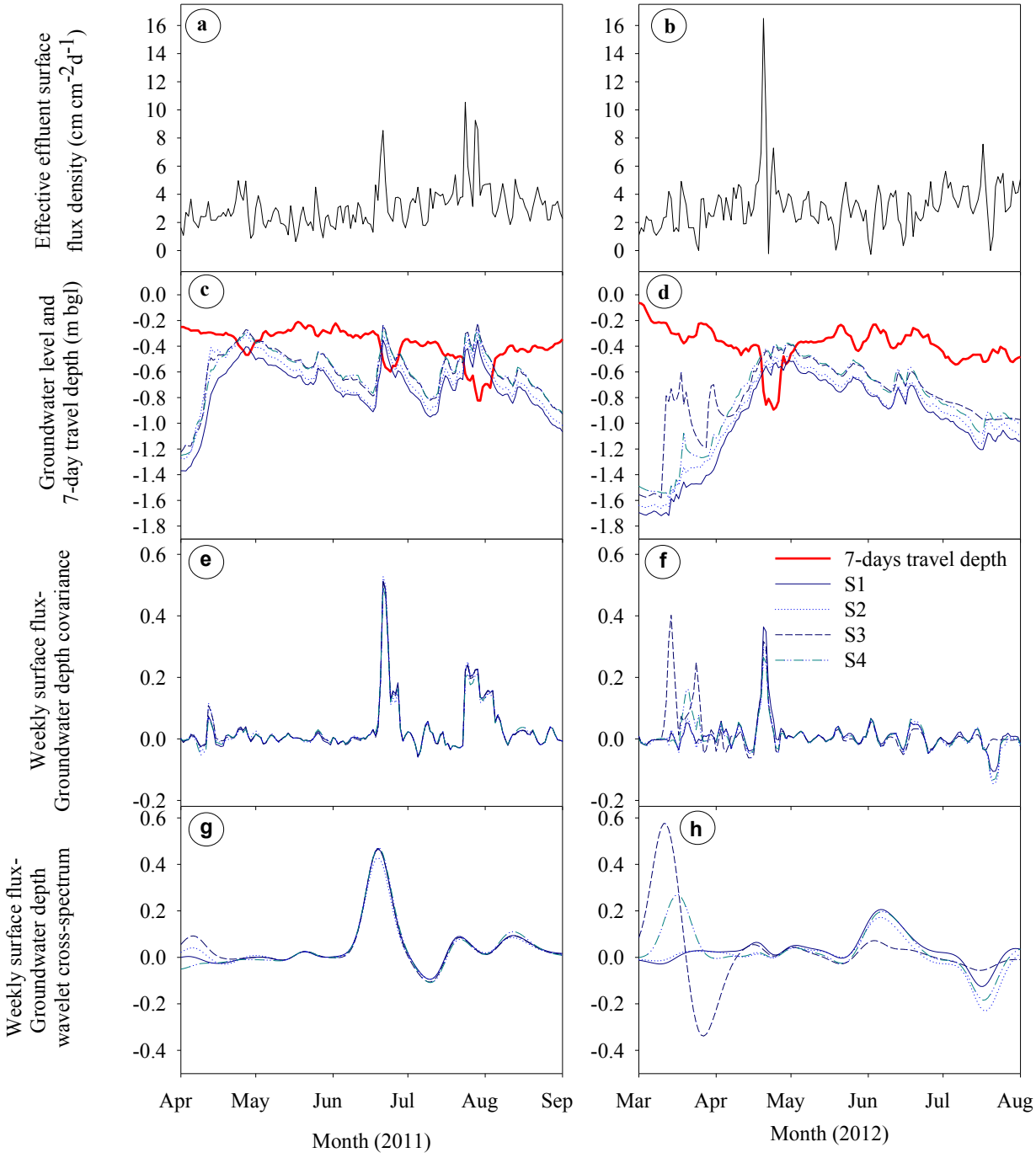

Figure 3-8: Time series focusing on the spring and summer periods for the two years (2011-2012). The graphs compare the weekly surface flux and groundwater depth covariance (e) and (f) and wavelet cross-spectrum (g) and (h) to the corresponding picks in the groundwater hydrograph (c) and (d) and effective surface flux density (a) and (b).

4. WASTEWATER FLOW AND PATHOGEN TRANSPORT FROM AT-GRADE LINE SOURCES TO SHALLOW GROUNDWATER

4.1. Introduction

Canada has approximately 7% of the world's renewable freshwater resources (Environment Canada, 2004). However, the Canadian people and industries are among the world's highest per capita water users, ranked second next to the United States. Approximately 30% of Canadians depend on groundwater supply and yet groundwater users frequently report municipal water shortages (Environment Canada, 2004). The Canadian population is also increasing and is projected to be close to 42.5 million by 2056 (Statistics Canada, 2008). With the increase in population, the demand for land development and maintaining a clean and adequate water supply is likely to grow. Therefore, in areas with water shortages use of treated wastewater may be a practical option (Menegaki *et al.,* 2007; Pedrero *et al.,* 2010). However, potential public and environmental health risks should be considered (Ganoulis, 2012; Hanjra *et al.,* 2012; Mutengu *et al.,* 2007; Pedrero *et al.,* 2010; Qadir *et al.,* 2010; Scandura and Sobsey, 1997; Weber *et al*., 2006).

Research has led to the invention of various wastewater treatment techniques including physical, chemical and biological systems that are operated at off-site (centralized) or on-site (decentralized) facilities. Nevertheless, the control of pathogenic microorganisms such as bacteria, viruses and protozoa and organic compounds that include pharmaceutical and personal care products, industrial and life-style compounds and caffeine remains a challenge. Elevated levels of organic compounds and emerging pathogens have been observed in the environment even following wastewater treatment (Crockett, 2007; Carrara *et al.,* 2008; Katz and Griffin, 2008; Katz *et al.,* 2009; Lapworth *et al.,* 2012; Lishman *et al*., 2006). To increase effluent treatment efficiency in on-site treatment systems, a combination of two or more treatment systems has been proposed – for example, ultraviolet wastewater disinfection combined with sand filtration (Crockett, 2007). In general, studies suggest revisions of the existing regulatory standards and industrial practices to address the aforementioned challenges.

Municipal wastewater consists of sanitary wastes collected in sewers from households, industry, commercial establishments and institutions; and typically contains human and other organic wastes, nutrients, microorganisms (pathogenic and nonpathogenic), suspended solids, household and industrial chemicals (CCME, 2009). In Canada, municipal effluents are managed

and regulated jointly by municipal, provincial/territorial and federal governments to improve environmental and human health protection (CCME, 2006).

In Canada, use of treated wastewater for toilet flushing, landscape and golf course irrigation is at an experimental stage (Exall*,* 2004; Exall *et al.,* 2006). Ordinarily, it is discharged to the environment after being treated. Canada discharges more than 3 billion cubic meters of treated effluent per year from over 3500 centralized wastewater treatment facilities to surface water bodies (CCME, 2006 and 2009). However, most of these treatment systems require repair and upgrading to avoid potential risks to human health and the environment (CCME, 2009; Gibson, 2014).

The magnitude and variability of pathogen transport through porous media depends on the level of saturation and pore size distribution. The solid-water-interface (SWI), air-water-interface (AWI) and the solid-water-air-interface (SWA) (see Figure 1-1 in Chapter 1) are believed as mechanisms for biocolloids' filtration or straining processes (Schijven and Hassanizadeh, 2000) but still there is controversy as to which of the processes is dominant (Hassanizadeh, 2012).

The attachment and detachment of biocolloids to soil particles has been an area of research in recent years at column or bench scales (Torkzaban *et al.,* 2006; Torkzaban *et al.,* 2008; Michen and Graule, 2010). Scaling-up these studies to field-scale could help better predict the magnitude and variability of these processes under prevailing field boundary conditions. The nature of the AWI changes with soil water content which affects the potential adsorption of bio-colloids. Spatially and temporally variable soil water content in response to transient infiltration of effluent are commonly observed in on-site wastewater treatment systems and the magnitude of these fluctuations depends on the magnitude and frequency of effluent applications.

Convective-dispersive transport processes for biocolloids and nonreactive tracers are dependent on soil structure variability and soil particle size distribution (Guber *et al.,* 2005; Pang *et al*., 2008). Pang *et al* (2008) reported more convective and less dispersive transport of microbes than that of bromide (Br) in structured soils as compared to a uniform, single-grain dune sand, resulting in slower velocity of microbes than Br in sandy soils (Pang *et al.,* 2008; Shelton *et al.,* 2003; Guber *et al.,* 2005). This has been explained by size exclusion (i.e., preferential transport of bacteria in large pores) and the presence of large inter-aggregate macropores in structured soils, which are absent in structureless sandy soils. Guber *et al* (2005)

also observed reduced biocolloid straining in high flow velocity fields. Microbes such as *E.coli* can be transported through the mobile portion of the soil water excluding the adsorbed phase (immobile phase), while Br may include the slow velocity zones near the solid surfaces, which might not be available for *E.coli* transport (Pang *et al.,* 2008).

Shallow groundwater conditions, low winter temperatures and elevated groundwater pH conditions has been shown to increase groundwater contamination risks (Bales *et al.,* 1995; Scandura and Sobsey, 1997). Bales *et* al (1995) observed pH-dependent attachment (at pH = 5.8) and detachment (at pH = 6-8) of viruses in a sandy soil. Scandura and Sobsey (1997) observed viral contamination of groundwater from on-site wastewater treatment systems during times of the year with shallow water table conditions and during the lowest winter temperatures in North Carolina. The authors, (Scandura and Sobsey, 1997), also observed extensive reduction of virus, bacteria and nutrients when the field soils of on-site septic systems contained ≥15% clay or when the vadose zone is ≥1 m thick. About $5\ log_{10}$ reduction in enteric viruses were also observed when they were exposed to 23°C compared to 10°C in 20 days (Blanc and Nasser, 1996).

Virus attenuation is also sensitive to soil moisture content with studies showing higher virus die-off in unsaturated soils than saturated (Blanc and Nasser, 1996). Similarly, Alhajjar *et al* (1988) reported higher inactivation rates of viruses under aerobic conditions and further proposed sorption of viruses to aquifer sediments was a reversible reaction under favorable conditions. Factors affecting attenuation - pH, ionic strength, flow rates and soluble organics – are subject to change (i.e., adsorption may be variable or reversible). Elevated virus counts with distance away from the effluent drain fields were observed with decreased levels of ionic strength in the groundwater (Alhajjar *et al.,* 1988). Viruses may remain infectious when sorbed to high ionic strength aquifer sediments suggesting that these sediments become potential sources of pathogenic microbes.

On-site wastewater treatment systems (OWTS) are alternative wastewater treatment options that are serving approximately 25% of Canadian and the United States populations (US-EPA, 1997). They are commonly used in individual homes in rural areas or in remote public park areas where centralized wastewater treatment systems are not practical. The OWTS are also used in some urban settings because of the high costs for building new centralized systems and maintaining the existing ones (McCray et al., 2005; McCray and Christopherson, 2008, Lowe *et al*., 2008; Durnie, 2008; Sen, 2011). In Alberta, an estimated 300,000 private sewage

systems are in use and increasing at a rate of 7,000 per year (Durnie, 2008). However, there are issues with the increasing use of private sewage systems, notably the availability of suitable land for OWTS, increasing development density, cumulative loading, localized groundwater mounding, regulatory needs, potential system failures and environmental contamination. Recently, the US-EPA (2013) issued concerns that approximately 10-20% of the OWTS systems in the US fail each year putting public health and the environment at risk.

A conventional OWTS has four main components: wastewater source, septic tank (pre-treatment unit), infiltration gallery and soil absorption field (McCray *et al.,* 2005). It is believed that most of the treatment processes take place in the soil absorption field and yet the nature of physical flow and transport processes through the soil absorption field are poorly understood (Sen, 2011). Alternative design approaches to the conventional septic system are being considered in areas where soil and site conditions are not suitable for treating septic tank effluents (e.g. restrictive layer or shallow water table) (Jantrania and Gross, 2006). The use of LFH at-grade soil-based dispersal systems is one of the alternative options being used in areas with shallow water table conditions (Jantrania and Gross, 2006; Verma, 2008; Motz *et al.*, 2011). In LFH at-grade systems the effluent is dispersed on the ground surface via pressured and perforated pipes that are laid a few centimeters above the ground and are covered with dome-shaped, plastic chamber and wood chips. The advantage of LFH at-grade systems is that use of the available soil depth above the restrictive layer such as shallow water table to filter the treated effluent as it passes through the soil, however, they are also more prone to fluctuations in temperature and soil moisture that could strongly impact pathogen removal (Verma, 2008 and Motz *et al.,*2011). As new systems in Alberta, regulators and the on-site wastewater industry wanted to quantify the effectiveness of the new LFH At-Grade soil based wastewater absorption and treatment system design (Safety Codes Council 2009 and 2012).

An on-site wastewater treatment system equipped with an ultraviolet (UV) wastewater disinfection system and pressurized at-grade line sources was established at the Wetaskiwin Rest Stop on Highway 2 by the Alberta Municipal Affairs in the fall of 2007. Disinfection by UV is one of the techniques used to kill pathogens in drinking waters as an alternative to chemical methods (Meulemans, 1987; US-EPA, 1999; Zimmer and Slawson, 2002). It is an effective method in killing most viruses, spores, and cysts within 250 to 270 nm wavelengths. The UV system works by transferring electromagnetic energy from a mercury arc-lamp to the organism's

genetic material (DNA and RNA) and it inactivates the reproductive ability of the organisms by destroying the reproductive cells (US-EPA, 1999). Nevertheless, the efficiency of the UV disinfection system depends on the characteristics of the wastewater, the intensity of UV radiation, the length of time microorganisms are exposed to the radiation, and the reactor configuration. Its function and effectiveness may be impaired by turbidity and high levels of total suspended solids (e.g. >30mg/L) and it is less effective at low UV intensities (US-EPA, 1999; Zimmer and Slawson, 2002; Shin *et al.,* 2010). Microorganisms may also have natural mechanisms to repair their DNA, that is, dark repair or photo repair mechanism. Zimmer and Slawson, (2002), observed the photo repair potential of *E. coli* following exposure to low-intensity and medium-intensity UV sources. Recently, Ben Said and Otaki (2013) observed reactivation of *E.coli* following UV disinfection and suggested post-UV treatment. In practice, it is likely that there is no 100% effective disinfection technique and pathogenic microorganisms can grow rapidly (WHO, 2004). In addition, UV wastewater treatment systems require operation and maintenance that increases treatment costs compared to other disinfection systems like chlorination (US-EPA, 1999; WHO, 2004; Health Canada, 2006).

For soil-based wastewater treatment systems, the Alberta Safety Code Council has developed regulations for many aspects of the system including a minimum vertical separation required between a point of effluent infiltration and a water table or an impervious layer (Safety Code Council, 2012). The vertical separation considers the quality of the effluent and the depth of the suitable soil required to achieve a 7-day travel depth to the treatment boundary. For primary and secondary treated effluents such as from septic tanks and wastewater treatment plants respectively, the recommended vertical separation between the infiltration surface and the water table is 1.5 and 0.9 m, respectively. Similar regulations are also available in other provinces of Canada. The British Columbia Municipal Wastewater Regulation (2012) indicates 6 to 10 days of subsurface travel time for a municipal effluent before it reaches a receptor. However, these regulations have not been verified using field measured data, and thus research was needed to determine a safe separation depth between the point of effluent entry and the groundwater.

The focus of this study is to better understand wastewater flow and transport processes from at-grade line sources installed on a shallow groundwater system. An in-situ field scale experimental approach was adopted using naturally existing biocolloids in the wastewater and

nonreactive tracers under boundary conditions typical of OWTS on shallow groundwater conditions. By turning off the UV, we introduced a step impulse of untreated effluent (*E. coli*) and also simultaneously applied a short pulse of bromide (conservative) to better understand the transport processes, transport pathways and environmental risks associated with OWTS. We are not aware of any similar experiments reported in the literature and hence it is a novel approach. The evaluation of the new OWTS with respect to the existing guidelines and standards of practice helps to develop appropriate guidelines and standard of practices for designing effective OWTS. The specific objectives were (i) to identify wastewater flow pathways and transport through the saturated and unsaturated zones; (ii) to quantify flow and transport parameters and (iii) to examine and evaluate effective vadose zone thickness that potentially filter/treat wastewater before pathogens reach the groundwater.

4.2. Materials and Methods

4.2.1. Site Description

The study was conducted at the Wetaskiwin Rest Stop (N52°53'43''and W113°38'33'') located 80 km south of Edmonton, Alberta, Canada. The Rest Stop was equipped with seven toilets, two urinals, seven hand washing sinks, septic tanks, and an Ultraviolet (UV) wastewater disinfection system. It generates an average of 8.94 m^3 wastewater daily. As a pilot project, the UV disinfection system was established in 2007 by the Alberta Municipal Affairs. A Detailed site description has been given in Chapter 2.

At the start of this study, the site had received UV-disinfected effluent for about four years. The wastewater from the Rest Stop was conveyed to settling tanks, where the solid fraction settled, and the liquid fraction was pumped forward to subsequent tanks for further treatment including FAST (Fixed Activated Sludge Treatment) and UV disinfection (refer to Figure 2-6b in Chapter 2). After UV-disinfection the effluent was pumped to infiltration fields via pressurized, at-grade line sources, polyvinyl chloride pipes each with 3.175 cm internal diameter, which are referred to hereafter as laterals. In total, there were three infiltration field zones, each with five laterals. The laterals were laid by raising them 10-cm above the ground surface and encompassed by an arc-like shape Quick4® standard chamber (width = 0.85 m and height= 0.31m) (Infiltrator Systems Inc., 2006) to guide the effluent infiltration and to ensure a uniform wetting of the infiltration bed. The chambers were also covered with a 30 cm thick

layer of wood chips to protect the laterals from freezing, rodents and for aesthetic reasons. Our study was conducted in one of the infiltration field zones with four laterals (Figure 2-3, Chapter 2). Each lateral was 40 m long by 0.61 m wide giving 24.4 m^2 infiltration bed area per lateral.

4.2.2. Soil Resources and Hydraulic Properties

The soils on the study site were classified as Black Chernozems overlying shallow groundwater at approximately ~1.1 m below ground surface (Figure 2-9 in Chapter 2). The soil particle size distribution for the upper 0 to 1.5 m depth below the ground surface is given in Table 4-1 (detailed site description is given in section 2.2.1.2). The soil samples were collected at 20 cm depth interval at three sites along transect A-A′ (Figure 4-1a).

Soil hydraulic properties were determined from undisturbed soil cores that were collected from three sites: Site A: 0-1.68 m, Site B: 0-2.20 m and Site C: 0-3.30 m (Figure 2-6 in Chapter 2) at 20 cm depth interval using a Geoprobe. The cores were sliced into 3-5 cm increments (4-5 cm ID) making a total of 110 core samples from the three sites. The soil water pressure head and soil water content were determined by a hanging water column and pressure extraction techniques (Reynold and Topp, 2006) at seven matric potential values (0, 0.05, 0.1, 0.3, 1, 5 and 15 bar) selected a priori. The hydraulic parameters - i.e. residual soil water content (θ_r,), saturated soil water content (θ_s,) [L^3 L^{-3}], and van Genuchten parameters, α, [L^{-1}] and n [-] (Table 2-2) - were obtained by fitting the van Genuchten-Mualem model (Equation 2-1 and 2-2) to the measured data using a RETC program ver. 6.02 (van Genuchten, 1980; van Genuchten *et al.,* 2009).

In-situ saturated soil hydraulic conductivity, Ks was measured from a nest of piezometers installed at the site as described in the following section (Figure 4-1). A bailer method was used where by the standing water was purged and subsequent rise in water level was recorded at a given time interval using Solinst water level meter. Saturated soil hydraulic conductivity was then estimated using piezometer and auger hole methods (Topp and Sattlecker, 1983) as:

$$K_s = \left(\frac{\pi r^2}{S\Delta t}\right) \ln\left(\frac{y_0}{y_t}\right) \qquad [4.1]$$

Where: Ks is saturated hydraulic conductivity (L T^{-1}), r is radius of the piezometer well (L), Δt the time interval (T), y_0 and y_t are heights of water below the equilibrium water level initially and at Δt later respectively, and S is the shape factor (L) for the measured cavity that depends on i) the distance of the measured cavity or surface below the water table, ii) the height of the cavity, iii) radius of the cavity and iv) the distance below the cavity to the impermeable layer. The value of S can be found in tables (Youngs 1968).

4.2.3. Field Tracer Experiment

4.2.3.1. Experimental set-up

Prior to the detailed wastewater flow and transport study, the groundwater hydrology and the extent of existing wastewater plume (Figure 4-1a) were characterized using groundwater level and water samples collected from a dense grid of 99 stand pipes (diameter = 1.25 cm) installed over a 1.5 ha area. The wastewater plume center of mass was estimated from the measurements of the spatial distribution of the groundwater EC using the Kriging linear interpolation method in the Surfer® program (Golden Software, Inc., 2009; Figure 3a).

Ten nests of piezometers (three piezometers per nest, N=30) were installed along the estimated groundwater EC plume center of mass and the average groundwater flow direction (Figure 4-1b). The piezometers are referred to hereafter as monitoring wells. These monitoring wells were used to track wastewater flow and pathogen transport over time and space. The nests were numbered as 1 to 10 starting from up- to down-gradient with respect to the at-grade line sources (laterals). Nests 1 and 2 were in the up-gradient, 3 to 5 were in the source zone and the remaining (6 to 10) were located in the down-gradient of the source zone. A schematic representation of the three dimensional transport domain and the effluent source tanks is also shown in Figure 4-2.

In each of the piezometer nests, the three monitoring wells (MWs) provided point measurements centered at 0.94 m, 1.29 m and 1.55 m below the ground surface (Figure 4-1b). The shallowest MW (0.94 m) was screened over a 0.5 m interval and the other two were screened over a 0.25 m interval. Before the start of the tracer experiment, the wells were developed by purging every two days for a week. In the first tracer experiment, we used two tracers: bromide (Br) as a nonreactive tracer and naturally occurring *Escherichia coli* (*E.coli)* as a biocolloid tracer. Bromide, as a pulse input, was added to the effluent source tank on July 27,

2011 (details are given in section 4.2.3.2) and two days later, on Jul 29, 2011, the UV disinfection system was turned off and untreated (i.e., no UV) effluent was applied to the infiltration field via pressured at-grade line sources for three months. The untreated wastewater *was* applied as a step function.

The experimental set-up and the tracer application time was delayed by a month from the original plan pending for installing wider wells that recover enough water volume for microbial analysis and resulted in a narrow window for background sampling. Therefore, water samples from the monitoring wells and the source tank were collected only once before the UV-disinfection system was turned off.

4.2.3.2. Bromide Injection and Tracer Pulse Duration

In the first experiment, 2 kg and 5.092 kg $CaBr_2$ and KBr respectively was dissolved in 4546 L of effluent volume in the source tank at one time to instantaneously bring the concentration to 2 g Br L^{-1} (Figure 4-2 and 4-3a). Similarly, a 4.546 kg Br mass in the form of KBr was added to effluent tank instantaneously to bring the concentration to 1 g Br L^{-1} in the second experiment period (Figure 4-2 and 4-3b). From the total effluent volume, 3637 L was applied to the infiltration area (97.6 m^2) via four laterals intersecting the monitoring well nests described above (the remaining 909 L was applied to the to the fifth line which was not included in the present study because its location was away from the influence of the monitored transect, see Chapter 2 for details). Therefore, the total Br mass added to the instrumented infiltration area was 41 g Br m^{-2} and 25 g Br m^{-2} in 2011 and 2012 respectively. The concentration of bromide in the source tank was measured on the same schedule as the monitoring wells (see next section) and declined significantly within two days after the injection due to removal of Br-rich effluent from the tank and being applied to the infiltration field, and subsequent dilution by the incoming of Br-free effluent to the source tank every time a the controlling system triggered a dosing event. For evaluation of Br transport, the dilution effect is represented by an exponential decay impulse response function (Figure 4-3). In both experiments, it took approximately 3 days for all of the Br-rich effluent to be removed from the source tank and be applied to the treatment zone and hence it was assumed as instantaneous input.

4.2.3.3. Groundwater Sampling and Laboratory Analysis

During the field tracer experiments, water samples from the effluent source tanks and the MWs were collected at weekly to biweekly intervals for one year after the first Br pulse, and for two months following the second Br pulse. The samples were analysed for Br, *E.coli*, total coliforms, EC, pH, and viruses. Additional groundwater and effluent samples were also collected for routine analysis four times: two before- and two after-Br injection. A total of 1596 groundwater and effluent samples were collected for chemical and microbiological analyses during the 2011-2012 field tracer experiments (Table 4-2).

The groundwater samples were collected from the MWs using dedicated tubing with a footvalve for each well to ensure no cross contamination. Two days prior to every sampling date, two to three well volumes were purged. A 20 mL sample for Br and 200 mL sample for *E.coli* and total coliforms were collected from each well and transferred to clean and sterile sampling bottles. The samples for the microbiological analysis (*E. coli* and total coliforms) were transferred into the sterile bottles containing a preservative, sodium thiosulphate ($Na_2S_2O_3.2H_2O$). All the samples were then stored in a cooler box with ice packs that kept the temperature at <4°C during transportation from the field to the laboratory.

Each sample for Br analysis was filtered through a 0.045 micron filter before analysis, and was analyzed within one to two weeks after the date of sampling by Ion Chromatography (IC; Dioxin 6000) in the Natural Resources Analytical Laboratory, department of Renewable Resources, University of Alberta. Analyses of *E.coli* and total coliforms were conducted within 24 hours of the sampling time using standard IDEXX Quanti-Tray®/2000 Colilert *E. coli* and total coliforms enumeration techniques in the Provincial Laboratory for Public Health (ProvLab), University of Alberta Hospital (APHA *et al*., 2012). The Quanty-Tray®/2000 Colilert is a semi-automated quantification method that works based on the standard method of Most Probable Number (MPN) model and the results were reported as MPN per 100 mL (IDEXX Laboratories Inc. 2002).

Electrical conductivity (EC) and pH were determined for each water sample on-site within 5 to 10 minutes of sampling using a portable Thermo-Orion 5-plus meter at biweekly to bimonthly intervals. Samples for the routine geochemical analysis for non-biological parameters (Table 4-3) were sent to Exova Environmental Laboratory and were determined using the

American Public Health Association (APHA) standard methods for the examination of water and wastewater (APHA, 1999).

Virus testing was conducted during the second season Br pulse experiment (Summer 2012). Water samples for virus analysis were sent to the Provlab, University of Alberta Hospital. The water samples were analyzed using a real time quantitative polymerase chain reaction (rtPCR) approach following the procedure developed by Pang *et al* (2012). A polymerase chain reaction is a molecular procedure used for virus detection in water samples (Fout *et al*., 2003) and it is more rapid and sensitive to detect enteric viruses compared to cultures (Pang *et al.,* 2012).

4.3. Data Analysis

4.3.1. Hydraulic Gradient Estimation

Pressure head in each of the piezometers along the main transect A-A' (Figure 4-1) were measured for more than 14 months from July 2011 to December 2012 using a Solinst water level meter at weekly to bi-weekly intervals before purging and water sampling events. The pressure head in the piezometers and the elevation of the center of the piezometers' screen were used to calculate total hydraulic heads which in turn were used to estimate the spatial and temporal distribution of hydraulic gradients along the transect and a seasonal average was obtained.

4.3.2. Groundwater and Effluent Geochemistry

The ionic strength (I) of a solution, a measure of the concentration of dissolved chemical constituents, in the groundwater and the effluent was determined using the expression by Bundschuh and Zilberbrand (2012) and Kennedy (1990) as follows:

$$I = \sum_{i-1}^{n} C_i Z_i^2 \qquad [4.2]$$

Where: C_i is concentration of the i^{th} species [mol L^{-1}], and Z_i is valence number of the i^{th} species. The calculation was made assuming a complete dissociation of the ions (that is, no association into ion pairs or complexes) because these associations, H^+ and OH^- do not likely contribute significantly to the ionic strength.

4.3.3. Bromide Transport

Spatial moment analysis was used to characterize the transport and dispersion processes from the Br plume observed during the experiment period. The spatial moments define integrated measures of total tracer mass, mean velocity and dispersivity of the tracer plume at the field scale (e.g. Ellsworth *et al.,* 1991; Jensen *et al.,* 1993). Moment analysis methods are nonparametric and model-independent approaches that do not need a priori assumptions about the transport processes while providing a physically sound plume characteristic (Ellsworth *et al.,* 1991). In this study, we calculated the zeroth moment, *Mo* [mass recovery; M L^{-2}]; first central moment, $E[k]_t$ [L]; and second central moment, $Var[k]_t$ L^2], where: k denotes a spatial coordinate either x or z depending on the direction of interest, (Freyberg, 1986; Ellsworth *et al.,* 1991, Garabedian *et al.,* 1991, Jensen *et al.,* 1993; Vanderborght and Vereecken, 2001; Kumar and Sekhar, 2005; Woods *et al*., 2006; Woods *et al*., 2013). These moments estimate the solute mass in the monitoring zone; the mean spatial location of the plume along the monitoring transect; and the spreading of the plume about the mean respectively. For a two-dimensional flow and transport analyses the spatial moments are given as:

$$M_{0,t} = \int_{-\infty}^{\infty} \int_{-\infty}^{\infty} p c_w(x', z, t)\, dx' dz \qquad [4.3]$$

$$M_{1,t} = \int_{-\infty}^{\infty} \int_{-\infty}^{\infty} p x' c_w(x', z, t)\, dx' dz \qquad [4.4]$$

$$M_{2,t} = \int_{-\infty}^{\infty} \int_{-\infty}^{\infty} p x'^2 c_w(x', z, t)\, dx' dz \qquad [4.5]$$

Where: p is porosity measured from soil cores under laboratory conditions assumed to be approximately equal to the average, mobile soil water content determined [L^3 L^{-3}], C_w is solution concentration [M L^{-3}], x' and z are spatial coordinates [L] and x' is horizontal coordinate parallel to the groundwater flow direction.

Steps of moment analyses

We followed a similar approach to that used by Woods *et al* (2006, 2013). First, a bromide (Br) concentration [M L^{-3}] profile was estimated using linear interpolation (*dz*=5 cm) of the measured Br concentrations at the wells in each nest and all values outside the sampling interval were assigned a zero value. For each nest, the Br mass, *Mo(t)* [M L^{-2}] was obtained for each sampling time (Breakthrough, BTC) by spatially integrating the estimated Br concentration profiles:

$$M_{0v,(x\prime,t)} = \int_0^Z pC_{w,(x\prime,t)}(z)\,dz \qquad [4.6]$$

Where: $M_{0v(x\prime,t)}$ is zeroth moment for the vertical direction [M L^{-2}] at location, x', at time, t. The subscript v indicates vertical direction, p is porosity [L^3 L^{-3}], C_w is solution concentration [M L^{-3}], and Z and z are vertical (depth) coordinates [L] and Z is equal to maximum sampling depth (~155 cm). The domain porosity (p = 0.56 cm^3cm^{-3}) was estimated from soil cores in the lab.

The first moment ($M_{1v(x',t)}$) [M L^{-1}] and second moment ($M_{2v,(x',t)}$) [M] were calculated as:

$$M_{1v,(x\prime,t)} = \int_0^Z zpC_{w,(x\prime,t)}\,dz \qquad [4.7]$$

$$M_{2v,(x\prime,t)} = \int_0^Z z^2pC_{w,(x\prime,t)}\,dz \qquad [4.8]$$

For the horizontal spatial moments, first the depth-integrated concentration average was obtained by dividing the zeroth moment of each nest per snapshot as:

$$aveC_{wz,(x\prime,t)} = \frac{M_{0v,(x\prime,t)}}{Z} = \frac{\int_0^Z pC_{w,(x\prime,t)}\,dz}{Z} \qquad [4.9]$$

Using $aveC_{wz,(x',t)}$ (M L^{-3}) for each BTC, horizontal Br concentration was linearly interpolated at a regular interval of dx'=10 cm. The zeroth ($M_{0h,t}$) [M L^{-2}], first ($M_{1h,t}$) [M L^{-1}] and second ($M_{2h,t}$) [M] moments along the horizontal direction were obtained from the linearly interpolated Br concentration as follows:

$$M_{0h,t} = \int_{X1}^{X2} aveC_{wz,(x',t)}\, dx' \qquad [4.10]$$

$$M_{1h,t} = \int_{X1}^{X2} x' aveC_{wz,(x',t)}\, dx' \qquad [4.11]$$

$$M_{2h,t} = \int_{X1}^{X2} x'^2 paveC_{wz,(x',t)}\, dx' \qquad [4.12]$$

Where: $M_{0h,t}\ [ML^{-2}], M_{1h,t}\ [ML^{-1}],\ M_{2h,t}[M]$ are the zeroth, first and second moments for the horizontal direction respectively, the subscript *h* indicates horizontal direction, *x'* is the horizontal coordinate [L], and X2-X1 is the maximum horizontal sampling distance in the domain. The zeroth moment were also used for estimating Br mass recovery by dividing it to the Br mass applied to the laterals surface area $[ML^{-2}]$.

The mean travel depth or distance and travel depth or distance variance about the means for the vertical and horizontal directions were calculated as follows.

First central moments in the vertical and horizontal directions

$$E[z]_t = \frac{M_{1v}(x',t)}{M_0 v(x',t)} \qquad [4.13]$$

$$E[x']_t = \frac{M_{1h}(t)}{M_{0h}(t)} \qquad [4.14]$$

Second central moments in the vertical and horizontal directions

$$Var[z]_t = \frac{M_{2v}(x',t)}{M_{0v}(x',t)} - \left(\frac{M_{1v}(x',t)}{M_{0v}(x',t)}\right)^2 \quad [4.15]$$

$$Var[x']_t = \frac{M_{2h}(t)}{M_{0h}(t)} - \left(\frac{M_{1h}(t)}{M_{0h}(t)}\right)^2 \quad [4.16]$$

The surface pulse application reference center was approximated at the center of the source zone at the fourth nest from up-gradient site located between the middle two at-grade line sources (Figure 4-2). Therefore, the center of mass displacement over time was estimated based on the reference point using a solute transport velocity (*V(t)* [L T^{-1}] expression:

$$V(t) = \frac{\Delta\{E[k]_t\}}{\Delta t} \quad [4.17]$$

4.3.4. *E.coli* and Virus Fate and Transport Analysis

The fate and transport of *E.coli* and viruses were examined from field-observed breakthrough curves (Figure 4-10 to 4-15 and 4-16). The fact that the MWs that showed detectable levels of *E.coli* were limited (likely because of attenuation), moment analyses was conducted only using the Br concentrations but breakthrough curves of *E.coli* and Br were compared in the monitoring wells where both Br and *E.coli* were simultaneously measured and detected. Similarly, breakthrough curves of Br and viruses were also compared.

4.4. Results and Discussion

4.4.1. Groundwater and Effluent Geochemistry

The hydrogeochemistry of the groundwater and the effluent before and after Br injection were comparable. The median coefficient of variation (CV) was within 10%, and hence the results were averaged. The average values of the groundwater and the effluent chemical characterization and the corresponding ionic strength are presented in Table 4-4. On average ionic strength increased with depth and this result was used in the virus transport section.

The spatial distribution of Nitrate-N (NO_3^--N) and Nitrite-N (NO_2^--N) below the source zone at two sampling times is given in Figure 4-5. The NO_3^--N and NO_2^--N plume indicate: (i) the impact of the wastewater on groundwater, as reflected with higher nitrate and nitrite levels in the source zone compared to the up- and down-gradient zones, and were higher than the drinking groundwater standard (Health Canada, 2012), (ii) wastewater plume movement along the general groundwater flow as indicated by the increased concentration of nitrate and nitrite in the down-gradient direction, and (iii) groundwater fluctuation and vertical gradients as shown by the irregularities in the plume shape and vertical extent of the plume. Manganese (Mn^{2+}) concentrations were also low in the source zone showing reducing conditions under the source zone resulting from the wastewater infiltration, but it is unclear whether these reducing conditions are a result of saturated conditions below the laterals, or increased biological oxygen demand in the wastewater.

4.4.2. Hydraulic Heads and Groundwater Flow Direction

The average seasonal spatial distribution of hydraulic head along the measurement transect in nests (at the up-gradient, source and down-gradient zones) with measurable hydraulic heads and approximate contour of equipotential lines is given in Figure 4-4. Hydraulic heads were on average 20 to 30 cm greater in 2011 compared to 2012, which is also reflected in the groundwater level data summarized in Chapter 3. In general, the direction of groundwater flow along the measurement transect, as interpreted from the spatial distribution of hydraulic head, was consistent over the spring and summer seasons of 2011 and 2012. In the horizontal direction, the hydraulic heads varied 20 to 40 cm over horizontal distances of 20 meters, resulting in a horizontal gradient of 0.01 - 0.02, consistent with that reported in Chapter 2. Because of the short vertical distance between well screens, there was significant uncertainty associated with the vertical hydraulic gradients. The vertical distance between well screens within a nest ranged from 25 to 40 cm. Water elevation measures likely had errors of at least 2 or 3 cm. Therefore, the estimation error associated with vertical hydraulic gradients was greater than the estimated horizontal gradient because of the relatively short vertical distance between well screens compared to their horizontal separation. In the spring 2011, spring 2012 and summer 2012 periods, hydraulic heads within nests did not differ by more than 3 to 5 cm which was within the range of measurement errors. In the summer of 2011, hydraulic heads differed by up to 30 cm between nests, suggesting downward vertical gradients of 0.1 to 0.2. Assuming these gradients

were representative of the long-term, the net groundwater flow direction is downward and to the northeast. The northeast flow direction indicated by the gradients was consistent with the EC plume presented in Chapter 2. Hereafter, then, the northeast direction will also be referred to as the down-gradient direction and the southwest will be referred to as the up-gradient direction.

4.4.3. Observed Tracer Movement

4.4.3.1. Br-Plume Transport and Spatial Moment Analysis

Hand-drawn contours of the bromide (Br) plume at different snapshots in time (from t=0 to 406 days) are presented in Figure 4-6a-f. The time after the second Br pulse was July 25, 2012 (t=364 days) and it is shown in Figure 4-6e. The contours were produced using linear interpolation of Br concentration data between sampling points**.** Spatial moments (zeroth, first and second moments as well as estimated first and second central moments and plume flow velocity are summarized in Tables 4-5 (horizontal moments) and 4-6 (vertical moments). The relationship between vertical and horizontal central moments is also given in Figure 4-7.

The minimum and maximum Br mass recoveries (Eq. [4-6] and Eq. [4-10] were 0% and 75% with an average of 27% during the first Br pulse experiment period (July 27, 2011 to July 28, 2012). The mass recovery was calculated as the total Br mass applied per the effluent application area under the laterals assuming no horizontal dispersion at the edges of the plume. A separate mass recovery for the second Br pulse was not practical because it was influenced by the remnant from the first pulse. However, when considering the Br mass applied in both pulse experiments, the maximum, minimum and average Br mass recovered after the second pulse (August 01, 2012 to September 12, 2012) were 32, 7 and 24% respectively. The differences in recovery were likely attributed to groundwater fluctuation; for example, 0% was recovered when most of the monitoring wells were dry before snow melt period. In addition, the analysis was based on that of Br mass that was obtained from the monitoring zone that is in the saturated zone within the monitoring wells' interval, however, unaccounted Br mass was expected in the un-sampled unsaturated zone. The percent recovery after the second pulse was low because the data was only collected for short period that is 49 days after the second pulse application.

Bromide-spiked effluent from the surface tank was first applied to the soil via the laterals on July 27, 2011. This time is set to t=0 in Figures 4-6, and 4-10 through 4-12. The first detectable concentrations of Br were observed in the nest of monitoring wells below the two

northern-most effluent laterals, followed by the wells located at 1.0 and 2.0 m down-gradient of the source zone (Figures 4-6 & 4-9). The first groundwater sampling date was four days after the first day (t=0) of Br pulse application and Br was detected in those samples from MWs 3 (0.97 m), 5 (0.94 m), 6 (0.95 m), 7 (0.94 m), 7 (1.33 m), 7 (1.58 m) and 8 (0.93 m). As shown in Figure 4-6, the transport of this first plume was consistent with the groundwater flow inferred from Figure 4-4, lending confidence to measured hydraulic gradients. The initial arrival of the Br in this location was likely because the groundwater table was about 40-cm closer to the surface at the down-gradient end of the source zone. During the week of Br pulse application (July 27 to Aug 02, 2011 inclusive), the average estimated 7-day travel depth was 0.72 m directly beneath the laterals. So it would have taken approximately 2 to 5 days for the effluent to reach the top of the groundwater level observed on July 27 and July 31 respectively. But the MWs were not directly below the laterals.

The initial infiltration and transport of the Br-spiked surface effluent was likely proportional to the quasi-steady 2-D/3-D flow field resulting from the previous effluent applications. The fastest travelling bromide, therefore, is within the streamline directly below the laterals. But because of the 2- and 3-D flow below the laterals, the 1-D approximation of the 7-day travel depth is likely greater than the actual multi-dimensional case. For example in MWs 5 (0.94 m) and 6 (0.95 m), located closest to two laterals but not directly below the laterals (Figure 4-2), a longer travel time was expected. The expected travel time of Br through the fastest streamlines would have been first to travel vertically through the vadose zone and then horizontally to the MWs. However, in these wells Br was detected earlier than the expected time.

After the second Br pulse application on July 25 2012, Br levels in the groundwater increased slowly starting from the nest between the two northern most laterals in the source zone. The first groundwater sampling date was three days after the second Br pulse application (t=367 days) Figure not shown because the Br plume concentration was similar to that observed at t=364, Figure 4-6e. At the time of the second Br pulse, the Br concentration in MW 6 (0.95 m) had returned to background levels and Br was not detected until 7 days after the second Br pulse. Even though, the earliest Br breakthrough was 3 days after the first pulse, it took 7 days for the Br to breakthrough after the second pulse. The difference was attributed to the increase in depth to groundwater below the ground surface observed in the summer 2012.

Bromide transport at times greater than 40 days after the first application were dominated by decreasing water table levels. As can be seen in Figure 4-6, with the seasonal drop in water table during the fall of 2011, majority of the initial bromide plume was transported to the lowest or below the lowest monitoring wells in the source zone (Figure 4-9c, d), with some Br remaining in the unsaturated zone. After the water table recovered in the spring of 2012, the Br plume was much more dilute and the center of mass had shifted up-gradient (Figure. 4-6e; Table 4-5). This backward shift in the Br plume center of mass is likely a result of a combination of the down-gradient transport of the original Br plume during the winter and the rising groundwater intercepting the slower-moving bromide in the unsaturated zone in the up-gradient area of the source zone during the spring.

In the summer of 2012, the total mass of Br injected into source zone was lower than that of 2011 (Figure 4-10). The groundwater elevation was also about 30-cm lower than it was in 2011. As a result of these two conditions, the second Br pulse did not influence the spatial moments significantly.

The influence of the decreasing groundwater table on the Br transport is apparent in the horizontal and vertical spatial moments of the Br plume (Table 4-6; Figures 4-7). In general, greater horizontal transport was associated with greater vertical transport. The vertical transport is dominated by increases or decreases in the elevation of the groundwater table.

413 days after the first Br pulse application and 49 days after the second pulse application, the center of groundwater Br mass was located at 526 cm down gradient from the center of the source zone (X'=0). The average, horizontal groundwater flow velocity was estimated as 1.37 cm d^{-1} giving rise to a 0.77 cm d^{-1} Darcy flux assuming the field observed porosity of 0.56 cm^3 cm^{-3}. These results were close to the Darcy flux estimate (0.54 cm d^{-1}) obtained using the average horizontal hydraulic gradient (-0.014 m m^{-1}) and average field measured hydraulic conductivity, ~38 cm d^{-1} (Table 4-3).

4.4.3.2. Br and *E.coli* Breakthrough

Cumulative probability distribution functions and time series of *E.coli* concentrations in the wastewater and surface loading rates with and without UV disinfection are given in Figure 4-8. Locally observed breakthrough curves (BTC) and loading rates (wastewater concentration multiplied by daily surface flux) of Br and *E.coli* for the wells that showed relatively high levels

of both Br and *E.coli* (at nests 5, 6 and 7) are presented in Figures 4-9 to Figures 4-12. Figures 4-9b,d,f show Br concentrations observed for the entire spectrum of sampling time from July 27, 2011 to September 12, 2012 and Figures 4-10 to 4-12 show for the first 131 days since the first Br pulse application that is from July 27 to December 04, 2011. In each of the Figures, Br and *E.coli* loading rates, groundwater hydrology and calculated 7-day travel depths are also compared to the BTCs.

The performance of the UV disinfection system appeared to be dependent on the intensity of facility use. Only one measurement of *E.coli* concentration was taken in July, 2011 prior to shutting off the UV disinfection system, but this concentration was within the range of concentrations measured while the UV disinfection system was shut off. There were a few *E.coli* samples that were collected by the facility maintenance office directly from the tank with the UV lamps (Appendix 4-A). However, no measurements were taken from the last tanks distributing the UV disinfected effluent to the laterals, where we had been monitoring *E.coli* concentrations simultaneously with the groundwater wells. These results may give some idea about performance of the UV-disinfection, but again the method of sampling and analysis were different from ours. The UV system was turned back on November 6, 2014 and there was a substantial decrease in *E.coli* concentrations over the fall and winter, but they increased close to untreated levels again in the spring of 2012 when a greater number of travelers were using the facilities increasing effluent dosing rates.

In terms of loading rates, approximately 38% of the loading rates estimated when the UV system was on were within the range of loading rates estimated when the UV system was shut off. The most likely reason for this result is the positive correlation between facility use, wastewater production and surface effluent application rates. When the facilities are used more frequently, more wastewater is generated and it appears that the UV disinfection system is less efficient during these times.

As can be expected, Br breakthrough in a nest was sequential with depth in that Br was first detected at the shallow monitoring wells followed by the middle and deep wells respectively, indicating the absence or minimal presence of preferential flow paths within the monitoring wells zone. All Br BTCs exhibited long tails which was likely associated with the decreasing surface flux and groundwater fluctuations following Br application.

The level of *E.coli* concentration in the untreated effluent ranged between $4\ log_{10}$ to $5.5\ log_{10}$ *E.coli* (MPN 100 mL^{-1}), and loading rates ranged from $2.5\ log_{10}$ to $4\ log_{10}$ (MPN $cm^{-2}\ d^{-1}$) (Figure 4-10a). In the monitoring wells, the highest *E.coli* concentrations appeared during the highest loading rates, but were not greater than $2.5\ log_{10}$ showing at least a 50% reduction of *E.coli* between the soil surface and monitoring wells. These findings indicated that approximately $2\ log_{10}$ to $3\ log_{10}$ *E.coli* (MPN 100 mL^{-1}) had been attenuated in the unsaturated soil before reaching the groundwater (Figures 4-10 to 4-12). In more than 90% of the monitoring wells (that is, all except the up-gradient wells), Br was detected but *E.coli* was only detected in 30% of the monitoring wells. In the wells in which both *E.coli* and Br were detected, their first times of arrival were similar (Figure 4-10 to 4-12 b,c,d) indicating similar transport pathways for both *E.coli* and Br. Figures 4-13 to 4-14 show a close look of *E.coli* and Br BTCs by zooming in to the months of July and August 2011. It is important to note, however, that the decrease in Br concentrations at late times are likely because of the pulse application whereas the concentration of *E.coli* decreased with time despite steady loading rates for a period of more than 3 months. As the groundwater level dropped to $d(t) \geq 0.88$ m at the source zone (Figure 4-10e; i.e., increase in vadose zone thickness), *E.coli* levels in the monitoring wells dropped below detection limit (Figure 4-10b-c). Therefore, these findings imply that 0.88 m is likely the critical depth to consider in groundwater contamination risk assessment, which is consistent with the Safety Code Council standard (Safety Code Council, 2012).

At the study site (particularly at the instrumented infiltration area), a significant groundwater fluctuation (~ 1.22 m) in response to regional as well as to the local effluent infiltration was observed during the experiment period. At the start of the experiment in July 2011, the average water table level below the source zone was at approximately 0.28 m below the ground surface (Figure 4-10e to 4-12e) and it dropped gradually to approximately 1.63 m below ground surface in February 2012 and then it rose back up to 0.43 m below the ground surface during the snow-melting season in April 2012. As shown in Chapter 3, high surface effluent fluxes influenced the groundwater depth at times when the groundwater table was already high and these conditions existed only for brief periods. The window in which *E.coli* were detected in the monitoring wells was consistent with or slightly longer than the window of high covariance between surface flux and groundwater level from the end of July to the middle of August 2011 (see Figure 3-3). Even though, the covariance between surface effluent flux and

groundwater levels were estimated using groundwater levels measured in different wells in the source zone, it is possible that *E.coli* were only detected in the monitoring wells during times of high covariance between the surface flux and groundwater depth. These windows of high covariance were identified as periods of high groundwater contamination risk and this is further confirmed because *E. coli* loading rates are likely high during these windows of high covariance.

Both *E.coli* and Br showed similar early breakthrough, but *E.coli* was detected earlier than Br in MW 5 (1.32 m) despite the fact that the UV system was shut off 2 days after the Br was applied (Figure 4-10c). However, because it appears that high loading rates are possible during periods of intensive facility use even when the UV disinfection system is on, it may be that *E.coli* observed at early times was from effluent applied prior to UV system shutoff. Nevertheless, an early breakthrough of *E.coli* compared to conservative tracers was reported in previous studies that were conducted in intact soil column and lysimeter experiments (e.g. Shelton *et al.,* 2003; Guber *et al.,* 2005; Levy *et al.,* 2007; Pang *et al*., 2008). This velocity enhanced transport of *E.coli* was believed to be a result of preferential pathways in structured soils, saturated flow conditions and size exclusion. In our study, the estimated 7-day effluent travel depth was greater than the depth to groundwater for approximately a week during the start of the experiment between July 27 to Aug. 03, 2011 (Figure 4-10e to 4-12e). In addition, as observed from the Br-BTC, Br-rich effluent reached MW 6, which was 0.95 m below the ground surface and 1 m down-gradient of the source zone, in two days suggesting the presence of preferential conduits. The preferential pathways include spatial variability of soil structure, root channels, fractures and animal burrows and these features expedite bacteria transport because bacteria may be excluded from the small pores on the bases of their size (Shelton *et al.,* 2003). At the study site, observations also indicate the potential presence of preferential flow path ways. The site was covered with aspen trees and tree roots were observed at the time of installing the monitoring wells (Figure 4-17). Firstly, the installation activity likely disrupted the tree roots leaving some of them dead or misplaced, creating preferential pathways. Secondly, the action of tree roots as they grow vertically and laterally may also create preferential pathways. Microbes such as *E.coli* were also believed to utilize the mobile portion of the soil water while that of Br may include the immobile phase as well (Pang *et al.,* 2008).

There was some evidence of variability in soil particle size and structure of the soils in the study area. The depth-averaged percentage of clay (0-1.40 m) was 21, 19 and 28% in the up-

gradient, source zone and down-gradient locations respectively. From the particle size distribution (Table 4-1) and field observations, more structured soils would be expected in the down-gradient zone. These observations likely contributed to the observed Br and *E.coli* transport variability as well. In monitoring well 6 (1.33 m), located at 1 m down gradient, *E.coli* was below detection limit throughout the sampling time while the shallower and deeper wells in the same nest showed detectable to higher levels of *E.coli*. Yet, Br was detected in nest 6 including monitoring well 6 (1.33 m). A close look of the particle size distribution at MW 6 (1.33 m) screen interval, revealed the highest percentage of silt (46-51%) that was recorded in the transect (Table 2-2, Chapter 2). In this case possible reasons were: i) *E.coli* was attenuated in the soil because silt loam soils are among the soil groups that were recommended for effective onsite wastewater treatment (EPA, 2000), and ii) saturated flow conditions and preferential pathways may have encouraged *E.coli* to bypass Br reaching the deepest well in the nest. Early researchers such as Guber *et al* (2005) and Pang *et al* (2008) also observed more convective and less dispersive transport of microbes than that of Br in structured soils compared to uniform, single-grain dune sand. The fact that silt loam is also relatively a structure less was also a benefit. In the uniform sandy soils, a slower velocity of microbial tracers than Br were expected.

4.4.3.3. Virus Fate and Transport

Enteric virus concentration (Log genome copies L^{-1}) and Br concentration are presented in Figure 4-16 and Table 4-7. Only two of the seven enteric virus types were detected in the groundwater samples. Similar to that of *E.coli* and Br, norovirus and rotavirus were detected in the shallow MW, 6 (0.95 m) (Figure 4-16 and Table 4-7). The concentration of viruses in the source tank is given in Table 4-6 and the concentrations for norovirus and rotavirus were the highest reaching 4.86±0.40 and 5.53±0.27 log genome copies L^{-1} respectively.

From our study, viruses were detected only in the shallow wells located at 0.95 m below the ground surface and their concentration also decreased with the drop in water table level below the ground surface (Table 4-7). On average, most of the enteric viruses that were detected in the effluent source tank had been either completely attenuated or reduced by approximately 1-Log genome copies L^{-1} (Table 4-7) as the effluent infiltrated through the vadose zone. Some of the reasons were likely attributed to soil water content, ionic strength and pH of the soil (Torkzaban *et al.,* 2006). Firstly, a relatively higher ionic strength (*I*) was observed in the deep MWs that would favor more attachment of viruses to negatively charged geologic materials

(Harvey and Ryan, 2004). Secondly, in the unsaturated soil (where the pores are partially filled with air), the transport volume is reduced and other processes of attachment (adsorption) would take place that retard virus transport as opposed to that in the saturated soil. Viruses are believed to attach to the solid-water interface (SWI), to the air-water interface (AWI) and to the air-water-solid interface (AWS) contact line (Schijven and Hassanizadeh, 2000; Michen and Graule, 2010). Such attachments delay virus transport and provide extra time for their inactivation and die-off. Therefore, except for norovirus and rotavirus that were reduced by only less than 1-log, the percent removal for the other viruses meets the Canadian guideline for drinking water. Health Canada (2012) requires a minimum of $4\ log_{10}$ reduction and/or inactivation of enteric viruses, which is consistent with the reduction observed in our study. Noroviruses are one of the highly contagious between humans responsible for causing about 50% of all gastroenteritis outbreaks in the world (Patel *et al*., 2009). In summary it can be said, therefore, that the UV-disinfection system does not work for viruses.

4.5. Conclusion

We investigated wastewater flow as well as microbes' fate and transport on a site with typical of OWTS with at-grade effluent disposal and shallow groundwater boundary conditions using Br and *E.coli* tracers. Firstly, wastewater plume flow was inspected from a two dimensional Br plume profile and using spatial moment analyses of data snapshots observed over one year (413 days) at weekly to biweekly intervals. The boundary conditions controlling the spatial distribution and shape of Br plume were identified and those were i) local effluent surface fluxes, ii) regional groundwater hydrology iii) vertical and horizontal hydraulic gradients, which in turn were dictated by soil properties such the particle size distribution, soil structure and hydraulic properties. Secondly, inspection of Br and *E.coli* breakthrough curves showed earlier arrival of *E.coli* in some of the monitoring wells and longer tailing of Br were observed indicating preferences of available flow paths between the two tracers. Bromide tracer had likely used most of the available pathways including the immobile phase the soil water, however, *E.coli* was believed to use only the mobile fraction of soil water due to size exclusion. Thirdly, our results demonstrated the effect of vadose zone thickness on *E.coli* and virus attenuation and transport. The thickness of the vadose zone was also dictated by the subsurface hydrology and transient surface effluent flux density. With the increase in vadose zone thickness, the concentration of *E.coli* and viruses decreased. In the shallow water table scenario, the removal

of *E.coli* and viruses were at least $1\ log_{10}$ higher compared to that of the deeper water table cases. As the vadose zone thickness increased, $> 3\ log_{10}$ removal of *E.coli* and viruses were observed except for norovirus and rotavirus species, in which the reduction was only $< 1\ log_{10}$. A critical depth to groundwater has been identified in that $d(t) \leq 0.88$ m would likely increase risks to groundwater contamination. In addition, spatial variability of soil structure, soil particle distribution and other sources of preferential pathways such as plant roots in combination with prevailing boundary conditions need to be considered when designing OWTS to avoid probable risks to groundwater contamination. This is because in the presence of preferential pathways expedite pathogen transport giving less residence time in the vadose zone.

As it has been discussed in the previous sections, the OWTS had a UV-distinction and the soil based treatment main units. The soil based treatment represents the unsaturated zone, also referred to as the vadose zone, a zone above the groundwater table that received the UV-disinfected effluent. The UV-disinfection system was not effective alone because more than $3\ log_{10}$ of *E.coli* were common in the source tank past the UV-disinfection that would need further treatment. Regardless of the UV-disinfection system, the vadose zone played a significant role in attenuation of *E.coli* to acceptable levels, however, it was not true for viruses particularly norovirus and rotavirus. It was observed that a vadose zone as thick as 0.88 m or more would potentially be safe under the prevailing boundary conditions.

In summary, as shown in Chapter 3, the hydrologic system of the study site was complex and many interrelated processes affected the subsurface flow and transport. However, in practice it would be too ambitious and impractical to acquire everything deemed necessary and hence we simplified and presented some key aspects that help understand the prevailing flow and transport processes, propose recommendations and future work directions. Our findings identify that groundwater fluctuation and depth below the ground surface from site conditions as well as particle size distribution and soil structure from soil properties to be considered in future research relevant to onsite wastewater treatment systems. The next chapter uses process-based modeling to better quantify the risks associated with OWTS in shallow and fluctuating groundwater conditions.

4.6. References

Alhajjar, B. J., S. L. Stramer, D. O. Cliver, and J. M. Harkin, 1988. Transport modeling of biological tracers from septic systems. *Water Res. 22:907-915.*

APHA, AWWA and WEF, 2012. Standard methods for the examination of water and wastewater. 22nd ed. Washington: American Public Health Association, America Water Work Association and Water Environment Federation.

APHA, 1999. Standard methods for water and wastewater by American Public Health Association, American Water Works Association, Water Environment Federation.

Bales, R. C., S. Li, K. M. Maguire, m. T. Yahya, C. P. Gerba, and R. W. Harvey, 1995. Virus and bacteria transport in a sandy aquifer, Cape Cod, MA. *Groundwater, 33:653-661.*

Ben Said, M. and M. Otaki, 2013. Enhancement of ultraviolet water disinfection process. *Afr. J. Biotechnol.:* 12:2932-2938. DOI: 10.5897/AJB12.1479

Blanc, R. and A. Nasser, 1996. Effect of effluent quality and temperature on the persistence of viruses in soil. *Water Sci. Tech. 33:237-242.*

British Columbia Municipal Wastewater Regulation, 2012. Municipal Wastewater Regulation. British Columbia Ministry of Environment: Municipal Wastewater Regulation and Amendments. Available online: http://www.env.gov.bc.ca/epd/mun-waste/regs/mwr/.

Bundschuh, J. and O. Sracek, 2012. Hydrogeochemistry principles for geochemical modeling. In J. Bundschuh J., M. Zilberbrand (Eds). Geochemical modeling of groundwater, vadose and geothermal systems. CRC Press, pp3-26.

Carrara, C., C. J. Ptacek, W. D. Robertson, D. W. Blowes, M. C. Moncur, ED Sverko, and S. Backus, 2008. Fate of pharmaceutical and trace organic compounds in three septic stsyem plumes, Ontario, Canada. *Environ. Sci. Technol. 42:2805-2811.*

CCME, 2006. Municipal wastewater effluent in Canada. Canada Council of Ministers of the Environment, Municipal wastewater effluent development committee. Available on line: http://www.ccme.ca/assets/pdf/mwwe_general_backgrounder_e.pdf

CCME, 2009. Canada-wide strategy for the management of municipal wastewater effluent. Available on line: http://www.ccme.ca/assets/pdf/cda_wide_strategy_mwwe_final_e.pdf

Crockett, C. S., 2007. The role of wastewater treatment in protecting water supplies against emerging pathogens. *Water Environ. Res. 79:221-232.*

Durnie, A, 2008. An on-site sewage and septage management framework in Alberta framework Alberta. Available on line: http://www.environmentconference.alberta.ca/docs/Session-33_presentation.pdf

Ellsworth, T. R., W. A. Jury, F. F. Ernst, and P. J. Shouse, 1991. A three-dimensional field study of solute transport through unsaturated, layered, porous media 1. Methodology, mass recovery, and mean transport. *Water Resour. Res., 27:951-965*.

Environment Canada, 2004. Threats to Water Availability in Canada. National Water Research Institute, Burlington, Ontario. NWRI Scientific Assessment Report Series No. 3 and ACSD Science Assessment Series No. 1. 128 p. Available on line: https://www.ec.gc.ca/inre-nwri/default.asp?lang=En&n=0CD66675-0&offset=4&toc=show Modified on 2013-07-23

EPA, 2000. Wastewater treatment manuals. Treatment systems for single house. Environmental Protection Agency, Ireland. 69pp. Available on line: http://www.tri-bio.com/fckeditor/upload/image/2008/08/epa_single_houses.pdf

Exall, K. 2004. A review of water reuse and cycling, with reference to Canadian practice and potential: 2. Applications. *Water Qual. Res. J. Canada. 39:13-28.*

Exall, K., J. Marsalek, and K. Schaefer, 2006. Water reuse in canada: Opportunities and challenges. In P. Hlavinek, T. Kukharchyk, J. Marsalek and I. Mahrikova (eds.), Integrated urban water resources management. *Proceedings of NATO Advanced Research Workshop. p 253–262*.

Fout, G. S., B. C. Martinson, M. W. Moyer, and D. R. Dahling, 2003. A multiplex reverse transcription-PCR method for detection of human enteric viruses in groundwater. *Appl. Environ Microbiol. 69:3158-64.*

Freyberg, D. L., 1986. A natural gradient experiment on solute transport in sand aquifer: 2. Spatial moments and the advection and dispersion of nonreactive tracers. *Water Resour. Res. 22:2031-2046.*

Ganoulis, J., 2012. Risk analysis of wastewater reuse in agriculture. *Inter. J. of Recycling of Org. Waste in Agri. 1:1-9.*

Garabedian S. P., D. R. Leblanc, L. W. Gelhar, and M. A. Celia, 1991. Large-scale natural gradient tracer test in a sand and gravel, Cape Cod, Massachusetts: 2. Analysis of spatial moments for a nonreactive tracer. *Water Resour. Res. 27:911-924*.

Gibson, K. E., 2014. Viral pathogens in water: occurrence, public health impact, and available control strategies. *Curr. Opin. Virol. 4:50–57*.

Golden Software, Inc. 2009. Surface mapping system. Surfer Version 9.11.947.

Guber, A. K., D. R. S. Shelton, and Ya. A. Pachepsky, 2005. Transport and retention of manure-borne coliforms in soil. *Vadose Zone J. 4:828-837.*

Hanjra, M. A., J. Blackwell, G. Carr, F. Zhang, T. M. Jackson, 2012. Wastewater irrigation and environmental health: Implications for water governance and public policy. *Int. J. Hyg. Envir. Heal. 215:255–269.*

Harvey, R. W. and J. N. Ryan, 2004. Use of PRD1 bacteriophage in groundwater viral transport, inactivation, and attachment studies. *FEMS Microbiol. Ecol. 49 (2004) 3–16*

Hassanizadeh, S. M., 2012. 2012 Henry Darcy Distinguished Lecture "Transport of Viruses in Partially Saturated Soil and Groundwater". Available on line http://www.youtube.com/watch?v=okSx8Y8AHv8

Health Canada, 2006. Guidelines for Canadian Drinking Water Quality: Guideline Technical Document — *Escherichia coli*. Water Quality and Health Bureau, Healthy Environments and Consumer Safety Branch, Health Canada, Ottawa, Ontario. Available on line: http://www.hc-sc.gc.ca/ewh-semt/alt_formats/hecs-sesc/pdf/pubs/water-eau/escherichia_coli/escherichia_coli-eng.pdf.

Health Canada, 2012. Guidelines for Canadian Drinking Water Quality - Summary table. Water, Air and Climate Change Bureau, Healthy Environments and Consumer Safety Branch, Health Canada, Ottawa, Ontario.

IDEXX Laboratories Inc. 2002. Quanti-Tray® and Quanti-Tray®/2000. An easy quantification method for Colilert®,Colilert®-18, Colisure® and Enterolert™. Available on line: http://www.environmental-expert.com/products/quanti-tray-quanti-tray-2000-coliform-and-e-coli-testing-13837.

Infiltrator Systems Inc., 2006. The Quick4® Standard Chamber. Available on line: www.infiltratorsystems.com

Jantrania A. R., and M. Gross, 2006. Advanced onsite wastewater systems technologies. Taylor and Francis. Boca Raton, Florida, USA.

Jensen, K. H., K. Bitsch, and P. L. Bjerg, 1993. Large-scale dispersion experiments in a sandy aquifer in Denmark: Observed tracer movements and numerical analyses. *Water Resour. Res. 29:673-696.*

Katz, B. G., and D. W. Griffin, 2008. Using chemical and microbiological indicators to track the impacts from the land application of treated municipal wastewater and other sources on groundwater quality in a karstic springs basin. *Environmental Geology 55: 801-821*.

Katz, B.G., D. W. Griffin, and J. H. Davis, 2009. Groundwater quality impacts from land application of treated municipal wastewater in a large karstic spring basin: chemical and micbiological indicators. *Sci. Total Environ. 407:2872-2886*.

Kennedy, C. D., 1990. Ionic strength and the dissociation of acids. Biochemistry

Kumar G. S. and M. Sekhar, 2005. Spatial moment analysis for transport of nonreactive solutes in fracturmatrix system. *J. Hydrol. Eng. 10:192-199.*

Lapworth, D. J., N. Baran, M. E. Stuart, and R. S. Ward, 2012. Emerging organic contaminants in groundwater: A review of sources, fate and occurrence. *Environ. Poll. 63:287-303*.

Levy, J., K. Sun, R. H. Findlay, J. Porter, K. L. Mumy, J. Tomaras, and A. Tomaras, 2007. Transport of *Escherichia coli* bacteria through laboratory columns of glacial-outwash sediments: Estimating model parameter values based on sediment characteristics. *J. Contam. Hydrol. 89:71-106*.

Lishman, L., S. A. Smyth, K. Sarafin, S. Kleywegt, J. Toito, T. Peart, B. Lee, M. Servos, M. Beland, and P. Seto, 2006. Occurrence and reductions of pharmaceuticals and personal care products and estrogens by municipal wastewater treatment plants in Ontario, Canada. *Sci. Total Environ. 367:544-558*.

Lowe, K. S., S. M. Van Cuyk, .R. L. Siegrist and J. E. Drewes, 2008. Field evaluation of the performance of engineered on-site wastewater treatment units. ASCE , *J. Hydrol. Engin. 735-743.*

McCray, J. E. and S. H. Christopherson, 2008. On-site wastewater systems and interactions with the environment. ASCE , *J. Hydrol. Engin. 653-654.*

McCray, J. E., S. L. Kirkland, R. L. Siegrist, and G. D. Thyne, 2005. Model parameters for simulating fate and transport of on-site wastewater nutrients. *Ground Water, 43:628-639.*

Menegaki, A. N., N. Hanley, and K. P. Tsagarakis, 2007. The social acceptability and valuation of recycled water in Crete: A study of consumers' and farmers' attitudes. *Ecol. Econ. 62:7–18.*

Meulemans, C.C.E., 1987. The basic principles of UV-disinfection of water. Ozone: Science & Engineering: *J. Intern. Ozone Assoc. 9:299-313, DOI: 10.1080/01919518708552146.*

Michen, B. and T. Graule, 2010. Isoelectric points of viruses. J. Appl. Microbiol. 109:388–397.

Motz, E. C., E. Cey, M. C. Ryan and A. Chu, 2011. Vadose zone microbial transport below at-grade distribution of wastewater effluent. *Water Air Soil Pollut.* DOI 10.1007/s11270-011-0901-y

Mutengu, S., Z. Hoko, and F. S. Makoni, 2007. An assessment of the public health hazard potential of wastewater reuse for crop production. A case of Bulawayo city, Zimbabwe. *Phys. Chem. Earth 32:1195–1203.*

Pang, L., M. McLeod, J. Aislabie, J. Šimůnek, M. Close, and R. Hector, 2008. Modeling transport of microbes in ten undisturbed soils under effluent irrigation. *Vadose Zone J. 7:97–111. doi:10.2136/vzj2007.0108*

Pang, X. L., B. E. Lee, K. Pabbaraju, S. Gabos, S. Craik, P. Payment, N. Neumann, 2012. Pre-analytical and analytical procedures for the detection of enteric viruses and enterovirus in water samples. *J. Virol. Meth. 184 (2012) 77– 83.*

Patel, M. M., A. J. Hall, J. Vinj´e, and U. D. Parashar, 2009. Noroviruses: a comprehensive review. *J. Clin. Virol. 44:1–8.*

Pedrero, F., I. Kalavrouziotis, J. J. Alarcón, P. Koukoulakis, and T. Asano, 2010. Use of treated municipal wastewater in irrigated agriculture—Review of some practices in Spain and Greece. *Agr. Water Manage. 97:1233–1241.*

Qadir, M., D. Wichelns, L. Raschid-Sally, P. G. McCornick, P. Drechsel, A. Bahri, and P. S. Minhas, 2010. The challenges of wastewater irrigation in developing countries. *Agr. Water Manage. 97:561–568.*

Reynolds, W. D. and G. C. Topp, 2006. Soil water desoprion and imbibition: Tension and pressure techniques. In M.R. Carter and E.G. Gregorich (eds.). Methods of soil analysis. 2nd ed. Taylor & Francis Group, LLC.

Safety Code Council, 2012. Alberta private sewerage systems 2009 standard of practice handbook. Available on line:

http://www.safetycodes.ab.ca/Public/Documents/PSSSOP_Handbook_Version_12_Online_Feb_21_2012b.pdf

Scandura, J. E. and M. D. Sobsey, 1997. Viral and bacterial contamination of groundwater from on-site sewage treatment systems. *Water Sci. Tech. 35:141-146.*

Schijven, J. F. and S. M. Hassanizadeh, 2000. Removal of viruses by soil passage: Overview of modeling, processes, and parameters. *Crit Rev Environ. Sci. Technol. 30:49–127.*

Sen, T. K., 2011. Processes in pathogenic biocolloidal contaminants transport in saturated and unsaturated porous media: A Review. *Water Air Soil Pollut. Springer*, DOI: 10.1007/s11270-010-0531-9

Shelton, D. R., Ya. A. Pachepsky, A. M. Sadeghi, W. L. Stout, J. S. Karns, and W. J. Gburek, 2003. Release rates of manure-borne coliform bacteria from data on leaching through stony soil. *Vadose Zone J. 2:34-39.*

Shin, G., K. G. Linden and G. Faubert, 2010. Reactivation of *Giardia lamblia* cysts after exposure to polychromatic UV light. *Letters in Appl. Microbiol. 51:395–399. doi:10.1111/j.1472-765X.2010.02908.x*

Statistics Canada, 2008. Canadian demographics at a glance. Statistics Canada demography division.

Topp, G. C. and S. Sattlecker, 1983. A rapid measurement of horizontal and vertical components of saturated hydraulic conductivity. *Can. Agri. Eng. 25:193-197.*

Torkzaban, S., S. A. Bradford, M. Th. van Genuchten, and S. L. Walker, 2008. Colloid transport in unsaturated porous media: The role of water content and ionic strength on particle straining. *J. Contamin. Hydrol. 96:113–127.*

Torkzaban, S., S. M. Hassanizadeh, J. F. Schijven, H. A. M. de Bruin, and A. M. de Roda Husman, 2006. Virus Transport in Saturated and Unsaturated Sand Columns. *Vadose Zone J. 5:877–885*.

US-EPA, 1997. Response to the Congress on the use of decentralized wastewater treatment systems. Available on line: http://water.epa.gov/infrastructure/septic/upload/septic_rtc_all.pdf

US-EPA, 1999. Wastewater technology fact sheet ultraviolet disinfection. EPA 832-F-99-064. September 1999. Available on line: http://www.epa.gov/owm/mtb/uv.pdf

US-EPA, 2013. Septic (Onsite/Decentralized) Systems. Available on line: http://water.epa.gov/infrastructure/septic/

Van Genuchten, M. Th., 1980. A closed-form equation for predicting the hydraulic conductivity of unsaturated soils. *Soil Sci. Soc. Am. J., 44: 892-898*.

Van Genuchten, M. Th., J. Simunek, F. J. Leij, and M Segina, 2009. Code for quantifying hydraulic functions of unsaturated soils. Available on line: www.hydrus3d.com.

Vanderborght, J. and H. Vereecken, 2001. Analysis of time series of locally measured bromide concentrations during the groundwater transport experiment at Krauthausen. *Tracers and Modeling in Hydrogeology: Proceedings of the TraM'2000 Conference IAHS Publ. No. 262, 2000*.

Verma, E. M., 2008. Soil-based wastewater dispersal systems: net die-off and sorption rate constants of *Escherichia coli* and *Enterococcus faecalis. MSc thesis*. *112pp*. University of Alberta.

Weber, S., S. Khan, and J. Hollender, 2006. Human risk assessment of organic contaminants in reclaimed wastewater used for irrigation. *Desalination 187:53–64.*

WHO, 2004. Guidelines for drinking water quality. 3rd ed. Volume 1 Recommendations, Geneva. Available on line: http://www.who.int/water_sanitation_health/dwq/GDWQ2004web.pdf

Woods, S. A. R. G. Kachanoski and M. F, Dyck, 2006. Long-term solute transport under semi-arid conditions: Pedon to field scale. *Vadose Zone J. 5:365-376.*

Woods, S. A., M. F. Dyck and R. G. Kachanoski, 2013. Spatial and temporal variability of soi horizons and long-term solute transport under semi-arid conditions. *Can. J. Soil Sci. 93:173-191.*

Youngs, E. G. 1968. Shape factors for Kirkham's piezometer method for measuring the hydraulic conductivity of soil in situ for soils overlying an impermeable floor or infinitely permeable stratum. *Soil Sci. 106:235-237.*

Zimmer, J. L. and R. M. Slawson, 2002. Potential repair of *Escherichia coli* DNA following exposure to UV radiation from both medium- and low-pressure UV sources used in drinking water treatment. *Appl. Environ. Microbiol. 68:3293–3299.*

Table 4-1: Average PSD[£] with depth along a transect perpendicular to the at-grade line sources

Depth (cm)	**Up-gradient**	**Source zone**	**Down-gradient**
cm	**Soil textural class**[†]		
0-20	Loam	Sandy Loam	Loam
20-40	Sandy Loam	Sandy Loam	Loam
40-60	Sandy Clay Loam	Sandy Loam	Clay Loam
60-80	Loam	Sandy Clay Loam	Clay Loam
80-100	Loam	Loam	Clay Loam
100-120	Loam	Loam	Silty Loam
120-140	Sandy Loam	Loam	Loam

[£] PSD=Particle size distribution
[†] Canadian soil texture classification system

Table 4-2: Number of samples collected during the field tracer experiments seasons in 2011-2012

Analysis type	Bromide[£]	*E.coli* and Total coliforms[‡]	Virus testing	Routine[¶] Analysis	**Total**
Number of samples	936	467	40	153	**1596**

[£]The number of samples for Br represents total of the two experimental periods: 2011 and 2012.
[‡]The number of samples for microbial analysis was reduced from that of Br focusing only on those wells that showed detectable *E.coli* hits during the experimental sampling period, with occasional sampling from the other wells as a check-up.
[¶]Routine analysis is a standard procedure for testing the common water quality parameters in Table 4-4.

Table 4-3: Field measured saturated hydraulic conductivity (*Ks*)

Nest number	1	4	5	6	7	8	9	10	Mean K_s (cm d^{-1})
Eff. $K_{s,v}$ (cm d^{-1})	36.38	38.53	29.05	57.15	37.22	34.80	42.76	25.02	38.27
Eff. $K_{s,h}$ (cm d^{-1})	36.38	38.53	29.95	63.05	37.31	36.84	43.45	25.83	

Eff. = effective, and the subscripts stand for: v = vertical and h = horizontal

Table 4-4: Average groundwater geochemistry observed in the nested monitoring wells††

Zone	Ave. Mid-screen depth	EC	Temp observed pH	pH	Na^+	K^+	Ca^{2+}	Mg^{2+}	SO_4^{2+}	Cl^-
	m	mS cm^{-1}	(^{0}C)		mg L^{-1}					
Up-gradient	0.92	2.60 (0.39)	20.4 (1.08)	7.56 (0.18)	236.11 (14.96)	1.54 (0.31)	275.38 (24.88)	53.89 (6.16)	97.16 (6.07)	648.00 (63.82)
	1.28	2.21 (0.23)	20.8 (1.52)	7.64 (0.14)	173.75 (9.79)	0.71 (0.10)	233.25 (20.41)	47.24 (3.73)	82.09 (6.43)	509.63 (44.36)
	1.56	2.91 (0.57)	20.6(1.12)	7.44 (0.22)	122.55 (16.90)	1.85 (0.34)	347.00 (54.58)	88.88 (11.21)	94.71 (10.69)	754.63 (125)
Source	0.95	2.88 (0.18)	21 (1.55)	7.57 (0.15)	243.42 (9.35)	2.76 (0.53)	275.17 (26.64)	76.27 (5.66)	133.50 (7.85)	519.92 (32.76)
	1.29	2.50 (0.28)	21.3 (1.44)	7.62 (0.19)	193.0 (19.51)	1.21 (0.14)	234.67 (23.50)	68.97 (8.42)	105.19 (10.07)	423.75 (48.57)
	1.54	3.84 (0.41)	21.0 (1.59)	7.52 (0.17)	232.67 (15.21)	2.22 (0.31)	419.50 (59.73)	132.96 (15.43)	267.03 (29.30)	823.33 (67.42)

Table 4-4: (cont...)

Zone	Ave. Mid-screen depth	EC	Temp observed pH	pH	Na^+	K^+	Ca^{2+}	Mg^{2+}	SO_4^{2+}	Cl^-
	m	mS cm^{-1}	(^{0}C)	pH	mg L^{-1}					
Down-gradient	0.95	2.48 (0.23)	21.5 (1.52)	7.62 (0.10)	160.95 (12.81)	3.13 (0.56)	248.40 (19.28)	81.51 (6.93)	132.29 (4.61)	412.75 (25.63)
	1.29	2.68 (0.36)	21.3 (1.51)	7.62 (0.16)	190.25 (17.96)	1.79 (1.06)	253.95 (27.25)	93.28 (8.74)	150.13 (12.08)	453.35 (39.74)
	1.55	2.77 (0.21)	21.3 (1.49)	7.58 (0.18)	212.35 (11.39)	1.67 (0.49)	257.45 (24.09)	97.30 (7.50)	166.25 (8.68)	487.25 (28.14)
Effluent	-	2.23 (0.44)	20.6 (1.10)	8.02 (0.16)	178.25 (17.04)	41.08 (6.31)	121.75 (20.29)	40.00 (7.96)	88.10 (10.51)	408.25 (52.71)

Table 4-4: (cont...)

Zone	Ave. Mid-screen depth	HCO_3^-	NO_2^--N	NO_3^--N	Fe^{3+}	Mn^{2+}	Total alkalinity as $CaCO_3$	TDS-cal	Ionic balance dissolved	Ionic strength$^+$
Zone	m	mg L^{-1}							(%)	mol L^{-1}
Up-gradient	0.92	472.00 (89.58)	6.50 (2.20)	6.53 (2.21)	0.024 (0.011)	0.339 (0.193)	387.00 (73.50)	1532.9 (116.03)	99.75 (5.52)	5.04×10^{-2}
	1.28	440.88 (79.15)	1.83 (0.55)	1.83 (0.55)	0.015 (0.000)	0.430 (0.195)	361.75 (64.97)	1262.9 (77.20)	98.50 (4.25)	4.63×10^{-2}
	1.56	468.38 (112.69)	2.83 (0.96)	2.84 (0.96)	0.020 (0.012)	0.411 (0.169)	384.25 (92.56)	1638.8 (232.08)	96.75 (6.13)	5.92×10^{-2}
Source	0.95	436.33 (147.98)	69.50 (4.98)	71.04 (4.49)	0.030 (0.012)	0.108 (0.049)	357.75 (121.32)	1461.7 (96.76)	103.75 (3.56)	5.46×10^{-2}
	1.29	436.92 (106.6)	59.03 (7.41)	60.53 (7.39)	0.018 (0.005)	0.044 (0.016)	358.25 (87.63)	1240.8 (106.30)	100.92 (7.15)	4.87×10^{-2}
	1.54	529.17 (205.14)	52.83 (5.82)	53.88 (5.97)	0.039 (0.002)	0.077 (0.035)	434.25 (168.76)	2138.3 (220.43)	101.83 (5.19)	7.68×10^{-2}

Table 4-4: (cont...)

Zone	Ave. Mid-screen depth	HCO_3^-	NO_2^--N	NO_3^--N	Fe^{3+}	Mn^{2+}	Total alkalinity as $CaCO_3$	TDS-cal	Ionic balance dissolved	Ionic strength[+]
	m	mg L^{-1}							(%)	mol L^{-1}
Down-gradient	0.95	504.20 (106.30)	47.02 (6.05)	50.08 (5.83)	0.023 (0.007)	0.117 (0.039)	413.75 (87.11)	1285.8 (95.03)	100 (4.22)	5.27×10^{-2}
	1.29	525.75 (132.07)	52.10 (4.30)	54.23 (4.61)	0.026 (0.009)	0.043 (0.013)	431.25 (108.35)	1401.4 (128.74)	101.35 (5.71)	5.65×10^{-2}
	1.55	558.20 (101.23)	53.58 (5.28)	54.42 (5.37)	0.030 (0.018)	0.138 (0.042)	457.75 (83.13)	1496.5 (67.01)	99.80 (6.18)	5.96×10^{-2}
Effluent	-	443.75 (176.71)	7.10 (1.40)	7.96 (2.64)	0.03 (0.01)	0.42 (0.07)	364.0 (144.76)	1098.50 (93.50)	85.00 (16.45)	3.97×10^{-2}

[††] The values in brackets are standard deviations.

[+] The contribution of H+ and OH- to the ionic strength was assumed insignificant and hence it was not included in the calculation.

Table 4-5: Summary of bromide plume transport parameter – a) Horizontal displacement

Sampling time	M0	M1	M2	E[X']	VAR[x']	Est. Velocity (at consecutive time interval)	Est. Velocity (at selected time intervals as shown in bold)
Date	mg cm^{-2}	mg cm^{-1}	mg	cm	cm^2	cm d^{-1}	cm d^{-1}
27-Jul-11	0.000	0.00	0.00	0.00	0.00	0.000	
31-Jul-11	0.786	356.29	205644.38	453.48	56095.69	113.369	
3-Aug-11	0.907	345.34	175144.60	**380.65**	48158.80	-24.277	
10-Aug-11	1.390	522.33	263335.53	375.68	48265.82	-0.710	
17-Aug-11	1.594	615.11	319427.81	385.90	51478.11	1.461	
24-Aug-11	1.683	683.52	377495.96	**406.12**	59357.72	2.888	**1.21**
28-Aug-11	1.945	773.34	413800.04	397.61	54658.36	-2.127	
31-Aug-11	1.848	738.68	395466.05	399.82	54194.77	0.736	
4-Sep-11	1.878	769.25	419772.49	409.51	55766.15	2.423	
18-Sep-11	0.613	351.99	233689.06	574.39	51418.76	11.777	
25-Sep-11	0.614	356.46	242379.05	580.98	57505.03	0.941	
2-Oct-11	0.313	203.33	154077.60	**648.60**	70803.45	9.660	**6.22**
23-Oct-11	0.293	213.81	176851.15	729.06	71497.85	3.831	
6-Nov-11	0.265	161.49	118163.74	608.67	74879.54	-8.600	
23-Nov-11	0.319	196.02	148409.35	**614.09**	87832.22	0.319	**-0.66**
4-Dec-11	0.298	172.60	125454.22	578.69	85729.03	-3.219	

Table 4-5 a) Horizontal displacement (cont….)

2-Jan-12	0.257	163.94	126175.85	**637.37**	84309.96	2.024	**0.58**
30-Jan-12	0.186	147.12	123506.48	790.89	38452.43	5.483	
13-Feb-12	0.127	98.70	82250.44	776.59	44097.04	-1.022	
27-Feb-12	0.000	0.00	0.00	nd	nd		
12-Mar-12	0.000	0.00	0.00	nd	nd		
28-Mar-12	0.313	225.56	194036.97	721.24	100258.98		
11-Apr-12	1.610	916.25	688042.83	569.04	103505.39	-10.872	
25-Apr-12	2.378	1280.71	920796.37	538.56	97163.61	-2.177	
9-May-12	2.982	1411.09	945147.12	**473.25**	93018.63	-4.665	**-1.28**
23-May-12	3.097	1413.22	928421.50	456.27	91567.44	-1.213	
18-Jul-12	2.185	1047.88	727420.12	479.54	102930.56	0.416	
25-Jul-12	1.676	771.59	545289.22	**460.44**	113390.80	-2.728	**-0.17**
28-Jul-12	1.578	727.69	512396.49	461.06	112075.58	0.206	
1-Aug-12	1.913	875.95	605398.15	457.89	106799.01	-0.791	
4-Aug-12	2.057	942.59	629911.18	458.23	96250.89	0.110	
8-Aug-12	1.976	975.42	689915.50	493.66	105466.20	8.858	
15-Aug-12	2.085	1117.70	836747.36	535.96	113982.19	6.044	
22-Aug-12	1.847	1029.88	732956.68	557.53	85951.63	3.081	
29-Aug-12	1.567	923.97	667535.53	**589.61**	78328.98	4.583	**3.69**
5-Sep-12	0.918	661.95	516792.41	721.17	42938.61	18.794	
12-Sep-12	0.491	339.43	267885.51	691.18	67758.00	-4.285	
Mean	1.189	581.898	392155.047	526.078	74453.921	3.833	1.370
SD	0.889	412.593	284944.688	150.415	26713.265	20.599	2.679
SE	0.146	67.830	46844.618	25.425	4515.366	3.533	1.013
%CV	74.812	70.905	72.661	28.592	35.879	537.435	195.515

SD = Standard Deviation, SE = Standard Error and CV = Coefficient of Variance.

Table 4-6: Summary of bromide plume transport parameter – b) Vertical displacement

‡Nest # →	1	2	3	4	5	6	7	8	9	10
‡‡**X′** (m)→	-11.60	-9.75	-5.59	0.00	4.48	8.18	9.12	9.94	10.99	12.64
Date of sampling	Central moment (cm)									
27-Jul-11	0	0	0	0	0	0	0	0	0	0
31-Jul-11	nd	nd	37.30	nd	64.62	79.71	99.61	84.29	nd	nd
3-Aug-11	nd	nd	nd	nd	68.14	82.90	95.35	84.29	nd	nd
10-Aug-11	nd	nd	74.73	nd	71.90	87.38	92.49	93.94	nd	nd
17-Aug-11	nd	15.00	74.73	nd	73.83	89.43	100.96	95.23	107.78	nd
24-Aug-11	nd	22.52	74.73	nd	73.67	92.04	102.89	94.61	109.74	nd
28-Aug-11	nd	nd	74.73	nd	73.86	93.61	103.20	98.63	108.28	nd
31-Aug-11	nd	nd	74.73	nd	73.67	94.04	105.51	98.03	108.49	nd
4-Sep-11	nd	nd	73.35	nd	72.92	94.81	105.05	98.01	107.85	nd
18-Sep-11	nd	nd	nd	nd	98.46	94.68	120.81	101.87	108.29	nd
25-Sep-11	nd	nd	nd	nd	98.18	95.95	120.25	103.06	107.85	nd
2-Oct-11	nd	nd	nd	nd	99.54	111.81	120.34	126.33	108.07	nd
23-Oct-11	nd	67.53	nd	nd	95.67	111.62	120.41	126.96	108.66	nd
6-Nov-11	nd	nd	nd	nd	97.94	111.65	120.25	126.68	120.90	nd
23-Nov-11	nd	nd	nd	nd	97.36	111.49	120.28	126.88	121.37	127.37
4-Dec-11	nd	nd	nd	nd	97.61	111.45	120.07	126.48	121.42	130.97
2-Jan-12	nd	nd	nd	nd	98.58	111.56	119.70	126.13	123.02	129.64
30-Jan-12	nd	nd	nd	nd	nd	111.93	120.08	126.36	123.23	126.92
13-Feb-12	nd	nd	nd	nd	nd	112.25	120.55	nd	123.38	129.64
27-Feb-12	nd	nd	nd	nd	nd	nd	nd	nd	nd	nd
12-Mar-12	nd	nd	nd	nd	nd	nd	nd	nd	nd	nd
28-Mar-12	nd	nd	nd	nd	99.35	111.52	114.13	103.34	110.87	113.76
11-Apr-12	nd	62.68	55.87	80.49	81.55	88.52	96.61	104.40	111.61	112.53

‡Nest-1 and 2 are located at the up-gradient site. Nest 3 to 5 within the source zone and Nest 6 to 10 are at the down-gradient site (see Figure 4-2).
‡‡X’ is horizontal location (m)

Table 4-6: b) Vertical displacement (cont…)

25-Apr-12	47.39	49.13	56.45	77.05	77.37	92.77	100.61	101.77	111.94	114.58
9-May-12	nd	53.39	58.79	74.74	80.09	96.07	101.76	100.04	110.88	119.81
23-May-12	nd	67.53	58.54	72.61	81.95	95.50	101.79	99.51	108.86	114.48
18-Jul-12	nd	62.93	53.45	70.97	78.31	101.55	101.71	104.63	107.76	111.62
25-Jul-12	nd	62.12	68.49	71.91	76.43	105.57	102.12	104.29	108.46	111.02
28-Jul-12	nd	nd	68.13	71.38	76.83	105.07	101.25	104.30	108.47	110.85
1-Aug-12	nd	nd	68.25	72.73	76.45	89.39	101.23	103.92	108.77	109.53
4-Aug-12	nd	70.67	65.31	73.19	78.98	85.62	101.58	104.53	108.72	109.78
8-Aug-12	nd	66.71	67.62	72.92	76.27	89.65	102.06	104.84	108.07	109.75
15-Aug-12	nd	65.49	67.76	72.71	78.45	93.59	103.97	104.99	108.86	108.89
22-Aug-12	nd	nd	68.54	90.06	79.56	95.91	105.57	105.47	108.96	109.46
29-Aug-12	nd	nd	69.15	89.98	99.31	97.48	106.49	104.13	108.61	108.69
5-Sep-12	nd	nd	nd	nd	106.02	96.14	120.01	104.73	108.86	108.51
12-Sep-12	nd	nd	nd	nd	98.84	112.61	119.84	125.29	121.49	124.61
Mean	47.39	55.47	65.53	76.21	84.43	98.68	108.49	106.61	111.92	116.31
SD	nd	23.29	17.09	21.34	18.84	19.38	20.56	22.03	20.57	26.06
SE	nd	6.72	3.82	5.92	3.33	3.32	3.53	3.83	3.69	5.69
%CV	nd	41.98	26.08	28.01	22.32	19.63	18.95	20.66	18.38	22.40

SD = Standard Deviation, SE = Standard Error and CV = Coefficient of Variance.

Table 4-7: Summary of virus test data matrix

WellID	Well Mid-Screen depth (m)	Depth to GW, d(t) (m)	Well Location vs source zone	Sampling date	Sample volume (L)	Viral concentration [Log (genome copies L^{-1})]						
						Norovirus	Rotavirus	Sapovirus	Astrovirus	Enterovirus	General Adenovirus	JC virus
†TANK#4	-		Source tank	18-Jul-12	2	4.40	5.74	3.78	3.23	Neg	3.95	4.97
††TANK#7	-		Source tank	18-Jul-12	2	4.45	5.41	4.17	3.55	4.06	3.80	5.50
†††DI-H_2O	-		De-ionized	18-Jul-12	2	Neg[5]	Neg	Neg	Neg	Neg	Neg	Neg
6 (0.95 m)	0.95	0.83	1-m down-	18-Jul-12	2	3.66	4.31	Neg	Neg	Neg	Neg	Neg
8 (0.93 m)	0.93	0.77	3-m down-	18-Jul-12	2	Neg	Neg	Neg	Neg	Neg	Neg	Neg
10 (0.96 m)	0.96	0.78	6-m down-	18-Jul-12	2	Neg	Neg	Neg	Neg	Neg	Neg	Neg
††TANK#7	-		Source tank	1-Aug-12	2	4.62	5.61	3.43	3.80	2.45	Neg	5.97
†††DI-H_2O	-		De-ionized	1-Aug-12	2	Neg	Neg	Neg	Neg	Neg	Neg	Neg
6 (0.95 m)	0.95	0.96	1-m down-	1-Aug-12	2	4.29	4.88	Neg	Neg	Neg	Neg	Neg
8 (0.93 m)	0.93	0.93	3-m down-	1-Aug-12	2	Neg	Neg	Neg	Neg	Neg	Neg	Neg
10 (0.96 m)	0.96	0.90	6-m down-	1-Aug-12	2	Neg	Neg	Neg	Neg	Neg	Neg	Neg

Table 4-7: Summary of virus test data matrix

WellID	Well Mid-Screen depth (m)	Depth to GW, d(t) (m)	Well Location vs source zone	Sampling date	Sample volume (L)	Viral concentration [Log (genome copies L^{-1})]						
						Norovirus	Rotavirus	Sapovirus	Astrovirus	Enterovirus	General Adenovirus	JC virus
†TANK#4	-		Source tank	15-Aug-12	2	5.16	6.22	3.99	5.59	3.92	2.95	5.71
††TANK#7	-		Source tank	15-Aug-12	2	4.82	5.70	4.21	5.74	3.91	Neg	5.27
†††DI-H_2O	-		De-ionized	15-Aug-12	2	Neg	Neg	Neg	Neg	Neg	Neg	Neg
6 (0.95 m)	0.95	0.90	1-m down-	15-Aug-12	2	Neg	4.51	Neg	Neg	Neg	Neg	Neg
8 (0.93 m)	0.93	0.85	3-m down-	15-Aug-12	2	Neg	Neg	Neg	Neg	Neg	Neg	Neg
10 (0.96 m)	0.96	0.80	6-m down-	15-Aug-12	2	Neg	Neg	Neg	Neg	Neg	Neg	Neg
††TANK#7	-		Source tank	29-Aug-12	1	5.60	5.89	Neg	4.51	3.07	4.12	6.21
DI-H_2O	-		De-ionized	29-Aug-12	1	Neg	Neg	Neg	Neg	Neg	Neg	Neg
6 (1.55 m)	1.55	1.13	1-m down-	29-Aug-12	1	Neg	3.73	Neg	Neg	Neg	Neg	Neg
8 (1.56 m)	1.56	1.09	3-m down-	29-Aug-12	1	Neg	Neg	Neg	Neg	Neg	Neg	Neg
10 (1.52)	1.52	1.06	6-m down-	29-Aug-12	1	Neg	Neg	Neg	Neg	Neg	Neg	Neg

Table 4-7: Summary of virus test data matrix

WellID	Well Mid-Screen depth (m)	Depth to GW, d(t) (m)	Well Location vs source zone	Sampling date	Sample volume (L)	Viral concentration [Log (genome copies L^{-1})]						
						Norovirus	Rotavirus	Sapovirus	Astrovirus	Enterovirus	General Adenovirus	JC virus
††TANK#7	-		Source tank	05-Sep-12	1	4.79	5.11	Neg	3.81	3.53	Neg	5.73
†††DI-H_2O	-		De-ionized	05-Sep-12	1	Neg	Neg	Neg	Neg	Neg	Neg	Neg
6 (1.55 m)	1.55	1.22	1-m down-	05-Sep-12	1	Neg	Neg	Neg	Neg	Neg	Neg	Neg
8 (1.56 m)	1.56	1.17	3-m down-	05-Sep-12	1	Neg	Neg	Neg	Neg	Neg	Neg	4.99
10 (1.52)	1.52	1.14	6-m down-	05-Sep-12		Neg	Neg	Neg	Neg	Neg	Neg	Neg
†TANK#4	-		Source tank	12-Sep-12	1	5.02	6.21	Neg	3.92	3.93	4.49	5.92
††TANK#7	-		Source tank	12-Sep-12	1	4.90	5.48	Neg	3.17	Neg	Neg	5.82
†††DI-H_2O	-		De-ionized	12-Sep-12	1	Neg	Neg	Neg	Neg	Neg	Neg	Neg
6 (1.55 m)	1.55	1.29	1-m down-	12-Sep-12	1	Neg	Neg	Neg	Neg	Neg	Neg	Neg
8 (1.56 m)	1.56	1.24	3-m down-	12-Sep-12	1	Neg	Neg	Neg	Neg	Neg	Neg	Neg
10 (1.52)	1.52	1.20	6-m down-	12-Sep-12	1	Neg	Neg	Neg	Neg	Neg	Neg	Neg

†Source tank before UV-disinfection but with a FAST system (Fixed Activated Sludge Treatment)
††Source tank after UV-disinfection
†††DI-H2O is de-ionized water used as a field control

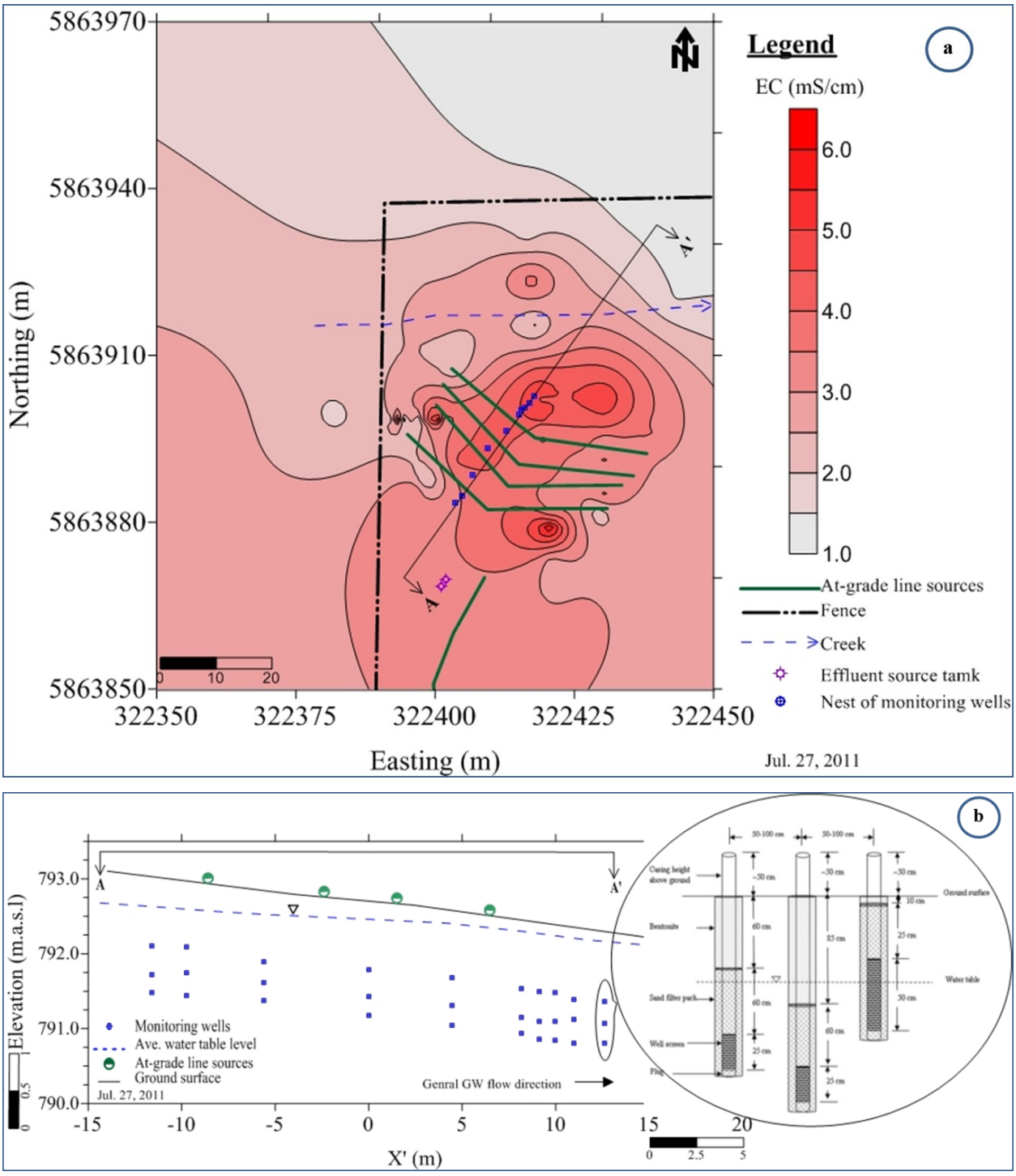

Figure 4-1: Groundwater EC plume and areal plan view of the nest of monitoring wells (a) and a two-dimensional view of the MWs along the A-A' transect (b). The coordinates were projected according to the North American Datum 83 (NAD 83) and are in zone 12.

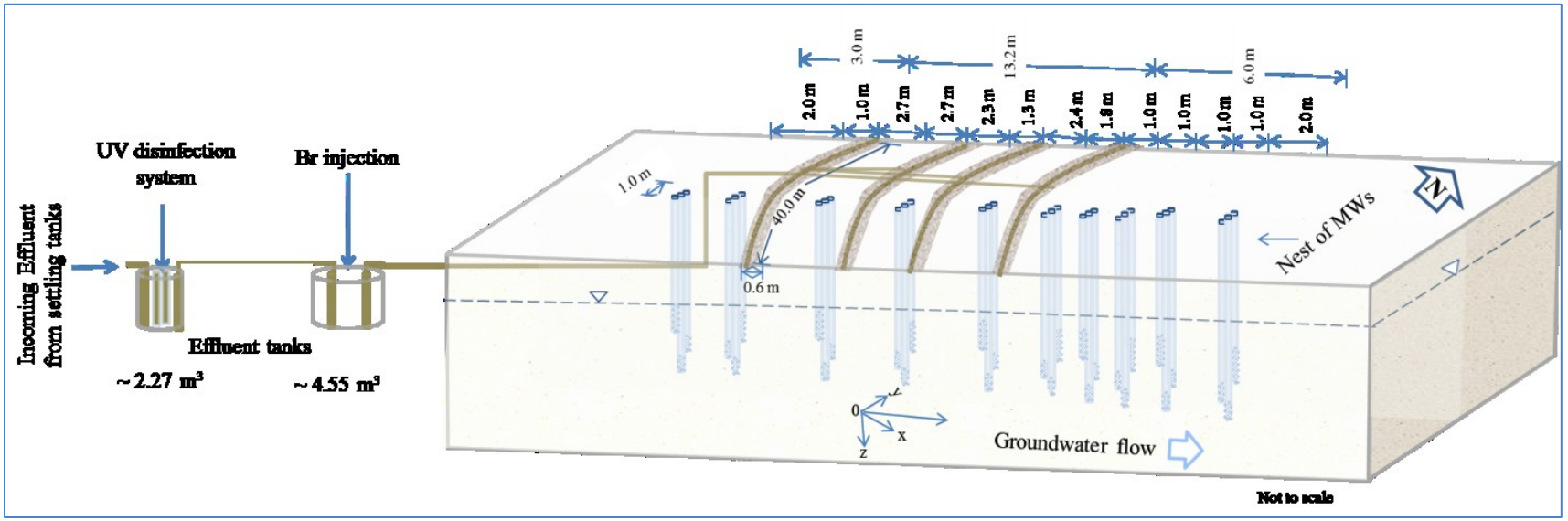

Figure 4-2: Three dimensional plan view of the monitoring wells, effluent source tank and distribution laterals layout. The nest of monitoring wells are numbered as 1 to 10 from up-gradient to downgradient direction.

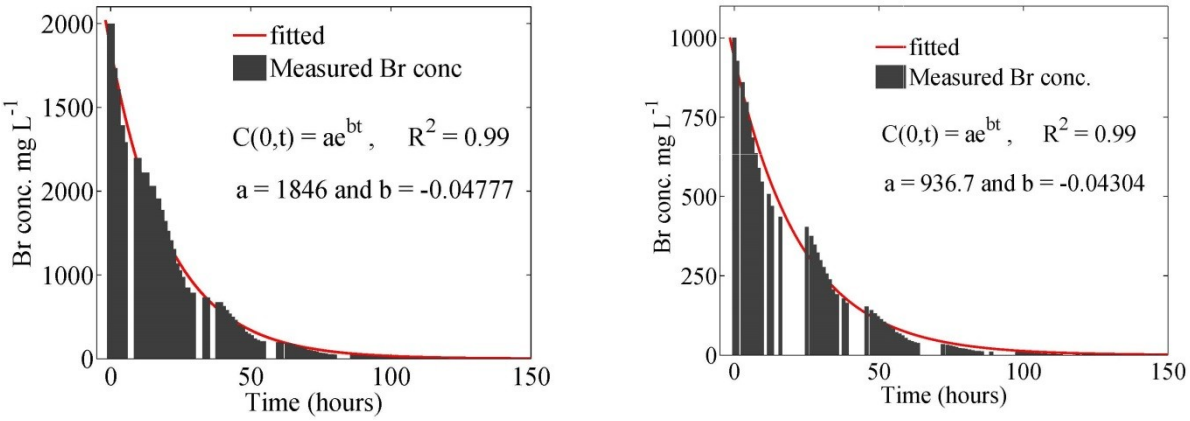

a) b)

Figure 4-3: Br injected to the source tank and pulse duration, a) Experiment 1, in 2011 and b) Experiment 2, in 2012.

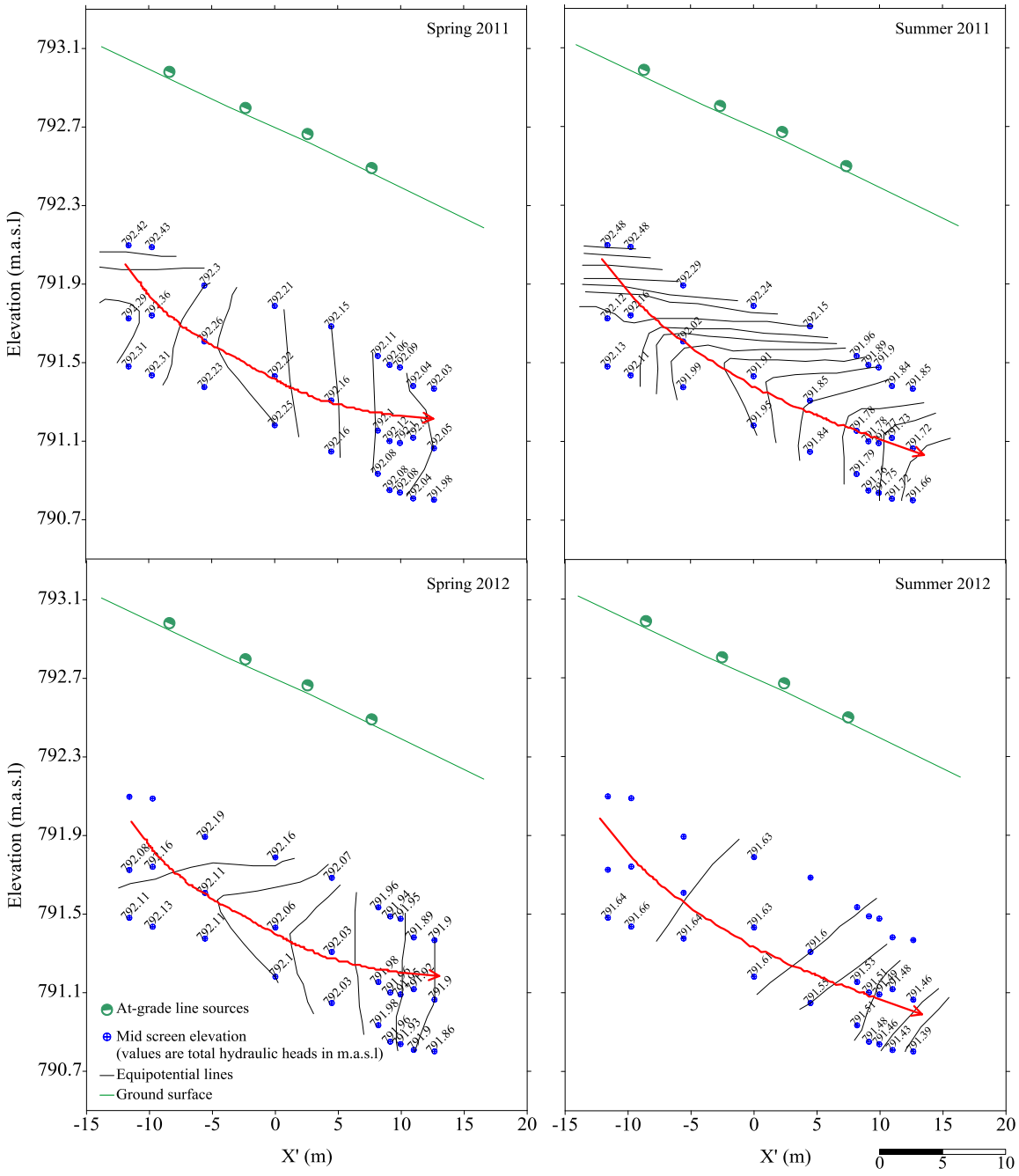

Figure 4-4: Seasonal hydrologic dynamic (Spring and summer periods) along the measurement transect. The arrows show average direction of general groundwater flow, which is downward and to the northeast direction. The data for Spring 2011 and 2012 included from April to June (on average SD ranged between 0.095 to 0.115) and for that of Summer 2011 and 2012 the data was from July to September (on average SD ranged between 0.095 to 0.218). SD=standard deviation. Overall average horizontal gradient was 0.017.

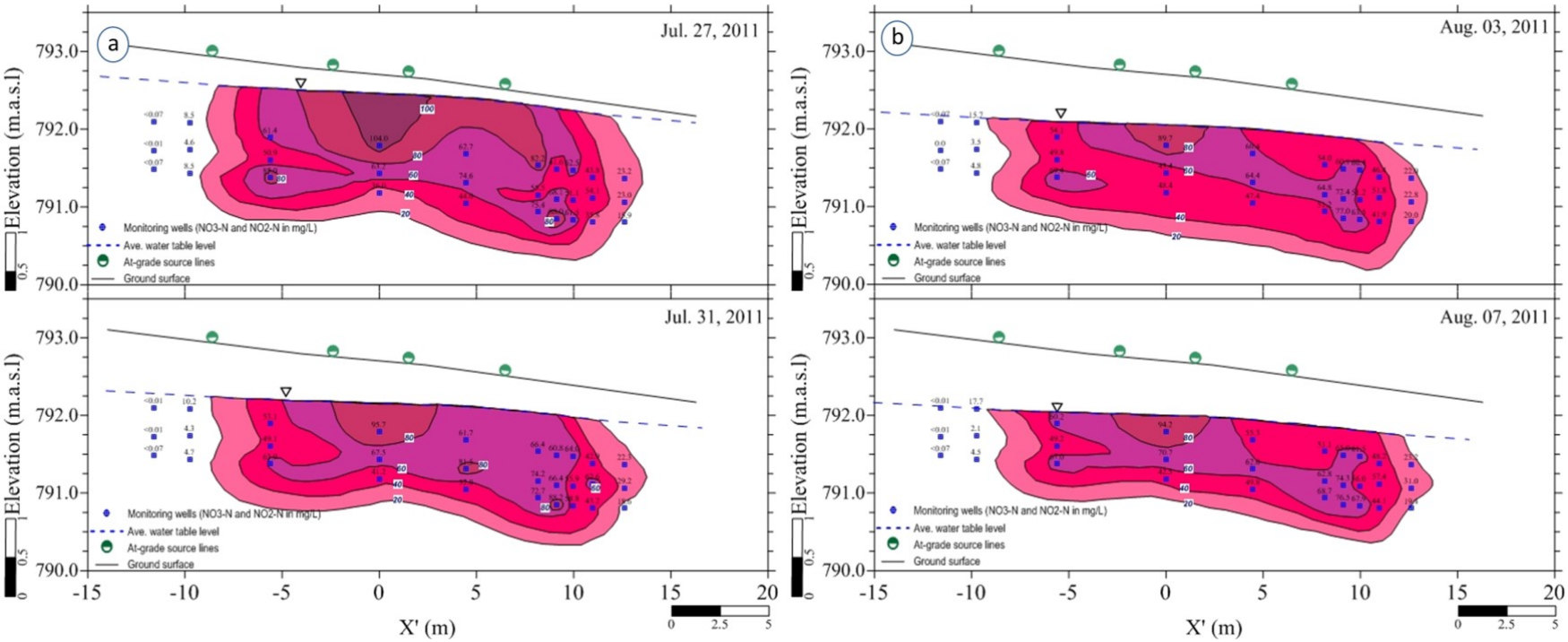

Figure 4-5: Spatial and temporal plume of nitrate-nitrogen and nitrite-nitrogen observed in the summer 2011 after about four year since the at-grade system started its operation. The plume indicates wastewater impact on the groundwater, wastewater dynamics and plume flow direction.

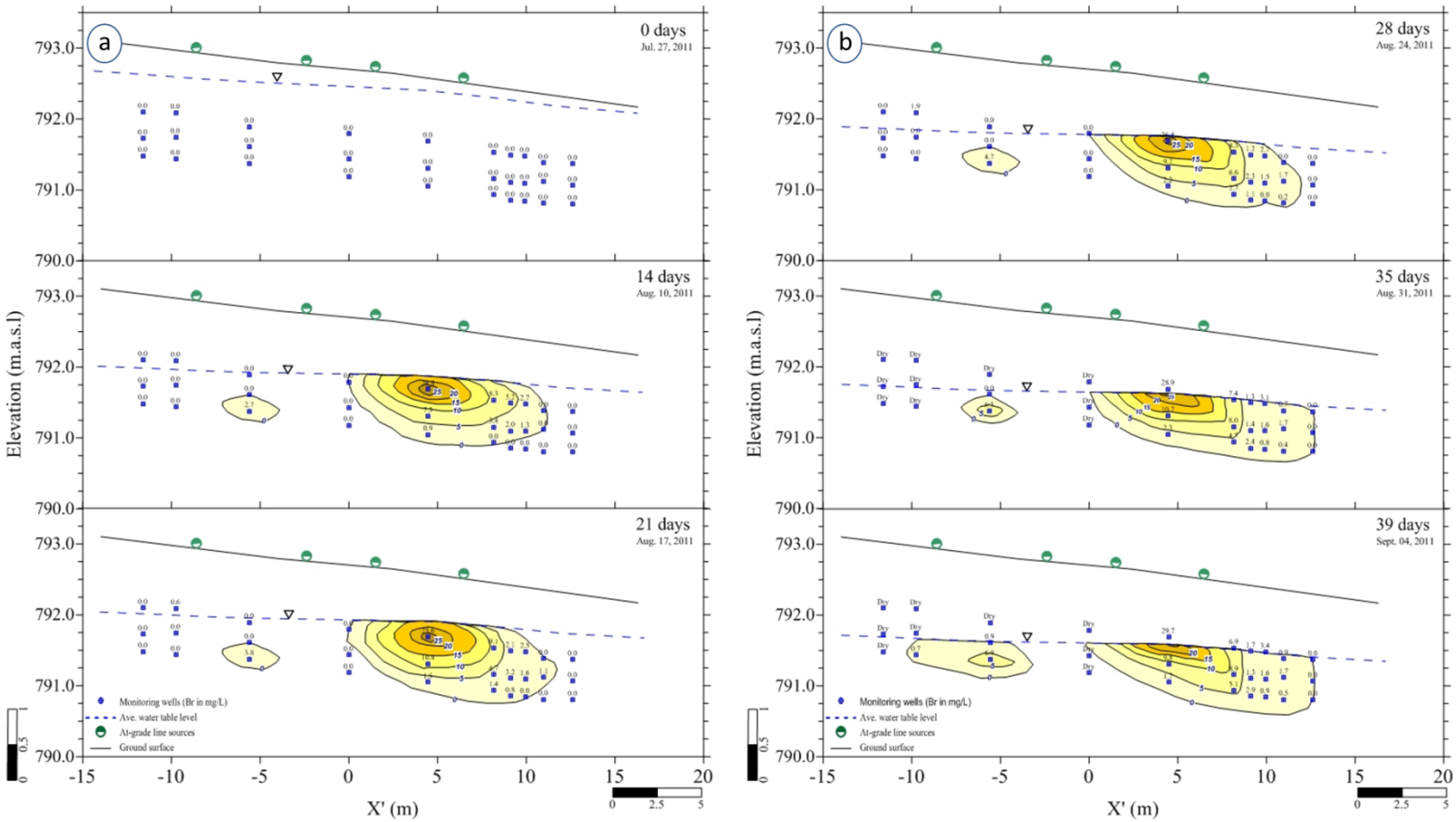

Figure 4-6: Visualization of two-dimensional bromide plume movement and displacement: (a) and (b) Jul. 27 to Sept. 04, 2011.

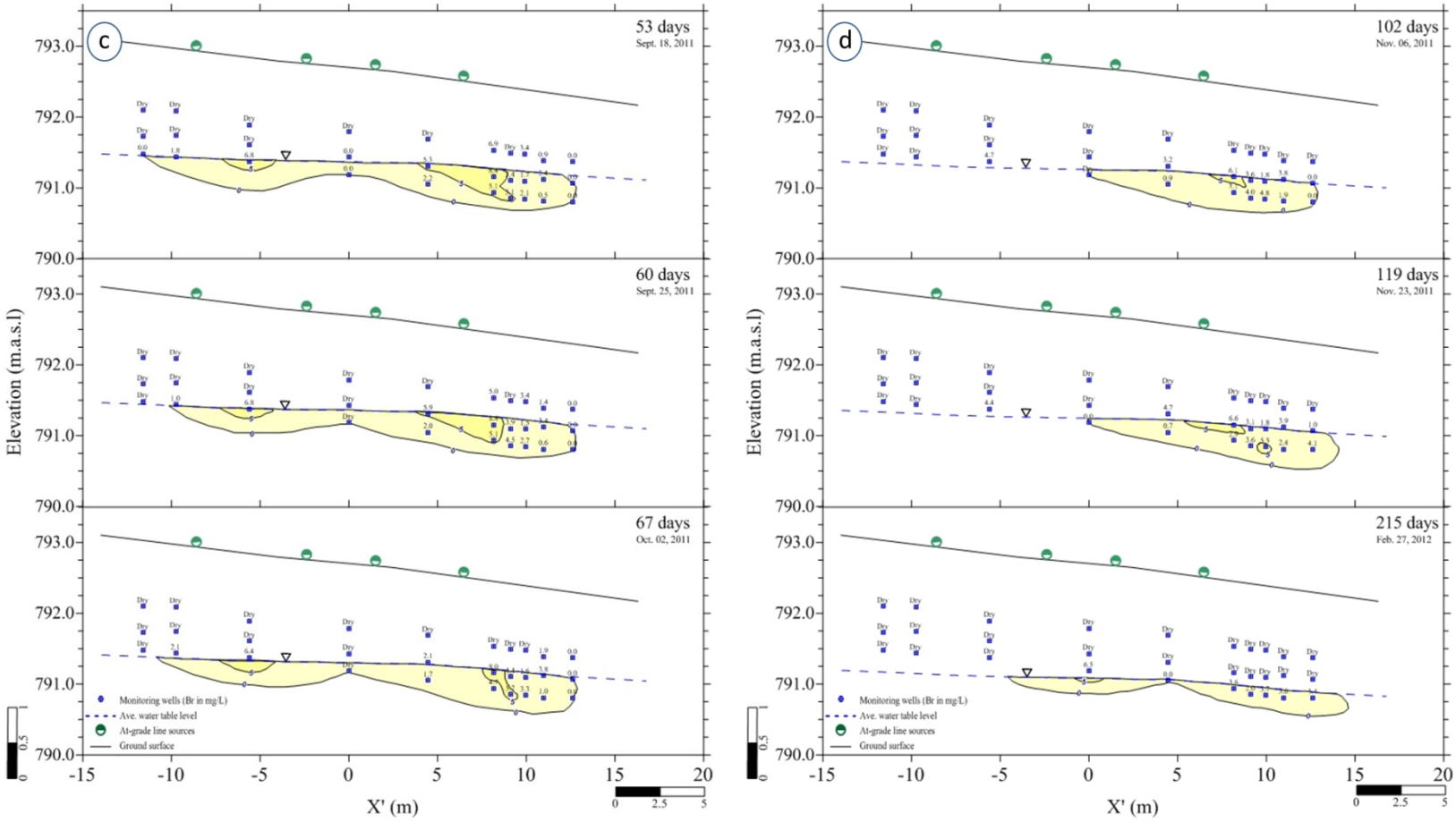

Figure 4-6: Visualization of two-dimensional bromide plume movement and displacement: (c) and (d) from Sept. 18, 2011 to Feb. 27, 2012.

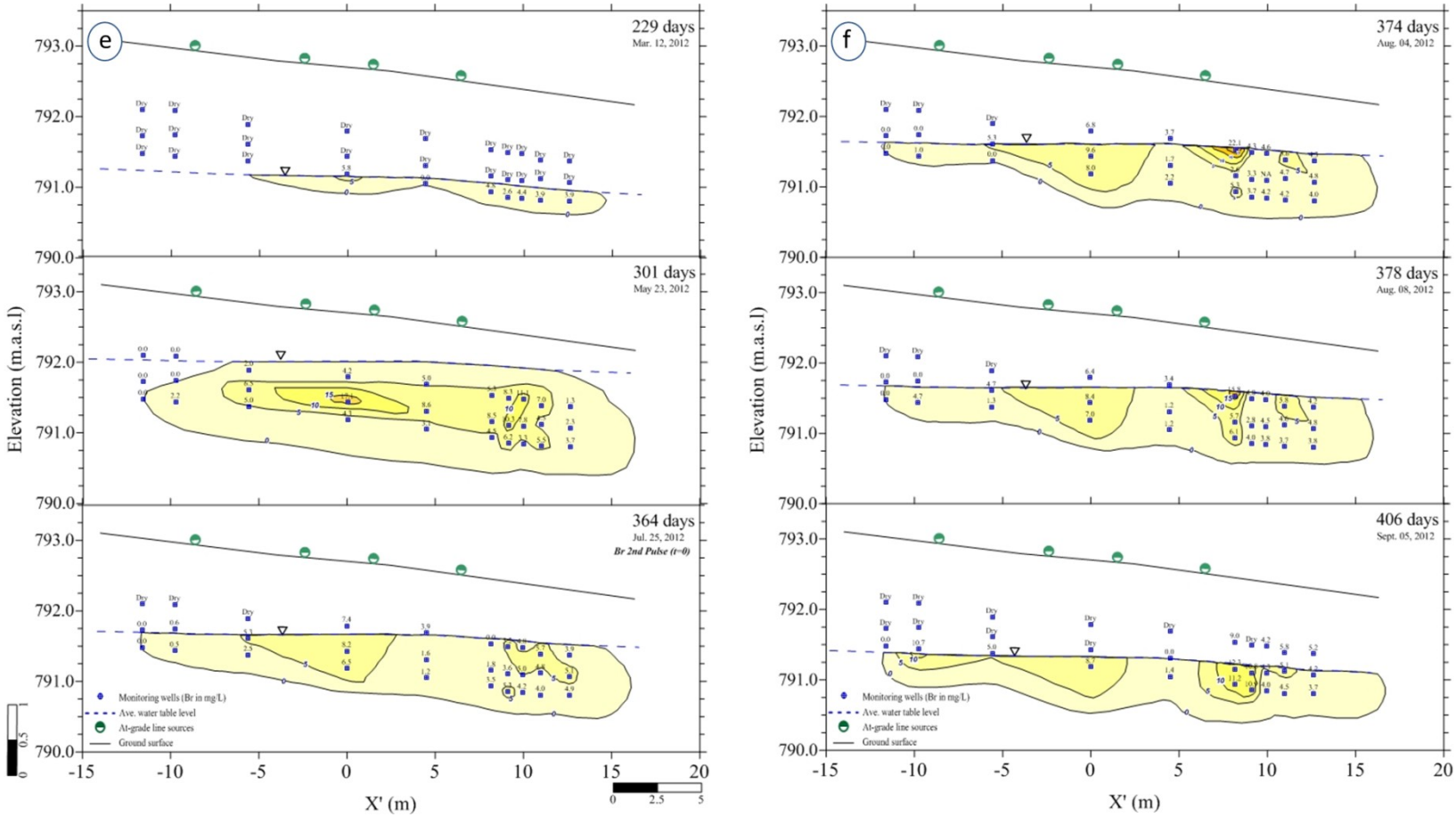

Figure 4-6: Visualization of two-dimensional bromide plume movement and displacement: (e) and (f) from Mar. 12, 2012 to Sept. 12, 212.

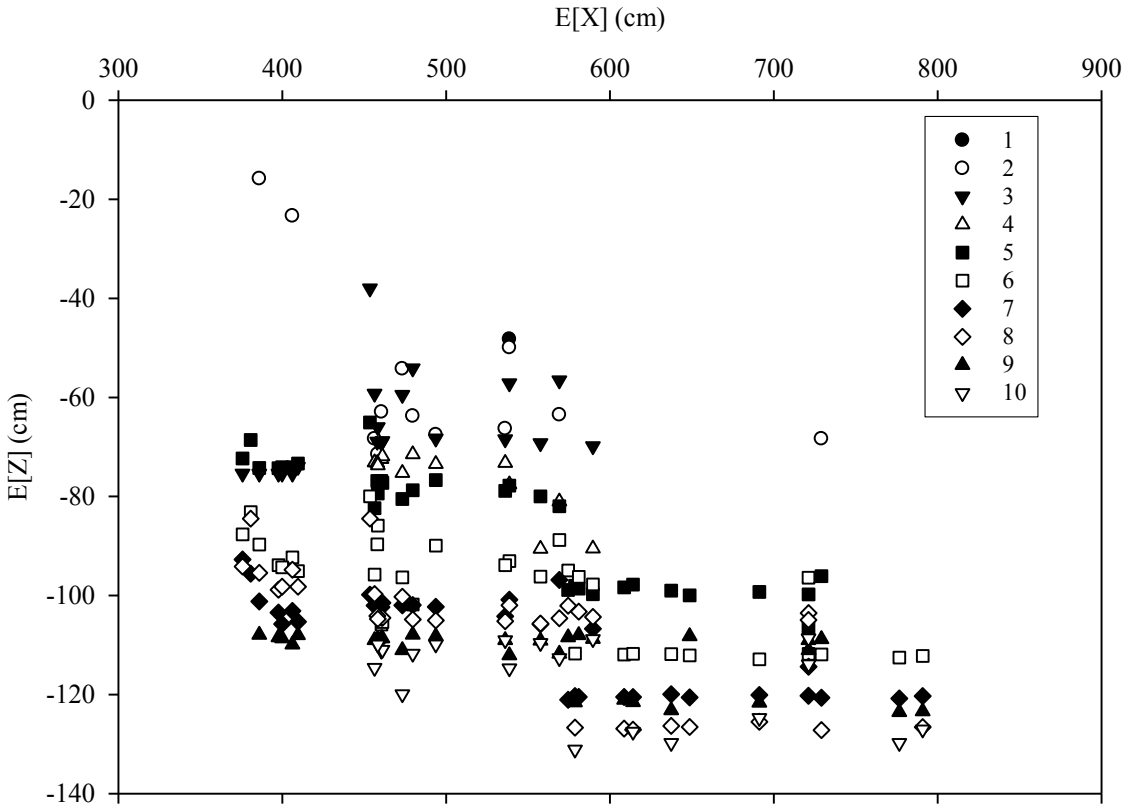

Figure 4-7: Estimated vertical and horizontal central moments for Br transport along the flow domain. The estimated plume center of mass displaced downward as it moved along the general groundwater flow direction. The numbers in the legend show nest number: 1-2 up-gradient zone, 3-5 in the source zone and the remaining 6-10 in the down-gradient zone. Each nest has three MWs with mid-screen depth from 0.93 to 1.58 m below the ground surface (Figure 4-1b and 4-2).

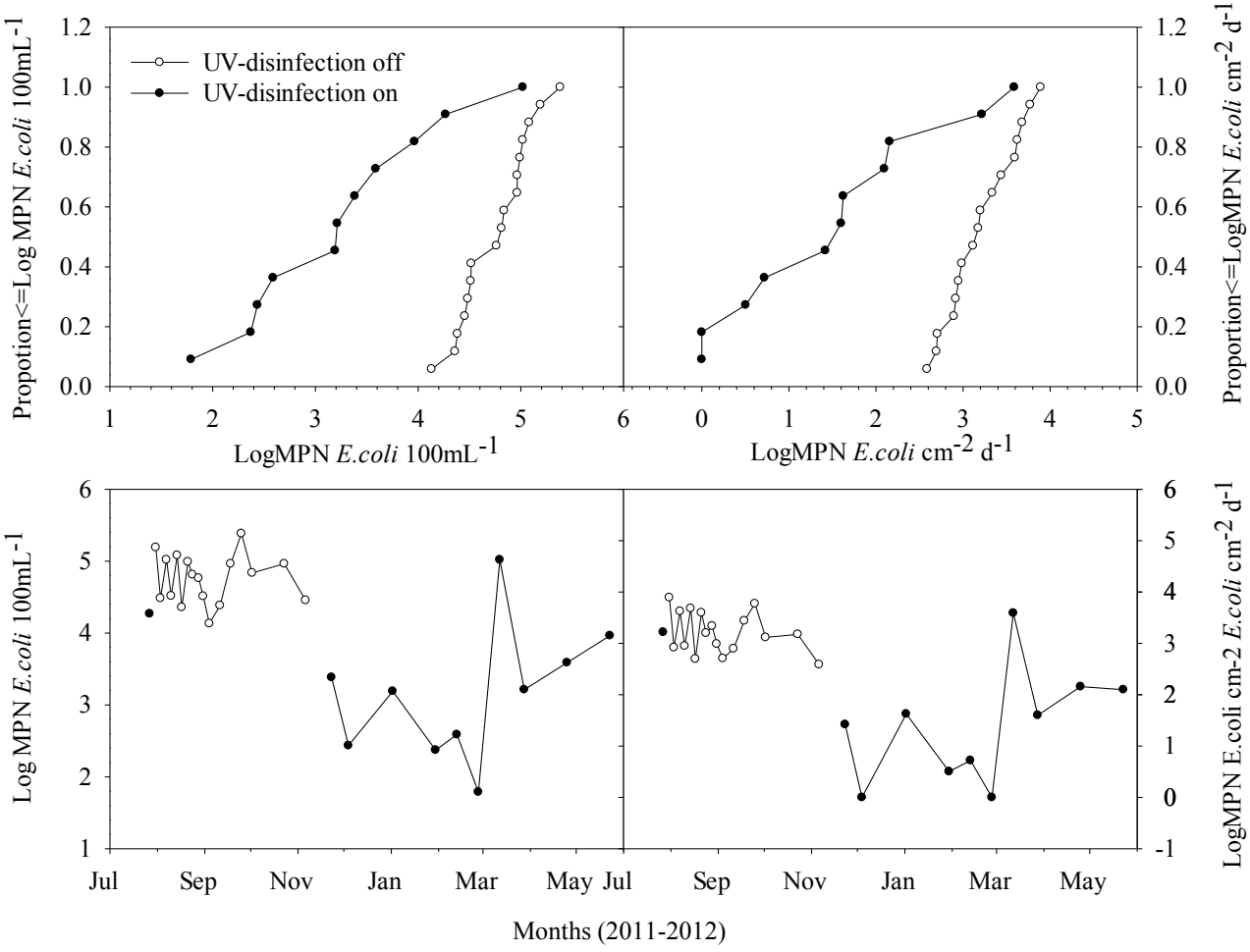

Figure 4-8: *E.coli* concentration in the source tank and daily loading rate to the infiltration field when the UV disinfection system was turned on and off observed during the sampling period from July 27, 2011 to March 23, 2012.

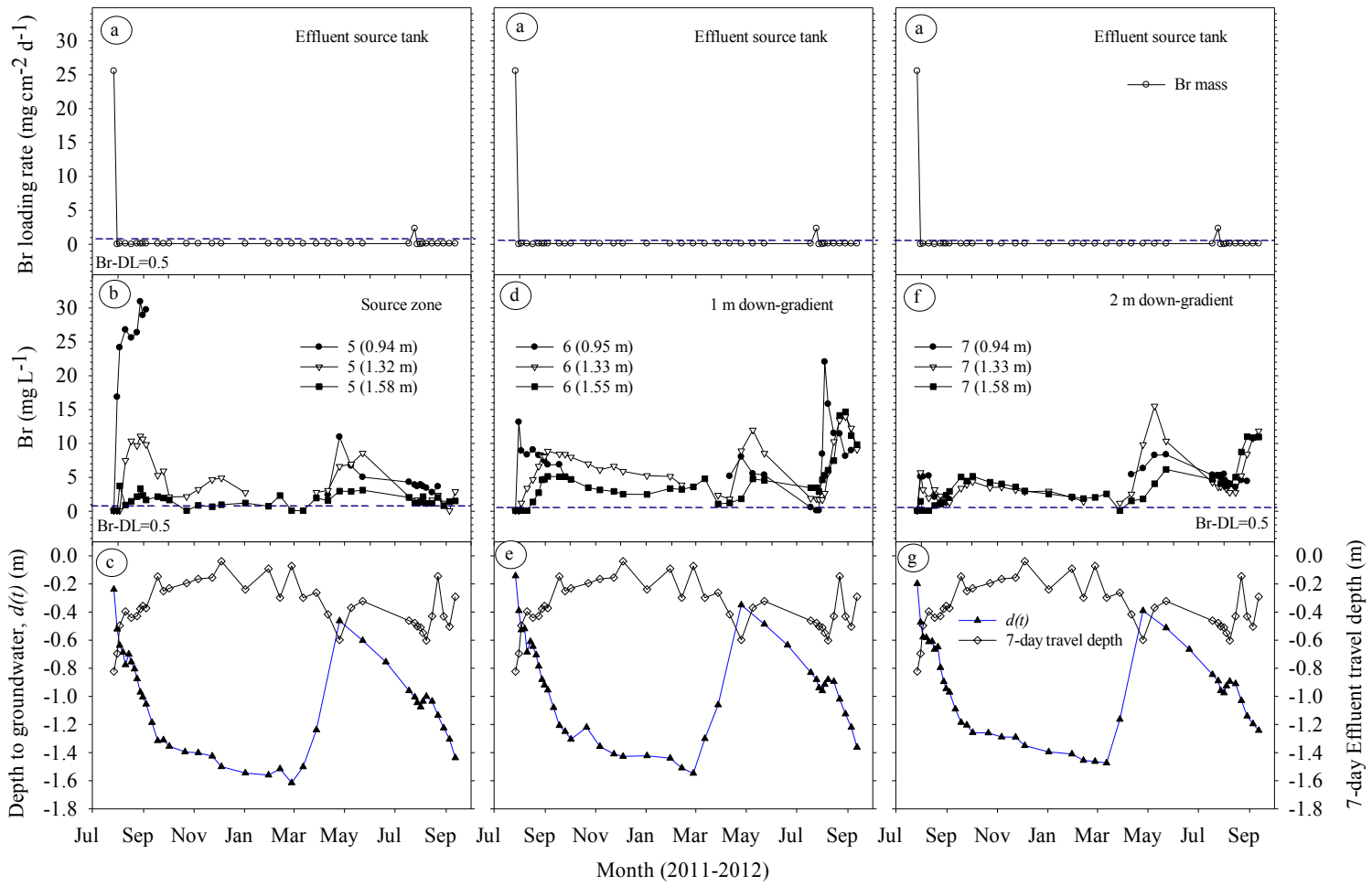

Figure 4-9: Observed Br loading rate (a) and breakthrough in selected wells: at the Source zone (b); 1 m down gradient (d); and 2 m down gradient (e). The bottom Figures (c, e and g) show corresponding depth to groundwater and 7-day effluent travel time observed from July 27, 2011 to Sept. 12, 2012 sampling time. The numbers 5, 6, 7 in b,d,f indicate nest number and the ones in brackets are corresponding mid-screen depth of the MWs below the ground surface. Br-DL is Br detection limit of the analytical instrument.

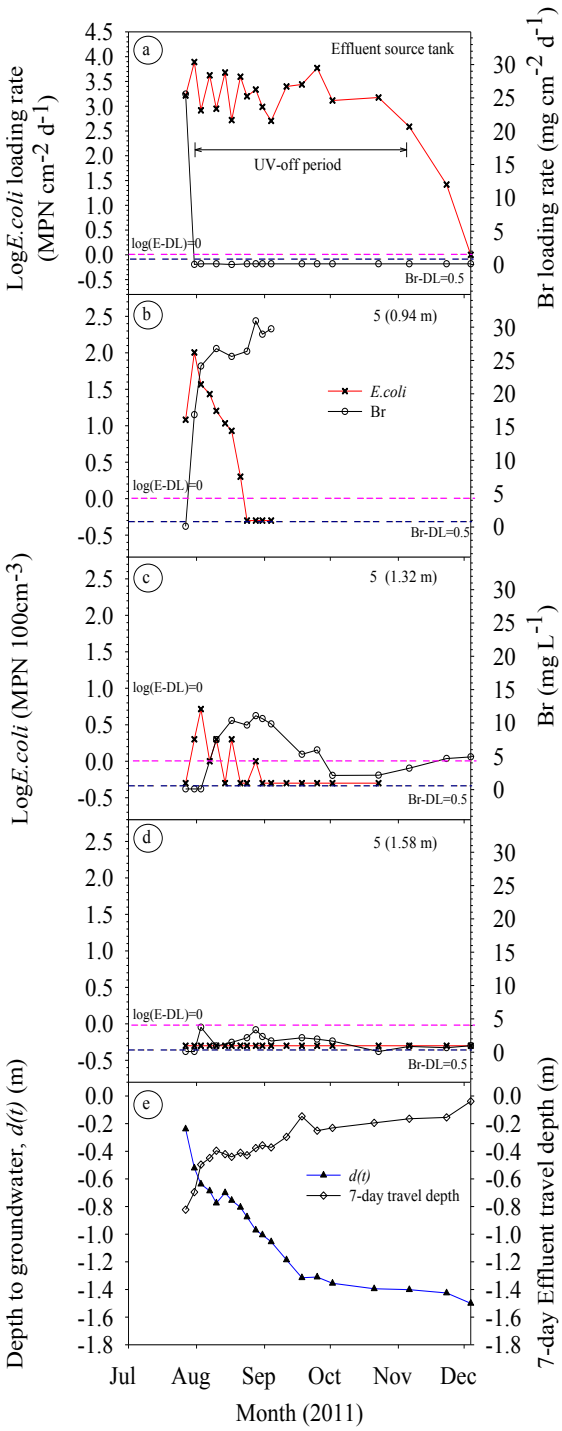

Figure 4-10: Br and *E.coli* loading rates (a); their breakthrough curves observed at the source zone nest at depths: (b) 0.94 m, (c) 1.32 m and (d) 1.58 m; and corresponding depth to groundwater and 7-day effluent travel time (e) observed from July 27 to December 04, 2011 sampling time. The number 5 in b, c, d indicate nest number and the ones in brackets are corresponding mid-screen depth of the MWs below the ground surface. E-Dl and Br-DL show *E.coli* and Br detection limits of the analytical instruments respectively.

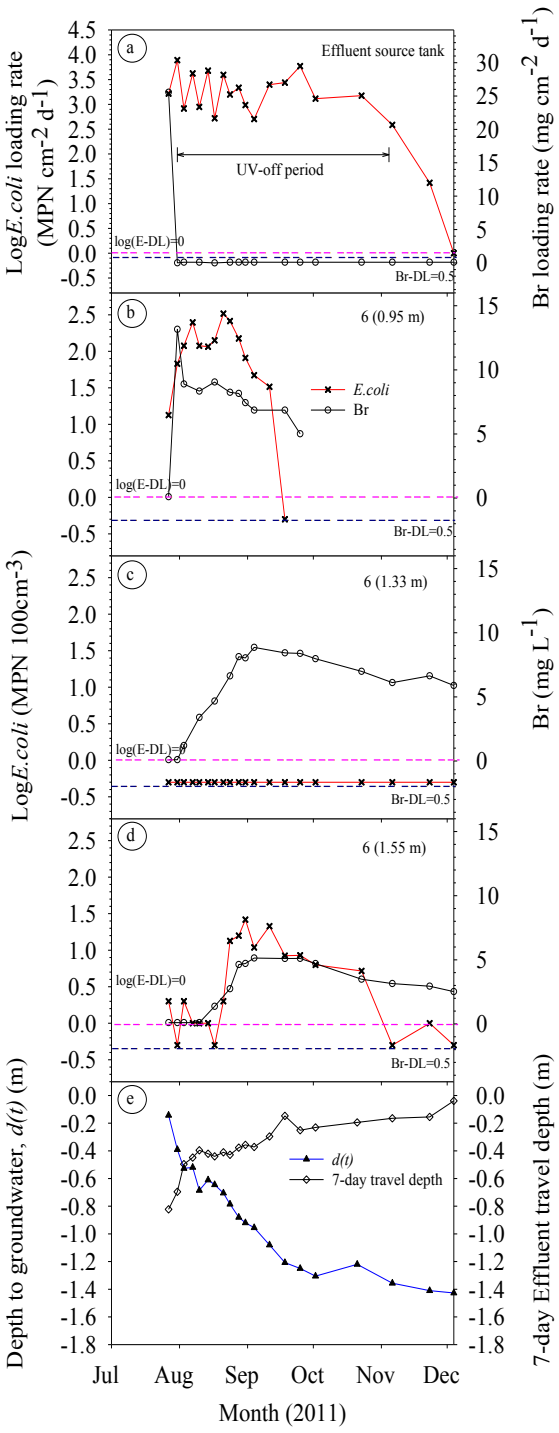

Figure 4-11: Br and E.coli loading rates (a); their breakthrough curves observed at the nest located 1 m down gradient of the source zone at depths: (b) 0.95 m, (c) 1.33 m and (d) 1.55 m; and corresponding depth to groundwater and 7-day effluent travel time (e) observed from July 27 to December 04, 2011 sampling time. The number 6 in b, c, d indicates nest number and the ones in brackets are corresponding mid-screen depth of the MWs below the ground surface. E-Dl and Br-DL show *E.coli* and Br detection limits of the analytical instruments respectively.

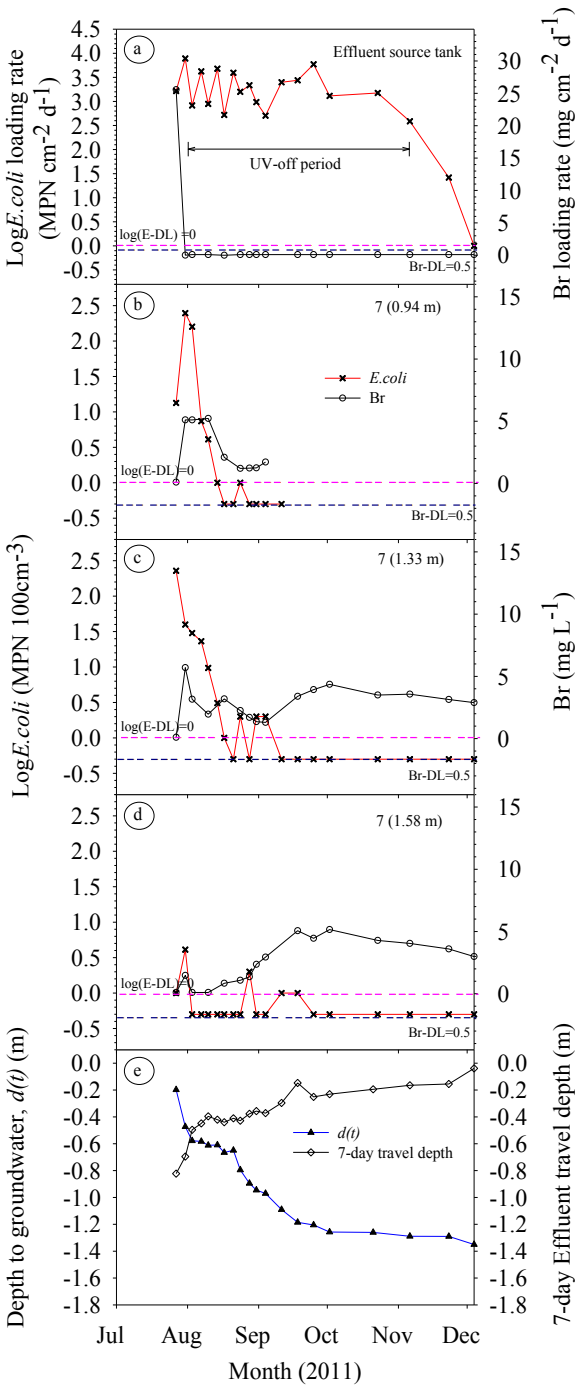

Figure 4-12: Br and E.coli loading rates (a); their breakthrough curves observed at the nest located 2 m down gradient of the source zone at depths: (b) 0.94 m, (c) 1.33 m and (d) 1.58 m; and corresponding depth to groundwater and 7-day effluent travel time (e) observed from July 27 to December 04, 2011 sampling time. The number 7 in b, c, d indicates nest number and the ones in brackets are corresponding mid-screen depth of the MWs below the ground surface. E-Dl and Br-DL show *E.coli* and Br detection limits of the analytical instruments respectively.

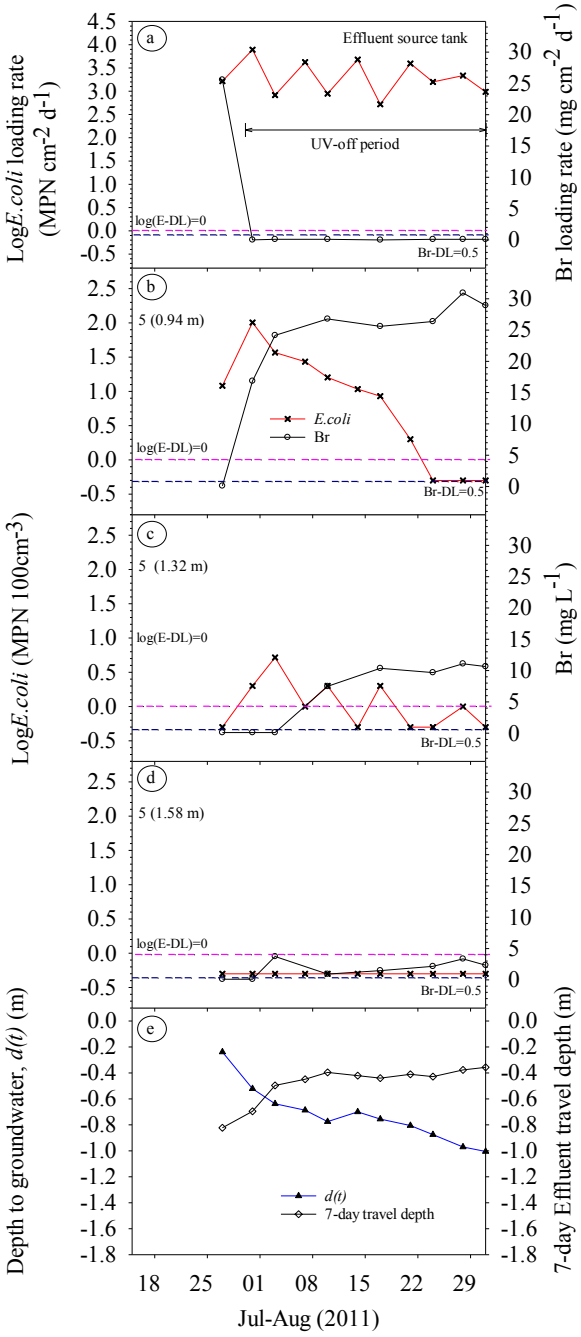

Figure 4-13: Br and *E.coli* loading rates (a); their breakthrough curves observed at the source zone nest at depths: (b) 0.94 m, (c) 1.32 m and (d) 1.58 m; and corresponding depth to groundwater and 7-day effluent travel time (e) observed from July 27 to August 31, 2011 sampling time. The number 5 in b, c, d indicate nest number and the ones in brackets are corresponding mid-screen depth of the MWs below the ground surface. E-Dl and Br-DL in (a) show *E.coli* and Br detection limits of the analytical instruments respectively.

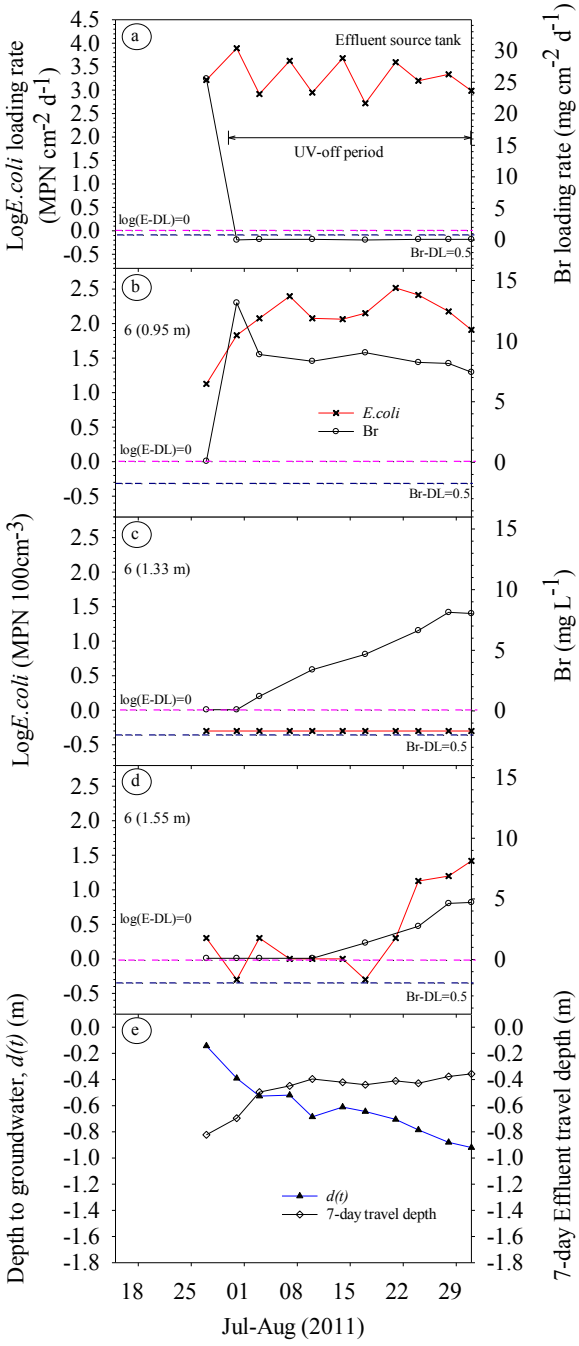

Figure 4-14: Br and E.coli loading rates (a); their breakthrough curves observed at the nest located 1 m down gradient of the source zone at depths: (b) 0.95 m, (c) 1.33 m and (d) 1.55 m; and corresponding depth to groundwater and 7-day effluent travel time (e) observed from July 27 to August 31, 2011 sampling time. The number 6 in b, c, d indicates nest number and the ones in brackets are corresponding mid-screen depth of the MWs below the ground surface. E-Dl and Br-DL in (a) show *E.coli* and Br detection limits of the analytical instruments respectively.

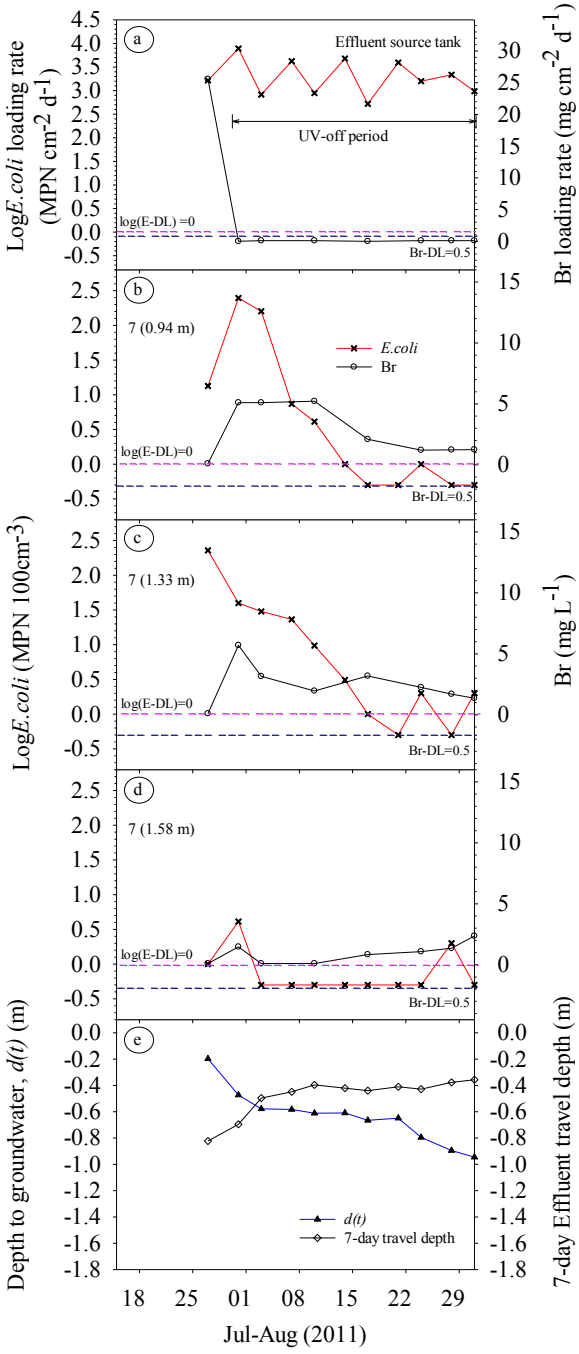

Figure 4-15: Br and E.coli loading rates (a); their breakthrough curves observed at the nest located 2 m down gradient of the source zone at depths: (b) 0.94 m, (c) 1.33 m and (d) 1.58 m; and corresponding depth to groundwater and 7-day effluent travel time (e) observed from July 27 to August 31, 2011 sampling time. The number 7 in b, c, d indicates nest number and the ones in brackets are corresponding mid-screen depth of the MWs below the ground surface. E-Dl and Br-DL in (a) show *E.coli* and Br detection limits of the analytical instruments respectively.

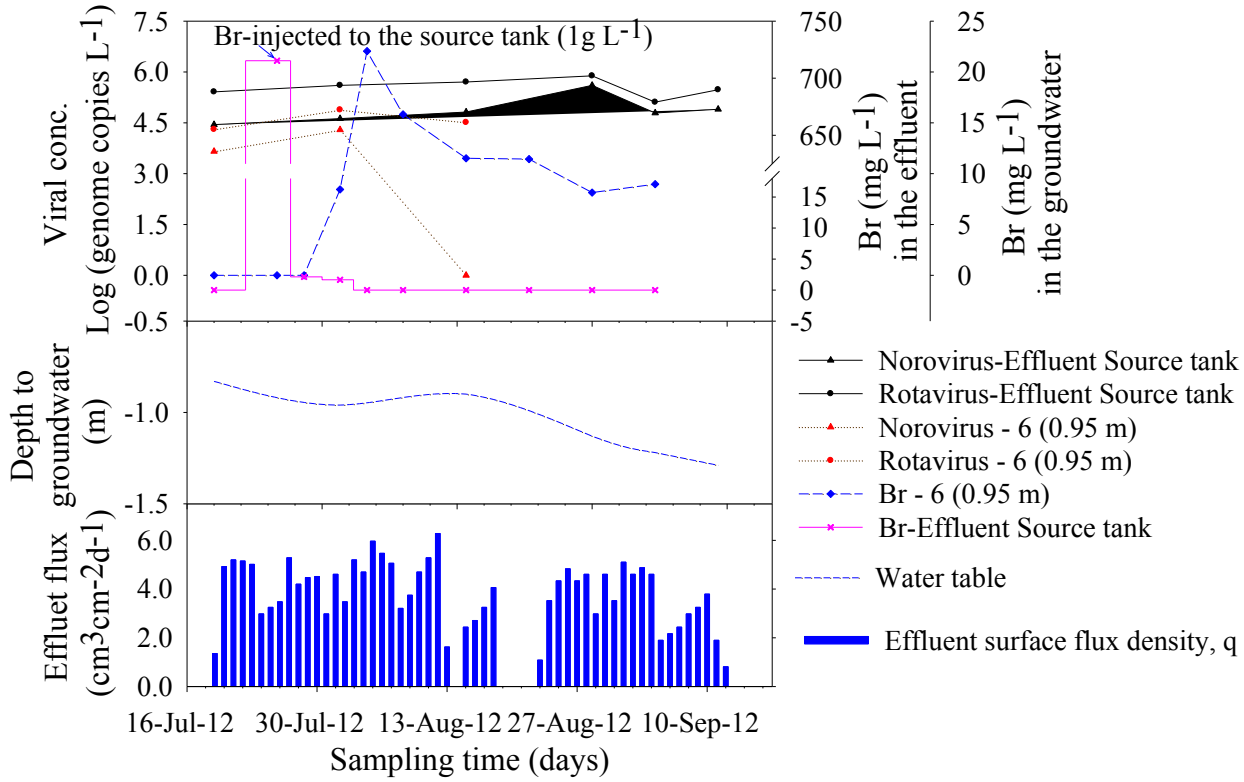

Figure 4-16: Norovirus, rotavirus and Br conc. in the effluent and the groundwater observed at MW 6 (0.95 m) (a) and depth to groundwater (b); and Effluent surface flux density observed

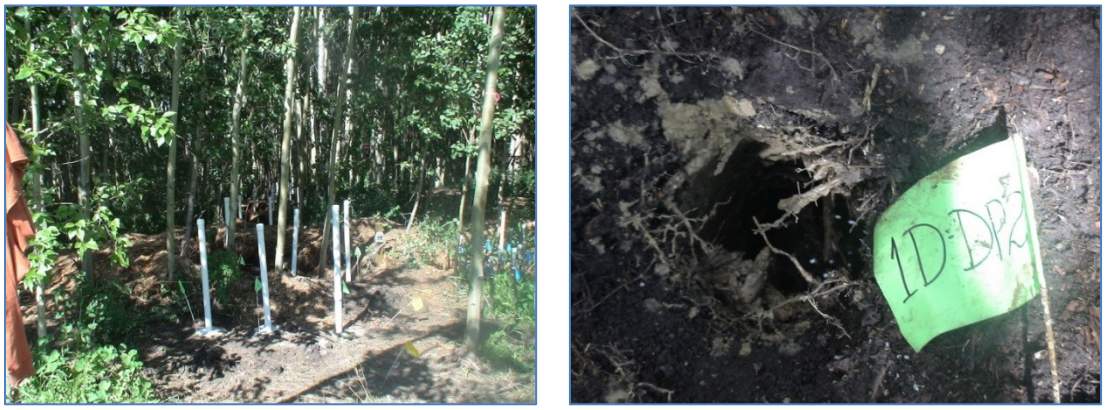

a) b)

Figure 4-17: Study site vegetative cover (a) and tree roots revealed during well installation (b). during the time of sampling (c). The number 6 in the legend indicates nest number and the ones in brackets are corresponding mid-screen depth of the MW below the ground surface**.**

5. PROCESS BASED MODELING WATER FLOW AND PATHOGEN TRANSPORT FROM AT-GRADE LINE SOURCES TO SHALLOW GROUNDWATER

5.1. Introduction

On-site wastewater treatment systems (OWTS) are becoming common wastewater treatment facilities in many parts of the world. A conventional OWTS has four main components: wastewater source, septic tank (pre-treatment unit), infiltration gallery and soil absorption field (Figure 5-1a). It is believed that most of the treatment is accomplished by the soil absorption field unit (McCray et al., 2005). The soil absorption field is the vadose zone between the point of effluent entry (ground surface or subsurface) and groundwater (saturated) zone, linking the atmosphere, soil and ground waters. Near-surface water balance and geochemical conditions are affected by vadose zone processes, which, in turn, can significantly influence the fate and transport of dissolved compounds and biocolloids. Lin (2010) described the vadose zone-groundwater interface as one of the critical interfaces controlling landscape-soil-water-ecosystem-climate relationships. Therefore, wastewater treatment in the soil absorption field is the outcome of complex transport and attenuation processes which are influenced by the physical, chemical and biological properties of soil. Studies on wastewater flow in the subsurface have been carried out over two decades. However, the physical flow processes from the infiltration surface through the soil treatment zone remain poorly understood (McCray and Christopherson, 2008; Close, 2010; Sen, 2011). Research findings have shown that the main treatment processes including filtration, microbial inactivation, attachment and detachment take place in the soil absorption field.

Shallow groundwater conditions with seasonal fluctuations affect the vadose zone thickness, expediting travel time of surface applied effluent reaching the groundwater and posing risks to groundwater contamination at times when the vadose zone gets thinner. The term, "risk", refers to the probability that a particular adverse event occurs during a stated period of time (Ferguson *et al*., 1998; Royal Society, 1992). As defined by Ferguson *et al* (1998), risk assessment is the scientific process addressing the informal question, "How risky is it for bad things to happen?" In on-site wastewater treatment systems, a shallow water table associated with high effluent dosing volumes/events may pose a risk to groundwater resources because in those scenarios contaminants that may exist in the effluent can reach groundwater by travelling short distances through the vadose zone. A shorter travel distance means contaminants have less

residence time in the unsaturated zone and less time and space for attenuation processes such as filtration, microbial inactivation, and other attachment processes to occur.

Risk assessment can be viewed in the form of source-pathway-receptor concept (Figure 5-1b). Some of the parameters used to quantify risks to groundwater contamination include: i) hydrogeologic properties - depth to groundwater table, groundwater recharge volume and hydraulic conductivity, ii) physiographic characteristics - slope or gradient of the vadose zone and aquifer layer, iii) contaminant properties - contaminant degradation rates and retardation factors and iv) soil properties - percentage of soil organic matter, fraction of organic carbon content in soil, soil volumetric water content, soil texture and structure. In this study, depth to groundwater (vadose zone thickness) was considered as a risk indicator parameter because a thinner vadose zone (shorter pathway) poses a greater risk to the groundwater receptor.

The main purpose of this chapter was to use a process model to simulate transport at the research site by introducing scenarios including shallow water table (shallow means close to the ground surface) and deep water table conditions. Although the specific results of these simulations may not be directly transferable to other OWTS, the simulation, risk assessment methodology is transferable. The HYDRUS 2D hydrological model (Šimůnek *et al*., 2006) was used to simulate wastewater infiltration, evapotranspiration and groundwater fluctuations at the site. The threshold levels of depth to groundwater and surface effluent fluxes that were identified in the previous chapters (Chapter 3 and 4) were also assessed and compared to simulated results to investigate risks.

5.2. Materials and Methods

5.2.1. Site Description

The model was developed based on an actual on-site wastewater treatment system (OWTS) at the Wetaskiwin Rest Stop (N52°53’43’’and W113°38’33’’) located 80 km south of Edmonton, Alberta, Canada. The Rest Stop was equipped with seven toilets, two urinals, seven hand washing sinks, septic tanks, and an Ultraviolet (UV) wastewater disinfection system resulting in an average production of 8.94 m^3 d^{-1} of wastewater. As a pilot project, the OWTS equipped with UV disinfection systems and at-grade line sources were established at the rest stop in 2007 by the Alberta Municipal Affairs. A Detailed site description has been given in Chapter

2, and more detailed investigations of groundwater elevation dynamics and solute and microbial transport were discussed in Chapters 3 and 4 respectively.

The model(s) discussed in this chapter represent a 2D vertical slice of the study site encompassing the sampling transect containing the 10 nested monitoring wells used for the solute and *E.coli* transport experiment in Chapter 4 (Figure 5-2). An example domain constructed in HYDRUS 2D graphical interface is presented in Figure 5.3. Because of the strong snowmelt-driven seasonal, regional groundwater dynamics observed in Chapter 3, and to minimize the influence of boundary conditions imposed on the sides of the domain, the horizontal scale (400-m) of the constructed domain is much greater than the scale of the monitoring well transect (22.2 m). Further, the actual complex topography of the site was simplified to a constant, slope of 2.5% resulting in an inclined domain. Therefore, as with all models, the models constructed for this work are a simplification of reality. The goal of the modelling exercise was to construct a model that captured the large-scale temporal groundwater dynamics.

5.2.2. HYDRUS 2D Model Description

This section will give a general description of the Hydrus model with the following sections covering specific implementation of the model. The HYDRUS 2D/3D model (Version 1.12.0070) is used to simulate water and solute movement in unsaturated, partly saturated or fully saturated porous media (Šimůnek *et al.*, 2006). The model uses Galerkin-type, linear finite element scheme to numerically solve the Richards equation for variably saturated water flow to simulate infiltration, root water uptake, evapotranspiration and groundwater recharge. The corresponding Richards equation is given as follows assuming negligible air phase effect in the liquid flow process

$$\frac{\partial \theta}{\partial t} = \left[\frac{\partial}{\partial x}\left(K(h)\frac{\partial h}{\partial x}\right) + \frac{\partial}{\partial z}\left(K(h)\frac{\partial h}{\partial z} + K(h)\right)\right] - S(h,z) - E_s(t) \qquad [5.1]$$

Where θ is volumetric soil water content [$L^3\ L^{-3}$], t is time [T], h soil water pressure head [L], x and z are the spatial coordinates [L], $K(h)$ is the unsaturated hydraulic conductivity [$L\ T^{-1}$], *S(h,z)* and *Es(t)* [$L^3\ L^{-3}\ T^{-1}$] are sink terms representing root water extraction and surface evaporation respectively in this particular application.

Hydrus solves Eq. [5.1] under user-defined initial and boundary conditions. The specific initial and boundary conditions used for the simulations in this chapter will be described in section 5.2.6.

Soil hydraulic parameters

The model simulations in this study use the van Genuchten (1980) model to describe the soil hydraulic properties as

$$\theta(h) = \begin{cases} \theta_r + \frac{\theta_s - \theta_r}{[1+|\alpha h|^n]^m} & h < 0 \\ \theta_s & h \geq 0 \end{cases} \quad [5.2]$$

$$K(h) = \begin{cases} K_s S_e^{0.5} \left[1 - \left(1 - S_e^{1/m}\right)^m\right]^2 & h < 0 \\ K_s & h \geq 0 \end{cases} \quad [5.3]$$

$$S_e = \frac{\theta - \theta_r}{\theta_s - \theta_r} \quad [5.4]$$

Where S_e is the normalized soil water content [-], θ is volumetric water content [L^3 L^{-3}], the subscripts *r* and *s* refer to residual and saturated volumetric water content respectively, α [L^{-1}], *n* and *m* are van Genuchten model parameters, m=1-1/n, and K_s is saturated hydraulic conductivity [L T^{-1}].

Root water uptake

The sink term (*S(h,z)*) is defined as the volume of water removed from the soil per unit of time due to plant water uptake. In this chapter, root water uptake by multiple aspen trees along the transect was modelled assuming a horizontally uniform distribution of the trees (width L_t, Appendix 5-3). Therefore, root water uptake was assumed only to vary with depth because a uniform atmosphere boundary was applied on the upper domain boundary nodes except for the nodes where wastewater was applied to the surface. Root water uptake was parameterized using the model of Feddes *et al* (1978) that was further expanded by van Genuchten (1987) to include osmotic stress:

$$S(h, h_\phi, z) = a(h, h_\phi) S_p(z) \quad [5.5]$$

Where S_p(z) is the potential water uptake rate [L^3 L^{-3} T^{-1}] and $a(h,h_\phi)$ is a dimensionless water stress response function of the soil water pressure, h and osmotic heads, h_ϕ [L]. The values of the function range between 0 and 1 ($0 \leq a \leq 1$), and more details about these expressions can be found in Šimůnek *et al* (2006).

The vertical root water uptake was assumed to decrease linearly with depth over the root zone similar to the model by Prasad (1988) where water uptake at the maximum root zone depth is expected to be zero and that near the surface, where root densities are greatest, would be high. The linear root water uptake distribution in the vertical direction was assigned equally and uniformly throughout the width of the domain. A detailed description of the plant species and their root distribution system is given in section 5.2.5.2.

The potential root water uptake rate, S_p, is given as (see also Appendix 5-3)*:*

$$S_p(\mathrm{z}, \mathrm{t}) = \left(\frac{Z_R - z}{Z_R}\right) \frac{L_t T_p(t)}{L_X} \quad [5.6]$$

Where: L_t is the width of the soil surface associated with the transpiration process [L], T_p is the potential transpiration rate [L T^{-1}], L_X and Z_R are horizontal and vertical dimensions of the two dimensional root zone domain [L] respectively, z is root depth with a maximum rooting depth of Z_R. When L_t=L_x under a complete ground cover condition, S_p reduces to $\left(\frac{Z_R - z}{Z_R}\right) T_p(t)$. Multiple aspen trees on the modelled transect were considered interconnected by their sucker roots contributing a spatially uniform transpiration rate along the transect.

As the HYDRUS model required inputs of potential transpiration, T_p and surface evaporation, Es separately, potential evapotranspiration (ET_0) was first partitioned into E_s and T_p following Beers law (Ritchie 1972) as follows:

$$\mathrm{T}_p = \mathrm{ET}_0 \, \mathrm{SCF} \quad [5.8]$$

$$\mathrm{E}_s = \mathrm{ET}_0 (1 - \mathrm{SCF}) \quad [5.9]$$

Where ET_0 is potential evapotranspiration [L T^{-1}], T_p is transpiration [L T^{-1}] and E_s is surface evaporation fluxes [L T^{-1}], SCF is dimensionless soil cover fraction defined as SCF=1-exp(-*k* LAI), LAI is leaf area index [L^2 L^{-2}], which refers to a ratio of one-sided green leaf area to ground surface area for broadleaved species, *k* is radiation extinction by canopy [-].

Because soil hydraulic conductivity decreases sharply with decreasing water content, the actual root water uptake simulated by Hydrus is less than the potentials expressed in Eq. [5.8] (see Eq. [5-5]). Similarly, the actual soil evapotranspiration is less than the potential soil evaporation in Eq. [5-9]. In addition, the total precipitation input into the model was adjusted to account for interception by the tree canopy. A detailed description of the top boundary conditions is given in section 5.2.6.1.

5.2.3. Model Construction, Space and Time Discretization

Space discretization

Two-dimensional (2D) flow domains were constructed in HYDRUS 2/3D to simulate effluent surface flux and transport (Šimůnek, *et al*., 2006 and 2007). Three 2D domain sizes with dimensions of X=10000, 20000, 40000 cm and Z=1700 cm, which are referred hereafter to Domain1, Doamin2 and Domain3 respectively, were constructed to select the best domain representing the site conditions. All the three domains had a 2.5% slope in the general groundwater flow direction (Figure 5-3). The vertical dimension (Z) of the model was the same in all the three domains representing the study site in terms of the lithological and hydrological setting (details of the site's hydrogeological description are available in Chapter 2 section 2.2.1.2).

Each of the 2D domains was discretized into unstructured finite-element (FE) triangular mesh using MeshGen2D module in HYDRUS with a target FE size of 5 cm. The FE sizes were finer on the surfaces near to the ground surface and coarser on the surfaces further away the ground surface, mostly the saturated zone (Figure 5-3 and Figure 5-5). A total number of 31976, 34659 and 44609 nodes were generated for Domain1, Domain2 and Domain3 respectively.

Time discretization

The time discretization in HYDRUS involved time adjustment associated with the numerical solution that started with the prescribed initial time increment, Δt_{init} (Šimůnek and

Šejna (2009). The time increment, Δt, was automatically adjusted at each time level following certain rules (refer to Šimůnek and Šejna, 2009 for details). For example, larger initial time steps were recommended for soil with less nonlinear soil hydraulic properties such as loam soils). The time discretizations given above were selected based on those set of rules recommended by Šimůnek and Šejna (2009).

5.2.4. Model Parameterization

5.2.4.1. Soil Hydraulic Properties

The domain material was assumed to be homogeneous and the soil hydraulic properties are presented in Table 5-1. The values of θs and K_s were measured, and those of α and n were HYDRUS default for loam soil. The soil saturated hydraulic conductivity, K_s was determined in-situ using piezometer and auger hole methods as described in Chapter 4 section 4.3.2. The residual volumetric water content, θr that was used in the simulations accounted for 10 times of its average value that was obtained by fitting to the measured data using a RETC program ver. 6.02 (van Genuchten, 1980; van Genuchten *et al.,* 2009) as shown in Table 2-3. The use of a higher residual water content was justified in that the average value of θ that was measured at -15 bar was 0.268 cm^3 cm^{-3} (Table 2-3), which was similar to θr and it also improved the model convergence.

5.2.4.2. Root Distribution Parameters

The common tree species in the study site was aspen (*Populus tremuloides*). Aspen has a wide ranging root system that varies with soil type on which it grows and tree age. Gifford (1966) observed aspen roots reaching a depth of 290-, 152- and 127-cm in sandy loam, loam and clay soils respectively for a 52-year old tree. Other researchers also reported a maximum rooting depth of 152 cm in gravely sandy loam soils (Brendt and Gibbons, 1958), 50 cm in an organic-clay-sand soil profile along hillslope transect with coarse and fine roots reaching between 200 to 500 cm (Devito *et al.,* 2005; Blanken *et al.,* 2001; Debyle *et al.,* 1985) and up to 70 cm in five regions of Central Northern Alberta (DesRochers, 2000). Although the sinker roots of aspen reach the depths mentioned above, most aspen roots are confined in the upper 30 to 120 cm of soil (Day, 1944; Gifford, 1966). Also aspen roots may spread laterally anywhere between 800 to

1500 cm (Gifford, 1966; Day, 1944, Berndt and Gibbons, 1958) and may reach up to 3000 cm in some instance when the entire clone was considered (Gifford, 1966).

Saturated conditions are not favorable for aspen in that aspen roots may die in saturated and anaerobic conditions (Bales *et al*., 1998). Therefore, with the frequent shallow water table conditions observed at the study site (Figure 3-3), the active roots of aspen were assumed to occur above the water table, reaching 60 cm vertically below the ground surface. The vertical root distribution was considered to decrease linearly from the ground surface to the bottom of the root zone located at approximately 60 cm below the ground, resulting higher water uptake near the surface and zero beyond 60 cm depth. The root water uptake was also assumed uniform in the lateral direction in that tree roots were interconnected via suckers (clone) as shown by DeByle (1985) resulting a uniform water uptake through the entire surface area associated with the transpiration process.

5.2.5. Boundary and Initial Conditions

5.2.5.1. Boundary Conditions

The flow of water in the HYDRUS model was controlled by prescribed pressure heads on the up- and down-stream boundaries that did not vary with time, and by variable effluent surface fluxes [L^3 L^{-2} T^{-1}], i.e., VarFl1, VarFl2, VarFl3 and VarFl4, at the upper boundary nodes representing the at-grade line sources (laterals). Each of the four at-grade line sources was represented by seven nodes giving approximately 60 cm width of one lateral. The remaining nodes on the upper boundary had atmospheric boundary conditions. All the bottom boundary nodes (BBC) were assigned a constant flux attempting to simulate vertical downward gradients (Table 5-3 and Figure 5-5). The lower boundary layer of the study site was located at approximately 1700 cm depth below the ground surface based on observations that the material at this depth is a clay or till (HCL, 2008), which is generally considered as very low permeability material, hence the imposed BBC gradient was smaller than the vertical gradients measured at the upper portion of the domain from the ground surface to 1.5 m depth (refer to section 5.4.2). The surface effluent flux of the experimental site was variable in magnitude and application interval; however, these conditions were the same in the all simulations.

Top Boundary Conditions (Atmospheric and variable surface effluent fluxes)

a) Evapotranspiration:

$$-\left[\left(K(h)\frac{\partial h}{\partial x}\right)+K(h)\left(\frac{\partial h}{\partial z}+1\right)\right] \leq |E_{max}| \quad \text{at } z=0 \qquad [5.11]$$

and

$$h_{min} \leq h \leq 0 \quad \text{at } z=0 \qquad [5.12]$$

Where E_{max} [L T^{-1}] is the maximum potential rate of evapotranspiration (ETo) or infiltration under the prevailing atmospheric conditions, and h_{min} is the minimum pressure head [L] allowed at the soil surface. This upper boundary condition can switch from a prescribed flux to a prescribed pressure head to ensure that the two limiting conditions in Eq. [5-2] are met (Simunek *et al.,* 2006). The growing season was assumed to start when the mean daily air temperature rose to ≥5^{o}C, a minimum threshold temperature for general plant growth (Alberta Agriculture and Rural Development, https://www.agric.gov.ab.ca/app49/imcin/about.jsp).

The atmospheric input variables: total rainfall, snow water equivalent (SWE), air temperature, wind speed, vapour pressure were recorded at an on-site weather station.

Potential (reference) evapotranspiration was calculated from the weather data when the daily air temperature was ≥5^{0}C during the study period (2011-2012) using two methods: i) Penman-Montieth for short grass (ET_{os}) (Allen *et al* (1998), and ii) two empirical expressions, ET_{tr} and ET_{tru}, developed by Maule *et al* (2006) for the Prairie region of Canada as follows

$$ET_{os}=\frac{0.408\Delta(R_n-G)+\gamma\dfrac{900}{T+273}u_2(e_s-e_a)}{\Delta+\gamma(1+0.34u_2)} \qquad [5.16]$$

$$ET_{tr}=0.053(T_{\max}-T_{\min})+0.134T+0.846\Delta R_a-3.18e_a+1.28 \qquad [5.17]$$

$$ET_{tru}=0.077(T_{\max}-T_{\min})+0.114T+0.832\Delta R_a-2.77e_a+0.269u_2+0.053 \qquad [5.18]$$

Where ET_{os} , ET_{tr} and ET_{tru} are reference evapotranspiration [mm d^{-1}], R_n is net radiation at the crop surface [MJ m^{-2} day^{-1}], G is soil heat flux density [MJ m^{-2} d^{-1}], R_a is extraterrestrial radiation [MJ m^{-2} d^{-1}], T is mean daily air temperature at 2 m height $\{(T_{max}+T_{min})/2)\}$[°C], T_{max} and T_{min} are maximum and minimum air temperatures respectively [^oC], u_2 wind speed at 2 m height [m s^{-1}], e_s and e_a are saturation vapour pressure and actual vapour pressure [kPa] respectively, e_s-e_a saturation vapour pressure deficit [kPa], Δ slope vapour pressure curve [kPa $°C^{-1}$], γ psychrometric constant [kPa $°C^{-1}$].

Comparison of ET_{tr} and ET_{tru} to ET_{os} is given in Appendix 5-15. Simulation results using the potential evapotranspiration values obtained from the two methods are given in Table 5-3, Figures 5-7 to 5-10 and Appendix 5-2.

b) Surface effluent application:

A daily surface effluent flux density was calculated from the volume of effluent that was discharged daily to the infiltration bed via the at-grade line sources (laterals) as follows:

$$q(t) = \frac{V(t)}{A \times t} \qquad [5.13]$$

Where *q(t)* is daily surface effluent flux density [L^3 L^{-2} T^{-1}], V(t) is volume of surface effluent flux [L^3], A is surface area of the effluent infiltration bed [L^2], and t is time [T].

c) Precipitation:

$$P = RF + Snowmelt \qquad [5.13]$$

Where P is precipitation [$L\,T^{-1}$] and RF is daily total rainfall [$L\,T^{-1}$].

The daily precipitation was applied to all nodes on the upper boundary of the flow domain but the effluent infiltration beds. Because the at-grade lines were covered with dome-shaped chamber and woodchips (Figure 2-10 in Chapter 2), there was no direct surface infiltration of precipitation in these locations.

Approximately 15% of the total precipitation was assumed as interception loss by aspen (*Populus tremuloides*) (Tate, 1995; Debyle, 1985; K. Devito, personal communication,

University of Alberta, Edmonton, AB). In our study, a net daily rainfall was estimated by deducting interception loss from the gross daily rainfall. The total precipitation was obtained by adding the net total daily rainfall and snow water equivalent (SWE).

The annual snowmelt input was estimated to be equal to the measured SWE at the site. Furthermore, the regional SWE was approximated by the locally measured SWE at the study site. In hydrus, this was implemented as part of the daily precipitation events and distributed equally over a 14 day period before daily potential evapotranspiration increased above zero.

Bottom Boundary Conditions

At the bottom of the entire flow domain a gradient equivalent to specified flux (q) was specified as:

$$\frac{\partial h}{\partial z} = g_0 \Rightarrow q = -K_s \frac{\partial h}{\partial z} = -K_s g_0 \qquad [5.14]$$

Where K_s is saturated hydraulic conductivity [LT^{-1}], h is pressure head [L], z is depth [L], g_0 specified gradient [-], and q is specified flux [LT^{-1}] (Figure 5-5). The bottom boundary gradient was specified based on try and error calibration and validation of the model with measured data.

Boundary Conditions at the Sides

The pressure heads on the upper- and down-gradient sides were equilibrated to the lowest nodal point at Z=1700 cm keeping the water table at a specified depth throughout the simulation time. The water table depth at the side nodes was decided to be at similar depth with the initial water table in the entire domain. However, after simulation was initiated, the initial water table level in all the nodes except those at the two sides was allowed to change in response to the top and bottom boundary conditions.

5.2.5.2. Initial Conditions

An initial pressure head distribution in the entire domain was set in equilibrium to the lowest nodal points at Z=1700 cm, that is from the smallest negative pressure head at the top surface boundary nodes (z=0) to the largest positive pressure head at the bottom boundary nodes (z=1700, Figure 5-4), resulting in the initial water table level at a constant depth from the ground

surface (z=*d(t)*) in the entire domain, h(z=*d(t)*, x, t=0)=0. Accordingly, the initial pressure head is given as:

$$h(x,z,t) = \left[\frac{z-1700}{z_{water\ table}-1700}\right] z_{water\ table} + \left[\frac{z-z_{water\ table}}{1700-z_{water\ table}}\right] 1700 \quad \text{for } t = 0 \quad [5.10]$$

Where $z_{water\ table}$ is equal to the elevation of water table at the start of the simulation. First, the model was run until steady state was achieved using zero flux on the top and bottom boundaries and an initial pressure distribution that kept the water table level at the average groundwater depth, $d(t_i)$ observed at the start of the simulation. The pressure head at steady state (no change in pressure head during the simulation) was used as the initial pressure head distribution for subsequent transient simulations.

The observation nodes used for the model validation were located at x = -470.12-, 29.33- and 378.96-cm representing approximately the three nests of monitoring wells horizontally in the source zone and at z = -100±0.15 cm below the ground surface (Figure 5-4)

5.3. Data Analysis

5.3.1. Sensitivity Analysis

Sensitivity analysis and model validation are important steps required in a modeling process (Smith *et al.,* 2008, Trucano *et al.,* 2006). The sensitivity of the model output to input parameters was assessed by changing each parameter, one-at-a-time and comparing the magnitude of the change in model output to the magnitude of the change in model parameters (Hamby, 1994).

The sensitivity of the model to each of the input parameters given in Table 5-2 was measured by testing one parameter-at-a-time while keeping constant all the other parameters, initial and boundary conditions. To assess model sensitivity to atmospheric inputs, initial and boundary conditions, we first ran water flow simulations assuming no surface fluxes at a fixed water table level of 120 cm below the ground surface (the average groundwater depth observed in the field) and ran the model to steady state. Subsequently, the upper boundary conditions were replaced with the time series surface fluxes (atmospheric and effluent fluxes) that were observed during the study period from 2011-2012 (e.g. Figure 5-8 to 5-10). The final time pressure head of the steady state simulation was used as an initial pressure head for the transient

simulations. The effect of each parameter was assessed using a simulated groundwater depth, *d(t)* below the ground surface as observed at a node location x=29.33 cm and z=-100±0.15 cm below the ground surface. The observation node represents approximately the center of the domain in the horizontal dimension.

The sensitivity index, a value that was used to test model sensitivity to input parameter, was estimated using the expression by Hoffman and Gardner (1983) as:

$$\mathrm{SI} = \frac{d(t)_{max} - d(t)_{min}}{d(t)_{max}} \qquad [5.19]$$

Where SI is dimensionless sensitivity index [-], *d(t)max* and *d(t)min* are the maximum and minimum output values of depth to groundwater [L] at each observation node, obtained from varying the input parameter over its entire range. The model was considered less sensitive to the parameters that have small SI values and vice versa to the parameters with large SI values.

The model input parameters were either measured on-site/in-situ at the research site or determined in the laboratory. The daily surface effluent flux and weather data were collected on-site using Aquaworx (Pinnacle Environmental Technologies, Ltd.) and Campbell Scientific data loggers respectively. Additional model input parameters and site characteristics including soil hydraulic properties, study site physiography, hydrogeology and plant species were either lab measured, characterized in the field or reviewed from literature (e.g. HCL, 2008).

5.3.2. Model Validation

The validation of a model is a process of testing the predictive capability of a code for a given application through comparison of calculations with a set of experimental data (Trucano *et al.,* 2006). It may involve a two-step calibration scheme, which is known as historical validation (Šimůnek *et al*., 2012). The first step tunes the model by manipulating the input parameters such as soil hydraulic properties and initial or boundary conditions within reasonable ranges until the simulated model results closely match the observed variables such as pressure heads, water contents and concentrations. While in the second step the data set serves to compare simulated and measured data using the parameters found during the calibration. Model validation can be achieved by trial and error techniques (Šimůnek *et al*., 2012).

The model was validated by comparing simulated and measured groundwater depths, *d(t)*s below the ground surface. The groundwater depth time series, *d(t)* were measured on-site using automated pressure transducers (Leveloggers) that were deployed into four monitoring wells located within the effluent disposal zone (source zone, Figure 5-2). In addition, groundwater level data were obtained using water level meter from the nest of monitoring wells located along the modeled transect.

Following the sensitivity analysis, validation of the HYDRUS 2D model was performed using the optimum domain size and input parameters found during the sensitivity analysis. Subsequent model calibration tests were conducted for a range of scenarios (domain slope, initial and boundary conditions, and soil hydraulic properties) to fine tune the best conditions that match the field conditions (Table 5-1 and 5-4 and Appendix 5-1). A simulated time series of water table depths, *d(t),* directly under the source zone were compared with the measured values. The root mean squared error (RMSE) is used to validate the precision of the model, a smaller RMSE value indicating a better fit or goodness of fit (Table 5-3 and Appendix 5-2).

$$\text{RMSE} = \left[\sum_{i=1}^{N}(O_i - P_i)^2\right]^{\frac{1}{2}} \qquad [5.20]$$

Where RMSE is root mean square error, O_i and P_i are the i^{th} measured and simulated values, and N is number of paired simulated and measured values. An average simulated value for the model validation was obtained from three observation nodes located at x = -470.12, 29.33 and 378.96 cm and z = -100±0.15 cm representing approximately the three nests of monitoring wells at the modeled transect of the source zone (Figures 5-3 to 5-4).

5.3.3. Groundwater Contamination Risk Analysis: Surface flux travel depth analysis

The probability of a 7-day effluent travel depth exceedance to simulated groundwater depths, *d(t)* were evaluated for assessing risks to groundwater contamination by considering three initial groundwater depth scenarios: 50 cm, 115 cm and 200 cm below the ground surface. These groundwater depths represented shallow, average and very deep groundwater depths respectively. Threshold levels of $d(t) \leq 0.5$ m and $q(t) \geq 5$ cm^3 cm^{-2} d^{-1} that were determined in the previous chapters (Chapter 3 and 4) were also evaluated with respect to the simulated *d(t)*

values. The probability of simulated *d(t)* below the threshold value (≤ 0.5 m) were calculated and compared for the three initial groundwater depth scenarios. Standard covariance between weekly effective surface fluxes and simulated *d(t)* calculated over 7-day windows were also estimated to verify dependence of the two variables.

To further quantify groundwater contamination risk, joint and conditional probabilities of the 7-day travel depth, effective surface fluxes, *q(t)* and simulated *d(t)* being greater than or less than the thresholds identified in Chapter 3 were computed for the three groundwater depth scenarios. Let A, B, C and N represent 7-day travel depth ≥0.5 m, *d(t)* ≤0.5 m, *q(t)* ≥5 $cm^3cm^{-2}d^{-1}$, and total number of observations respectively. The probabilities of single event, P(B), joint, $P(B \cap C)$, and conditional, $P(B|C)$ are calculated as

$$P(j) = \frac{\#\ of\ occurence\ of\ j}{N}, j = A, B\ or\ C \quad [5.21]$$

$$P(B \cap C) = \frac{\#\ of\ occurence\ of\ B\ and\ C}{N} \quad [5.22]$$

$$P(B|C) = \frac{P(B \cap C)}{P(C)}\ , P(C) > 0 \quad [5.23]$$

$$P(C|B) = \frac{P(B \cap C)}{P(B)}\ , P(B) > 0 \quad [5.24]$$

Since the 7-day travel depth is highly dependent on the effluent surface flux, most of the risk analysis is based on the probability of *q(t)* exceeding the given threshold.

5.4. Results and Discussion

5.4.1. Domain Size and Input Parameter Sensitivity

The influence of the specified head boundary conditions imposed on the sides of the domain were assessed by running the model to steady state with zero flux top and bottom boundary conditions with an initial groundwater depth of 120 cm below the surface. When the top surface boundary conditions were set to allow precipitation, evapotranpiration and

wastewater infiltration, there was a significant influence of domain size on the water table levels in the center of the domains during the winter months (Figure 5-7), groundwater mounding at the center of the smaller domains (Domain1 and Domain2) was observed after approximaelty 260 simulated days.. It appears that the boundary conditions at the sides in the smaller domains create groundwater mounding that is not a result of the surface atmospheric and effluent fluxes. Therefore, for the rest of the sensitivity analyses, the largest domain (Domain 3: 40000 cm by 1700 cm) was selected.

The results of HYDRUS 2D model sensitivity to input parameters for the largest domain size are summarized in Table 5-2. Graphical representation of simulated output values showing the sensitivity of the model to the different parameters for the large domain are given in Appendix 5-4 to 5-10. Sensitivity of the model to the parameters was quantified using the sensitivity index of groundwater depth below the ground surface as an output variable. The model was sensitive to the parameters in the following order: ET > K_s > Domain size > LAI > k > Z_R > z*. Where ET is evapotranspiration [L T^{-1}], Ks is saturated hydraulic conductivity [L T^{-1}], LAI = leaf area index [L^2 L^{-2}], k is radiation extinction by canopy [-], Z_R is maximum rooting depth [L] and z* is empirical parameter [L].

5.4.2. Model Validation

To investigate the predictive capability of the model, the historical validation technique was employed, which was fine tuning the model by changing the upper atmospheric boundary conditions (ET and SWE), the bottom boundary, saturated hydraulic conductivity (K_s) and ET models to match measured values. Simulated and measured *d(t)* were compared and results for 30 scenarios that best mimic the site conditions are given in Figures 5-8 to 5-10, Appendices 5-B, 5-K to 5-O. The most significant adjustments required for model validation were in the boundary conditions. After considerable efforts to validate the model, we noticed that the minimum simulated water table level was costrained to values at or above the initial condition (1.2 m) by the elevation of the fixed head boundary conditions at the sides of the domain. During the winter periods, however, actual observed groundwater elevations were usually much lower. Further, signficant vertical, downward gradients were observed and reported in Chapter 4. Therefore, a constant flux boundary condition -0.03 cm d^{-1}, which roughly corresponds to a gradient, g_0 of 0.0008 to 0.0012 depending on the K_s used, was imposed at the bottom of the domain for the remaining validation simulations (Appendix 5-14). At the study site, downward

vertical average gradients of 0.1 to 0.2 were observed in the summer 2011 while in the spring 2011, spring 2012 and summer 2012 the difference in hydraulic heads was on average within the measurement error, 3 to 5 cm difference, suggesting negligible vertical gradients in those seasons. Furthermore, simulated results were better for scenarios with evapotranspiration estimated using the Maule *et al* (2006) expression (ET_{tr}) compared to ET_{os} estimated by the Penman Monteith method (Allen *et al*., 1998, Table 5-3).

The top nine scenarios (lowest RMSE) are given in Table 5-3 and Figure 5-8. Figures 5-8 and Appendices 5-K to 5-L compare simulated and measured groundwater depths and soil water content for the top nine best scenarios. The best scenarios representing the site conditions were determined by simulating water flow at an initial groundwater depth of 120 cm below the ground surface (Figures 5-3 to 5-5) and comparison of those scenarios are presented in Figures 5-8 to 5-10. Using the first top scenario (#23), groundwater contamination risks were assessed by varying initial groundwater depth below the ground surface and are discussed below.

5.4.3. Groundwater Contamination Risk Assessment

5.4.3.1. Wastewater Travel Depth and Groundwater Depth Analysis

To investigate the influence of the thickness of the vadose zone on the probability of wastewater reaching the groundwater, and therefore assessing risks to groundwater contamination, three initial groundwater depths (50, 115 and 200 cm) were selected as model scenarios. The model was tested at the three initial water table levels using the parameters for the first three top scenarios (#23, 9 and 26) that were shown in Table 5-3.

When the initial water table was at 50 cm depth below the ground surface scenario, the snow water equivalent (SWE) contribution to the surface flux inputs was reduced by 75% in the water flow simulation because the model did not converge when 100% of the SWE was added as part of the surface flux inputs. In this case, 75% of the SWE was assumed as being lost in the form of surface runoff due to saturated surface boundary conditions, accounting for approximately 82 mm and 75 mm of the SWE in 2011 and 2012 respectively. Even though only 25% of the SWE was considered as surface flux input in the 50 cm initial water table scenario simulated groundwater level rose up approaching the ground surface during the months of March to August (Figure 5-11 c and d). In the other two initial water table scenarios (115 cm and 200 cm), all the SWE for a given year was added as part of the surface fluxes.

Figures 5-11 to 5-13 show simulated *d(t)* focusing on the months when the water table level was rising close to the ground surface (commonly from March to August) each year. In each of the figures, 7-day travel depth of effective surface flux, covariance weekly surface flux and groundwater depth are also included for comparison purposes. For the risk analysis, average *d(t)*s was obtained from four observation nodes located beneath each laterals at x=-769.85-, -220.42-, 129.22-, and 528.81-cm and z=-99.68±0.24 cm (Figure 5-5). The observation nodes were chosen to investigate the probability an effluent reaching the top of the groundwater located vertically beneath the laterals.

Comparing the simulated and measured *d(t)*, 7-day travel depth of the surface flux, and covariance of weekly surface fluxes and groundwater depth for the three initial water table conditions showed both surface effluent fluxes and *d(t)* were co-dependent. As expected, the covariance level decreased as the initial groundwater dropped to 200 cm below ground surface (Figure 5-16), indicating relatively lower impact of the surface fluxes to the underlying groundwater body when the initial groundwater level gets deeper. When the initial water table level was lowered from 115 cm to 200 cm below the ground surface (a decrease by about 74%), the covariance of weekly surface flux and depth to groundwater decreased by approximately 98.5%. As expected, the deeper groundwater depths do not vary as much as the shallow depths in response to surface fluxes.

5.4.3.2. Probability Distribution of Groundwater Depth and Risk Analysis

The HYDRUS 2D model was used to simulate *d(t)* by varying initial groundwater depth while keeping other flow parameters the same for two years. The probability distribution of simulated *d(t)* were compared to the threshold levels of *d(t)* and *q(t)*, which were estimated in the previous Chapters (3 and 4) focusing on the months when the groundwater depth was observed close to the ground surface (between March and August). In Chapter 4, $d(t) \leq 0.8$ m was investigated as an *E.coli* threshold depth.

When simulated *d(t)* was less or equal to 0.5 m and $q(t) \geq 5$ cm^3 cm^{-2} d^{-1}, the groundwater was considered at risk because there was high probability that effluent and accompanying contaminants would reach the groundwater. Therefore, groundwater contamination risk was assessed based on the probabilities of wastewater effluent reaching the groundwater when the *d(t)* was closer to the ground surface during a given year. A summary probability table in which

surface fluxes would reach groundwater for the three initial *d(t)* scenarios as well as the measured *d(t)* are given in Table 5-4. Comparison of probabilities of *d(t)*s and groundwater depth are also given in Figure 5-14.

As expected, an inverse relationship was found between initial groundwater depth and probability of effluent reaching the groundwater (Figure 5-14). The probability of $d(t) \leq 0.5\ m$ given that $q(t) \geq 5\ cm^3\ cm^{-2}\ d^{-1}$indicated that up to 40% likelihood that effluent would reach groundwater when the initial water table was at 0.95 m depth below the ground surface (average mid screen of the shallowest monitoring wells of the nests in the source zone, 5-0.95 m; interpolated from Figure 5-14). Similarly, when initial water table was used at monitoring wells 5-1.29 and 5-1.54, there would up to 26% and 16% probability that effective surface fluxes would result in a 7-day travel depth greater than the groundwater table respectively.

When considering the conditional probability of $q(t) \geq 5\ cm^3\ cm^{-2}\ d^{-1}$, given $d(t) \leq 0.5\ m$, there was up to 6.0% , 4.4% and 3.2% probability that the surface fluxes would result in a 7-day travel depth greater than the groundwater table when the initial water table was at 0.95 m, 1.29 and 1.54 m depths below the ground surface respectively.

When the initial water table was at 200 cm below the ground surface, groundwater did not respond to surface effluent infiltration until effluent flux density ≥ 15 $cm^3\ cm^{-2}\ d^{-1}$ (Figure 5-13) as indicated by the 7-day covariance windows. Therefore, surface fluxes ≥15 $cm^3\ cm^{-2}\ d^{-1}$ and initial water table depth at ≥ 200 cm below the ground surface could be assumed as threshold values for safe groundwater.

5.5. Summary and Conclusion

The HYDRUS 2D model was used to investigate risks associated with on-site wastewater treatment systems to groundwater resources. Probability distributions of *d(t)* were investigated for a range of initial water table scenarios to help define a minimum vertical separation between at-grade line sources and groundwater table in designing effective on-site wastewater treatment systems.

The coincidence of snow melting and increased surface effluent flux events in the months of March to May shorten the vertical separation and hence lower the attenuation potential of the vadose zone for contaminants that may exist in the infiltrating effluent. The findings showed

that *d(t)* was less than the threshold depth for more than 40% of the time when initial water table was located at 0.95 m below the ground surface of $q(t) \geq 5\ cm^3\ cm^{-2}\ d^{-1}$.

Lowering the initial groundwater depth by 130% (from 50 cm to 115 cm) lowered the probability of surface effluent flux reaching the groundwater by 65%. The implication of this finding was to define a safe groundwater depth below at-grade line sources. In a seasonally high water table (water table close to the ground surface) exhibiting a range of fluctuation is a required design factor for on-site wastewater treatment systems. Typically, it is the maximum or high water table (high water table means groundwater level close to the ground surface) that is required for design criteria. From the three initial groundwater depths, wastewater flow simulation results showed that surface fluxes $\geq 15\ cm^3\ cm^{-2}\ d^{-1}$ and initial water table depth at ≥ 200 cm below the ground surface could be assumed as threshold values for safe groundwater.

Future direction of research in this line would include on assessing loading rate scenarios by varying the mean and variance of the observed effluent surface flux data to assessing risks to groundwater contamination, investigating effluent travel depth probability by varying soil material, and evaluating onsite wastewater treatment system using HYDRUS 3D model.

5.6. References

Allen, R., L.S. Pereira, D. Raes, and M. Smith, 1998. Crop evapotranspiration – Guidelines for computing crop water requirements. FAO Irrigation and Drainage Paper N° 56. Rome, Italy.

Bates, P.C.; E. Sucoff, S. R. Blinn, 1998. Short-term flooding effects on root suckering of quaking aspen. *Northern Journal of Applied Forestry 15: 169–173.*

Berndt, H. W. and R. D. Gibbons, 1958. Root distribution of some native trees and understory plants growing on three sites within ponderosa pine watersheds in Colorado. *Forest Service, Rocky Mountain Forest & Range Exp. Sta. Paper 37. 14 p*.

Blanken, P. D, T.A. Black, H.H. Neumann, G. den Hartog, P.C. Yang, Z. Nesic, X. Lee, 2001. The seasonal water and energy exchange above and within a boreal aspen forest. *J. Hydrol. 245: 118–136.*

Close, M., 2010. Critical review of contaminant transport time through the Vadose Zone. Environmental Canterbury Technical Report. Report No. R10/113 ISBN 978-1-927137-

54-3. Available on line: http://ecan.govt.nz/publications/Reports/critical-review-contaminant-transport-vadose-zone-000610.pdf

Day, M. W. 1944. The root system of aspen. *Amer. Midl. Natur., 32:502-509*.

DeByle, N. V., 1985. Water and watershed. In N. V. DeByle and R. P. Winokur (eds) Aspen: ecology and management in the western United States. *Gen. Tech. Rep. RM-119*. Fort Collins, CO: U.S. Department of Agriculture, Forest Service, Rocky Mountain Forest and Range Experiment Station: 153–160.

DesRochers, A. 2000. Clonal root connections and respiration in aspen. Ph.D. Thesis. University of Alberta, Edmonton, AB.

Devito, K. J. Devito, I. F. Creed and C. J. D. Fraser, 2005. Controls on runoff from a partially harvested aspen-forested headwater catchment, boreal plain, Canada. *Hydrol. Process. 19:3–25*.

Feddes, R. A., P. J. Kowalik, and H. Zaradny, 1978. Simulation of Field Water Use and Crop Yield. John Wiley & Sons, New York, NY.

Ferguson, C., D. Darmendrail, K. Freier, B.K. Jensen, J. Jensen, H. Kasamas, A. Urzelai and J. Vegter (eds), 1998. Risk Assessment for Contaminated Sites in Europe. Volume 1. Scientific Basis. LQM Press, Nottingham.

Gifford, G. F., 1966. Aspen root studies on three sites in northern Utah. *Am. Midl. Nat., 75: 132-141.*

Hamby, D. M., 1994. A review of techniques for parameter sensitivity analysis of environmental models. *Environ. Monit. Assess. 32: 135-154.*

HCL, 2008. Regional groundwater assessment. For country of Wetaskiwin. Part of North Saskachwan river basin. Parts of Tp 044 to 048, R 22 to 28, W4M & Tp 045 to 047, R 01 to 07, W5M. Prepared for the country of Wetaskiwin. hydrogeological consultants ltd. (hcl) 1.800.661.7972 . File No.: 07-771.03

Hoffman, E. O. and R. H. Gardner, 1983. Evaluation of uncertainties in environmental radiological assessment models, in: Till, J. E.; Meyer, H. R. (eds) Radiological Assessments: a Textbook on environmental dose assessment. Washington, DC: U.S. Nuclear Regulatory Commission; Report No. NUREG/CR-3332.

Lin, H. 2010. Earth's critical zone and hydropedology: Concepts, characteristics, and advances. *Hydrol. Earth Syst. Sci. 14:25–45. doi:10.5194/hess-14-25.*

Maulé, C., W. Helgason, S. McGinn and H. Cutforth, 2006. Estimation of standardized reference evapotranspiration on the Canadian Prairies using simple models with limited weather data. *Can. Biosys. Eng. 48:1-11*.

McCray, J. E. and S. H. Christopherson, 2008. On-site wastewater systems and interactions with the environment. ASCE , *J. Hydrol. Engin. 653-654*.

McCray, J. E., S. L. Kirkland, R. L. Siegrist, and G. D. Thyne, 2005. Model parameters for simulating fate and transport of on-site wastewater nutrients. *Ground Water, 43:628-639*.

Prasad, R. 1988. A linear root water uptake model. *J. Hydrol. 99: 297-306*.

Ritchie, J. T., 1972. Model for predicting evaporation from a row crop with incomplete cover. *Water Resour. Res. 8:1204-1213.*

Royal Society, 1992. Risk: Analysis, Perception and Management. *The Royal Society*, London (ISBN 0-85403-467-6).

Sen, T. K., 2011. Processes in pathogenic biocolloidal contaminants transport in saturated and unsaturated porous media: A Review. *Water Air Soil Pollut. Springer*, DOI: 10.1007/s11270-010-0531-9

Šimůnek, J. and M. Šejna, 2009. Notes on spatial and temporal discretization (when working with HYDRUS). This text was last modified on December 7, 2009. Available on line: http://www.pc-progress.com/Images/Pgm_Hydrus3D2/Notes_on_Spatial_and_Temporal_Discretization.pdf.

Šimůnek, J., M. Šejna and M. Th. van Genuchten, 2007. The HYDRUS software package for simulating the two- and three-dimensional movement of water, heat and multiple solutes in variably-saturated media. User Manual, Version 1.02. PC Progress, Prague, Czech Republic.

Šimůnek, J., M. Th. van Genuchten, and M. Šejna, 2006. The HYDRUS software package for simulating the two- and three-dimensional movement of water, heat and multiple solutes in variably-saturated media. Technical Manual, Version 1.0. PC Progress, Prague, Czech Republic.

Šimůnek, J., M. Th. van Genuchten, and M. Šejna, 2012. HYDRUS: model use, calibration and validation. *Trans. ASABE. 55:1261-1274*.

Smith, E. D., F. Szidarovszky, W. J. Karnavas and A. T. Bahill, 2008. Sensitivity analysis, a powerful system validation technique. *TOCSJ, 2:39-56.*

Tate, K. W., 1995. Interception on rangeland watersheds. *California Rangelands and Information Center. Fact Sheet. No. 36.*

Trucano, T.G., L. P. Swiler, T. Igusa, W. L. Oberkampf, M. Pilch, 2006. Calibration, validation, and sensitivity analysis: What's what. *Reliab Eng Syst Saf. 91:1331–1357.*

van Genuchten, M. Th. 1987. A numerical model for water and solute movement in and below the root zone. Research Report No 121, U.S. Salinity laboratory, USDA, ARS, Riverside, California.

van Genuchten, M. Th., J. Simunek, F. J. Leij, and M Segina, 2009. Code for quantifying hydraulic functions of unsaturated soils. Available on line: www.hydrus3d.com

Table 5-1: Soil hydraulic properties

θs	θr	α	n	K_s
$cm^3\ cm^{-3}$	$cm^3\ cm^{-3}$	cm^{-1}	-	$cm\ d^{-1}$
0.560	0.21	0.036	1.56	38.27 (Ave. field measured)
0.560	0.21	0.036	1.56	24.96 (loam soil – Hydrus default)

Table 5-2: Summary model input parameters and sensitivity indices (SI)

Index	ETtr (75-200%)	K_s (12.5 to 100 cm d^{-1})	LAI (1.5-12)	k (0.25-2)	Z_R=60-150	z*(30-150)	z*(10-60)	Measured
		ETtr (100%)	k=0.49	LAI=6	z*=30	Z_R=150	Z_R=60	
MIN-d(t)	0.0112	0.0237	0.0839	0.2979	0.3234	0.3389	0.3389	0.2808
MAX-d(t)	1.7697	1.8028	1.5940	1.5943	1.6913	1.6914	1.5903	1.6627
SI	0.9936	0.9869	0.9474	0.8132	0.8088	0.7996	0.7869	

Where ET is evapotranspiration [$L\ T^{-1}$], Ks is saturated hydraulic conductivity [$L\ T^{-1}$], LAI = leaf area index [$L^2\ L^{-2}$], k is radiation extinction by canopy [-], Z_R is maximum rooting depth [L] and z* is empirical parameter [L].

Table 5-3: Top 9 best scenarios that were selected based on the RMSE

Rank	Scenario	Domain size	SLP	d(t)	Depth	K_s	Bottom Boundary flux	Potential Evapotranspiration (method of determination)[£]	SWE‡	# of days SWE applied		RMSE
										2011	**2012**	
	No.	cm	%	cm	cm	cm d^{-1}	cm d^{-1}					
1	23	40000 x 1700	2.5	120	0-1700	25.00	-0.030	Full ETtr	3	14	14	0.2056
2	9	40000 x 1700	2.5	120	0-1700	25.00	-0.030	Full ETtr	2	14	14	**0.2066**
3	26	40000 x 1700	2.5	120	0-1700	25.00	-0.030	Full ETtr	4	14	14	**0.2080**
4	25	40000 x 1700	2.5	120	0-1700	38.27	-0.030	Full ETos	4	14	14	**0.2106**
5	18	40000 x 1700	2.5	120	0-1700	38.27	-0.030	Full ETos	2	14	14	**0.2140**
6	19	40000 x 1700	2.5	120	0-1700	38.27	-0.030	Full ETos	3	14	14	**0.2148**
7	24	40000 x 1700	2.5	120	0-1700	25.00	-0.035	Full ETtr	3	14	14	**0.2202**
8	11	40000 x 1700	2.5	120	0-1700	25.00	-0.035	Full ETtr	2	14	14	**0.2219**
9	4	40000 x 1700	2.5	120	0-1700	38.27	-0.030	Full ETos	1	14	12	**0.2227**

[£]ETtr and ETos are evapotranspiration values determined by Maule *et al (*2006) method developed for the Prairie region of Canada and by Penman Monteith method (Allen *et al.,* 1998) respectively,

‡Snow Water Equivalent (SWE) values indicate: 1 = SWE 2011=109 mm and 2012=78 mm, 2 = SWE 2011=109 mm and in 2012 SWE increased from 78 mm to 100 mm, 3 = SWE 2011=109 mm and in 2012 SWE increased from 78 mm to 100 mm application way changed and 4 = SWE 2011=109 mm and in 2012 SWE increased from 78 mm to 100 mm and applied in 14 consecutive days.

In addition, LAI = 6 cm^2 cm^{-2}, k = 0.49, maximum rooting depth (Z_R) = 60 cm were used in all the validation simulations.

Table 5-4: Probability table: Joint and Conditional probabilities of $B=d(t) \leq 0.5$ m and $C=q(t) \geq 5$ cm^3 cm^{-2} d^{-1}

		2011			2012			Conditional probability[!]		
Initial d(t) (m)		d(t)≤0.5	d(t)>0.5	Total	d(t)≤0.5	d(t)>0.5	Total		2011	2012
0.50	q(t)<5	0.4314	0.5163	0.9477	0.0000	0.9412	0.9412	P(C|B)	0.0704	-
0.50	q(t)≥5	**0.0327**	0.0196	0.0523	**0.0000**	0.0588	0.0588	P(B|C)	**0.6250**	0.000
0.50	Total	0.4641	0.5359	1.0000	0.0000	1.0000	1.0000			
1.15	q(t)<5	0.1699	0.7778	0.9477	0.0000	0.9412	0.9412	P(C|B)	0.0714	-
1.15	q(t)≥5	**0.0131**	0.0392	0.0523	**0.0000**	0.0588	0.0588	P(B|C)	**0.2500**	0.000
1.15	Total	0.1830	0.8170	1.0000	0.0000	1.0000	1.0000			
2.00	q(t)<5	0.0000	0.9477	0.9477	0.0000	0.9412	0.9412	P(C|B)	-	-
2.00	q(t)≥5	**0.0000**	0.0523	0.0523	**0.0000**	0.0588	0.0588	P(B|C)	**0.0000**	0.000
2.00	Total	0.0000	1.0000	1.0000	0.0000	1.0000	1.0000			

[!]The conditional probabilities indicate both events were related. (Covary together) or were dependent each other

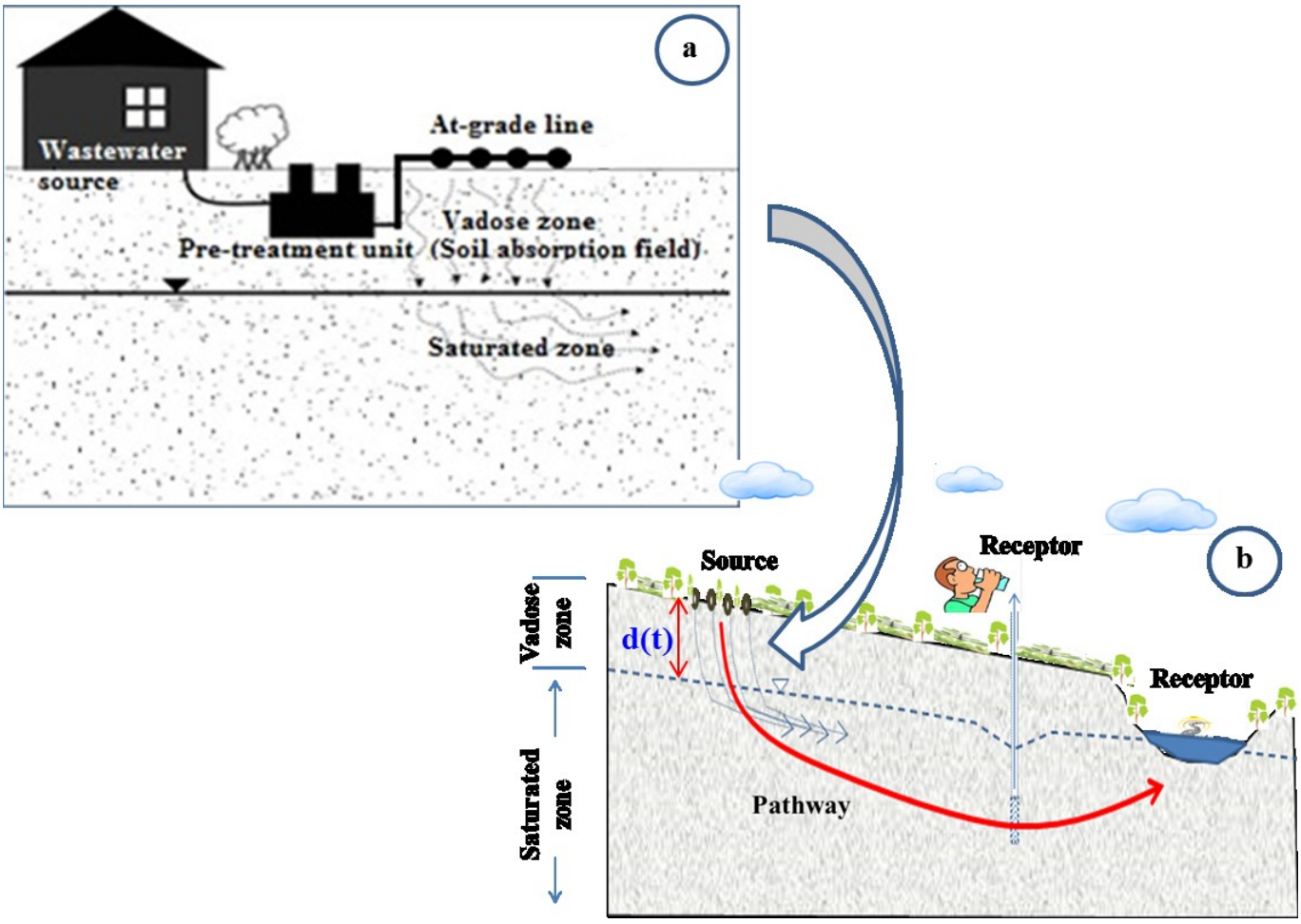

Figure 5-1: a) Typical conventional OWTS (Modified from McCray et al., 2005) and b) conceptual representation of assessing risks to groundwater contamination.

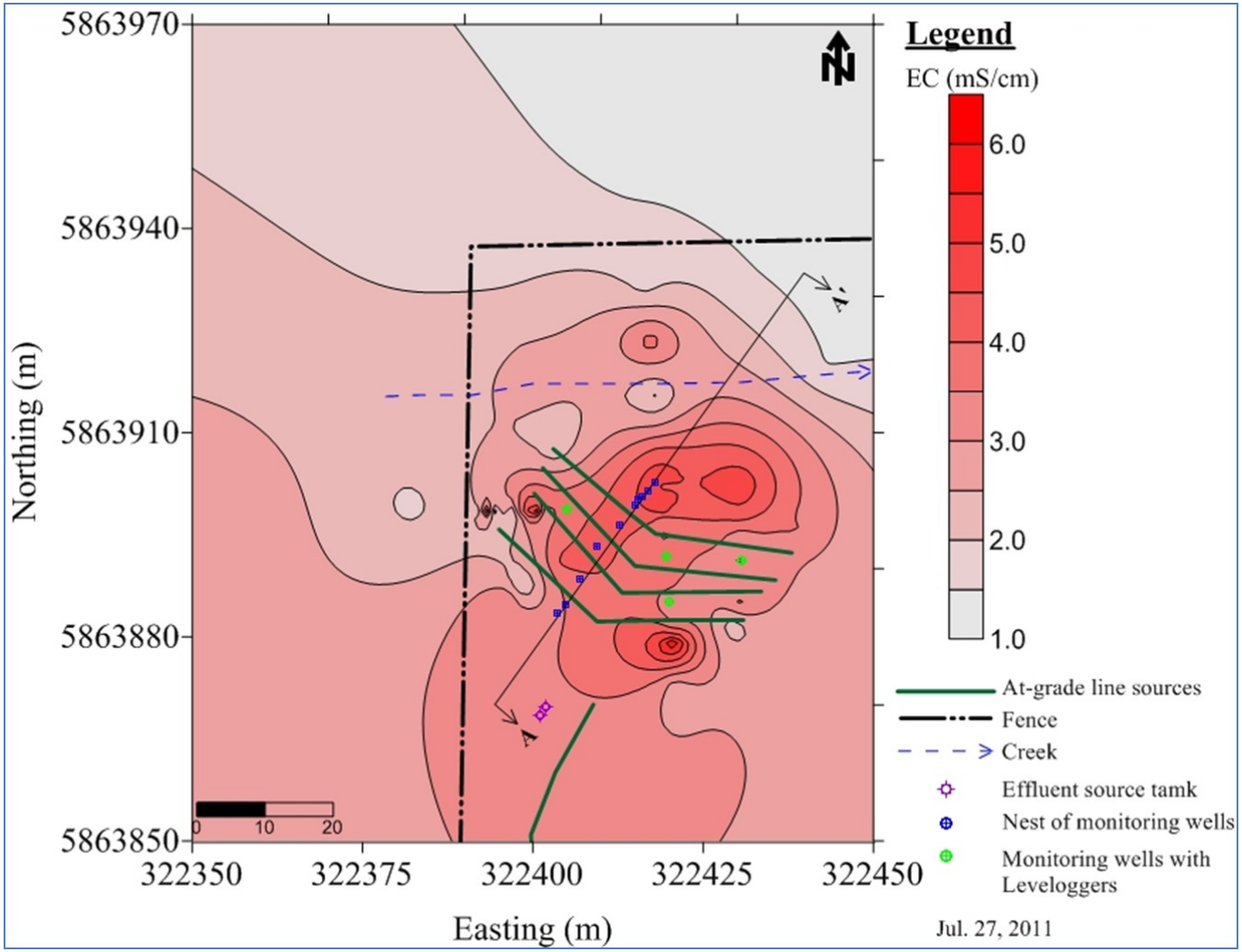

Figure 5-2: Top view of the at-grade line sources and monitoring wells along transect A-A'. The three dimentional plan view and two dimensional cross-section along transect A-A' are given in Figure 4-2 and Figure 5-3 respectively. Details of the spatial distribution of electrical conductivity is also available in chapter 2 and 4. The coordinates were projected according to the North American Datum 83 (NAD 83) and are in zone 12.

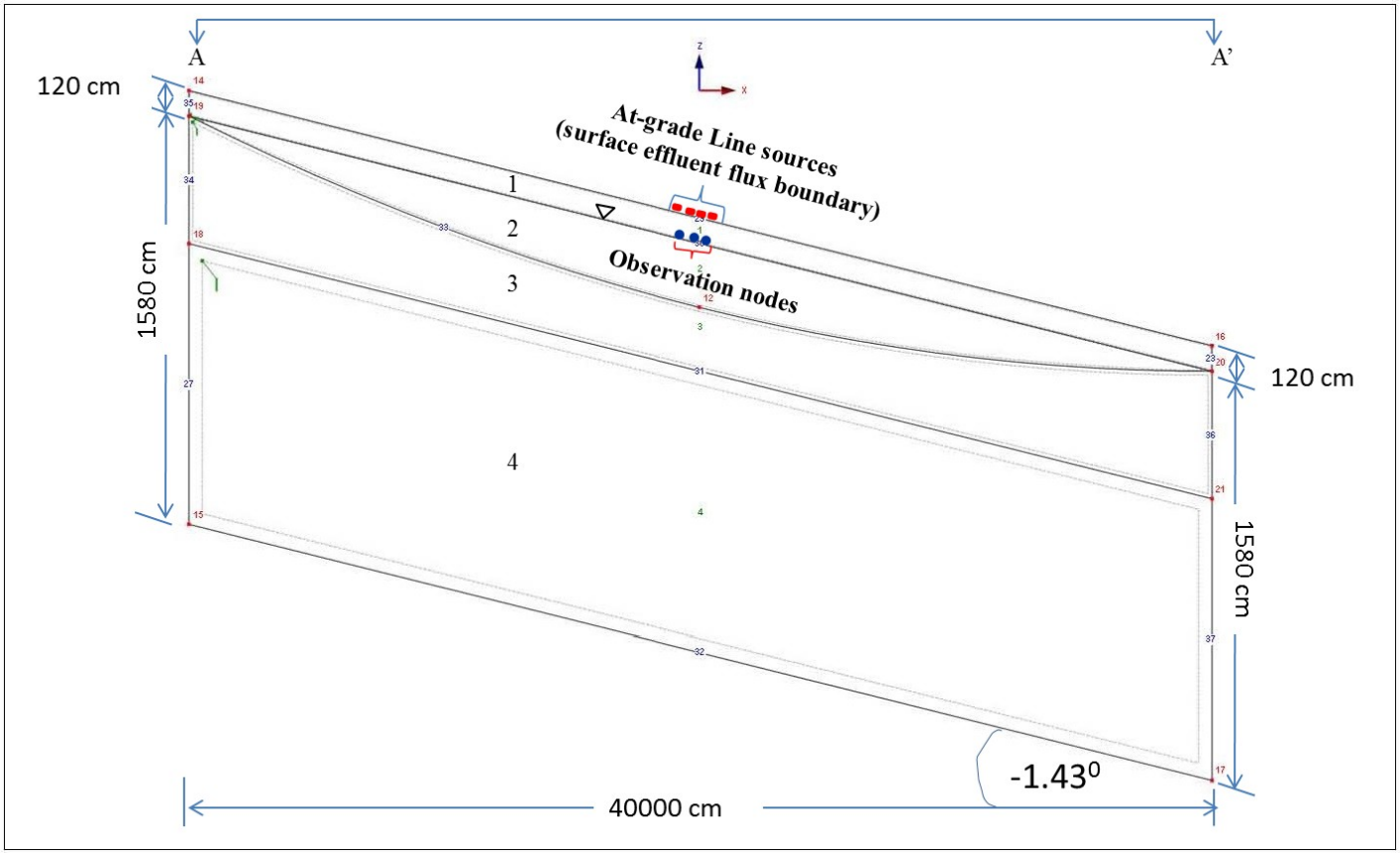

Figure 5-3: Two dimensional geometry for the 40000 cm by 17 cm domain size showing cross-sectional view of A-A' in Figure 5-2. The entire domain has a 2.5% slope and has four surfaces to help spatial discretization. The surfaces had a target finite element (FE) mesh sizes of 5 cm. The upper two surface (1 and 2)were discretized by 5 cm FE size, surface 3 by 25 cm and surface 4 was 50 cm, giving a finer discretiozation close to the ground surface where flow and transport parameters are important. the current discretization produced a total of 44609 nodes in the entire domain.

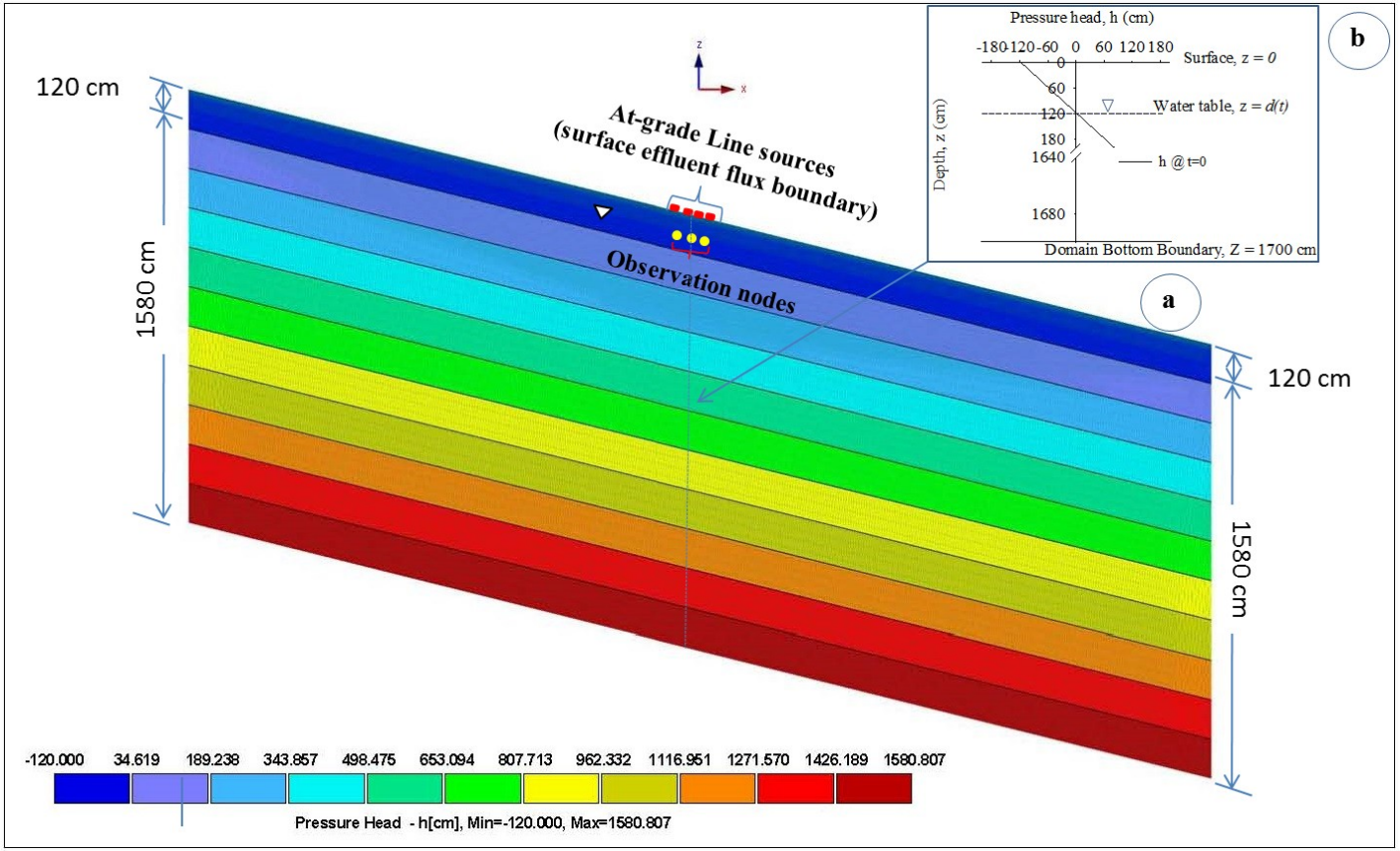

Figure 5-4: a) Initial pressure head conditions for the two-dimensional domain and b) Pressure head profile of the central cross-section at the center of the domain and refernce points. The initial condition was in equlibrium from the lowest nodal points throughout the bottom boundary of the domain keeping the water table level at 120 cm below the ground surface. The observation nodes represent approximately the nest of MWs locations (see Figure 4-1b) in the source zone at approximately -100±0.15 cm below the ground surface at which simulated *d(t)s* were compared with the measured data duinrg model validiation tests.

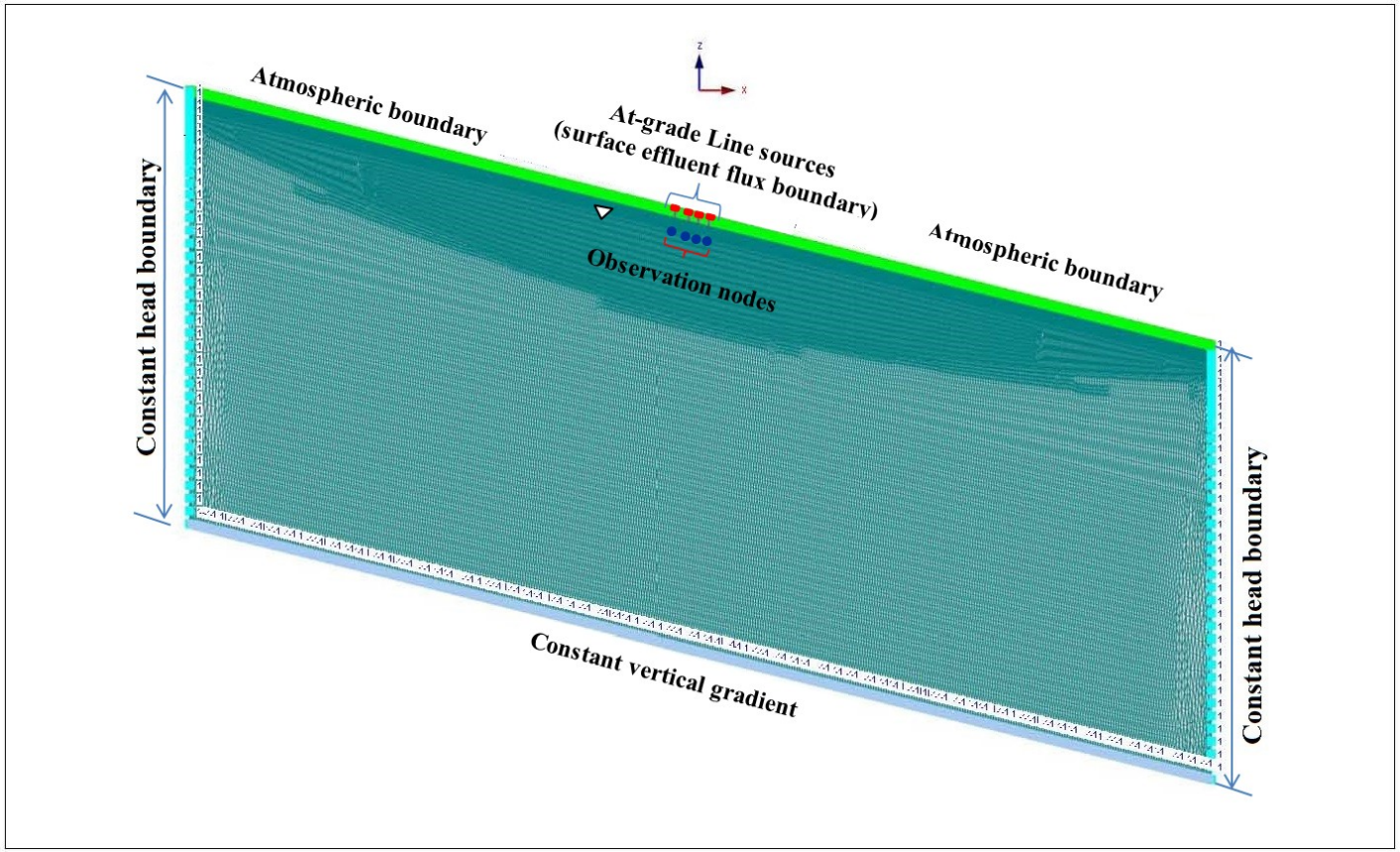

Figure 5-5: Boundary conditions for the two-dimensional domain. The up- and down-stream sides were specified a fixed head boundary condition keeping the water table level at 120 cm below the ground surface. The top boundary was open to the atmosphere and surface effluent fluxes, while the bottom bourady was speficied a constant vertical gradient. The observation nodes were located approximately beneath the center center of each lateral at -99.68±24 cm below the ground surface at these locations simulated *d(t)s* were calculated for risk analysis.

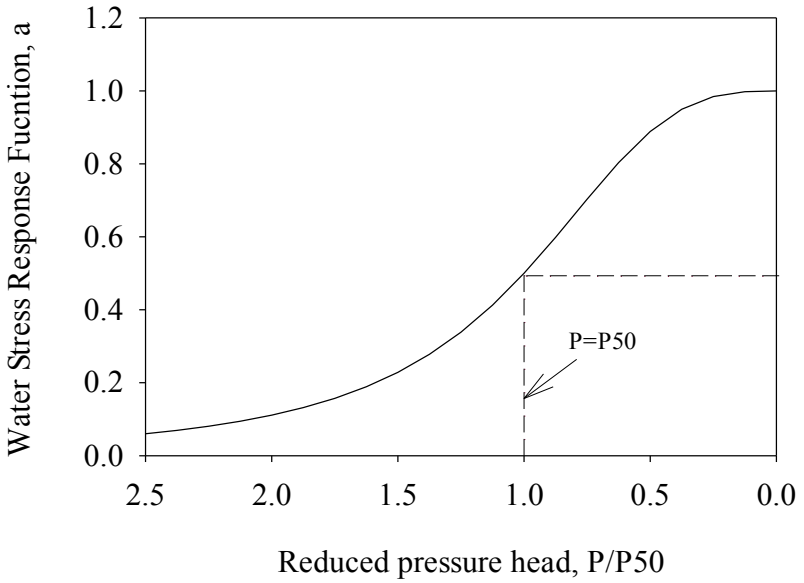

Figure 5-6: Schematic of the water stress response function for Aspen used in the simulation

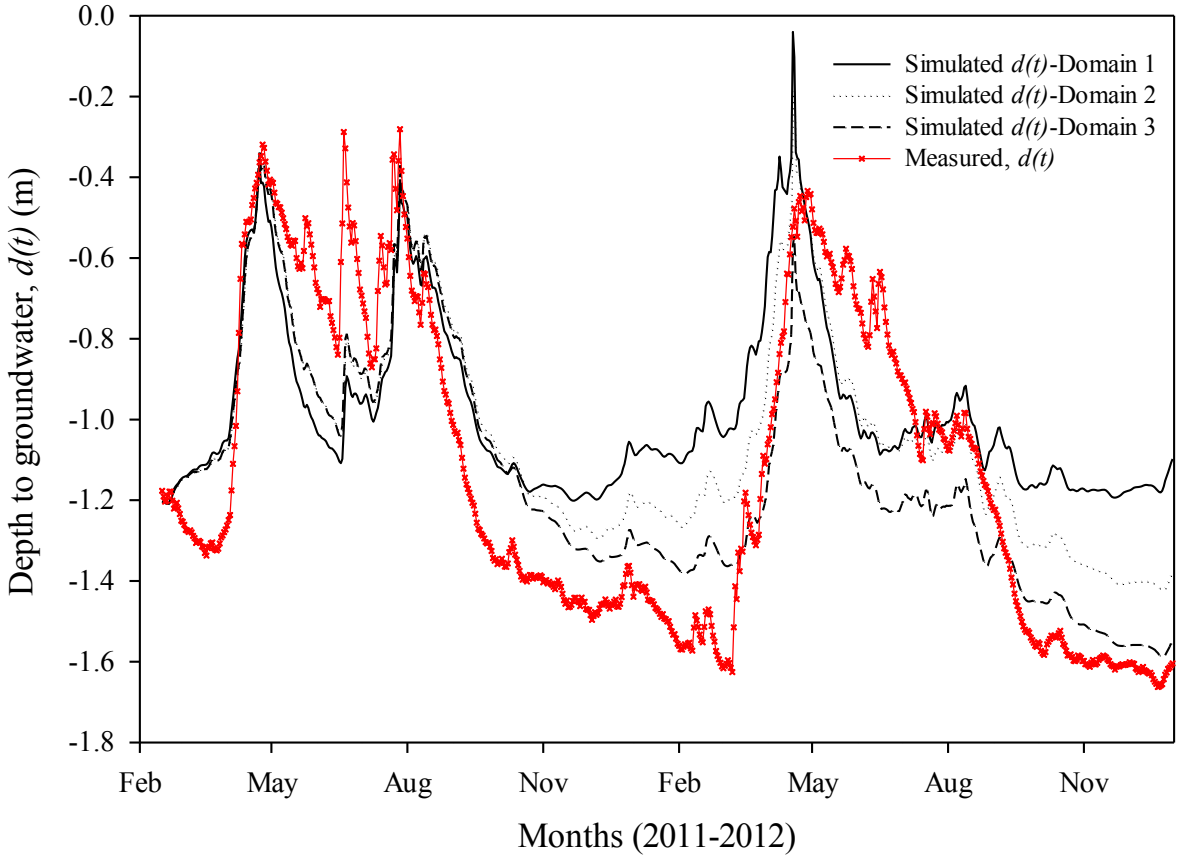

Figure 5-7: Domain size selection. The domain sizes were: Domain 1 = 10000 cm x 1700 cm, Domain 2 = 20000 cm x 1700 cm and Domain 3 = 40000 cm x 1700 cm. RMSE beteween simulated and measured d(t) of domain 1, 2 and 3 were 0.3073, 0.2172 and 0.2041 respectively. Groundwater mounding was also observed for domains 1 and 2 after approximately 260 days since simulation started. Therefore, comparing the three domain sizes, Domain 3 was selected as the best size to mimic the site conditions.

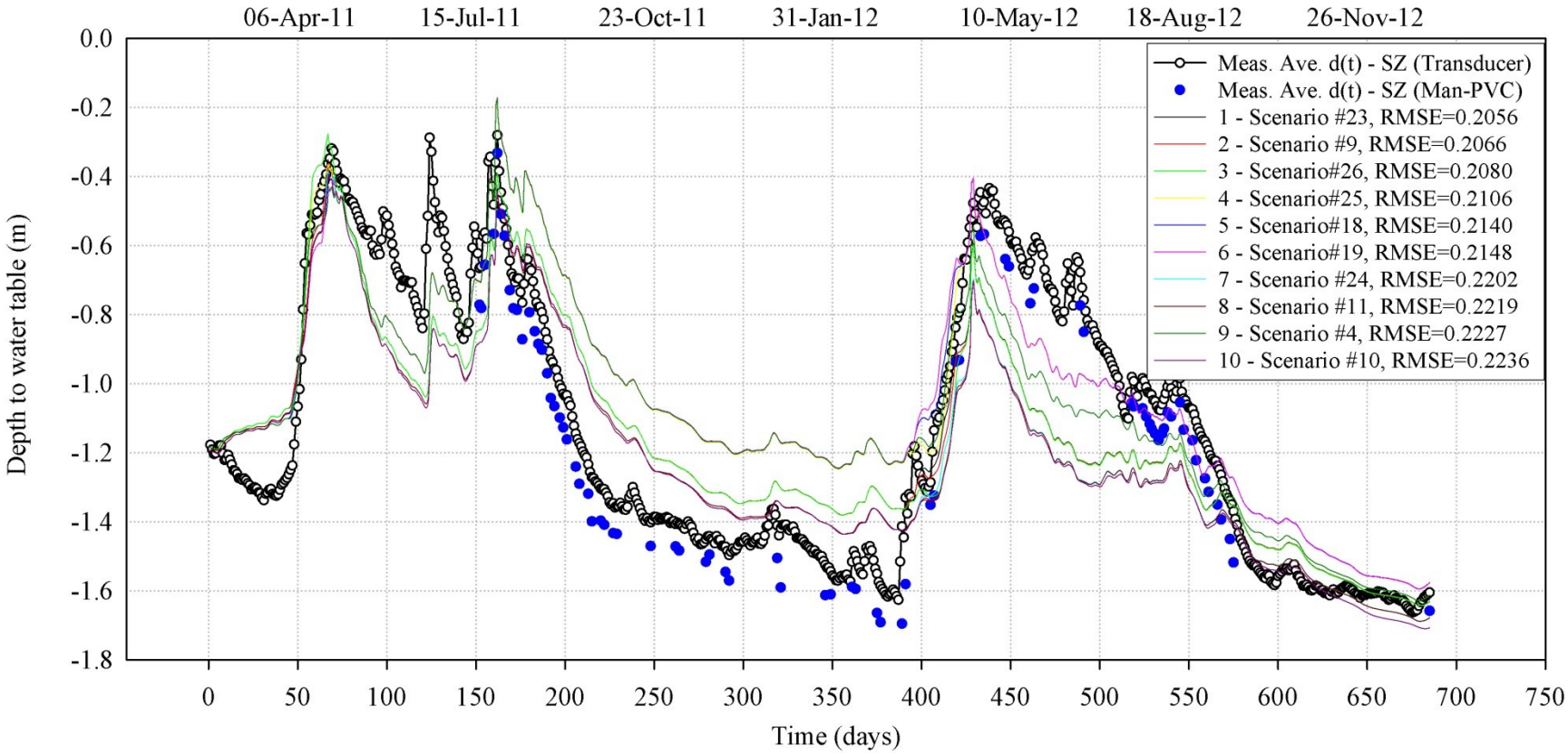

Figure 5-8: Measured and simulated d(t) of the top ten scenarios ranked based on root mean squared error (RMSE) as shown in Table 5-3. The ranking was made from the preliminary observations of the lowest RMSE between the measured and simulated depth to water table d(t)). SZ- and Man-PVC represent source zone and manually measured water level from PVC wells respectively.

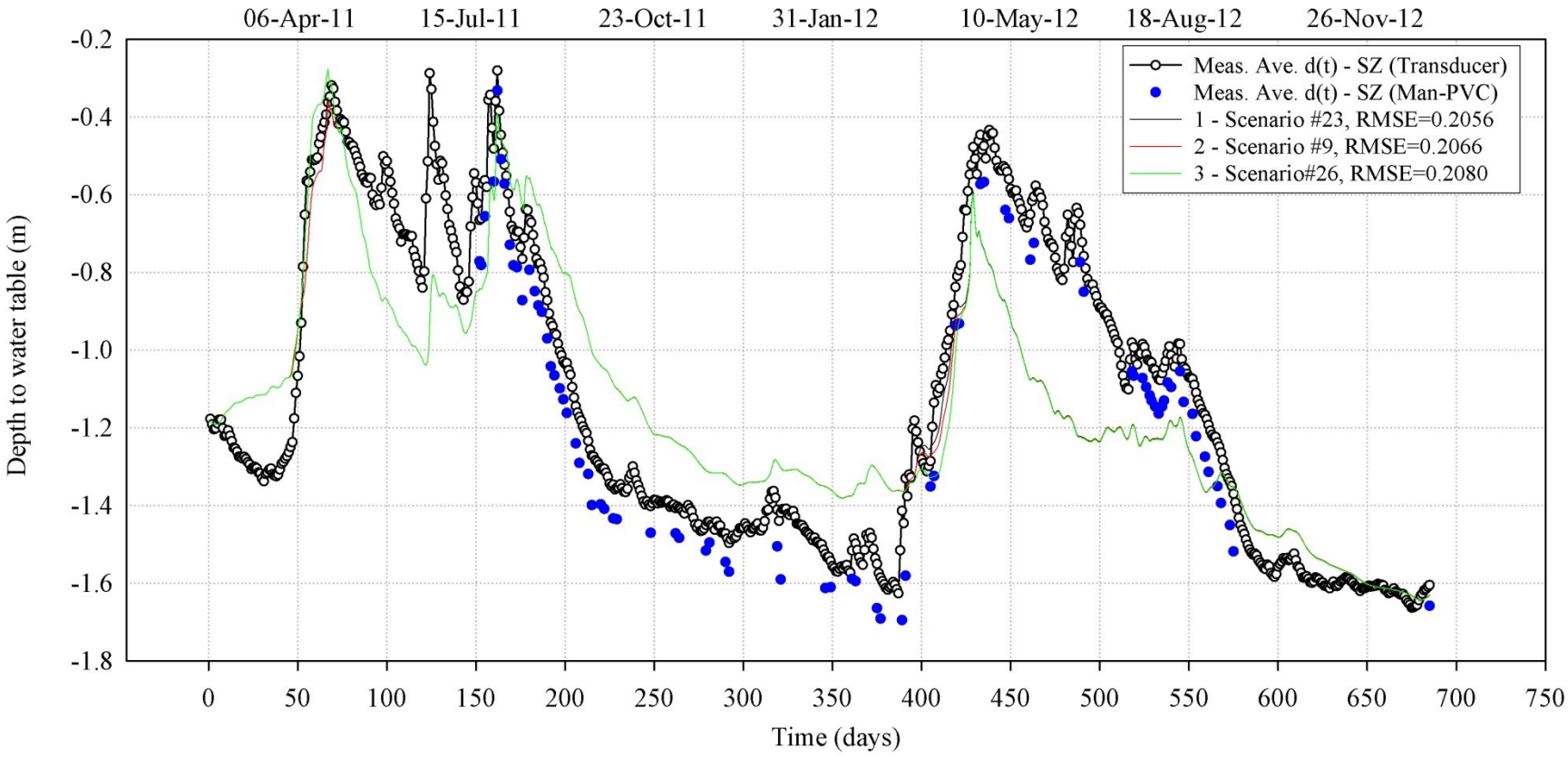

Figure 5-9: Measured and simulated d(t) for the best scenario (K_s = 25 cm d^{-1}, a constant flux of -0.030 at the bottom boundary, and ET_{tr}) that were given in Figure 5-7.

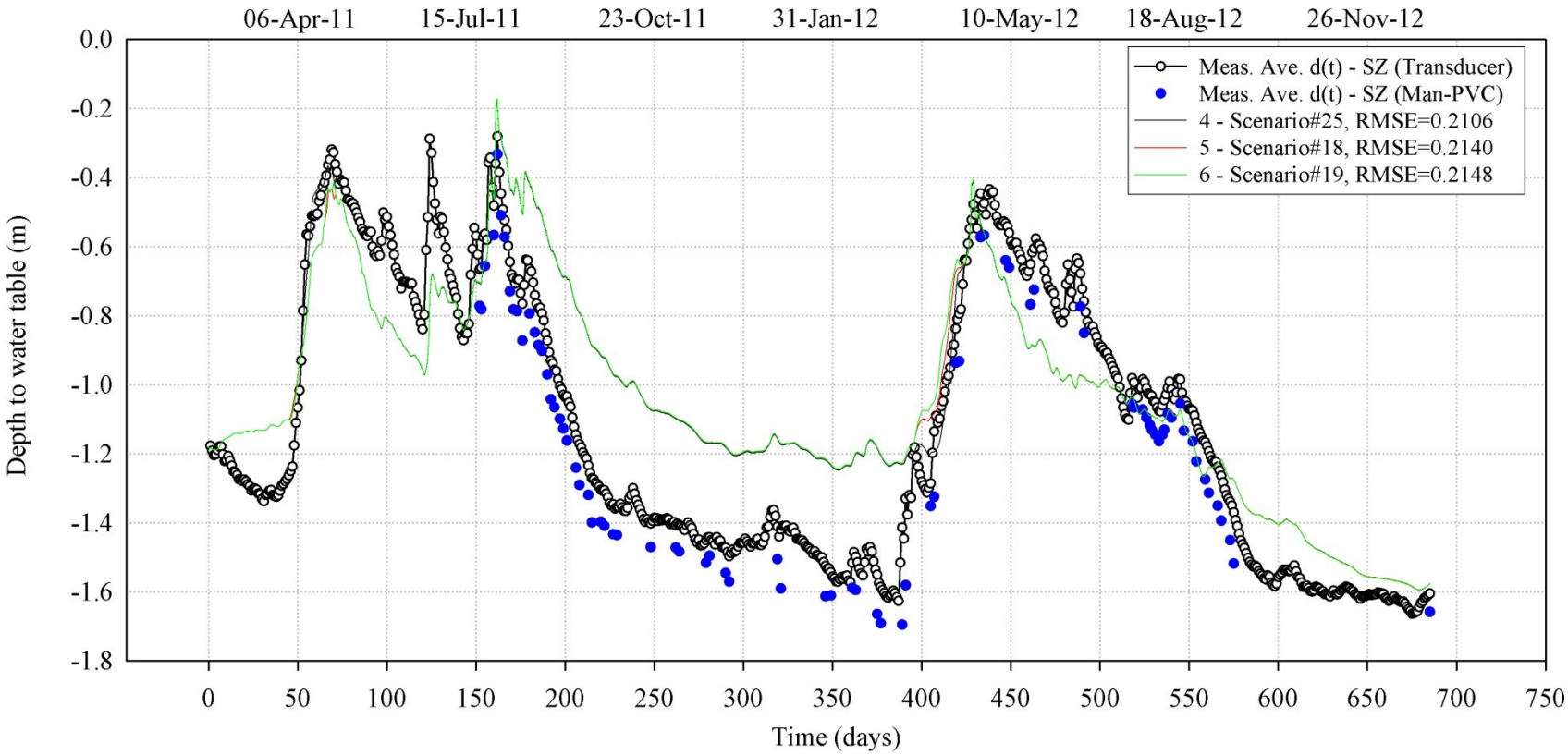

Figure 5-10: Measured and simulated d(t) for the 2nd best scenario (K_s = 38.27 cm d^{-1}, a constant flux of -0.030 at the bottom boundary, and ET_{os}) that were given in Figure 5-7.

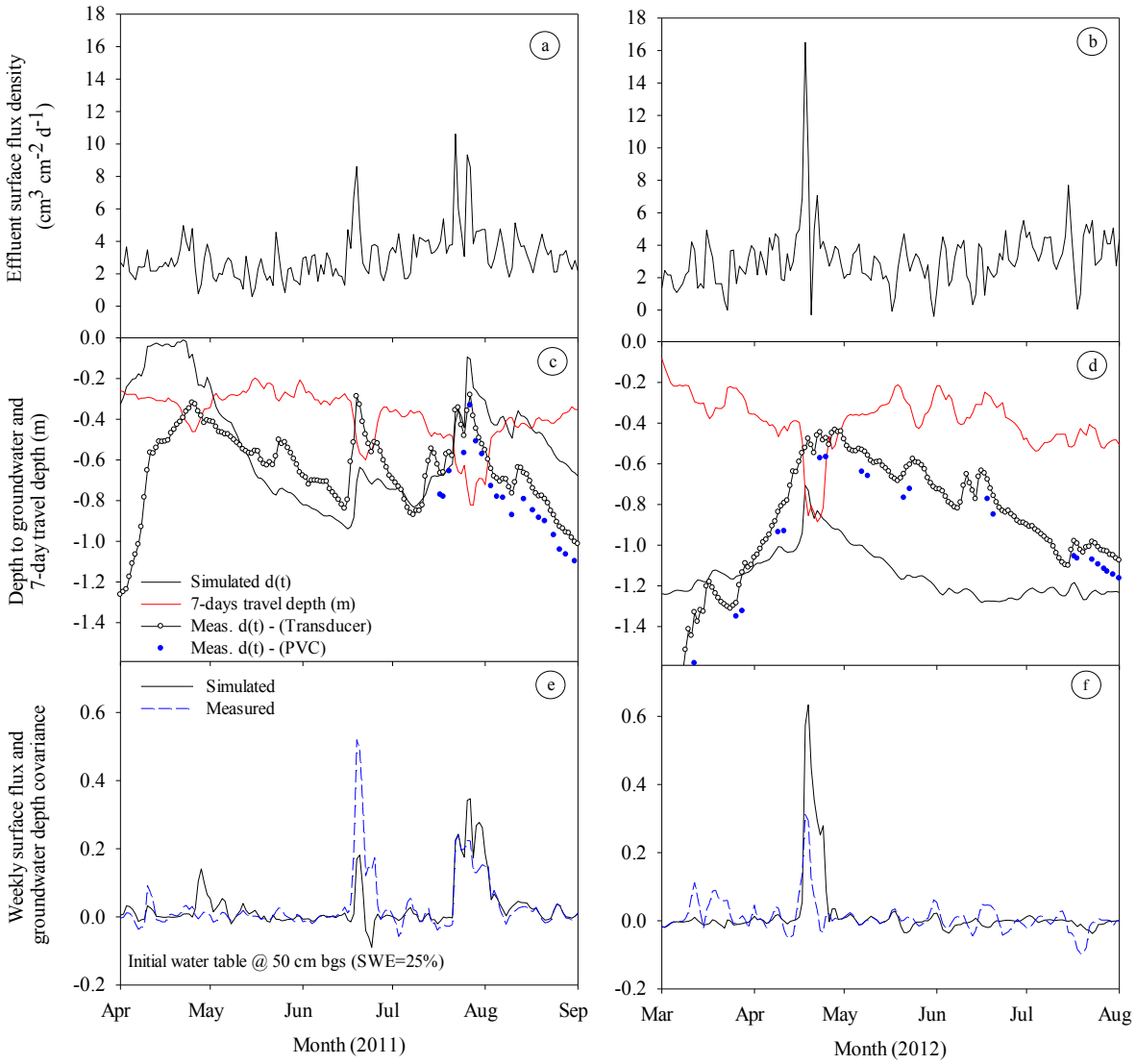

Figure 5-11: Measured and simulated time series groundwater level below the ground surface when the initial water table level was at 50 cm below the ground surface and assuming 25% SWE focusing on the spring and summer periods for the two years (2011-2012). The graphs compare the effective surface flux density (a) and (b), groundwater hydrographs and 7-day travel depth (c) and (d), and weekly surface flux and groundwater depth covariance (e) and (f). ET_{tr} calculated using Maule *et al.,* 2006.

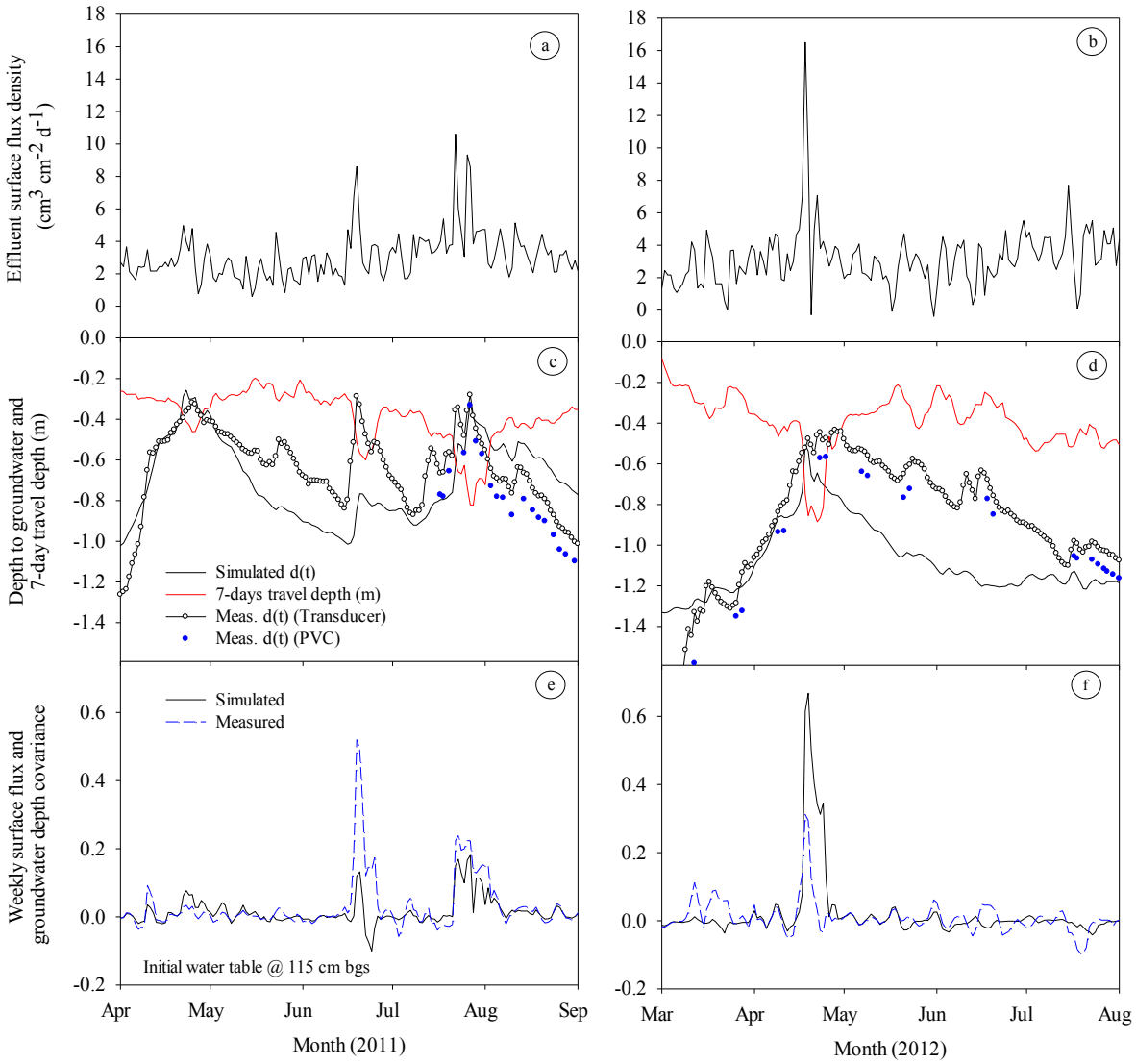

Figure 5-12: Measured and simulated time series groundwater level below the ground surface when the initial water table level was at 115 cm below the ground surface and assuming 100% SWE focusing on the spring and summer periods for the two years (2011-2012). The graphs compare the effective surface flux density (a) and (b), groundwater hydrographs and 7-day travel depth (c) and (d), and weekly surface flux and groundwater depth covariance (e) and (f). ET_{tr} calculated using Maule *et al.,* 2006.

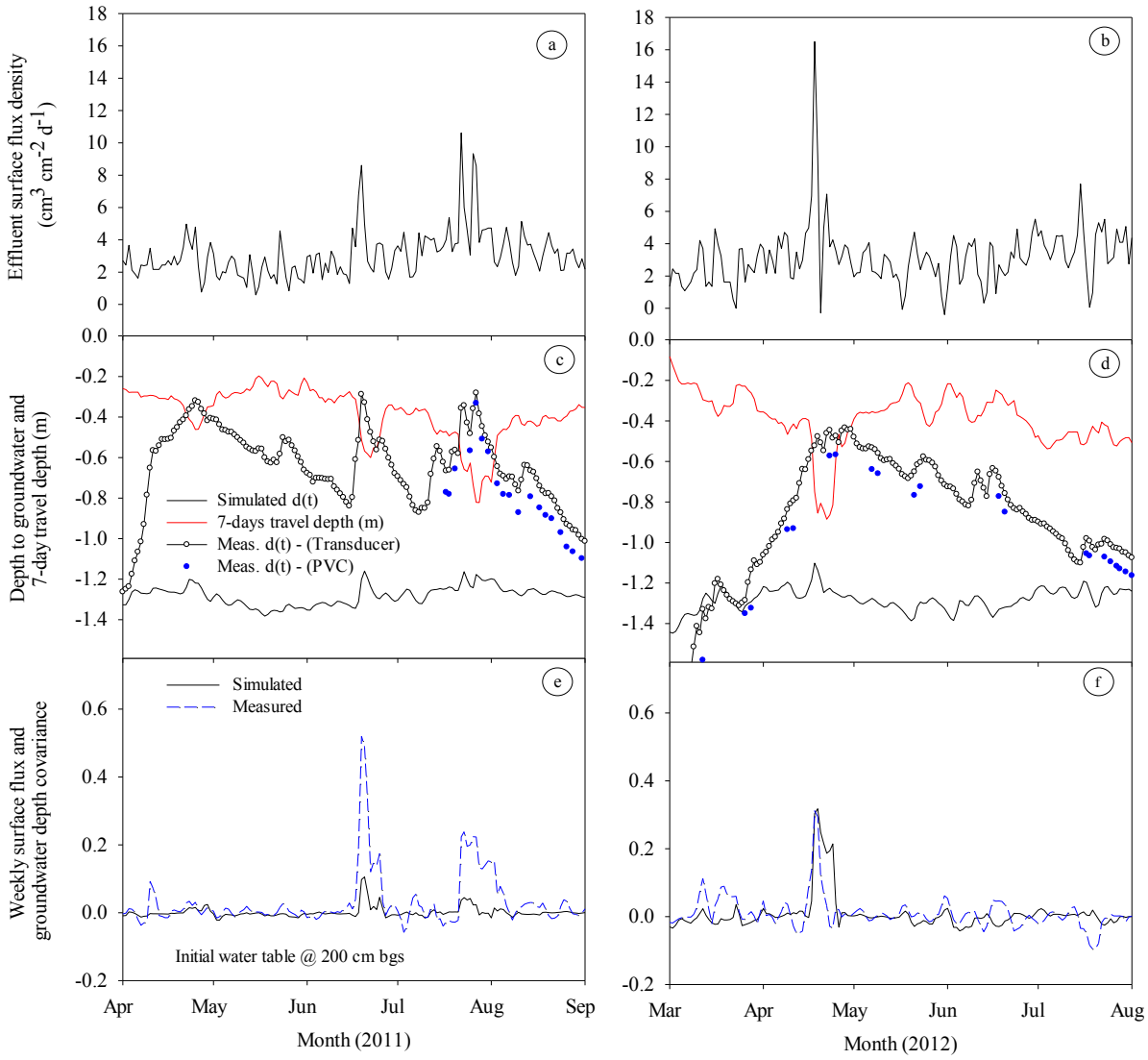

Figure 5-13: Measured and simulated time series groundwater level below the ground surface when the initial water table level was at 200 cm below the ground surface and assuming 100% SWE focusing on the spring and summer periods for the two years (2011-2012). The graphs compare the effective surface flux density (a) and (b), groundwater hydrographs and 7-day travel depth (c) and (d), and weekly surface flux and groundwater depth covariance (e) and (f). ET_{tr} calculated using Maule *et al.,* 2006.

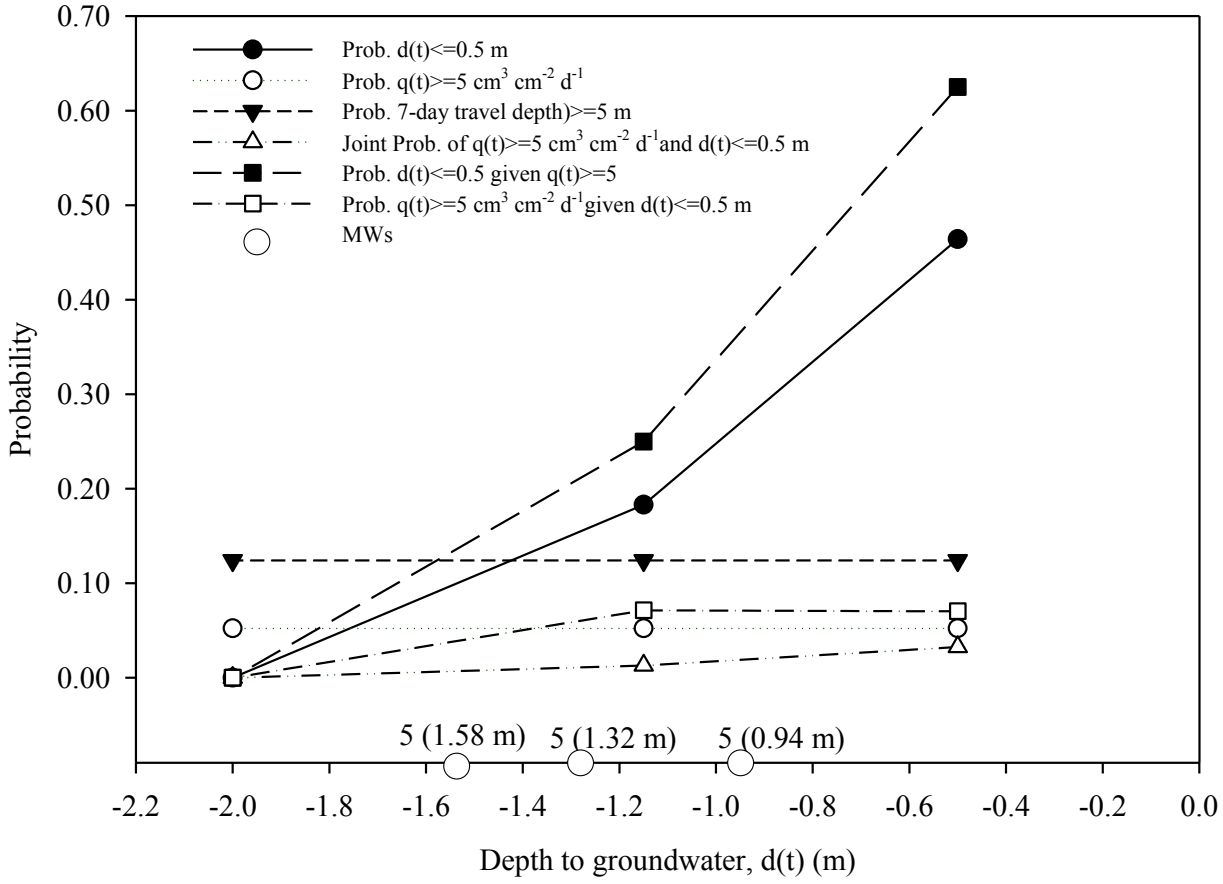

Figure 5-14: Joint and conditional probability of d(t) and q(t). The monitoring wells at the source zone nest # 5 at 0.94, 1.32 and 1.58 m depth below the ground surface (see Figure 4-2 in Chapter 4).

6. GENERAL CONCLUSION AND DISCUSSION

6.1. Summary and Contribution of This Thesis

The major objective of this thesis was to increase our understanding of multi-dimensional unsaturated and saturated flow and transport under boundary conditions typical of on-site wastewater treatment systems (OWTS) under shallow groundwater conditions and to quantifying groundwater contamination risks associated with these systems. Field investigations evaluating performance of at-grade effluent treatment systems are required to include these systems in the Alberta standard of practice for on-site wastewater treatment. A field research program was executed at the Wetaskiwin rest stop located 80 km south of Edmonton to accomplish the objective. The performance of the OWTS was evaluated by measuring the hydrologic response to surface effluent infiltration and wastewater flow and transport. The site-specific measurements of the flow and transport processes were used to validate a numerical flow and transport model. The model was then used to assess risks of groundwater contamination associated with OWTS. The major contributions and conclusions of this thesis are:

1. An existing wastewater plume and its flow direction were identified using a combination of non-contacting geophysical instruments (Electromagnetic Induction, EM38 and EM31) and by installing inexpensive aluminum wells (Chapter 2). The methodology can be adopted and implemented in similar field studies.
2. Hydrologic response to surface effluent infiltration was quantified and a threshold value of effective surface flux, $q(t)$ for a given depth to groundwater, $d(t)$ has been identified for the OWTS under the prevailing boundary conditions (Chapter 3). It was observed that surface effluent reached the groundwater in less than 7 days for approximately 15% of the time in the spring and summer periods when effluent loading rate of ≥ 5 cm^3 cm^{-2} d^{-1} encountered groundwater at ≤ 0.5 m below the ground surface. These conditions also coincided with the significant 7-day cycles of the effluent input function due to traffic on the highway and use of the facilities. The results suggest considering not only surface effluent loading but also site hydrologic conditions, particularly during periods of high covariance between depth to groundwater and surface effluent loading rates, when designing at-grade

wastewater treatment systems to minimize potential groundwater contamination risks.

3. Wastewater flow and transport was investigated using a pulse of Bromide and a step input of *E.coli* (Chapter 4). The step input of microbiological contaminant was a novel approach implemented in our study and the results will contribute to our understanding of flow, pathogen fate and transport processes on a site with typical OWTS and shallow groundwater boundary conditions. The step input resulted in a quasi steady state application of microbe rich-effluent for an extended period, simulating the UV-disinfection system malfunction. With increasing vadose zone thickness, $> 3\ log_{10}$ removal of *E.coli* and viruses were observed except for norovirus and rotavirus species, in which the reduction was only$< 1\ log_{10}$. Based on the observed results, *E.coli* present in the infiltrating effluent was lowered to acceptable levels when the groundwater level was ≥0.88 m below the ground surface achieving the 7-day effluent travel depth design criteria (Safety Code Council, 2012). However, some viruses such as the noroviruses and rotaviruses were observed in higher concentrations for groundwater levels ≤ 1.0 m, indicating performance failure of the at-grade effluent dispersal system under the prevailing boundary conditions at certain periods of the year. These risky periods were observed during the spring snow melt and the summer precipitation periods simultaneously with high covariance between depth to groundwater and effluent loading rates.

4. Assessing the risks associated with OWTS requires characterization of the complex flow and transport processes. However, from a regulatory perspective, it would be too onerous and impractical to undertake the detailed characterization described in this thesis for every new OWTS system. Hence it was simplified and some key aspects are presented that help understand the prevailing flow and transport processes and propose the following recommendations for future work. Typically, considering groundwater fluctuation and groundwater depth below the ground surface during the risky periods of a year as mentioned above as well as particle size distribution as the key factors in designing at-grade effluent treatment systems. We used the site-specific measurements of the flow and transport

processes to validate a numerical flow and transport model, HYDRUS 2D (Šimůnek *et al.,* 2006, Chapter 5) and then probability distribution of *d(t)* for various initial water table depth scenarios has been developed for use in similar site conditions. Accordingly, surface fluxes ≥15 cm^3 cm^{-2} d^{-1} and initial water table depth at ≥200 cm below the ground surface could be assumed as threshold values for safe on-site wastewater treatment systems and it can be applicable to sites with similar boundary and site conditions.

5. In summary, understanding of the effluent loading rates, soil hydraulic properties and temporal site hydrologic conditions are important for designing effective at-grade effluentt treatment systems. The following points were set as possible recommendations: i) reduce daily surface effluent loading rates on shallow groundwater systems, for example, by containing effluents in storage tanks especially during potentially risk periods, ii) adopt performance based approaches for at-grade systems an approach accounting for treatment and dispersal in the soil absorption field with the performance objective to protect public health and the environment (McMurtrie *et al.,* 2013), and iii) Minimize daily surface effluent flux density, for example by increasing application surface area (if applicable).

6.2. At-Grade Line Sources and Soil-Based Wastewater Treatment System

At-grade line sources use laterals placed on (or raised slightly above) the ground surface as effluent dispersal lines. These systems commonly use soil based wastewater treatment systems installed on shallow groundwater conditions to increase the vadose zone thickness (vertical separation between the point of effluent entry and the groundwater level). The increased thickness increases residence time of the effluent and attenuation of contaminants that may exist in the effluent before reaching the groundwater. However, in areas with considerable seasonal groundwater fluctuation, the vadose zone thickness change the hydrologic condition, flow and transport processes. In periods of groundwater rise close to the ground surface, surface applied effluent would reach the groundwater in shorter travel time than the time required for attenuation of contaminants putting groundwater at risk.

6.3. Future Research

This thesis provides a foundation for several future research directions. Possibly the most obvious is extending further process based modeling of the flow and transport processes by varying mean and variance of the surface effluent flux loading, using layered soils and testing it in HYDRUS 2D and HYDRUS 3D model.

- Simulate pathogen transport in a 2D model (using the data for bacteria to validate the model)
- Repeat the field experiment by switching the step input of untreated effluent (considering *E.coli* and Viruses as microbial tracers) to the winter and spring seasons and simultaneously measure/monitor concentrations in groundwater and in the vadose zone (as applicable)
- Assess loading rate scenarios by varying the mean and variance of the observed effluent surface flux data to assessing risks to groundwater contamination
- Investigate effluent travel depth probability by varying soil material
- Evaluate groundwater contamination risk in HYDRUS 3D in homogenous soil using the existing dataset
- Develop a process-based model using layered soils (heterogeneous domain) and the existing dataset in HYDRUS 2D and 3D.

6.4. References

McMurtrie, R., Payne, M., and Ralston, I., 2013. APEGBC Professional practice guidelines onsite sewerage systems. APEGBC Version 1.2 – January 07, 2013. British Columbia.

Safety Code Council, 2012. Alberta private sewerage systems 2009 standard of practice handbook. Available on line: http://www.safetycodes.ab.ca/Public/Documents/PSSSOP_Handbook_Version_12_Online_Feb_21_2012b.pdf

Šimůnek, J., M. Th. van Genuchten, and M. Šejna, 2006. The HYDRUS software package for simulating the two- and three-dimensional movement of water, heat and multiple solutes in variably-saturated media. Technical Manual, Version 1.0. PC Progress, Prague, Czech Republic.

7. APPENDICES

Appendix 2-A: Appendix D: Alberta one-call line clearance map

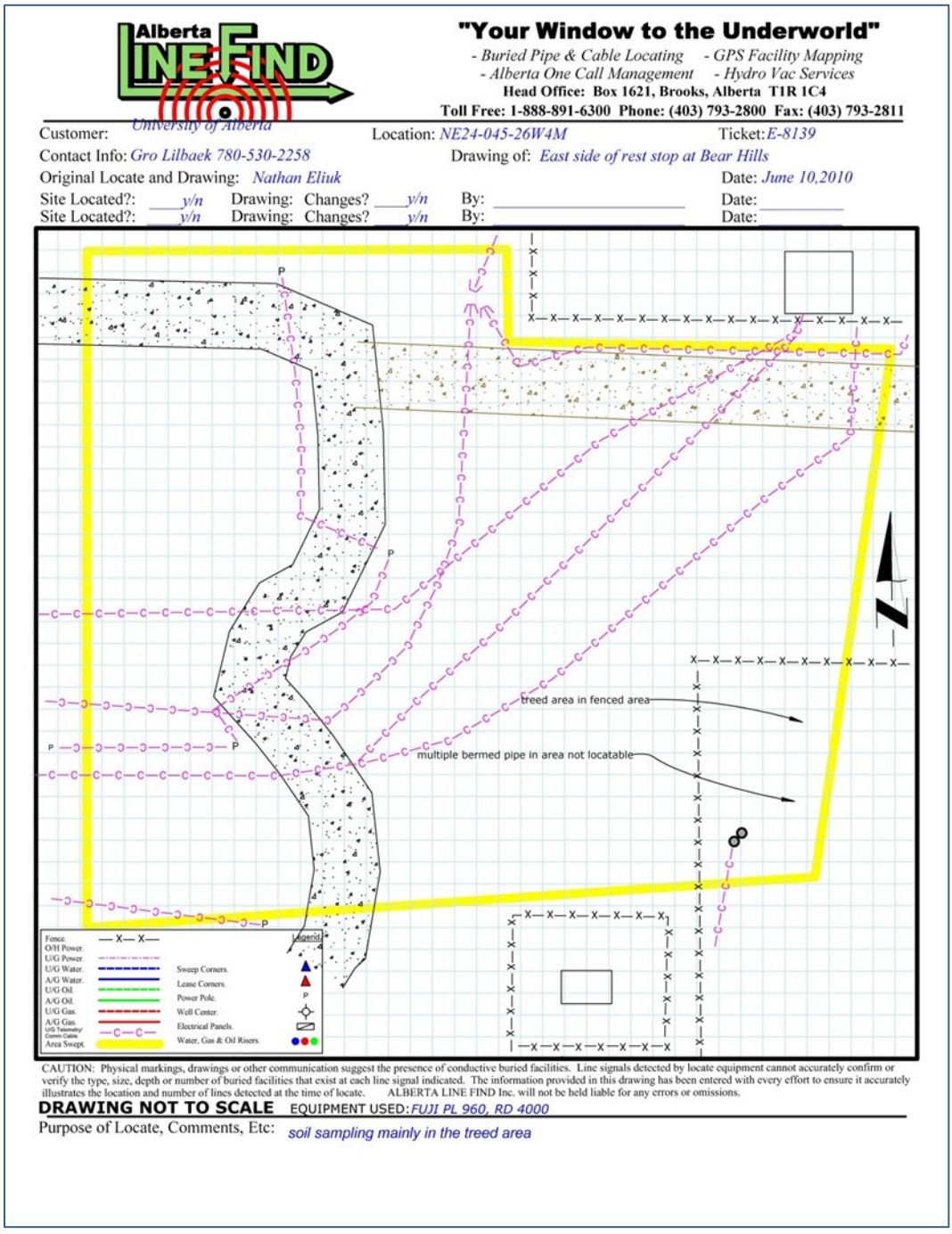

Appendix 4-A. Historical as well as on-going biochemical data for samples collected from the UV-disinfection tank (Source: Cherdan Construction Comp)

Parameter	Unit	19-Jan-11	12-Apr-11	Detection limit	Method	Unit	20-Jul-11	20-Apr-12	14-Nov-12	Detection limit	Method
BOD	mg/L	12.0	14.0	4	5 Days	mg/L	11.0	10.0	10.0	4	5 Days
TSS	mg/L	17.0	<2	2	Total Suspended solids	mg/L	52.0	<5	6.0	5	Total Suspended solids
Total Kjeldahl N						mg/L			142.0	0.2	
pH		8.1	7.9		Routine water		nd	nd	nd	nd	APHA
E.coli	MPN/100 mL	nd	490.0		MPN	CFU/100 mL	<5	nd	nd	nd	nd
Fecal Coliforms	MPN/100 mL	nd	490.0		MPN	CFU/100 mL	<5	<1	<5	5	nd
Total Coliforms	MPN/100 mL	nd	1300.0		MPN	CFU/100 mL	>1000	153.0	50.0	5	nd

BOD=Biochemical Oxygen Demand: Modified from APHA 5210B

Fecal Coliforms (water): Modified from APHA 921E

TKN (water): Modified from APHA 450-NC

Total Coliforms (water): Modified from APHA 92B

Total Suspended Solids=TSS: Modified from APHA 2540D

Appendix 5-A: Summary input parameters to the HYDRUS 2D model used for water flow simulation

Parameters and variables	Values	
1. Project	*2D Water flow simulation*	
2. Flow and transport domain		
Geometry	2D vertical plane XZ general dimension	
Domain sizes	X (cm)	Z (cm)
	10000	1700
	20000	1700
	40000	1700
Slope	-1.43^0 (2.5%) and -0.57^0 (1%) to the general groundwater flow direction	
Length units	cm	
Fine element Mesh	Generated with MeshGen2D	
Number of materials in the flow domain	Homogeneous soil material (with hydraulic properties given below)	
3. Main processes	Water flow, root water uptake	
4. Time discretization		
Time units	Days	
Initial time	0 (16 Feb. 2011)	
Final time	365 (15-Feb-2012) and 685 (31-Dec-2012)	
Initial time step	0.010466 (15 min recommended for loam)[a]	
Minimum time step	0.000012	
Maximum time step	0.041666	
Number of time-variable boundary records	365 and 685	

Appendix 5-A: (Cont…)

Parameters and variables	Values
Spatial discretization	
Target mesh size	5 cm
Surfaces	1-2 = 5 cm
Surfaces	3 = 15 cm
Surfaces	4 = 20 cm
Smoothing factor	2
Mesh stretching	2
5. Iteration criteria	
Maximum number of iterations	10 (default)
Water content tolerance	0.001(default)
Pressure head tolerance	1 (default)
Lower optimal iteration range	3 (default)
Upper optimal iteration range	7 (default)
Lower time step multiplication factor	1.3 (default)
Upper time step multiplication factor	0.7 (default)
Lower limit of the tension interval	0.0001 (default)
Upper limit of the tension interval	10000 (default)
Initial condition	Prescribed pressure head
6. Soil hydraulic properties (Sandy Loam)	
Hydraulic model	Van Genuchten-Mualem
Hysteresis	No
Residual water content (θr), [cm^3cm^{-3}]	0.21
Saturation water content (θs), [cm^3cm^{-3}]	0.56
α of the soil water retention function, [cm^{-1}]	0.036
n of the soil water retention function, [-]	1.56

Appendix 5-A: (Cont…)

Parameters and variables	Values
Saturated hydraulic conductivity (K_s), [cm d^{-1}]	25, 38.27 and 19.135
l of the soil water retention function	0.5
7. Root water uptake model and parameters	
Water uptake reduction model	S-Shape (van Genuchten, 1987)
Root distribution	Linear distribution with depth from the surface to the bottom of the root zone at 60cm. Laterally uniformly distributed along the entire surface area associated with transpiration
Ph50[b]	-800 cm (default)
o[c]	3 (default)
PWP[d]	-10^{-10} cm (default)
Z_R	60 cm
z*	30 cm
P_z	1
8. Time variable boundary condition records	
Flux density	Daily observed effluent flux density
Precipitation, Potential evaporation and transpiration	Daily values calculated from weather data and vegetation characteristics (Aspen tree)
hCritA	15000 cm
Surface area associated with transpiration	Length of transect for 2D domain
9. Initial conditions	
Pressure head in equilibrium from the lowest located nodal point and the water table was set at 100 cm below the ground surface	

Appendix 5-A: (Cont…)

Parameters and variables	Values
10. Boundary conditions	
Constant boundary condition	Up-and down-gradient pressure head in equilibrium from the lowest located nodal point and water table located at 100 cm below the ground surface.
Atmospheric boundary condition	Top boundary nodes EXCEPT the effluent line sources
Variable flux boundary	Top boundary nodes representing the effluent line sources
No flow boundary	Bottom nodes
Domain properties	
Material distribution	Homogeneous loam soil
Root water uptake	Linearly distributed with depth from the surface to the bottom of the root zone located at 60cm (i.e., high root distribution close to the surface);
Depth of observation nodes (cm)	~25, ~100, ~130, ~155 cm below the ground surface.

[a] Larger initial time step (e.g. 15 min) was suggested for soils with less nonlinear soil hydraulic properties (e.g. Loam) (Šimůnek *et al.,* 2006).
[b] Pressure head value, h_{50}, at which root water uptake is reduced by 50% (Šimůnek *et al.,* 2006).
[c] Exponent *o* in the S-shaped root water uptake stress response function. Recommended value is 3 (Šimůnek *et al.,* 2006).
[d] PWP = Wilting point, i.e., the pressure head below which the root water uptake ceases (Šimůnek *et al.,* 2006).
[e] hcritA critical threshold pressure head value (Šimůnek *et al.,* 2006).

Appendix 5-B:RMSE of scenarios considered during model validation process

Scenario#	Domain size	SLP	*d(t)*	Depth	K_s	Bottom Boundary flux	Potential Evapotranspiration (method of determination) [£]	Snow water equivalent (SWE) [†]	# of days SWE applied[††]		RMSE
									2011	2012	
	Cm	%	cm	cm	cm d^{-1}	cm d^{-1}					
1	20000 x 1700	2.5	120	0-1700	38.27	-0.025	Full ETtr	1	14	12	0.2281
2	40000 x 1700	2.5	120	0-1700	38.27	-0.025	Full ETtr	1	14	12	0.2539
3	40000 x 1700	2.5	120	0-1700	38.27	-0.025	Full ETtru	1	14	12	0.2510
4	40000 x 1700	2.5	120	0-1700	38.27	-0.030	Full ETos	1	14	12	0.2227
5	40000 x 1700	2.5	120	0-1700	25.00	-0.030	Full ETtr	1	14	12	0.2274
6	40000 x 1700	2.5	120	0-1700	25.00	-0.035	Full ETos	1	14	12	0.2477
7	40000 x 1700	2.5	120	0-1700	25.00	-0.040	Full ETos	1	14	12	0.2304
8	40000 x 1700	2.5	120	0-1700	25.00	-0.050	Full ETos	1	14	12	0.2423
9	40000 x 1700	2.5	120	0-1700	25.00	-0.030	Full ETtr	2	14	14	0.2066
10	40000 x 1700	1	120	0-1700	25.00	-0.035	Full ETtr	2	14	14	0.2236
11	40000 x 1700	2.5	120	0-1700	25.00	-0.035	Full ETtr	2	14	14	0.2219
12	40000 x 1700	2.5	120	0-1700	25.00	-0.040	Full ETtr	2	14	14	0.3147
13	40000 x 1700	2.5	120	0-1700	25.00	-0.050	Full ETtr	2	14	14	0.3145
14	40000 x 1700	2.5	120	0-1700	19.14	-0.050	Full ETtr	2	14	14	0.2645
15	40000 x 1700	1	120	0-1700	38.27	-0.025	Full ETtr	2	14	14	0.2317
16	40000 x 1700	2.5	120	0-1700	38.27	-0.025	Full ETtr	2	14	14	0.2298

Appendix 5-B:(Cont…)

Scenario#	Domain size	SLP	d(t)	Depth	K_s	Bottom Boundary flux	Potential Evapotranspiration (method of determination) [£]	Snow water equivalent (SWE)[‡]	# of days SWE applied		RMSE
									2011	2012	
	Cm	%	cm	cm	cm d^{-1}	cm d^{-1}					
17	40000 x 1700	2.5	120	0-1700	38.27	-0.300	Full ETtr	2	14	14	0.2540
18	40000 x 1700	2.5	120	0-1700	38.27	-0.030	Full ETos	2	14	14	0.2140
19	40000 x 1700	2.5	120	0-1700	38.27	-0.030	Full ETos	3	14	14	0.2148
20	40000 x 1700	2.5	120	0-1700	38.27	No Flow	Full ETtr	3	14	14	0.2433
21	40000 x 1700	2.5	120	0-1700	38.27	-0.025	Full ETtr	3	14	14	0.2286
22	40000 x 1700	2.5	120	0-1700	38.27	-0.300	Full ETtr	3	14	14	0.2523
23	40000 x 1700	2.5	120	0-1700	25.00	-0.030	Full ETtr	3	14	14	0.2056
24	40000 x 1700	2.5	120	0-1700	25.00	-0.035	Full ETtr	3	14	14	0.2202
25	40000 x 1700	2.5	120	0-1700	38.27	-0.030	Full ETos	4	14	14	0.2106
26	40000 x 1700	2.5	120	0-1700	25.00	-0.030	Full ETtr	4	14	14	0.2080
27	40000 x 1700	2.5	120	0-1700	25.00	-0.035	Full ETtr	4	14	14	0.2237
28	40000 x 1700	2.5	120	0-1700	38.27	No Flow	Full ETtr	4	14	14	0.2371
29	40000 x 1700	2.5	120	0-1700	38.27	-0.025	Full ETtr	4	14	14	0.2318
30	40000 x 1700	2.5	120	0-1700	38.27	-0.030	Full ETtr	4	14	14	0.2565

[£]ETtr and ETos are evapotranspiration values determined by Maule *et al (*2006) method developed for the Prairie region of Canada and by Penman Monteith method (Allen *et al.,* 1998) respectively, ‡Snow Water Equivalent (SWE) values indicate: 1 = SWE 2011=109 mm and 2012=78 mm, 2 = SWE 2011=109 mm and in 2012 SWE increased from 78 mm to 100 mm, 3 = SWE 2011=109 mm and in 2012 SWE increased from 78 mm to 100 mm application way changed and 4 = SWE 2011=109 mm and in 2012 SWE increased from 78 mm to 100 mm and applied in 14 consecutive days.

Appendix 5-C: Schematic of the potential water uptake distribution function, *b(x,z)*, in the soil root zone *(S)* a) for a single plant (After Šimůnek *et al*., 2011) and b) extended 2D for multiple plants (n = number of plants)

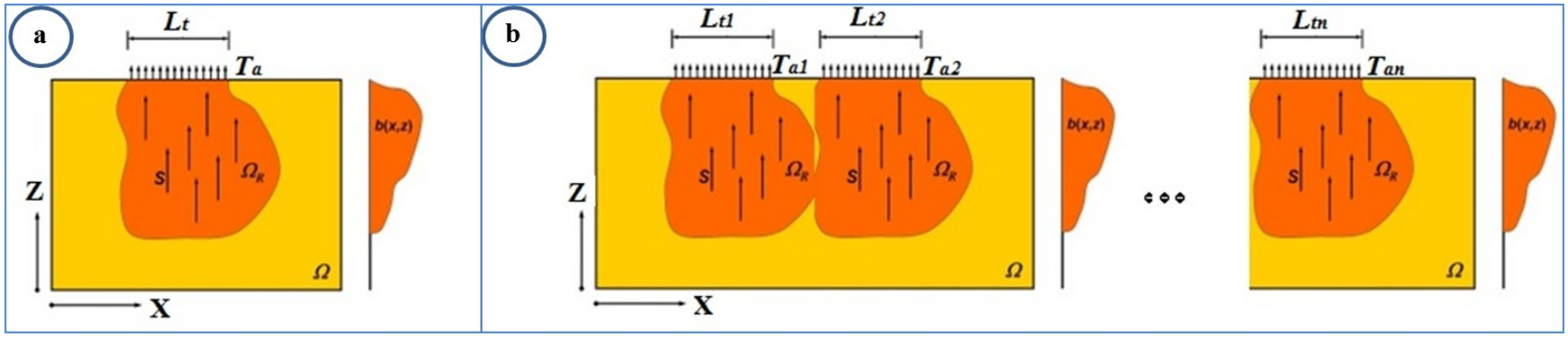

Appendix 5-D: Simulated *d(t)* showing sensitivity of HYDRUS 2D model to ET_{tr}. Domain size: 40000 cm x 1700 cm

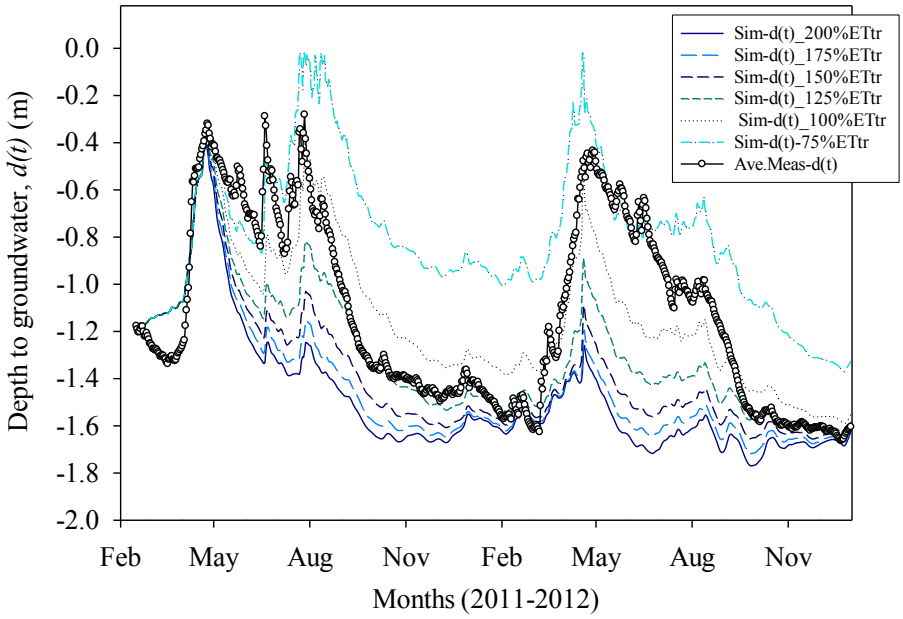

Appendix 5-E: Simulated *d(t)* showing sensitivity of HYDRUS 2D model to saturated hydraulic conductivity, K_s. Domain size: 40000 cm x 1700 cm

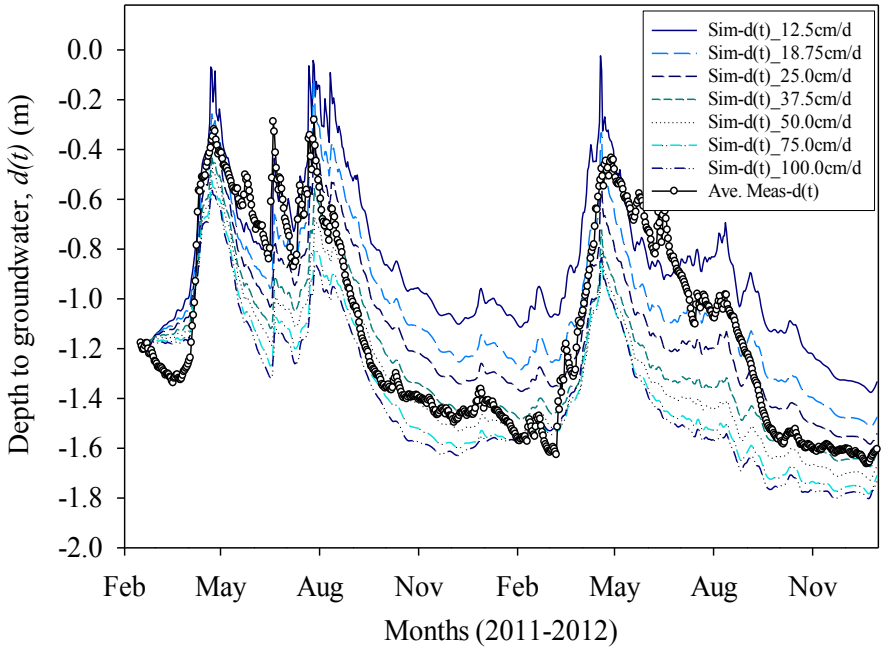

Appendix 5-F: Simulated *d(t)* showing sensitivity of HYDRUS 2D model to *LAI*. Domain size: 40000 cm x 1700 cm

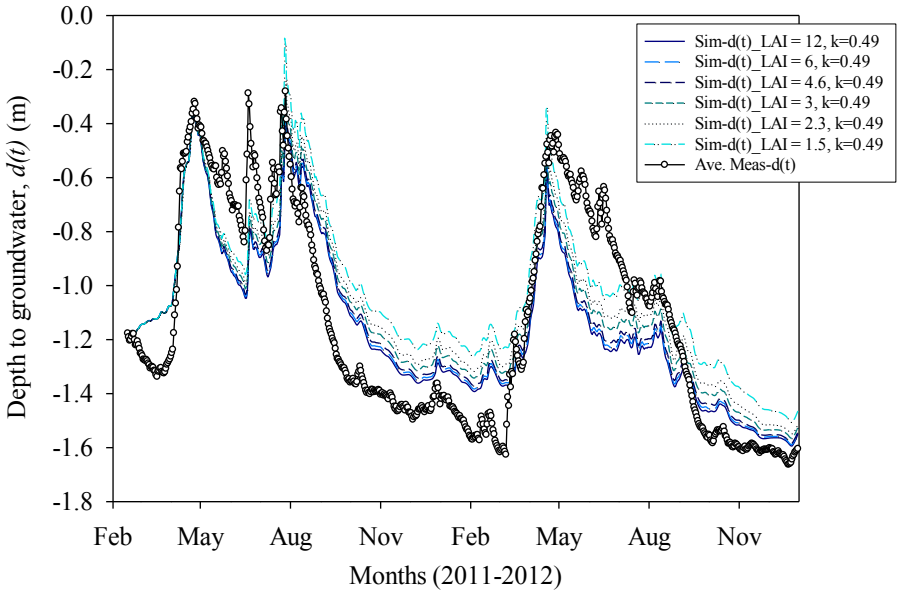

Appendix 5-G: Simulated *d(t)* showing sensitivity of HYDRUS 2D model to *k*. Domain size: 40000 cm x 1700 cm

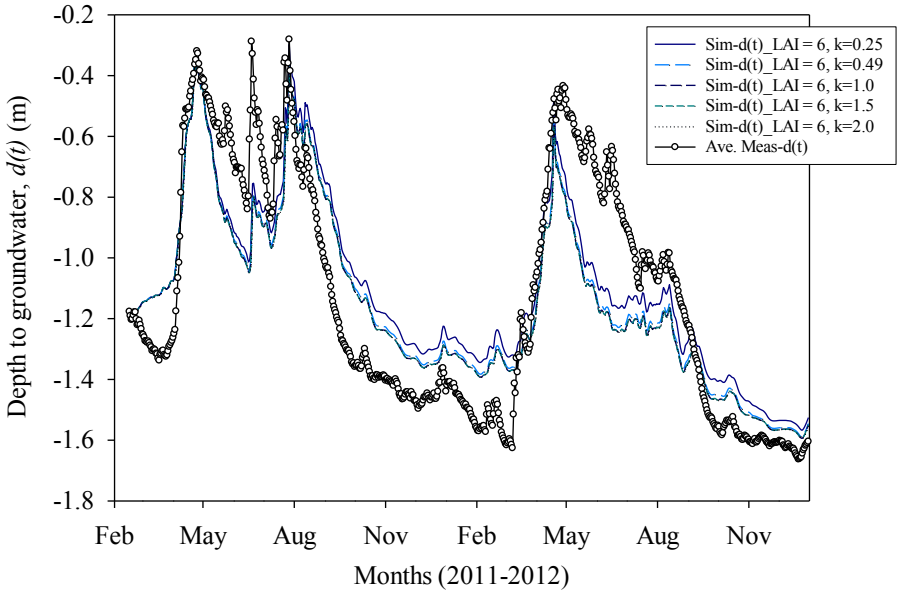

Appendix 5-H: Simulated *d(t)* showing sensitivity of HYDRUS 2D model to maximum rooting depth, Z_R. Domain size: 40000 cm x 1700 cm

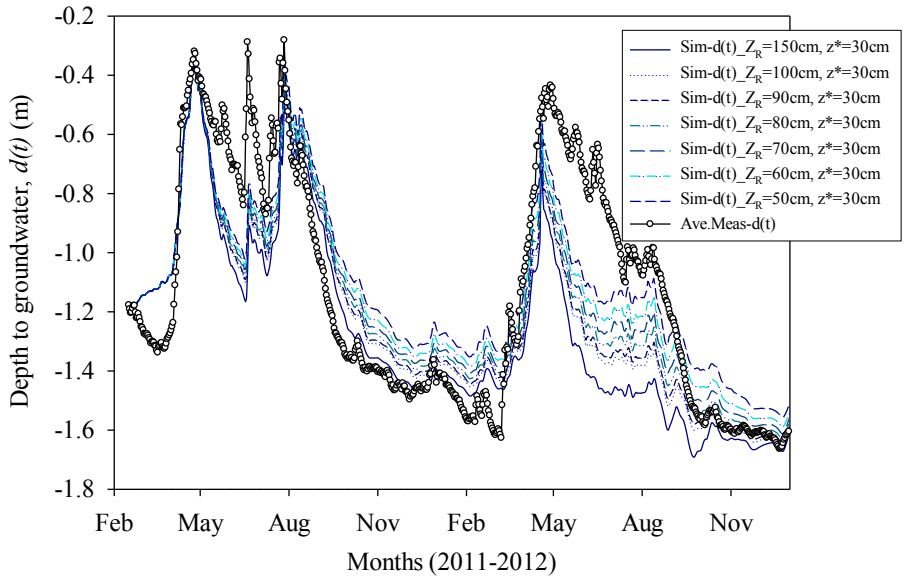

Appendix 5-I: Simulated *d(t)* showing sensitivity of HYDRUS 2D model to depth of maximum intensity, r* a) at Z_R=60 cm. Domain size: 40000 cm x 1700 cm

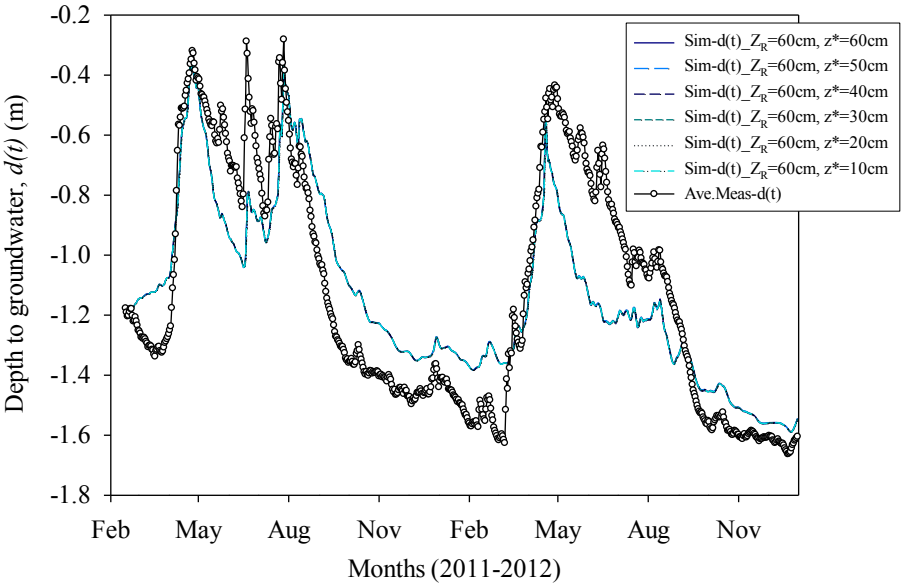

Appendix 5-J: Simulated *d(t)* showing sensitivity of HYDRUS 2D model to depth of maximum intensity, r* b) at Z_R=150 cm. Domain size: 40000 cm x 1700 cm

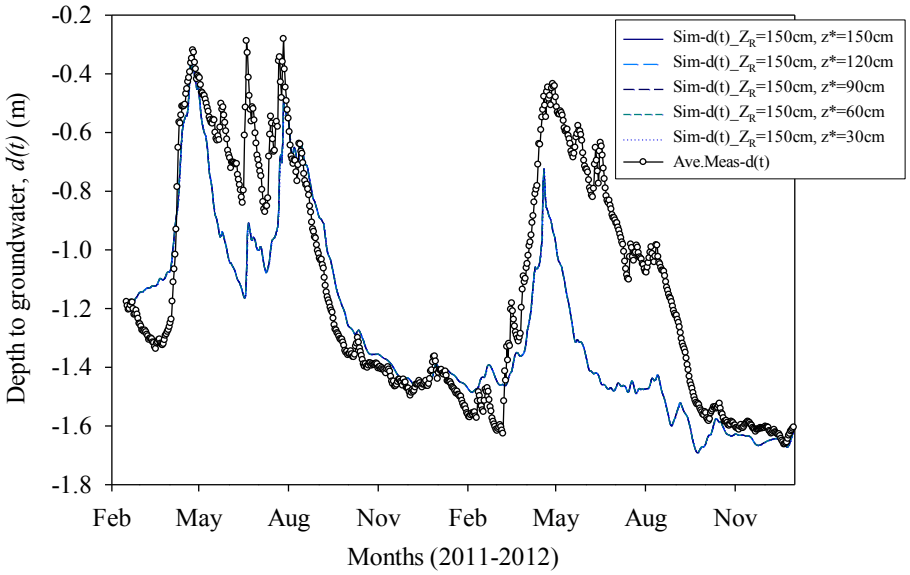

Appendix 5-K: Measured and simulated water content for the 1st top best three scenarios (K_s = 25 cm d^{-1}, a constant flux of -0.030 cm d^{-1} at the bottom boundary, and ET_{tr}). The simulated water content was an average of six observation nodes from 0-25 cm depth beneaththe center of each line source consistent with the TDR probe mearement depth , 25 cm. Domain size: 40000 cm x 1700 cm

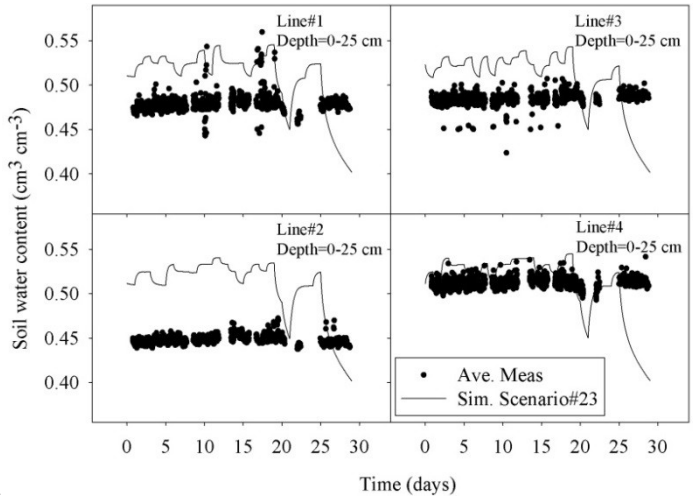

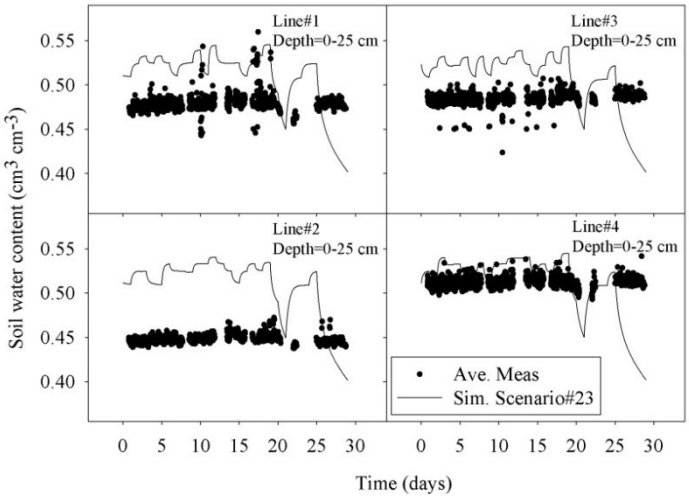

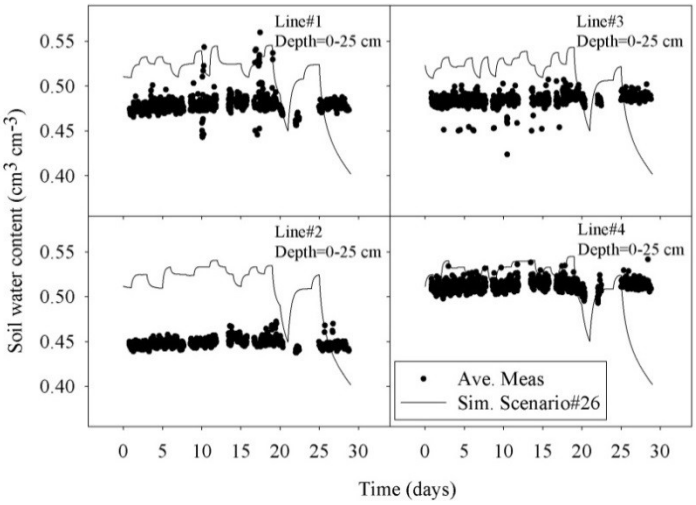

Appendix 5-L: Measured and simulated water content for the 2nd top best three scenarios (K_s = 38.27 cm d^{-1}, a constant flux of -0.030 cm d^{-1} at the bottom boundary, and ET_{os}). The simulated water content was an average of six observation nodes from 0-25 cm depth beneaththe center of each line source consistent with the TDR probe mearement depth , 25 cm. Domain size: 40000 cm x 1700 cm

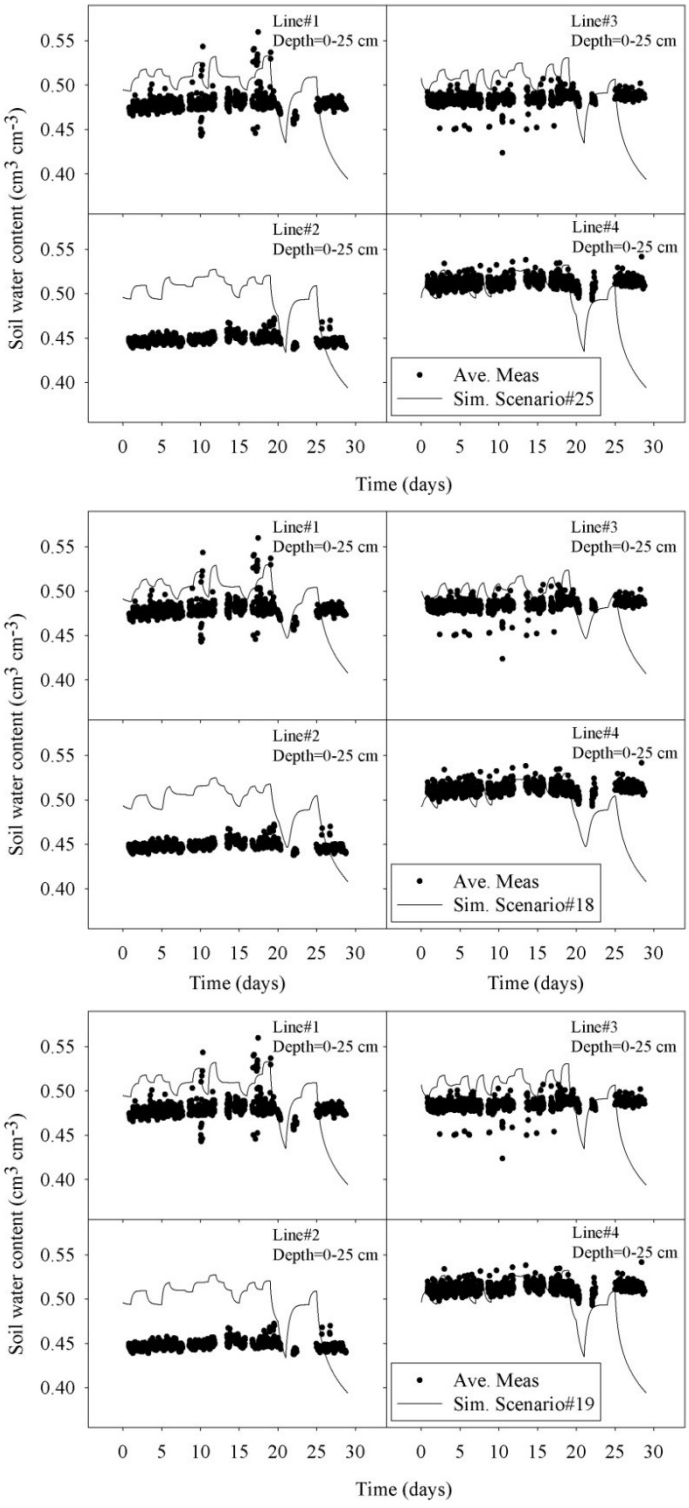

Appendix 5-M: Domain size comparison. The smaller domain size (20000 cm by 1700 cm) showed earlier mounding (the circled area) before the spring snowmelting period, which reflects the effect of a fixed head boundary on the up-and down-stream sides of the domain. The effect of the fixed head boundary was not noticeable on the larger domain size (40000 cm by 1700 cm), which was safer to be used for further flow and transport simulations

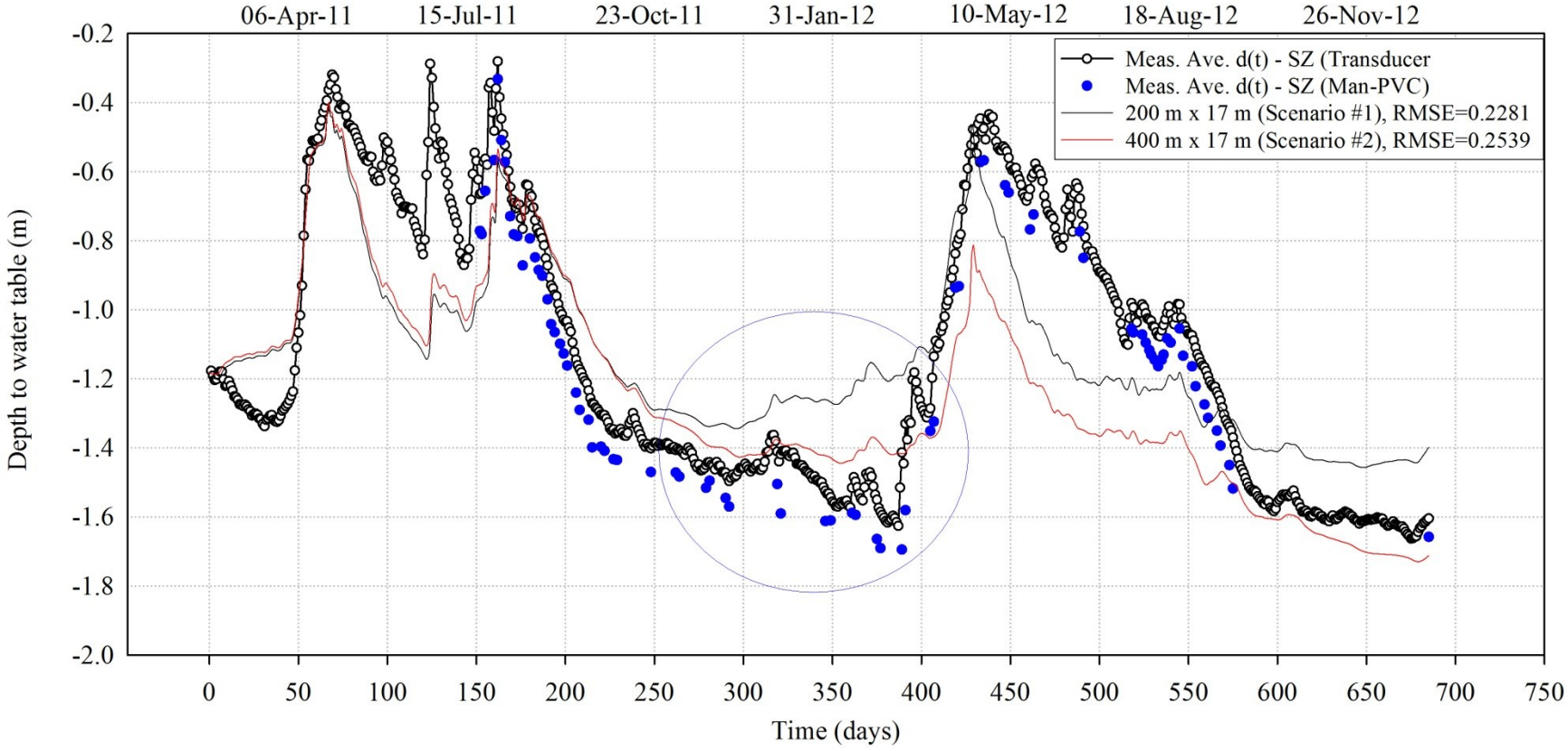

Appendix 5-N: Domain slope comparison for the 40000 cm by 1700 cm domain and there was no difference between the graphs from the 1% and 2.5% slope domains. The graphs from the domain slopes of 1% and 2.5% overlap each other for i) Scenarios 10 and 11 (K_s = 25 cm d-1 and a constant flux of -0.035 cm d-1and ETtr) and ii) Scenarios 15 and 16 (K_s = 25 cm d-1 and a constant flux of -0.035 cm d-1and ETtr)

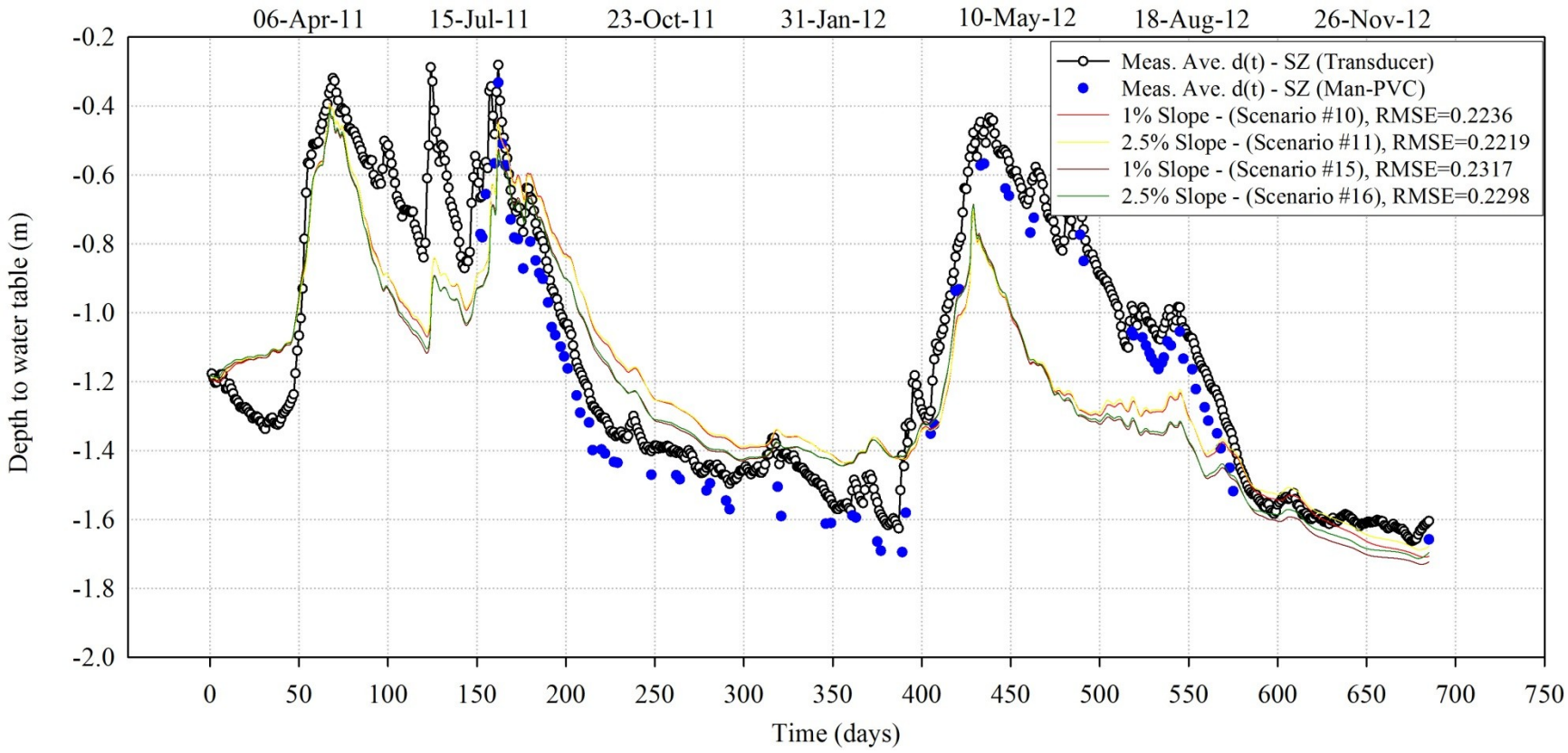

Appendix 5-O: Bottom boundary condition (BBC) comparison for the 40000 cm by 1700 cm domain. the effect of imposing constant flux or gradient at the bottom boundary was signifincat. The solid and dashed blue lines show when no flow was imposed at the bottom boundary and kept the water table level at or above the initial condition during the winter period

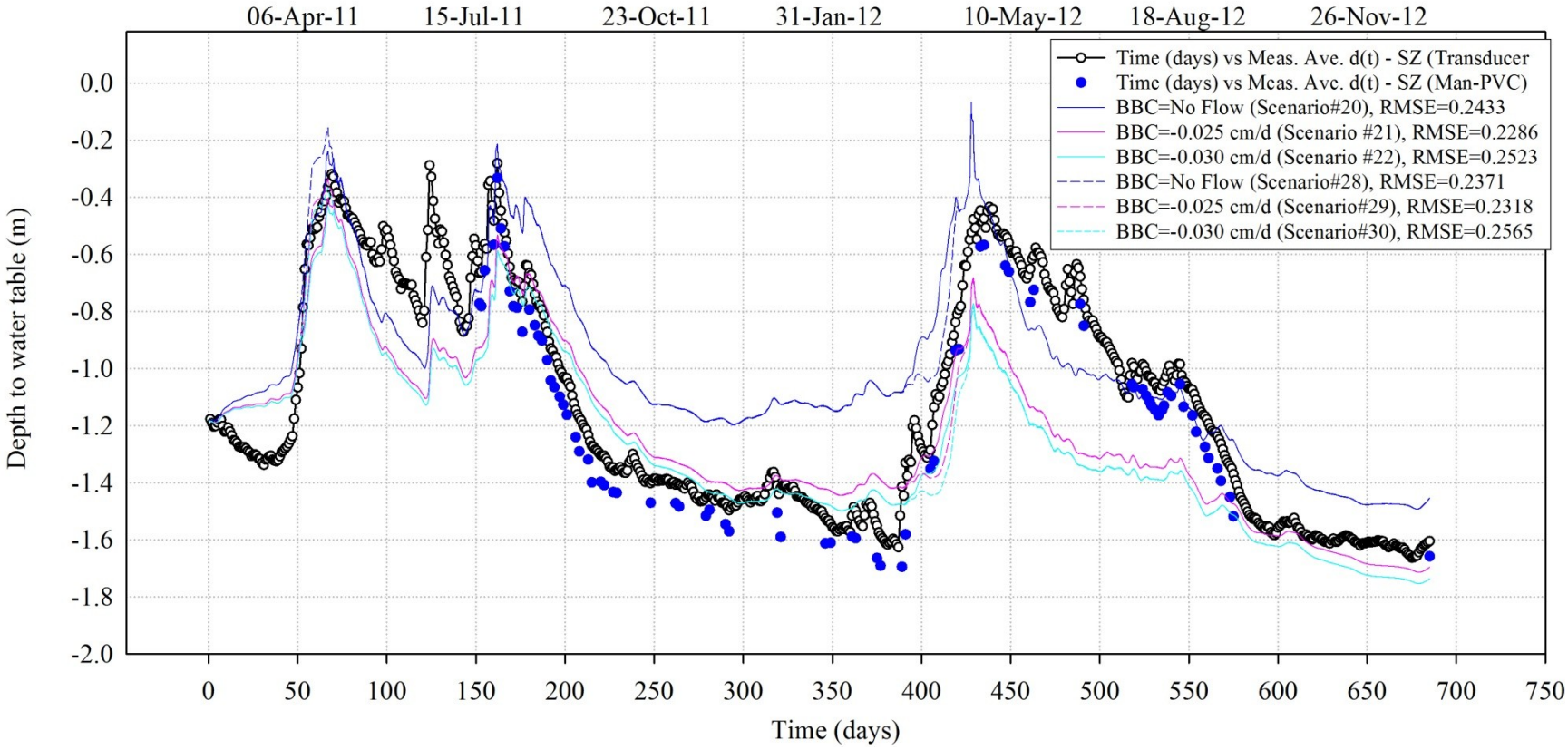

Appendix 5-P: Comparison of potential evapotranspiration calculated using three methods: ETos, ETtr and ETtru.